



DEVELOPMENT OF IMPROVED 3DOF ANALYSIS CAPABILITIES IN THE AEDC-VKF CONTINUOUS WIND TUNNELS

M. O. Varner

ARO, Inc., a Sverdrup Corporation Company

VON KARMAN GAS DYNAMICS FACILITY
ARNOLD ENGINEERING DEVELOPMENT CENTER
AIR FORCE SYSTEMS COMMAND
ARNOLD AIR FORCE STATION, TENNESSEE 37389

April 1978

Final Report for Period July 1976 — September 1977

Approved for public release; distribution unlimited.

UNCLASSIFIED REPORTS
FULL COPY

Property of U. S. Air Force,
AEDC-TR-78-10
100000000000

Prepared for

ARNOLD ENGINEERING DEVELOPMENT CENTER/DOTR
ARNOLD AIR FORCE STATION, TENNESSEE 37389

NOTICES

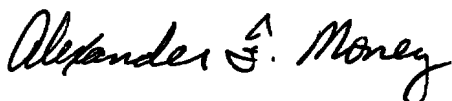
When U. S. Government drawings, specifications, or other data are used for any purpose other than a definitely related Government procurement operation, the Government thereby incurs no responsibility nor any obligation whatsoever, and the fact that the Government may have formulated, furnished, or in any way supplied the said drawings, specifications, or other data, is not to be regarded by implication or otherwise, or in any manner licensing the holder or any other person or corporation, or conveying any rights or permission to manufacture, use, or sell any patented invention that may in any way be related thereto.

Qualified users may obtain copies of this report from the Defense Documentation Center.

References to named commercial products in this report are not to be considered in any sense as an indorsement of the product by the United States Air Force or the Government.

APPROVAL STATEMENT

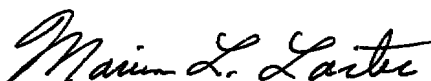
This report has been reviewed and approved.



ALEXANDER F. MONEY
Project Manager, Research Division
Directorate of Test Engineering

Approved for publication:

FOR THE COMMANDER



MARION L. LASTER
Director of Test Engineering
Deputy for Operations

UNCLASSIFIED

REPORT DOCUMENTATION PAGE		READ INSTRUCTIONS BEFORE COMPLETING FORM
1 REPORT NUMBER AEDC-TR-78-10	2 GOVT ACCESSION NO. 	3 RECIPIENT'S CATALOG NUMBER
4 TITLE (and Subtitle) DEVELOPMENT OF IMPROVED 3DOF ANALYSIS CAPABILITIES IN THE AEDC-VKF CONTINUOUS WIND TUNNELS		5 TYPE OF REPORT & PERIOD COVERED Final Report, July 1976 - September 1977
		6 PERFORMING ORG. REPORT NUMBER
7 AUTHOR(s) M. O. Varner, ARO, Inc.		8 CONTRACT OR GRANT NUMBER(s)
9 PERFORMING ORGANIZATION NAME AND ADDRESS Arnold Engineering Development Center Air Force Systems Command Arnold Air Force Station, TN 37389		10 PROGRAM ELEMENT, PROJECT, TASK AREA & WORK UNIT NUMBERS Program Element 65807F
11 CONTROLLING OFFICE NAME AND ADDRESS Arnold Engineering Development Center (DOS) Air Force Systems Command Arnold Air Force Station, TN 37389		12. REPORT DATE April 1978
		13. NUMBER OF PAGES 182
14 MONITORING AGENCY NAME & ADDRESS (if different from Controlling Office)		15. SECURITY CLASS. (of this report) UNCLASSIFIED
		15a. DECLASSIFICATION/DOWNGRADING SCHEDULE N/A
16 DISTRIBUTION STATEMENT (of this Report) Approved for public release; distribution unlimited.		
17. DISTRIBUTION STATEMENT (of the abstract entered in Block 20, if different from Report)		
18 SUPPLEMENTARY NOTES Available in DDC.		
19 KEY WORDS (Continue on reverse side if necessary and identify by block number) data reduction wind tunnel tests aerodynamic characteristics three-degrees-of-freedom simulation		
20 ABSTRACT (Continue on reverse side if necessary and identify by block number) This report presents improved data reduction and analysis procedures for 3DOF data from continuous wind tunnels. The Chapman-Kirk method is employed in the development of programs designed to extract aerodynamic coefficients from 3DOF motion. Noise sources inherent in the 3DOF gas bearing measurement system and found in typical test environments are studied. The validity		

UNCLASSIFIED

UNCLASSIFIED

20. ABSTRACT (Continued)

of extracted aerodynamic coefficients in the presence of these noise sources is addressed.

UNCLASSIFIED

PREFACE

The work reported herein was conducted by the Arnold Engineering Development Center (AEDC), Air Force Systems Command (AFSC), under Program Element 65807F. The results were obtained by ARO, Inc., AEDC Division (a Sverdrup Corporation Company), operating contractor for the AEDC, AFSC, Arnold Air Force Station, Tennessee, under ARO Project Number V32A-A4A. Major K. B. Harwood was the Air Force project manager. The manuscript was submitted for publication on January 5, 1978.

The author wishes to thank G. E. Burt, ARO, Inc., Supervisor, Dynamics Section, Aerodynamics Projects Branch, von Kármán Gas Dynamics Facility, for his assistance in obtaining the experimental data used in this report and for his guidance in this effort.

CONTENTS

	<u>Page</u>
1.0 INTRODUCTION	7
2.0 METHODS OF 3DOF ANALYSIS	7
3.0 MATHEMATICAL DEVELOPMENT	
3.1 Governing Equations for 3DOF Motion	10
3.2 Formulation of Parameter Extraction Method	17
4.0 DESCRIPTION OF COMPUTER PROGRAM	
4.1 Input	23
4.2 Output	23
5.0 RESULTS OF VALIDATION TESTS	
5.1 Computer-Generated Motion	24
5.2 Bench Test Data	28
5.3 Tunnel A Experimental Results	32
6.0 CONCLUDING REMARKS	36
REFERENCES	37

ILLUSTRATIONS

Figure

1. Arbitrary Body Showing Axis System for 3DOF Equation Development	39
2. Plane-Fixed Coordinate System Showing Euler Angles and Velocity Components Relative to Space-Fixed System	40
3. Physical Description of Symmetry Operations on Axis Systems	41
4. Flow Chart: Symmetric and Asymmetric Parameter Extraction Program	42
5. Graphical Solution Corresponding to Table 6, $\sigma = 0.05$ deg	43
6. Photograph of 3DOF Balance and Sting	47
7. 3DOF Balance Photographs	48
8. 3DOF Balance Schematic	49
9. Roll Interaction Effect for Sting Roll Position $\Omega = 0$ deg	50
10. Roll Interaction Effect for Sting Roll Position $\Omega = 45$ deg	52
11. Roll Interaction Effect for Sting Roll Position $\Omega = 90$ deg	54
12. Roll Interaction Effect for Sting Roll Position $\Omega = 180$ deg	56
13. Schematic of Bench Test Mechanism	58
14. Bench Test Results for 100-psi Bearing Pressure	59

<u>Figure</u>	<u>Page</u>
15. Bench Test Results for High Angle of Attack and 400-psi Bearing Pressure	65
16. Bench Test Results for Small Angle of Attack and 400-psi Bearing Pressure	70
17. Tunnel A	73
18. Model Schematic	74
19. Experimental 6.7-deg Sharp Cone Data Taken in Tunnel A at Mach Number 4.02 and 3.6 Million per Foot Reynolds Number	75
20. Experimental $d_N/d = 0.2275$, $\theta_c = 6.7$ -deg Sphere Cone Data Taken in Tunnel A at Mach Number 4.02 and 3.6 Million per Foot Reynolds Number	78
21. Graphical Solution of Sharp Cone Data Given in Fig. 19 for a Fit Interval of 8.44 sec with No Tunnel-Fixes Process Noise	81
22. Graphical Solution of Sharp Cone Data Given in Fig. 19 for a Fit Interval of 4.4 sec with Fixed Aerodynamics	89
23. Graphical Solution of Sharp Cone Data Given in Fig. 19 for a Fit Interval of 8.4 sec with Fixed Aerodynamics	93
24. Graphical Solution of Sphere Cone Data Given in Fig. 20 for a Fit Interval of 5.16 sec	99
25. Graphical Solution of Sphere Cone Data Given in Fig. 20 for a Fit Interval of 8.32 sec	104
26. Graphical Solution of Sphere Cone Data Given in Fig. 20 for a Fit Interval of 11.98 sec	114

TABLES

1. Fortran Listing: Symmetric Parameter Extraction Program	124
2. Fortran Listing: Asymmetric Parameter Extraction Program	142
3. Subroutine Descriptions for Both Asymmetric and Symmetric Programs	162
4. Input Variable Definitions for Symmetric and Asymmetric Programs	163
5. Effect of Number of Cycles and Number of Points per Cycle on C_{mq} RMS Deviation in Percent of C_{mq}	169
6. Effect of Measurement Noise on Linear and Nonlinear Coefficients and Their RMS Deviations	170
7. Tabular Results of Sharp Cone Analysis Using the Asymmetric Program for Fixed Model Aerodynamics	170
8. Tabular Results of Sphere Cone Analysis Using the Asymmetric Program for Fixed Values of $C_{lp} = -0.0027$ 1/rad, $t_1 = 0.017$ 1/rad, $t_4 = 0$, $\theta_T = 0$, $\psi_T = 0$	171

APPENDIX

A. MATHEMATICAL DEVELOPMENT: ASYMMETRIC VERISION	173
NOMENCLATURE	176

1.0 INTRODUCTION

During the past few years, improvements made on the AEDC von Kármán Gas Dynamics Facility (VKF) three-degree-of-freedom (3DOF) test mechanism have led to greater usage and increased emphasis on data quality and data reduction techniques. These improvements consist primarily of the addition to the original system as reported in Ref. 1 of roll position measurement and increased axial and normal load capacity.

Before the system alterations were made, only a limited amount of data was reduced to final form. This was due primarily to the relatively large computer time involved in the analysis of data and the limitations imposed by the data reduction procedure. The analysis of data for the extraction of meaningful aerodynamic coefficients was hampered by the use of data reduction procedures based on linear aerodynamics and on mass and aerodynamic symmetry properties of the model (Ref. 2). Since the majority of models tested fail to conform to either one or both of these restrictions, more exact data reduction techniques are required.

The capability of the 3DOF system to measure the roll position accurately permits data to be analyzed in the body-axis system. Use of this system allows analysis of the effects of model inertia anomalies and asymmetric aerodynamics on 3DOF motion. Moreover, increased emphasis has been placed on studying the effects of nonlinear aerodynamics for both symmetric (Ref. 3) and asymmetric configurations (Ref. 4).

This report presents improved data reduction and analysis procedures so that the increased capabilities of the 3DOF system may be utilized. A modified Newton-Raphson technique (hereafter referred to as the Chapman-Kirk method, Ref. 5) was employed to develop two programs designed to extract aerodynamic coefficients from 3DOF data. The asymmetric and symmetric programs utilize the full dynamic and kinematic equations and assume mirror plane symmetry and axial symmetry, respectively. Other data reduction methods currently used in aerodynamic parameter extraction are discussed in Section 2.0. The formulation of the mathematical aspects of the Chapman-Kirk method and the development of the governing 3DOF equations to be used in the extraction methods are presented in Section 3.0. Section 4.0 gives a detailed description of the resulting programs. In Section 5.0, the validity of the improved coefficient extraction technique is studied using computer-generated motion and 3DOF data from Tunnel A. In addition, bench test data are used to support error estimates of the extracted coefficients.

2.0 METHODS OF 3DOF ANALYSIS

During the past 20 years, much progress has been made in parameter identification techniques. Early methods were difficult to implement and time consuming in application.

The need for improved techniques was shown by the disagreement found between extrapolated wind tunnel and flight test results (Ref. 6). The following discussion concentrates on several types of identification techniques currently used in processing data, both in the wind tunnel and in full scale. The advantages and drawbacks of each type are addressed.

Parameter extraction methods may be broadly classified into three categories: 1) the so-called equation error methods, 2) output error methods, and 3) advanced methods. The equation error methods assume a performance criterion (i.e., a set of differential or algebraic constraints on the vehicle aerodynamics and/or motion) that minimizes the square of the equation error. All methods that fall into this group are basically least squares methods, and generally all response variables and derivatives must be measured. Application of this method gives a set of n linear equations with n unknowns. Since the equations to be solved are linear, the equation error methods are single-step processes. As such, they are normally used only as a startup method for output error methods. In addition, equation error methods are known to give biased estimates in the presence of measurement noise.

Output error methods minimize the square of the error between the actual system output and the modeled output. Characteristic of these methods is the ability to extract meaningful parameters in the presence of measurement noise. In addition, process noise (modeling errors) produces biased results in the extracted coefficients and may result in lack of convergence of the iterative scheme. Typical output error methods are Newton-Raphson, gradient, Kalman filter, and modified Newton-Raphson. The modified Newton-Raphson method, also referred to as the differential correction or quasilinearization method, can be shown to be identical to the Kalman filter method for the case of no measurement noise.

The maximum likelihood method (as described in Ref. 7) is the most advanced parameter identification technique currently available and is capable of handling both process and measurement noise. This technique may be subdivided into three basic steps. The first step employs the Kalman filter to estimate the magnitude of the states and to generate a residual sequence. A modified Newton-Raphson algorithm is then used for the parameter estimates. The final step uses an algorithm to estimate the noise statistics (the mean and variance of both process and measurement noise). With this approach used for parameter identification, the lower bound on the variances of parameter estimates and the models for the measurement and process noise disturbances may be determined.

The majority of experience gained over the past 20 years in parameter identification in the ballistic range and wind tunnel has been accumulated using some form of the

differential correction method (see Murphy, Ref. 8, and Nicolaides, Ref. 9, for example). The maximum likelihood method has seen limited use in the analysis of free-flight aircraft test data. Thus, even though the maximum likelihood method appears to hold promise for improved data analysis, the differential correction methods as used in the wind tunnel and ballistic range are still of primary interest due to their relative ease of application and proven reliability.

The differential correction method as used by Murphy (Ref. 8), Nicolaides (Ref. 9), and others, is essentially a linear or slightly nonlinear analysis. Under suitable linearizing assumptions, the angular motion equations of a basically symmetric model may be solved in closed form. The coefficients in the analytic solution which are functions of the vehicle aerodynamics are determined by fitting the solution to the data using the method of least squares. This approach can be used only to extract relatively simple aerodynamic coefficients from the experimental data. Furthermore, complex motion must usually be analyzed in small time segments, and thus any cumulative nonlinearities that may be present in the data are destroyed.

In the late 1960's a different approach to the differential corrections method was developed that did not rely on the existence of analytic solutions. This technique, hereafter referred to as the Chapman-Kirk method (Ref. 5), is also based on the minimization of the least squares function. The partial derivatives as required in the method of least squares are determined by numerically integrating parametric differential equations which are derived from the governing equations of motion. This approach can satisfactorily handle highly nonlinear aerodynamic moments and forces, but it requires substantially more computational effort since, in addition to the integration of the governing equations, a set of parametric differential equations must be solved.

The discussion of output error methods thus far has dealt with parameter identification techniques that are deterministic in nature in that the aerodynamic modeling does not account for measurement or process noise. All ballistic and wind tunnel angular motion data contain a finite amount of measurement and process noise, however. The effect of such noise usually appears in the higher order nonlinear coefficients, as pointed out in Ref. 10, in the form of abnormally large variance and bias. The extended Kalman filter method (as discussed in Ref. 11) provides an approach in which measurement noise can be satisfactorily modeled. This method provides direct estimates of the states of noisy systems as well as estimates of the state variable uncertainties. Even though the extended Kalman filter method provides more detailed information on the measurement noise of experimental data, it provides no estimate of process noise, which is a serious noise source in nonlinear systems. In this regard, the extended Kalman filter method has no distinct advantages over the Chapman-Kirk method in processing real 3DOF data.

Thus, the Chapman-Kirk method is used to develop an improved 3DOF data analysis capability for use in continuous wind tunnels. Even though this approach does not yield detailed information on measurement noise, as does the extended Kalman filter method, it does afford sufficient insight into the effects of the measurement noise on the extracted coefficients. In the absence of process (modeling) noise, it may be shown that the probable error of the extracted coefficients for random measurement noise, using the Chapman-Kirk method, is equal to the root-mean-square (RMS) deviation from the true value.

3.0 MATHEMATICAL DEVELOPMENT

The preceding section has dealt extensively with the different types of parameter identification techniques that may be used for 3DOF data analysis. It was concluded that the Chapman-Kirk method as described in Ref. 5 provided the best compromise in mathematical complexity, reliability, and versatility of the methods considered. This section presents in a concise manner the mathematical details of the Chapman-Kirk method as applied to 3DOF data for axisymmetric bodies of revolution taken in continuous wind tunnels. A similar development of the important equations for models with mirror plane aerodynamic and geometric symmetry is given in Appendix A.

3.1 GOVERNING EQUATIONS FOR 3DOF MOTION

The 3DOF governing equations of motion are derived from Newton's second law of motion, which may be written as

$$\vec{M} = \frac{d\vec{h}}{dt} \quad (1)$$

where \vec{M} is the external moment acting at the mass center of gravity (cg) equal to $M_x\vec{i} + M_y\vec{j} + M_z\vec{k}$, and \vec{h} is the moment of momentum referred to the axis system as shown in Fig. 1. For a rigid body, the moment of momentum may be shown (Ref. 12) to reduce to Eq. (2).

$$\begin{aligned} \vec{h} = h_x\vec{i} + h_y\vec{j} + h_z\vec{k} = & (p I_{xx} - q I_{xy} - r I_{xz}) \vec{i} \\ & + (-p I_{xy} + q I_{yy} - r I_{yz}) \vec{j} \\ & + (-p I_{xz} - q I_{yz} + r I_{zz}) \vec{k} \end{aligned} \quad (2)$$

Here p , q , and r are the components of the angular velocity vector along the x , y , z axis system (see Fig. 1), respectively, referenced to a space-fixed axis system, and I_{xx} , I_{yy} , I_{zz} , I_{xy} , I_{xz} , and I_{yz} are the moments and products of inertia as defined in the standard way by Kolk (Ref. 13) and others.

Utilizing Eq. (2) in Eq. (1), the governing Euler moment equations for a plane-fixed axis system may be written in the form of Eq. (3), where the caret denotes the aeroballistic axis system.

$$\begin{aligned}\hat{M}_x &= \dot{h}_x - \hat{q} h_z - \hat{r} h_y \\ \hat{M}_y &= \dot{h}_y + \hat{r} h_x - \hat{p} h_z \\ \hat{M}_z &= \dot{h}_z + \hat{p} h_y - \hat{q} h_x\end{aligned}\quad (3)$$

The dot as used here indicates differentiation of the scalar quantity with respect to time, and \hat{p} , \hat{q} , and \hat{r} are the angular velocities of the plane-fixed axis system relative to the space-fixed axis. For the case in which the body axis is a principal axis, the products of inertia, I_{xy} , I_{xz} , and I_{yz} , are identically zero. If it is further assumed that the body is axially symmetric about the x axis, then $I_y = I_z \equiv I$.

In order to derive the Euler moment equations in terms of angular measurements, the Eulerian angles ψ , θ , and ϕ are defined. Figure 2 illustrates the Euler angles ψ , θ , and ϕ for the aeroballistic axis system. Vectors in the space-fixed coordinate system may be transformed to the aeroballistic axis system by successive rotations about the Z axis through the yaw angle, ψ , and about the \hat{y} axis through the pitch angle, θ .

The Euler angles ψ , θ , and ϕ are related to the angular velocities through Eq. (4),

$$\begin{aligned}p &= \dot{\phi} - \dot{\psi} \sin \theta \\ q &= \dot{\theta} \\ r &= \dot{\psi} \cos \theta\end{aligned}\quad (4)$$

with the plane-fixed angular velocities given as follows:

$$\begin{aligned}\hat{p} &= -\dot{\psi} \sin \theta \\ \hat{q} &= \dot{\theta} \\ \hat{r} &= \dot{\psi} \cos \theta\end{aligned}\quad (5)$$

Inserting Eqs. (4) and (5) into the governing moment equations and simplifying, the governing differential equations of angular motion may be shown to reduce to the form of Eq. (6).

$$\begin{aligned}
\ddot{\phi} &= \bar{M}_x - \dot{\psi} \dot{\theta} \cos \theta + \bar{M}_y \tan \theta - (2 - R) \dot{\psi} \dot{\theta} \tan \theta \sin \theta \\
&\quad - R \dot{\phi} \dot{\theta} \tan \theta \\
\ddot{\theta} &= \bar{M}_y - (1 - R) \dot{\psi}^2 \sin \theta \cos \theta - R \dot{\phi} \dot{\psi} \cos \theta \\
\ddot{\psi} &= \bar{M}_z / \cos \theta + (2 - R) \dot{\psi} \dot{\theta} \tan \theta + R \dot{\phi} \dot{\theta} / \cos \theta
\end{aligned}
\tag{6}$$

Here the definitions $\bar{M}_y = \hat{M}_y/I$, $\bar{M}_z = \hat{M}_z/I$, $\bar{M}_x = \hat{M}_x/I_x$ and $R = I_x/I$ have been utilized. The above equations describe the angular motion of an axially symmetric body about its cg caused by aerodynamic moments \hat{M}_x , \hat{M}_y , and \hat{M}_z in the aeroballistic axis system.

The solution of Eq. (6) depends on the form chosen for the moments as functions of the dependent variables. In order to provide the most general form of the moment coefficients for axially symmetric bodies, the ideas of Tobak, Ref. 14, have been utilized. The moments are written as functionals of the parameters that directly influence the moments. Thus, it is assumed that the moment coefficients, C_l , C_m , and C_n are functions of the velocity ratios v/U_∞ and w/U_∞ and the angular velocities p , q , and r , as shown in Eq. (7).

$$\begin{aligned}
\hat{M}_x &= q_\infty S d C_l(\alpha, \beta; p, q, r) \\
\hat{M}_y &= q_\infty S d C_m(\alpha, \beta; p, q, r) \\
\hat{M}_z &= q_\infty S d C_n(\alpha, \beta; p, q, r)
\end{aligned}
\tag{7}$$

The variables α and β are the velocity ratios w/U_∞ and v/U_∞ , respectively, as depicted in Fig. 1. The dynamic pressure, reference area (base area), and reference length (base diameter) are denoted by q_∞ , S , and d , respectively. By expanding the moment coefficients about α and β and dropping nonlinear coefficients in $\dot{\alpha}$, $\dot{\beta}$, p , q , and r , the coefficients of Eq. (7) may be reduced to

$$\begin{aligned}
C_l(\alpha, \beta; p, q, r) &= C_l(\alpha, \beta) + \frac{d}{2U_\infty} \left[p C_{lp}(\alpha, \beta) \right. \\
&\quad \left. + q C_{lq}(\alpha, \beta) + r C_{lr}(\alpha, \beta) + \dot{\alpha} C_{l\dot{\alpha}}(\alpha, \beta) + \dot{\beta} C_{l\dot{\beta}}(\alpha, \beta) \right] \\
C_m(\alpha, \beta; p, q, r) &= C_m(\alpha, \beta) + \frac{d}{2U_\infty} \left[p C_{mp}(\alpha, \beta) \right. \\
&\quad \left. + q C_{mq}(\alpha, \beta) + r C_{mr}(\alpha, \beta) + \dot{\alpha} C_{m\dot{\alpha}}(\alpha, \beta) + \dot{\beta} C_{m\dot{\beta}}(\alpha, \beta) \right] \\
C_n(\alpha, \beta; p, q, r) &= C_n(\alpha, \beta) + \frac{d}{2U_\infty} \left[p C_{np}(\alpha, \beta) \right. \\
&\quad \left. + q C_{nq}(\alpha, \beta) + r C_{nr}(\alpha, \beta) + \dot{\alpha} C_{n\dot{\alpha}}(\alpha, \beta) + \dot{\beta} C_{n\dot{\beta}}(\alpha, \beta) \right]
\end{aligned}
\tag{8}$$

As can be seen, the new coefficients as defined in Eq. (8) are functions of the parameters α and β only. Before the expansion of the new coefficients about α and β equal to zero is accomplished, the relations describing α and β and their derivatives as functions of the Euler angles will be presented. Using this information will result in simplifications which ultimately will reduce the number of unknown parameters. Noting that the only component of velocity that exists in a continuous wind tunnel situation in the space-fixed coordinate system is $-U_\infty$ along the X axis, transformation to the aeroballistic axis system results in

$$\begin{aligned}\alpha &= \frac{u}{U_\infty} = \cos \psi \sin \theta \\ \beta &= \frac{v}{U_\infty} = -\sin \psi\end{aligned}\quad (9)$$

with rates of change of α and β given by

$$\begin{aligned}\dot{\alpha} &= -\dot{\psi} \sin \psi \sin \theta + \dot{\theta} \cos \psi \cos \theta \\ \dot{\beta} &= -\dot{\psi} \cos \psi\end{aligned}\quad (10)$$

A comparison of Eqs. (10) and (4) makes it evident that for small pitch and yaw angles, $\dot{\alpha}$ is approximately equal to $\dot{\theta}$. This of course assumes that θ and ψ are of the same order, a valid assumption for bodies with axial symmetry or with relatively small asymmetries. Thus, the rates $\dot{\alpha}$ and $\dot{\beta}$ are approximate linear combinations of the angular rates q and r and approach exact linear combinations in the limit as ψ and θ approach zero. Moreover, in Section 5.1 it is shown that for reasonable levels of measurement noise, the effects of the rate terms $\dot{\alpha}$ and $\dot{\beta}$ cannot be satisfactorily separated from the angular velocities q and r . Thus, to avoid over specification of the aerodynamics, it is assumed that $\dot{\alpha} = e_1 r$ and $\dot{\beta} = e_2 r$ where e_1 and e_2 are constants. This reduces the coefficient expansion as given in Eq. (8) to the form

$$C_i(\alpha, \beta; p, q, r) = C_i(\alpha, \beta) + \frac{d}{2U_\infty} \left[p C_{ip}(\alpha, \beta) - q C_{iq}(\alpha, \beta) + r C_{ir}(\alpha, \beta) \right] \quad (11)$$

where i equals l , m , or n .

In order to allow for a high degree of versatility in the coefficient expansions in terms of α and β , while at the same time retaining functional simplicity, Taylor series expansions are made about α and β equal to zero for each of the coefficients C_i , C_{ip} , C_{iq} , and C_{ir} . Terms involving the magnitude of α and β have also been included in the expanded coefficients. Retaining terms cubic and lower in α and β , for $C_i(\alpha, \beta)$, and

quadratic and lower for C_{ip} , C_{iq} , and C_{ir} , the expanded form of the coefficients is given in Eq. (12).

$$\begin{aligned}
C_i(\alpha, \beta) = & a_{i0} + a_{i1}\alpha + a'_{i1}|\alpha| + a_{i2}\alpha^2 + a'_{i2}\alpha|\alpha| \\
& + a_{i3}\alpha^3 + a'_{i3}\alpha^2|\alpha| + a_{i4}\beta + a'_{i4}|\beta| + a_{i5}\beta^2 \\
& + a'_{i5}|\beta|\beta + a_{i6}\beta^3 + a'_{i6}|\beta|\beta^2 + a_{i7}\alpha\beta + a'_{i7}|\alpha|\beta \\
& + a''_{i7}\alpha|\beta| + a'_{i7}|\alpha\beta| + a_{i8}\alpha^2\beta + a'_{i8}\alpha^2|\beta| \\
& + a''_{i8}|\alpha\beta|\alpha + a_{i9}\alpha\beta^2 + a'_{i9}|\alpha|\beta^2 + a''_{i9}\beta|\alpha\beta| \\
C_{iq}(\alpha, \beta) = & b_{i0} + b_{i1}\alpha + b'_{i1}|\alpha| + b_{i2}\alpha^2 + b'_{i2}\alpha|\alpha| \\
& + b_{i3}\beta + b'_{i3}|\beta| + b_{i4}\beta^2 + b'_{i4}\beta|\beta| + b_{i5}\alpha\beta \\
& + b'_{i5}|\alpha|\beta + b'_{i5}\alpha|\beta| + b''_{i5}|\alpha\beta| \quad (12) \\
C_{ir}(\alpha, \beta) = & c_{i0} - c_{i1}\alpha + c'_{i1}|\alpha| + c_{i2}\alpha^2 + c'_{i2}\alpha|\alpha| \\
& - c_{i3}\beta + c'_{i3}|\beta| + c_{i4}\beta^2 - c'_{i4}\beta|\beta| - c_{i5}\alpha\beta \\
& + c'_{i5}|\alpha|\beta - c''_{i5}\alpha|\beta| + c''_{i5}|\alpha\beta| \\
C_{ip}(\alpha, \beta) = & f_{i0} - f_{i1}\alpha + f'_{i1}|\alpha| + f_{i2}\alpha^2 - f'_{i2}\alpha|\alpha| \\
& + f_{i3}\beta - f'_{i3}|\beta| + f_{i4}\beta^2 - f'_{i4}\beta|\beta| + f_{i5}\alpha\beta \\
& + f'_{i5}|\alpha|\beta - f''_{i5}\alpha|\beta| + f''_{i5}|\alpha\beta|
\end{aligned}$$

Here, the coefficients a_i , b_i , c_i , and f_i are independent constants that are functions of the free-stream conditions (such as Mach number and Reynolds number) and body geometry.

Further simplification of Eq. (12) is not possible unless flow-field symmetry arguments are employed. The primary justification for implementation of the symmetry conditions is based on small angular motion about ψ and θ equal to zero. Since the maximum angular displacement of the 3DOF gas bearing system is 10 deg, flow-field symmetry that is compatible with geometric symmetry is implied. Thus, symmetry arguments as given by Maple and Synge, Ref. 15, are used to reduce the number of unknown constants in Eq. (12). To reduce the coefficients as given in Eq. (12) to those for a body symmetric about

the x axis (see Fig. 3), two covering operations are required. A covering operation for mirror symmetry about the x, z plane is performed first and is followed by a covering operation for 90-deg rotational symmetry about the x axis. The mirror symmetry condition results in

$$\begin{aligned} C_m(\alpha, -\beta; -p, q, -r) &= C_m(\alpha, \beta; p, q, r) \\ C_n(\alpha, -\beta; -p, q, -r) &= -C_n(\alpha, \beta; p, q, r) \\ C_g(\alpha, -\beta; -p, q, -r) &= -C_g(\alpha, \beta; p, q, r) \end{aligned} \quad (13)$$

Under the restrictions of Eq. (13), the moment coefficients as given by Eq. (12) reduce as follows:

$$\begin{aligned} C_m(\alpha, \beta) &= a_{m0} + a_{m1}\alpha + a'_{m1}|\alpha| + a_{m2}\alpha^2 + a'_{m2}\alpha|\alpha| \\ &\quad - a_{m3}\alpha^3 + a'_{m3}\alpha^2|\alpha| + a'_{m4}|\beta| - a_{m5}\beta^2 \\ &\quad - a'_{m6}|\beta|\beta^2 + a''_{m7}\alpha|\beta| - a'''_{m7}|\alpha\beta| + a'_{m8}\alpha^2|\beta| \\ &\quad + a''_{m8}|\alpha\beta|\alpha + a_{m9}\alpha\beta^2 + a'_{m9}|\alpha|\beta^2 \\ C_{mq}(\alpha, \beta) &= b_{m0} + b_{m1}\alpha + b'_{m1}|\alpha| + b_{m2}\alpha^2 + b'_{m2}\alpha|\alpha| \\ &\quad + b'_{m3}|\beta| + b_{m4}\beta^2 - b''_{m5}\alpha|\beta| + b'''_{m5}|\alpha\beta| \\ C_{mr}(\alpha, \beta) &= C_{m3}\beta + C'_{m4}\beta|\beta| + C_{m5}\alpha\beta + C'_{m5}|\alpha|\beta \\ C_{mp}(\alpha, \beta) &= f_{m3}\beta + f'_{m4}\beta|\beta| + f_{m5}\alpha\beta + f'_{m5}|\alpha|\beta \\ C_i(\alpha, \beta) &= a_{i0} + a_{i4}\beta + a'_{i5}\beta|\beta| + a_{i6}\beta^3 + a_{i7}\alpha\beta \\ &\quad + a'_{i7}|\alpha|\beta + a_{i8}\alpha^2\beta + a'_{i9}\beta|\alpha\beta| \\ C_{iq}(\alpha, \beta) &= b_{i3}\beta + b'_{i4}\beta|\beta| + b_{i5}\alpha\beta + b'_{i5}|\alpha|\beta \\ C_{ir}(\alpha, \beta) &= c_{i0} + c_{i1}\alpha + c'_{i1}|\alpha| + c_{i2}\alpha^2 + c'_{i2}\alpha|\alpha| \\ &\quad + c'_{i3}|\beta| + c_{i4}\beta^2 - c''_{i5}\alpha|\beta| - c'''_{i5}|\alpha\beta| \\ C_{ip}(\alpha, \beta) &= f_{i0} + f_{i1}\alpha + f'_{i1}|\alpha| + f'_{i2}\alpha^2 + f_{i2}\alpha|\alpha| \\ &\quad - f'_{i3}|\beta| + f_{i4}\beta^2 + f''_{i5}\alpha|\beta| + f'''_{i5}|\alpha\beta| \end{aligned} \quad (14)$$

Here, $i = n, \ell$. The coefficient expansions as given in Eq. (14) are valid for asymmetric configurations with the symmetry plane of the body in the x, z plane of the body-fixed axis system. A 90-deg rotational symmetry requirement will result in a four-fold symmetry of the body. The four-fold symmetry coupled with mirror plane symmetry is sufficient for the specification of axial symmetry. A covering operation performed on a 90-deg rotation of the axis system results in the coefficient constraints as given in Eq. (15).

$$\begin{aligned}
 C_n(\beta, -\alpha) &= C_m(\alpha, \beta) \\
 C_{nr}(\beta, -\alpha) &= C_{mq}(\alpha, \beta) \\
 -C_{nq}(\beta, -\alpha) &= C_{mr}(\alpha, \beta) \\
 C_\ell(\beta, -\alpha) &= C_\ell(\alpha, \beta) \\
 -C_{\ell q}(\beta, -\alpha) &= C_{\ell r}(\alpha, \beta) \\
 C_{\ell p}(\beta, -\alpha) &= C_{\ell p}(\alpha, \beta) \\
 C_{np}(\beta, -\alpha) &= C_{mp}(\alpha, \beta)
 \end{aligned} \tag{15}$$

Employing these constraints with the additional restriction that, for zero spin rate, an axially symmetric body will have no moments in the plane normal to the total angle-of-attack plane, the aerodynamic coefficient expansions as shown in Eq. (16) will result.

$$\begin{aligned}
 C_{m0}(\alpha, \beta)/\alpha &= a_1 + a'_2(|\alpha| + |\beta|) + a_3(\alpha^2 + \beta^2) + a''_8|\alpha\beta| \\
 C_{mq}(\alpha, \beta) - c_5\beta^2 &= b_0 + b'_1(|\alpha| + |\beta|) + b_2(\alpha^2 + \beta^2) + b''_5|\alpha\beta| \\
 C_{mr}(\alpha, \beta) &= c_5\alpha\beta \\
 C_{mp}(\alpha, \beta)/\beta &= d_3 + d'_5|\alpha| + d'_4|\beta| \\
 -C_{n0}(\alpha, \beta)/\beta &= C_{m0}(\alpha, \beta)/\alpha \\
 C_{nq}(\alpha, \beta) &= C_{mr}(\alpha, \beta) \\
 C_{nr}(\alpha, \beta) - c_5\alpha^2 &= C_{mq}(\alpha, \beta) - c_5\beta^2 \\
 C_{np}(\alpha, \beta)/\alpha &= d_3 + d'_5|\beta| + d'_4|\alpha| \\
 C_{\ell o}(\alpha, \beta) &= e_0 \\
 C_{\ell p}(\alpha, \beta) &= f_0 + f'_1(|\alpha| + |\beta|) + f_2(\alpha^2 + \beta^2) \\
 C_{\ell r}(\alpha, \beta)/\alpha &= g_3 - g'_5|\beta| + g'_4|\alpha| \\
 C_{\ell q}(\alpha, \beta)/\beta &= g_3 + g'_5|\alpha| + g'_4|\beta|
 \end{aligned} \tag{16}$$

The above expressions as used in Eq. (11) yield the required moment coefficients.

It is important to note here that the expansions as given in Eq. (16) are not unique in describing axially symmetric body aerodynamics. Indeed, other expansions, such as those in terms of the total angle of attack as used by Whyte (Ref. 16) and others, are also valid. The "correct" expansion of coefficients describing the aerodynamics of a body, in the parameter identification sense, is that which yields the "best" fit to the experimental data and does not violate established symmetry constraints. With the establishment of the required aerodynamic coefficients, the governing equations of motion, Eq. (6), may be solved.

3.2 FORMULATION OF PARAMETER EXTRACTION METHOD

In order to determine the coefficients describing the aerodynamic model as given in Eq. (16) for axial symmetry or in Eq. (14) for mirror plane symmetry, a parameter extraction technique must be used. The 3DOF gas bearing as described in Ref. 1 yields angular position measurements in yaw, pitch, and roll which provide the experimental data necessary to extract the unknown parameters. In Section 1.0 the Chapman-Kirk method was selected as the parameter identification technique to be employed here. This technique is an output error method and, as such, uses the method of least squares to minimize the cumulative error between observed and calculated motion.

Normally when one is fitting data with a least squares method, the function to be fitted is given with constant coefficients that appear linearly in the function. This results in a set of simultaneous linear equations that may be solved in a noniterative fashion for the unknown coefficients. For nonlinear functions, the coefficients must be evaluated by the differential corrections method. This technique provides corrections to improve the estimates of the unknown parameters and, as a result, is an iterative process.

Since the 3DOF governing equations as given in Eq. (6) are nonlinear and the unknown parameters as given in Eq. (16) are complicated functions of the Euler angles, ϕ , θ , and ψ , the differential corrections method will be used. Consider the problem of fitting the 3DOF motion of a model to known functions of the unknown parameters. If the variables $\phi_{m\ell}$, $\theta_{m\ell}$, and $\psi_{m\ell}$ are defined as the experimental values of the roll, pitch, and yaw positions at each time point ℓ , residuals (u_ℓ , v_ℓ , w_ℓ) yielding the difference between the measured and calculated data may be expressed by Eq. (17).

$$\begin{aligned} u_\ell &\equiv \phi_\ell - \phi_{m\ell} \\ v_\ell &\equiv \theta_\ell - \theta_{m\ell} \\ w_\ell &\equiv \psi_\ell - \psi_{m\ell} \end{aligned} \quad (17)$$

Here, ϕ_l , θ_l , and ψ_l are the calculated values of the roll, pitch, and yaw, respectively, which are functions of a set of independent constants, a_i . These constants are the aerodynamic coefficients to be determined as shown in Eq. (16). In order to determine the change in the coefficients, Δa_i , required to reduce the residuals in the least squares sense, a Taylor series expansion of the calculated solution is made. Expanding ϕ_l , θ_l , and ψ_l , and discarding second and higher order terms and using the definitions as given in Eq. (17), one obtains Eq. (18).

$$\begin{aligned} u_l + \phi_{ml} &= \phi_{lo} + \sum_{i=1}^{N_c} \Delta a_i \frac{\partial \phi_l}{\partial a_i} \\ v_l + \theta_{ml} &= \theta_{lo} + \sum_{i=1}^{N_c} \Delta a_i \frac{\partial \theta_l}{\partial a_i} \\ w_l + \psi_{ml} &= \psi_{lo} + \sum_{i=1}^{N_c} \Delta a_i \frac{\partial \psi_l}{\partial a_i} \end{aligned} \quad (18)$$

The functions ϕ_{lo} , θ_{lo} , and ψ_{lo} correspond to the values of ϕ_l , θ_l , and ψ_l , respectively, evaluated at each time point for the given constants a_i , and N_c is the total number of parameters a_i to be determined. The best fit of ϕ_l , θ_l , and ψ_l to the experimental data is established by minimizing the sum of the squares of the residuals for all time points considered. Thus,

$$\begin{aligned} \sum_{l=1}^N (u_l^2 + v_l^2 + w_l^2) &= \sum_{l=1}^N \left[\left(\sum_{i=1}^{N_c} \Delta a_i P_{1il} - R_{1l} \right)^2 \right. \\ &\quad \left. + \left(\sum_{i=1}^{N_c} \Delta a_i P_{2il} - R_{2l} \right)^2 + \left(\sum_{i=1}^{N_c} \Delta a_i P_{3il} - R_{3l} \right)^2 \right] \end{aligned} \quad (19)$$

is subject to the minimization condition as given in Eq. (20).

$$\frac{\partial}{\partial \Delta a_i} \sum_{l=1}^N (u_l^2 + v_l^2 + w_l^2) = 0 \quad (20)$$

where

$$P_{1il} = \frac{\partial \phi_l}{\partial a_i}, \quad P_{2il} = \frac{\partial \theta_l}{\partial a_i}, \quad P_{3il} = \frac{\partial \psi_l}{\partial a_i},$$

N is the total number of time points considered, and

$$R_{1\ell} = \phi_{m\ell} - \phi_{\ell 0} \cdot R_{2\ell} = \theta_{m\ell} - \theta_{\ell 0} \cdot R_{3\ell} = \psi_{m\ell} - \psi_{\ell 0}$$

Performing the indicated partial differentiation in Eq. (20) and combining terms results in

$$C_{ij} \Delta a_i = D_j \quad (21)$$

where C_{ij} is a symmetric ($N_c \times N_c$) matrix of parametric influence coefficients given by

$$C_{ij} = \sum_{\ell=1}^N (P_{1i\ell} P_{1j\ell} - P_{2i\ell} P_{2j\ell} - P_{3i\ell} P_{3j\ell}) \quad (22)$$

and D_j is a residual influence matrix with the form

$$D_j = \sum_{\ell=1}^N (R_{1\ell} P_{1j\ell} - R_{2\ell} P_{2j\ell} + R_{3\ell} P_{3j\ell}) \quad (23)$$

Since Eq. (21) is linear in Δa_i , it may be inverted, yielding the required correction to the coefficients, a_i . Thus, given a set of initial estimates for the independent constants, determination of Δa_i will result in corrected values of a_i which will cause the computed motion to more closely approach the experimental data. In the limit of no process or measurement noise, iteration on a_i will provide the best fit in the least squares sense of the computed to the experimental motion.

Implied in this development are two important facts that can seriously disrupt or destroy the convergence of a_i to the "best" values. If measurement noise exists, the definition of the residuals, Eq. (19), assumes that the dependent variables ϕ , θ , and ψ have the same relative uncertainty. For practical applications, the relative uncertainty of the measurements ϕ , θ , and ψ may differ by as much as an order of magnitude. This effect can be accounted for in the parametric influence coefficients by redefining C_{ij} as

$$C_{ij} = \sum_{\ell=1}^N \left(\frac{P_{1i\ell} P_{1j\ell}}{\sigma_\phi^2} + \frac{P_{2i\ell} P_{2j\ell}}{\sigma_\theta^2} + \frac{P_{3i\ell} P_{3j\ell}}{\sigma_\psi^2} \right) \quad (24)$$

and D_j as

$$D_j = \sum_{\ell=1}^N \left(\frac{R_{1\ell} P_{1j\ell}}{\sigma_\phi^2} + \frac{R_{2\ell} P_{2j\ell}}{\sigma_\theta^2} + \frac{R_{3\ell} P_{3j\ell}}{\sigma_\psi^2} \right) \quad (25)$$

where σ_ϕ , σ_θ , and σ_ψ are the standard deviations of the relative uncertainty in the roll, pitch, and yaw measurements, respectively (see Ref. 17). Also implied in Eq. (18) is the assumption that the coefficients (a_i) used to generate ϕ_{ℓ_0} , θ_{ℓ_0} , and ψ_{ℓ_0} are close to the best values. If a significant difference exists between the initial value of the coefficients and the actual or best values, the expansions as given in Eq. (18) are not valid and will result in divergence of the corrections, Δa_i , or convergence on invalid solutions. The closeness of the initial values of the coefficients to the best values for correct convergence is a function of the character of the motion fitted.

As stated previously, in the absence of measurement or process noise, correct application of the differential corrections method will yield parameters with no relative error. In the presence of these noise sources, however, bias may be introduced into the converged parameters. According to Ref. 18, for statistically random measurement noise in the data, it may be shown that the root-mean-square (RMS) deviation between the experimental data and converged solution is given by

$$E = \sqrt{\frac{\sum_{\ell=1}^N \left(R_{1\ell}^2 / \sigma_\phi^2 + R_{2\ell}^2 / \sigma_\theta^2 + R_{3\ell}^2 / \sigma_\psi^2 \right)}{3(N-1) - N_r + 1}} \quad (26)$$

with the corresponding RMS error in each of the coefficients, δa_i , equal to

$$\delta a_i = E \sqrt{B_i} \quad (27)$$

where B_i represents the diagonal components of the inverse matrix of C_{ij} . Equations (26) and (27) provide mathematically rigorous estimates of the measurement-noise-generated RMS deviation in the coefficients and solution. They do not, however, give reliable estimates of the RMS deviation or error for measurement noise that is not statistically random, noise which may result when data time samples are too small, or for process noise caused by inappropriate aerodynamic modeling.

The differential corrections method just presented requires the value of each of the partial derivatives, as illustrated in Eq. (18), at each time point. Previous users of the differential corrections method such as Eikenberry (Ref. 2) relied on the use of analytic solutions for the angular motion to generate the required partial derivatives. Since the equations of motion as used here are highly nonlinear and cannot be solved in closed form, the values of the influence coefficients ($\partial\phi/\partial a_i$, $\partial\theta/\partial a_i$, and $\partial\psi/\partial a_i$) are determined by numerically integrating a set of parametric differential equations. These equations are derived by differentiating the governing equations of motion with respect to each parameter, a_i , and inverting the order of differentiation. Performing the indicated operations on Eq. (6) results in the following:

$$\begin{aligned}
\ddot{P}_{1i} = & M_{1i} + \dot{\theta} \dot{P}_{3i} \cos \theta + \dot{\psi} \dot{P}_{2i} \cos \theta - \dot{\psi} \dot{\theta} P_{2i} \sin \theta \\
& + M_{3i} \tan \theta + \bar{M}_z P_{2i} \sec^2 \theta + (2 - R) (\dot{\theta} \dot{P}_{3i} + \dot{\psi} \dot{P}_{2i}) \tan \theta \sin \theta \\
& + (2 - R) \dot{\psi} \dot{\theta} P_{2i} \sin \theta (1 - \sec^2 \theta) + R \dot{\theta} \dot{P}_{1i} \tan \theta \\
& + R \dot{\phi} \dot{P}_{2i} \tan \theta + R \dot{\phi} \dot{\theta} P_{2i} \sec^2 \theta \\
\ddot{P}_{2i} = & M_{2i} - 2(1 - R) \dot{\psi} \dot{P}_{3i} \sin \theta \cos \theta - (1 - R) \dot{\psi}^2 P_{2i} (1 - 2 \sin^2 \theta) \quad (28) \\
& - R \dot{\psi} \dot{P}_{1i} \cos \theta - R \dot{\phi} \dot{P}_{3i} \cos \theta + R \dot{\phi} \dot{\psi} P_{2i} \sin \theta \\
\ddot{P}_{3i} = & M_{3i} \sec \theta + \bar{M}_z \dot{P}_{2i} \tan \theta \sec \theta + (2 - R) \tan \theta (\dot{\psi} \dot{P}_{2i} + \dot{\theta} \dot{P}_{3i}) \\
& + (2 - R) \dot{\psi} \dot{\theta} P_{2i} \sec^2 \theta + R \dot{\theta} \dot{P}_{1i} \sec \theta + R \dot{\phi} \dot{\theta} \tan \theta \sec \theta P_{2i} \\
& + R \dot{\phi} \dot{P}_{2i} \sec \theta
\end{aligned}$$

where $M_{1i} \equiv \frac{\partial \hat{M}_x}{\partial a_i}$, $M_{2i} \equiv \frac{\partial \hat{M}_y}{\partial a_i}$ and $M_{3i} \equiv \frac{\partial \hat{M}_z}{\partial a_i}$ are evaluated in a similar manner through the moment expansions. The above equations are second order and, thus, require two boundary conditions for the evaluation of each influence coefficient. These are obtained from the boundary conditions on the angular motion given by

$$\begin{aligned}
\phi(0) &= a_{N_c-5} \\
\dot{\phi}(0) &= a_{N_c-4} \\
\theta(0) &= a_{N_c-3} \\
\dot{\theta}(0) &= a_{N_c-2} \\
\psi(0) &= a_{N_c-1} \\
\dot{\psi}(0) &= a_{N_c}
\end{aligned} \quad (29)$$

If one differentiates the boundary conditions given in Eq. (29), the boundary conditions on the governing equations for the influence coefficients may be derived.

$$\begin{aligned}
P_{1i}(0) &= \delta_{N_c - 5, i} \\
\dot{P}_{1i}(0) &= \delta_{N_c - 4, i} \\
P_{2i}(0) &= \delta_{N_c - 3, i} \\
\dot{P}_{2i}(0) &= \delta_{N_c - 2, i} \\
P_{3i}(0) &= \delta_{N_c - 1, i} \\
\dot{P}_{3i}(0) &= \delta_{N_c, i}
\end{aligned} \tag{30}$$

Here δ_{ij} is the Kronecker-Delta function with $\delta_{ij} = 1$ for $i = j$ and $\delta_{ij} = 0$ for $i \neq j$. In order to utilize the differential corrections method to extract aerodynamic coefficients of interest, one must solve the governing angular motion equations and parametric differential equations simultaneously. With the angular motion and influence coefficient solutions determined for a given set of initial coefficient values, corrections to the coefficients are evaluated through Eq. (21). For example, if there are thirty coefficients to be identified [which include, generally, both the boundary conditions, Eq. (20), and the aerodynamic coefficients, Eq. (16)], a maximum of 186 differential equations must be solved simultaneously.

4.0 DESCRIPTION OF COMPUTER PROGRAM

The computer program as described here extracts aerodynamic coefficients from 3DOF data defined by the measured yaw, pitch, and roll angles as a function of time. The code is based on the Chapman-Kirk technique as detailed in Section 3.0. Both symmetric and asymmetric versions of the program have been developed and are listed in Tables 1 and 2.

The symmetric version is written in double precision Fortran IV for use on the IBM 370/165 computer. In the form listed here, core requirements are 164 K bytes using the G compiler. As many as 30 coefficients may be extracted from 3DOF data with actual computation time proportioned to τ as shown in Eq. (31).

$$\tau \propto n(N_c + 1) t_{max} / \Delta t \tag{31}$$

Here n is the number of iterations, N_c is the total number of constants varied, t_{max} is the total integration time, and Δt is the integration time interval.

The program is written in a logical sequence so that changes in internal program structure such as alteration of the functional form of the moment coefficient expansions

can be made easily. A flow chart showing the important logic and branching points is provided in Fig. 4. Table 3 contains a brief description of each of the subroutines employed in the code.

The asymmetric version of the code is functionally the same as the symmetric version. Only the core requirements, coefficient arrays in the main program, and subroutines directly involving the kinematic or dynamic equations for the 3DOF motion are altered. Core requirement for the asymmetric program is 266 K bytes when the G compiler is used. In addition, up to 72 coefficients can be extracted from 3DOF data using this version.

In both programs, integration of the kinematic, dynamic, and parametric differential equations is performed with a fourth-order Runge-Kutta, fixed time step scheme. The coefficients to be extracted from the data are reiterated as outlined in Section 3.2 until convergence is achieved. Convergence is assumed when consecutive iterations yield a change in the probable error of the fit less than a specified error bound.

4.1 INPUT

The input information necessary to execute either version of the coefficient extraction program is very similar. The actual 3DOF experimental data to be analyzed is input to both programs through a direct access input file. Data are stored in this file in 1,003 word records, in which the first three words define the data group number, data block number, and data type indicator, in that order, and are integers. The data type indicator defines the variable being accessed and may take on values from one to four corresponding to arrays of time, ϕ versus time, θ versus time, and ψ versus time, respectively, all of which are single precision variables.

The initial values of the coefficients and the parameters providing branching instructions and body and flow-field information are input using namelist statements. No default value is provided in the program for required variables not defined in the initial namelist statement. The namelist input format was used to provide versatility in constructing sequential runs by updating prior information. Table 4 gives the namelist variables, their meaning, and their nominal values needed for execution of either the symmetric or asymmetric coefficient extraction program.

4.2 OUTPUT

Output variables as used in both the symmetric and asymmetric programs are similar and are compatible with input variable definitions. Only portions of the output data from a typical run which are not self explanatory will be discussed.

During normal data reduction using either program, each iteration of the parameters (aerodynamic coefficients and boundary conditions) is listed with the corresponding change in the parameter (DELTA CON) according to the theory of Section 3.2. The variables defined as the new and old probable error are the previous and present values of the RMS deviation between the experimental data and converged solution, respectively, as defined in Eq. (26). The sum of the residuals is defined as follows:

$$\text{Sum of Residuals} = \sqrt{\sum_{l=1}^N R_{1l}^2/\sigma_{\phi}^2 + R_{2l}^2/\sigma_{\theta}^2 + R_{3l}^2/\sigma_{\psi}^2} \quad (32)$$

The iterations are continued until convergence of the solution, as discussed in Section 4.0, is achieved or until the input value of the maximum number of iterations is reached. The final values of the parameters are then listed along with corresponding values of the RMS error in each coefficient as defined in Eqs. (26) and (27). A comparison of the fit of the theoretical solution (denoted by FIT) to the experimental data (denoted by EXP) is also shown. The theoretically generated solution of ψ and θ (denoted by PSI and THETA, respectively) and the difference between the theoretical and experimental values of ψ and θ ($\psi - \psi_m \equiv \text{PSI} - \text{PSIM}$, $\theta - \theta_m \equiv \text{THETA} - \text{THETAM}$) are stored for later use as data for graphical output.

5.0 RESULTS OF VALIDATION TESTS

Verification of the improved parameter identification technique as presented in Sections 3.0 and 4.0 requires, in addition to checks on the program using computer-generated motion, an assessment of the measurement and process noise inherent in the gas bearing and in typical tunnel test data. This is necessary since the "best" coefficients, as produced by output error methods such as the one discussed here, are directly influenced by the cumulative effects of modeling errors and measurement noise. Thus, this section addresses three areas concerned with validation of the improved coefficient extraction technique: numerically-generated 3DOF motion, including Gaussian noise, is employed to simulate measurement noise effects on the probable error in extracted coefficients; a bench test is used to assess the accuracy of the 3DOF measurement system; and 3DOF data taken in Tunnel A are used to indicate some of the capabilities of the parameter identification technique.

5.1 COMPUTER-GENERATED MOTION

In order to arrive at the final form of the aerodynamic coefficients as given in Eq. (14) for the asymmetric and Eq. (16) for the symmetric analysis, the α and β coefficients were linearly combined with the q and r rate coefficients, respectively. This was a direct

result of similarity of the $\dot{\alpha}$, q and $\dot{\beta}$, r relations [(see Eqs. (4) and (10))] in terms of the Euler angles. In order to verify this hypothesis, 3DOF motion was generated both with and without noise with the $\dot{\alpha}$ and $\dot{\beta}$ coefficients included. The initial conditions and parameters employed to specify the motion are listed below.

$$S = 0.390 \text{ ft}^2, I_x = 0.0372 \text{ slugs-ft}^2, I = 0.244 \text{ slugs-ft}^2$$

$$C_{m\alpha} = -0.236 \text{ 1/rad}, C_{mq} = -1.762 \text{ 1/rad}, C_{m\dot{\alpha}} = -0.881 \text{ 1/rad}$$

$$\phi_0 = 0, \dot{\phi}_0 = 641 \text{ deg/sec}, \theta_0 = 5.18 \text{ deg}, \dot{\theta}_0 = -26.356 \text{ deg/sec}$$

$$\psi_0 = -2.589 \text{ deg}, \dot{\psi}_0 = -7.77 \text{ deg/sec}$$

$$U_\infty = 4,774 \text{ ft/sec}, q_\infty = 150.4 \text{ lbf/ft}^2$$

The symmetric version of the parameter identification program was used to extract the variables listed above from the generated data. The parameters C_{mq} and $C_{m\dot{\alpha}}$ were both extracted with nominal values of -1.74 per radian and -0.90 per radian, respectively, and RMS deviations of ± 0.05 per radian. This deviation is a measure of the character of data fitted and the numerical accuracy of the program. Gaussian noise with one standard deviation equal to 0.01 deg was then added to the generated values of ϕ , θ , and ψ . With noise added, C_{mq} and $C_{m\dot{\alpha}}$ were both extracted from the data and yielded values of -5.87 per radian and 3.2 per radian, respectively, with RMS deviations of ± 18 per radian. The noise added is representative of the levels of measurement noise inherent in the 3DOF measurement system. Moreover, the motion examined contained only linear aerodynamics. This should have resulted in the smallest RMS deviations of the extracted coefficients as influenced by modeling. Thus, based on the results of this example, it is not feasible to separate the effects of C_{mq} and $C_{m\dot{\alpha}}$ from typical 3DOF measurements where 1σ measurement errors are 0.01 deg or higher.

The definitions of α and β can also play a role in the extraction of the "best" coefficients for a given set of 3DOF measurements. In Tobak's developments, Ref. 14, α and β were defined as

$$\alpha_v = \frac{w}{U_\infty}, \beta_v = \frac{v}{U_\infty} \quad (33)$$

Much of the past work, however, has employed α and β in terms of the angle of attack and sideslip leading to,

$$\alpha_a = \tan^{-1} \frac{w}{u}, \beta_a = \tan^{-1} \frac{v}{u} \quad (34)$$

Written in terms of the Euler angles in the aeroballistic axis system, a_v , β_v may be related to a_a , β_a , resulting in

$$\begin{aligned} a_a &= a_v \left[\frac{1}{\cos \psi} + \frac{1}{6} \frac{a_v^2}{\cos^3 \psi} + \dots \right] \\ \beta_a &= \beta_v \left[\frac{1}{\cos \theta \cos \psi} + \frac{1}{3} \frac{\beta_v^2}{\cos^3 \theta \cos^3 \psi} + \dots \right] \end{aligned} \quad (35)$$

Thus, for small values of θ and ψ , $a_a \approx a_v$ and $\beta_a \approx \beta_v$. Over a large number of cycles of data, the cumulative effect of these small differences will appear as higher order terms in the coefficient expansions [compare Eqs. (35) and (16), for example]. Both definitions of α and β as given in Eqs. (33) and (34) have been incorporated in the parameter identification programs as developed here. Comparisons of generated data using the two definitions of α and β were made which confirmed the results derived from Eq. (35).

The accuracy and validity of generated 3DOF motion from the programs as listed in Tables 1 and 2 were examined through comparison with results from an existing 6DOF code, Ref. 19. Calculations were made using the 6DOF code and the asymmetric program as described in this report for two sets of initial body and flow-field conditions as listed below.

CHECK CASE I

$$S = 0.3898 \text{ ft}^2, d = 0.7038 \text{ ft}$$

$$I_y = I_z = 0.2444 \text{ slugs-ft}^2, I_x = 0.03723 \text{ slugs-ft}^2, I_{xz} = 0$$

$$U_\infty = 4,774 \text{ ft/sec}, q_\infty = 364.66 \text{ lbf/ft}^2$$

$$C_{m\alpha} = -C_{n\beta} = -0.2355 \text{ 1/rad}, C_{mq} = C_{nr} = -2.6434 \text{ 1/rad}$$

$$C_{lp} = -0.00745 \text{ 1/rad},$$

$$\theta_o = 5.18 \text{ deg}, \psi_o = -2.589 \text{ deg}, \phi_o = 0, p_o = 641.7 \text{ deg/sec}$$

$$q_o = -26.356 \text{ deg/sec}, r_o = -7.735 \text{ deg/sec}$$

CHECK CASE II

$$S = 1.228 \text{ ft}^2, d = 1.25 \text{ ft}$$

$$I_y = I_z = 700 \text{ slugs-ft}^2, I_x = 20 \text{ slugs-ft}^2, I_{xz} = -100 \text{ slugs-ft}^2$$

$$U_{\infty} = 1,500 \text{ ft/sec}, q_{\infty} = 675 \text{ lbf/ft}^2$$

$$C_{m\alpha} = -C_{n\beta} = 16.7132 \text{ 1/rad}$$

$$\theta_o = 5 \text{ deg}, \psi_o = 5 \text{ deg}, \phi_o = 0, p_o = q_o = r_o = 0$$

Typical results of the calculations are shown below and indicate excellent agreement between the two codes in the computed values of ϕ , θ , and ψ .

Results: Check Case I

	<u>t, sec</u>	<u>θ, deg</u>	<u>ψ, deg</u>	<u>ϕ, deg</u>
Present 3DOF Code	30	-4.270	0.702	-23.798
6DOF Code (Ref. 19)	30	-4.2704	0.7001	-23.762

Results: Check Case II

	<u>t, sec</u>	<u>θ, deg</u>	<u>ψ, deg</u>	<u>ϕ, deg</u>
Present 3DOF Code	19.90	-0.429	5.388	25.766
6DOF Code (Ref. 19)	19.90	-0.4289	5.3883	25.7659

To attain the best possible coefficients from 3DOF data with measurement noise, the quantity and character of the data sampled are of fundamental importance. A less than optimum data sample will yield extracted coefficients with high RMS deviations or, in some cases, lack of convergence of the solutions. The extraction of optimum coefficients was studied using the generated motion as discussed previously with 0.05-deg, 1- σ Gaussian noise added to the data and $C_{m\dot{\alpha}} = 0$, $C_{mq} = -2.64$ per radian where σ is one-standard deviation. Table 5 shows the results of this study where the RMS deviation in percent of C_{mq} is shown as a function of the number of data points per cycle of data and the total number of cycles of data analyzed. From this table it may be generally concluded that accuracy in the extracted value of C_{mq} is improved faster by increasing the data sample size than by increasing the number of points per cycle. This same trend and the rate of improvement of the extracted parameter was also found to hold true for $C_{m\alpha}$ and, moreover, for the nonlinear expansions of $C_{m\alpha}$ and C_{mq} [see Eq. (16)].

The effect of the magnitude of the measurement noise on the extracted coefficients was examined by generating noisy 3DOF data for the same conditions as previously used

but with $C_{m\alpha\delta^2} = 5.81/\text{rad}^3$, $C_{mq} = -4.0$ per radian, and $C_{mq\delta^2} = 98.5/\text{rad}^3$. The symmetric version of the parameter identification program was used and yielded the results shown in Table 6. Here the extracted parameters and their RMS deviation are shown as a function of the measurement noise added to the generated values of ϕ , θ , and ψ . The generated data analyzed contained 40 cycles of data with 20 points per cycle. Initial parameter estimates were set at $C_{m\alpha} = -0.2$ per radian and $C_{mq} = C_{mq\delta^2} = C_{m\alpha\delta^2} = 0$. Typical plots of calculated θ and ψ values versus time for a measurement noise level of $\sigma = 0.05$ deg are shown in Fig. 5. Residuals showing the difference between the generated data with noise and the calculated values of θ and ψ and graphs indicating the fit of the computed solution to the generated data are also provided.

Two important conclusions may be drawn from the magnitude and variation of the RMS deviation of each of the coefficients in Table 6. It is apparent that the magnitude of the RMS deviation is approximately a linear function of the measurement noise level denoted by σ . In addition, the magnitude of the deviation appears to be a good estimate of the actual error in the values of the extracted coefficients. This result is, in fact, verification of those statements made in Section 3.2 concerning the theoretical meaning of δa_i [Eq. (27)].

5.2 BENCH TEST DATA

The previous section discussed the effects of measurement noise on the extracted coefficients. The noise source considered was Gaussian and random in nature.

When 3DOF motion including Gaussian noise is viewed in the frequency plane, the noise contributes no distinct frequencies or regions of high spectral density. In most cases, however, the effect of modeling noise on the extracted coefficients is more pronounced than the effect of measurement noise. Most modeling sources occur over finite spectrums with median frequencies occurring near aerodynamic frequencies of interest. Moreover, in such regions modeling noise may have high power levels which may be the same order of magnitude as noise caused purely by aerodynamics. Thus, a critical assessment of the important modeling errors present in typical 3DOF data must be made to gain the optimum capabilities of the improved parameter identification technique.

Some of the important categories of modeling noise are 1) incorrect aerodynamic modeling of the specific configuration, 2) modeling errors introduced through the effects of tunnel flow nonuniformities, and 3) errors associated with nonlinearities and coupling effects caused by the gas bearing. This section will consider modeling errors due to the gas bearing only.

The VKF spherical gas bearing as described in Ref. 1 provides a nearly frictionless pivot in roll, pitch and yaw, and thus is ideal for 3DOF motion simulation. Model oscillations of up to 10 deg in the combined pitch, yaw plane and unlimited roll orientation are possible using this mechanism. Figs. 6 and 7 are photographs of the gas bearing assembly. Details of the balance mechanism and the angular measurement system are shown in Fig. 8. Pitch and yaw angular displacements are measured using an eccentric as shown in Fig. 7 positioned on the outer race of the bearing and two pairs of orthogonal E-cores fixed on the bearing instrument ring. Motion in pitch or yaw causes a change in the distance between the eccentric and the E-core surfaces. The accompanying change of the reluctance of the E-cores provides an analog signal proportional to angular displacement. The measurement of roll position is made using light-emitting diodes and alternating reflective and nonreflective lines affixed to the eccentric as shown in Figs. 7 and 8.

The measurement of angular position in pitch and yaw using the gas bearing is affected by two sources of error. During calibration, adjustments to the bearing are made so that the E-core output varies approximately linearly with the actual angular displacement. Calibration factors are then established for both the pitch and yaw measurements using a linear least squares curve fit. Although this approach provides a very simple and fast technique for reducing raw data into angular displacements, it can introduce error into the resulting measurements. Nonlinearities on the order of 0.02 deg or less for pitch and yaw measurements of up to ± 5 deg are typical for bearing calibration. For pitch or yaw measurements approaching 8 deg, the nonlinearity generally increases in magnitude, reaching values as high as 0.1 deg.

An additional source of error is the interaction of roll position on the pitch and yaw measurements. This effect is most probably a result of the machining tolerances of the eccentric and the alignment of the E-cores and has been found to change following reassembly of the bearing. A systematic investigation of this interaction effect was conducted to provide the variation of the measured pitch and yaw angle with roll position. Some typical results of this investigation are shown in Figs. 9 through 12. Data were taken of the variation in ψ and θ as a function of ϕ and the total angle in the vertical plane for sting roll positions in 15-deg increments. Accuracy of the measurements is within ± 0.01 deg in θ and ψ . The sting roll position, Ω , and total angle of attack, δ , are related to the Euler angles for $\phi = 0$ as follows:

$$\delta = \sqrt{\sin^2 \psi + \cos^2 \psi \sin^2 \theta} \quad (36)$$

$$\tan \Omega = \frac{\sin \psi}{\cos \psi \sin \theta} \quad (37)$$

Figs. 9 through 12 reveal some important facts concerning the roll interaction effect upon θ and ψ measurements. With reference to these figures, the magnitude of the correction approaches 0.1 deg for practically all combinations of δ and Ω . In addition, there is significant variation of the correction as a function of ϕ with no apparent symmetry about particular sting roll positions. If the interaction was caused by imperfections in the eccentric only, symmetry should have appeared as evidenced by matching corrections as a function of ϕ in 90-degree sting roll positions (compare Figs. 9, 11, and 12). Apparently the E-core, bearing alignment, and eccentric imperfections all play a major part in the lack of symmetry of the roll interaction effect.

In addition to the modeling or process noise resulting from the roll interaction effect and from the methods used for bearing calibration, process noise due to bearing moments can also be present in typical 3DOF data. These bearing moments are small and highly nonlinear and vary with the bearing gas pressure. A special pendulum designed for the gas bearing was used to study nonlinear bearing moments and their effect on 3DOF motion. Assuming that no aerodynamic moments act on the pendulum, the only moment caused by the pendulum is that resulting from the cg displacement from the vertical axis as depicted in Fig. 13. Then, in the aeroballistic system, it may be shown that

$$\begin{aligned}\hat{M}_y &= -W \ell \cos \psi \sin \theta \\ \hat{M}_z &= -W \ell \sin \psi\end{aligned}\tag{38}$$

where ℓ is the distance between the bearing pivot point and the pendulum center of mass and W is the pendulum weight. Comparison of Eq. (38) with Eqs. (9) and (16) yields $a_1 \equiv -W\ell/q_\infty S d$. Geometric properties of the pendulum and assumed conditions for data analysis are listed below.

$$\text{Weight} = 10.38 \text{ lbf}, I_x = 0.0305 \text{ slugs-ft}^2$$

$$I_y = I_z = 0.04747 \text{ slugs-ft}^2, \ell = 0.058 \text{ ft}$$

$$S = 0.3975 \text{ ft}^2, d = 0.7092 \text{ ft}$$

$$U_\infty = 1 \text{ ft/sec}, q_\infty = 0.5 \text{ lbf/ft}^2$$

Experimental ϕ , θ , and ψ data were taken using the configuration as shown in Fig. 13 for variations in the bearing pressure, total angle of attack of the pendulum, and roll rate. For low bearing pressure equal to 100 psi, analysis of the 3DOF data resulted in excellent fit of the linear moment distribution as given in Eq. (38). Typical plots of the resulting solution and the residuals in both θ and ψ are shown in Fig. 14. Analysis was

performed employing the symmetric version of the coefficient extraction code, Table 1, yielding an equivalent $C_{m\alpha}$ of -3.70 1/rad. With reference to Fig. 14, all residuals are of the same level as measurement errors caused by the roll interaction effect discussed earlier. In addition, a small rolling-moment coefficient, $C_{l_0} = -0.79 \times 10^{-4}$ 1/rad, was extracted from the data.

As the bearing pressure was increased, the resulting 3DOF motion became highly nonlinear. Large differences in the equivalent $C_{m\alpha}$ for small compared to moderate angles of attack were detected. The extracted values of the equivalent $C_{m\alpha}$ for the moderate and small angles of attack were -3.79 1/rad and -1.32 1/rad, respectively. The corresponding roll moment coefficient increased from -0.000079 1/rad for moderate angles to -0.00121 1/rad for small angles. Thus, as bearing pressure is increased from 100 to 400 psi, the bearing-induced roll torque increases by an order of magnitude from -1.1×10^{-5} ft-lbf to -1.7×10^{-4} ft-lbf.

Figures 15 and 16 show the fit of the computed solution to the experimental data for a bearing pressure of 400 psi at moderate and small angles of attack, respectively. The moderate angle-of-attack data exhibited large deviations from motion produced by the moments as given in Eq. (38). This is evident when the magnitude and character of the residuals as given in Fig. 15 are compared to those for low bearing pressure, Fig. 14. The results of the small angle-of-attack data, Fig. 16, indicate good agreement between the data and the computed solution based on the moment expressions as given in Eq. (38); however, the magnitude of the equivalent $C_{m\alpha}$ is a factor of three smaller than the expected value.

Thus, for normal operation of the gas bearing at bearing pressures of 400 psi, nonlinear moments, near ψ and θ equal to zero, induced by the bearing are present in typical 3DOF data with magnitudes proportional to $\hat{M}_y = 0.330 \alpha$ ft-lbf and $\hat{M}_z = -0.330 \beta$ ft-lbf. As bearing pressure is decreased from 400 psi, nonlinear bearing-induced moments are substantially reduced. For a Mach number 4 test environment with $q_\infty = 460$ psf and a slightly blunted sphere-cone with reference dimensions of $d = 0.7$ ft and $S = 0.35$ ft², the contribution of the bearing-induced moment at 400 psi operating pressure is on the order of 1 percent of the model aerodynamic pitching-moment coefficient with $C_{m\alpha} = -0.22$ 1/rad.

The previous discussion has revealed the existence of pitch and yaw measurement errors caused primarily by the roll interaction effect. In addition, there are errors present in the roll position measurement. The accuracy with which roll position can be measured is directly influenced by the number of alternating reflective and nonreflective lines on the eccentric (see Figs. 7 and 8). Currently, a change in roll orientation is sensed every two degrees by the digital system. Thus, for moderately high roll rates compared to the

median frequency in the pitch-yaw plane, a roll uncertainty of ± 1 deg appears in the data as approximately random noise. As the roll rate is decreased toward the median pitch-yaw plane frequencies, the roll uncertainty appears less random and can introduce significant errors in extracted coefficients depending on the duration of the data and the character of the motion to be fitted.

5.3 TUNNEL A EXPERIMENTAL RESULTS

In Sections 5.1 and 5.2, errors associated with the gas bearing measurement system were examined. The ability to extract correct aerodynamic coefficients (up to ± 0.1 deg in pitch and yaw) in the presence of random measurement noise caused by the gas bearing was shown to exist. Even though these errors are not random, successful analysis of low bearing pressure bench test data indicates that these measurement errors for linear systems may be treated as random measurement noise. The successful application of the parameter identification method as developed here, however, also strongly depends on the precise definition of process noise associated with tunnel flow nonuniformities. Depending upon the exact form of these flow nonuniformities, extracted aerodynamic parameters with large bias may result. In order to examine the ability of the present method to extract "correct" aerodynamic coefficients from typical wind tunnel results, 3DOF data were taken in the AEDC-VKF Tunnel A at a Mach number and Reynolds number of 4.02 and 3.6 million per foot, respectively.

Tunnel A is a continuous, closed-circuit, variable density wind tunnel with an automatically driven flexible-plate-type nozzle and a 40- by 40-in. test section (Fig. 17). The tunnel can be operated at Mach numbers from 1.5 to 6.0 at stagnation pressures from 29 to 200 psia, respectively, and at stagnation temperatures up to 750°R depending upon Mach number and pressure level. Minimum operating pressures range from about one-tenth to one-twentieth of the maximum at each Mach number. The tunnel is equipped with a model injection system which allows removal of the model from the test section while the tunnel remains in operation.

The configurations tested were a 6.7-deg sharp and 6.7-deg spherically blunted cone with mass and geometric properties as listed below (see Fig. 18).

$$d = 0.6667 \text{ ft}, S = 0.3491 \text{ ft}^2$$

$$\text{cg location} = 12.00 \text{ in. from model base}$$

$$\text{sharp cone: } I_x = 0.0301 \text{ slugs-ft}^2, I_y = 0.2583 \text{ slugs-ft}^2, I_z = 0.2565 \text{ slugs-ft}^2$$

$$\text{sphere cone: } I_x = 0.0304 \text{ slugs-ft}^2, I_y = 0.2519 \text{ slugs-ft}^2, I_z = 0.2514 \text{ slugs-ft}^2, \\ d_n/d = 0.2275$$

These two configurations do not sufficiently challenge the analysis capabilities of the asymmetric or symmetric program in terms of model aerodynamics. They do, however, provide baseline data on bodies whose aerodynamics are known. This information may be used to assess the influence of small tunnel flow-field nonuniformities on the sensitivity of the coefficient extraction technique.

The data analyzed are shown in Figs. 19 and 20 where the variables ϕ , θ , and ψ are plotted against time. Figure 19 shows typical data for the sharp cone model. Sphere-cone results are given in Fig. 20 with initial conditions similar to those for the sharp cone. Comparison of θ and ψ versus time in Fig. 19 shows unexpected frequency variations and damping effects normally not associated with motion of a sharp cone. For the flow-field and body constraints listed above, analysis of the sharp cone data should yield symmetric aerodynamic coefficients with

$$-C_{n\beta} = C_{m\alpha} = -0.23 \text{ 1/rad}, C_{m\alpha\delta^2} = -C_{n\beta\delta^2} = -1.13 \text{ 1/rad}^3$$

$$C_{nr} = C_{mq} = -5.5 \text{ 1/rad}, C_{lp} = -0.0081 \text{ 1/rad (Ref. 20)}$$

Analysis of the data as given in Fig. 19 was made using the symmetric program assuming linear aerodynamics and no flow-field-induced process noise. Analysis of 8.44 sec of the data resulted in extracted coefficients with

$$C_{m\alpha} = -0.225 \text{ 1/rad}, C_{mq} = -6.0 \text{ 1/rad}$$

with RMS deviations in the coefficients of

$$E(C_{m\alpha}) = 0.0003 \text{ 1/rad}, E(C_{mq}) = 0.23 \text{ 1/rad}$$

Comparison of the extracted with the corresponding expected value of each of the coefficients reveals good agreement which is reflected in the size of the calculated RMS deviations. However, examination of the residuals and the fit of the calculated solution to the experimental data as shown in Fig. 21 does not substantiate the validity of these coefficients.

Correct aerodynamic coefficients will not be extracted from the sharp cone data until the process noise in the experimental data is properly modeled. Tunnel-fixed flow nonuniformities are the most probable source of the process noise causing the poor fit of calculated and experimental data. Thus, as a first approximation in the modeling of the process noise, tunnel-fixed stiffness and damping moments that may differ in both the X, Y and X, Z planes are assumed as shown in Eq. (39).

$$\begin{aligned}
M_{yT} &= q_{\infty} S d (t_1 \theta + \frac{d}{2U_{\infty}} t_2 \dot{\theta}) \\
M_{zT} &= q_{\infty} S d (t_3 \psi + \frac{d}{2U_{\infty}} t_4 \dot{\psi})
\end{aligned}
\tag{39}$$

In the aeroballistic and body-fixed axis systems, the moments as given in Eq. (39) transform to

$$\begin{aligned}
\hat{M}_x &= M_{yT} \sin \psi \cos \theta - M_{zT} \sin \theta \\
\hat{M}_y &= M_{yT} \cos \psi \\
\hat{M}_z &= M_{yT} \sin \psi \sin \theta + M_{zT} \cos \theta
\end{aligned}
\tag{40}$$

$$\begin{aligned}
M_x &= M_{yT} \sin \psi \cos \theta - M_{zT} \sin \theta \\
M_y &= M_{yT} \cos \psi \cos \phi + (M_{yT} \sin \psi \sin \theta + M_{zT} \cos \theta) \sin \phi \\
M_z &= -M_{yT} \cos \psi \sin \phi + (M_{yT} \sin \psi \sin \theta + M_{zT} \cos \theta) \cos \phi
\end{aligned}
\tag{41}$$

Thus, tunnel-fixed flow effects as described by Eq. (39) may be extracted from 3DOF data using the symmetric or asymmetric programs by including the moment expansions as given in Eqs. (40) and (41), respectively. In the presence of other unknown process noise, it is not possible to extract the coefficients t_1 , t_2 , t_3 , and t_4 and the linear aerodynamic damping and pitching-moment coefficients simultaneously from 3DOF data. This is due to the overspecification of the linear stiffness and damping effects in the moment expansions. This may be shown by considering the linear stiffness terms for moments about the y axis in the body-axis system. A parallel derivation may be shown for the damping terms. If one substitutes Eq. (39) into Eq. (41), neglecting terms involving $\sin \psi \sin \theta$, and uses the results of Eq. (14), Eq. (42) results, as follows:

$$\begin{aligned}
C_m &= t_1 \theta \cos \psi \cos \phi + t_3 \psi \cos \theta \sin \phi \\
&\quad + a_{m1} (\sin \psi \sin \phi + \cos \psi \sin \theta \cos \phi) + \dots
\end{aligned}
\tag{42}$$

If one expands terms involving ψ and θ in Eq. (42) and rearranges, Eq. (42) reduces to

$$C_m = (t_1 + a_{m1}) \theta \cos \phi + (t_3 + a_{m1}) \psi \sin \phi + \dots
\tag{43}$$

Examination of Eq. (43) shows that the coefficients a_{m1} , t_1 , and t_3 for small angular motion are not independent. Thus, only two of the three parameters (a_{m1} , t_1 , and t_3) can be extracted from 3DOF data simultaneously. Attempts at extracting all three coefficients will lead to divergence of the iteration scheme in the parameter extraction

technique. As stated previously, similar constraints on the stiffness and damping coefficients in the aeroballistic axis system and on the damping coefficients in the body-fixed axis system may be shown to apply.

In addition to the tunnel-fixed stiffness and damping effects, constant bias in the measured pitch and yaw displacements may also be present. These can be caused by imprecise alignment of the zero yaw/pitch axes with respect to the tunnel-fixed axis and/or flow nonuniformities causing tunnel-fixed trim moments. This effect has been included in the form of artificial flow angularity corrections in the pitch and yaw planes (θ_T and ψ_1 , respectively).

The asymmetric parameter identification program presented in Table 2 was employed to extract the tunnel-fixed process noise (as described above) from the sharp cone data (Fig. 19). Results of the analysis are shown in Table 7. As indicated in the table, only the tunnel-fixed process noise, I_{zx} , C_{l_0} , and the boundary conditions were allowed to vary. Due to the constraints on the tunnel-fixed process noise, the model aerodynamics were fixed at theoretical estimates given previously. The calculated solution, residuals, and fit of the computed solution to the experimental data are shown in Figs. 22 and 23 for two data sample periods.

Analysis of the results presented in Table 7 indicates the existence of tunnel stiffness effects in both the pitch and yaw planes. In addition, a small product of inertia was extracted from the data. Tunnel-fixed damping effects were also extracted, indicating decreasing magnitudes for increasing data sample intervals. This effect may be caused by higher order coefficients in the tunnel-fixed damping terms. Examination of Fig. 22 shows excellent fit of the computed to the experimental data with residuals in θ and ψ bounded by ± 0.1 deg. The best fit of the experimental data to the calculated solution is bounded by the measurement errors caused by the gas bearing as discussed in Section 5.2. Doubling of the data sample interval as shown in Fig. 23 resulted in larger residuals with a dominate frequency approximately the same as the fundamental frequency of the experimental data (compare Figs. 23c and d with Figs. 19a and b, respectively). This is most probably an effect of frequency mismatch caused by higher order terms not included in the tunnel stiffness model, Eq. (39). Considering the results given in Table 7 and depicted in Figs. 22 and 23, the fit of the calculated 3DOF solution to the experimental sharp cone data is significantly improved over that given in Fig. 21. Thus, tunnel-fixed process noise governed by Eq. (39) and I_{zx} appear to be valid contributions to the parameters to be evaluated.

In order to further evaluate the tunnel-fixed process noise and the ability of the asymmetric program to extract model aerodynamics in the presence of this process noise,

the sphere cone data as shown in Fig. 20 were analyzed. Using the asymmetric program, aerodynamic moment coefficients and tunnel-fixed process noise were extracted from the data as given in Fig. 20 and are shown in Table 8. Since model aerodynamic coefficients were allowed to vary, one damping and one stiffness coefficient describing the tunnel-fixed effects were held constant. Considering the RMS deviations and values of t_1 , t_2 , t_3 , and t_4 as given in Table 7, the stiffness term, t_1 and damping term, t_2 , were assumed constant and equal to 0.017 1/rad and 0, respectively. Examination of Table 8 shows large variations in the extracted aerodynamic coefficients for different data sample intervals. Moreover, since the sphere cone is axially symmetric, the relationship given in Eq. (16) should hold. As the data sample interval increases in Table 8, the extracted coefficients tend to become less like those caused by an axisymmetric body. These effects are further illustrated by comparison of the graphical results in Figs. 24, 25, and 26 which correspond to this table. Thus, in addition to those sources of process noise described here, others must exist which cause the significant disagreement in the generated solution and experimental data. Even though the preceding analysis of the sphere cone data as given in Fig. 20 does not yield acceptable extracted aerodynamic coefficients, it does indicate some problem areas encountered in the analysis of 3DOF data taken in continuous wind tunnels as well as concepts for establishing process noise models.

6.0 CONCLUDING REMARKS

The previous sections have presented the mathematical development of coefficient extraction programs and practical application of the programs in continuous wind tunnel flow fields. The programs developed here are based on the principals governing output error methods. As such, extracted parameters are highly sensitive to measurement and process noise. Thus, identification of sources of both process and measurement noise and modeling of these effects were extensively examined.

Noise attributable to the gas bearing, tunnel flow nonuniformities, and inappropriate aerodynamic modeling was catagorized as being the most important. Measurement noise caused by the gas bearing was shown to contribute errors in ψ and θ measurements up to ± 0.1 deg with the magnitude of these errors dependent upon the value of ψ , θ , and ϕ and the gas bearing pressure. In addition, small, bearing-induced moments were also identified. Even though the magnitude of the bearing-induced errors can be large, it was concluded that these errors for most situations could be modeled as random noise. This allows for accurate parameter identification, assuming sufficiently large data samples and no other noise sources.

In order to define the effects of process noise on the extracted coefficients, sharp and spherically blunted cone data taken in Tunnel A were analyzed.

It was shown that the process noise inherent in the sharp cone and sphere cone data was large and could not be treated satisfactorily as linear, tunnel-fixed stiffness and damping moments independent of the model configuration. In addition, this process noise was of sufficient level to cause significant error in the extracted coefficients. The analysis of the sharp cone and sphere cone data did provide, however, concepts for establishing process noise models in similar situations. Further studies are planned on the definition of process noise in Tunnel A and on the effects of these noise sources on extracted aerodynamic coefficients. Also, more work is planned on the application methods of the programs developed herein.

REFERENCES

1. Ward, L. K., Jr. and Hodapp, A. E., Jr. "A Three-Degree-of-Freedom Dynamic Stability Balance for Use in the VKF Continuous Flow Hypersonic Tunnels ($M_\infty = 6$ through 12)." AEDC-TR-68-62 (AD832200), May 1968.
2. Eikenberry, Robert S. "Analysis of the Angular Motion of Missiles." SC-CR-70-6051, Prepared by the University of Notre Dame, February 1970.
3. Walchner, Otto and Sawyer, Frank M. "'In Plane' and 'Out of Plane' Stability Derivatives of Slender Cones at Mach 14." ARL-73-0090, July 1973.
4. Walchner, Otto. "Asymmetric Nose Bluntness Effects on the Aerodynamics of a Slender Cone at Mach-14. ARL-73-0072, April 1973.
5. Chapman, G. T. and Kirk, D. B. "A Method for Extracting Aerodynamic Coefficients from Free-Flight Data." AIAA Journal, Vol. 8, No. 4, April 1970, pp. 753-758.
6. Rediess, Herman A. "An Overview of Parameter Estimation Techniques and Applications in Aircraft Flight Testing," in "Parameter Estimation Techniques and Applications in Aircraft Flight Testing." NASA TN-D-7647, April, 1974, pp. 1-18.
7. Stepner, David E. and Mehra, Raman K. "Maximum Likelihood Identification and Optimal Input Design for Identifying Aircraft Stability and Control Derivatives." NASA CR-2200, March 1973.
8. Murphy, C. H. "Free Flight Motion of Symmetric Missiles." BRL R-1216 (AD442757), July 1963.
9. Nicolaidis, J. D. "On the Free-Flight Motion of Missiles Having Slight Configurational Asymmetries." BRL Report 858 (AD27405), June 1953.

10. Chapman, Gary T. and Kirk, Donn B. "Aerodynamics of Bodies from Motion Analysis." AGARDograph 138, pp. 267-350.
11. Brown, Charles M. Jr. "An Extended Kalman Filter for Estimating Aerodynamic Coefficients." AFATL-TR-76-158, December 1976.
12. Etkin, Bernard. Dynamics of Flight: Stability and Control. John Wiley and Sons, Inc., New York, 1959, pp. 94-104.
13. Kolk, W. Richard. Modern Flight Dynamics. Prentice-Hall, Inc., Englewood Cliffs, New Jersey, 1961, pp. 3-12.
14. Tobak, Murray and Schiff, Lewis B. "A Nonlinear Aerodynamic Moment Formulation and Its Implications for Dynamic Stability Testing." AIAA Paper No. 71-275, presented at AIAA 6th Aerodynamic Testing Conference, Albuquerque, New Mexico, March 10-12, 1971.
15. Maple, C. G. and Synge, J. L. "Aerodynamic Symmetry of Projectiles." Quarterly of Applied Mathematics, Vol. VI, No. 4, January 1949, pp. 345-366.
16. Whyte, Robert H. and Hathaway, Wayne H. "Aeroballistic Range Data Reduction Technique Utilizing Numerical Integration." AFATL TR-74-41, February 1974.
17. Bevington, Philip R. Data Reduction and Error Analysis for the Physical Sciences. McGraw-Hill Book Company, New York, 1969, pp. 72-75.
18. Hildebrand, F. B. Introduction to Numerical Analysis. McGraw-Hill Book Company, New York, 1956, pp. 258-269.
19. Young, Fay O. "Six-Degree-of-Freedom Flight Path Study Generalized Computer Program (SDFCP) User's Manual." AFFDL-TR-75-1, July 1975.
20. Uselton, James C. "Roll-Damping Derivatives on Cones." AEDC-TR-69-11 (AD850237), April 1969.
21. Welsh, C. J. and Lawrence, W. R. "Motion Analysis Procedure for Asymmetric Vehicles." AEDC-TR-75-158 (ADA024674), May 1976.

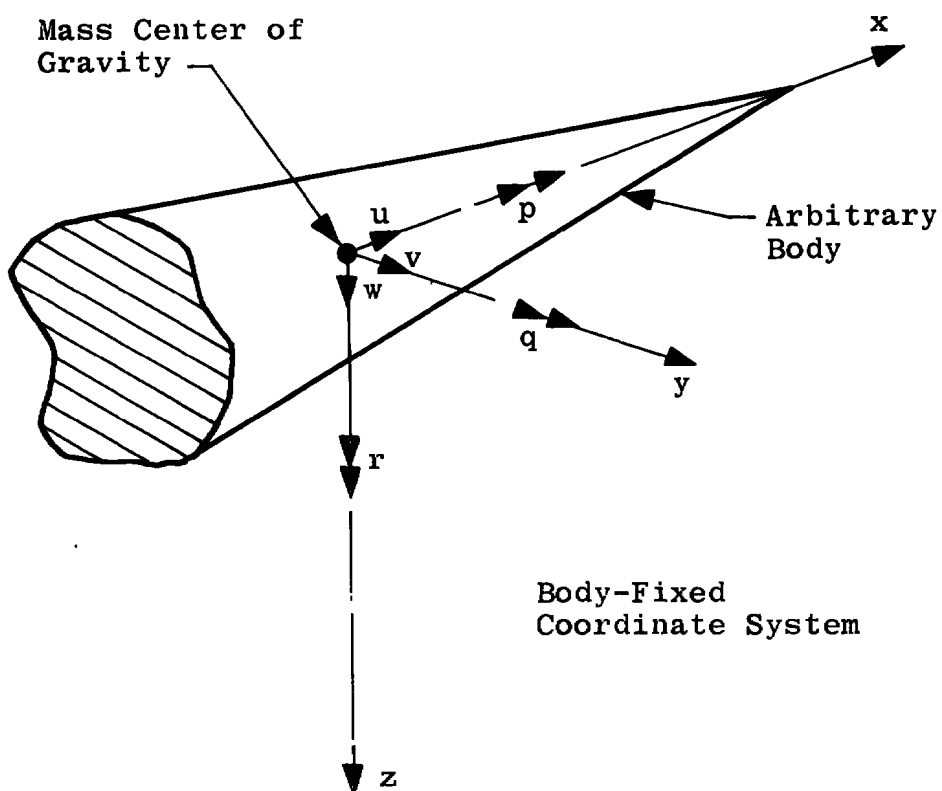


Figure 1. Arbitrary body showing axis system for 3DOF equation development.

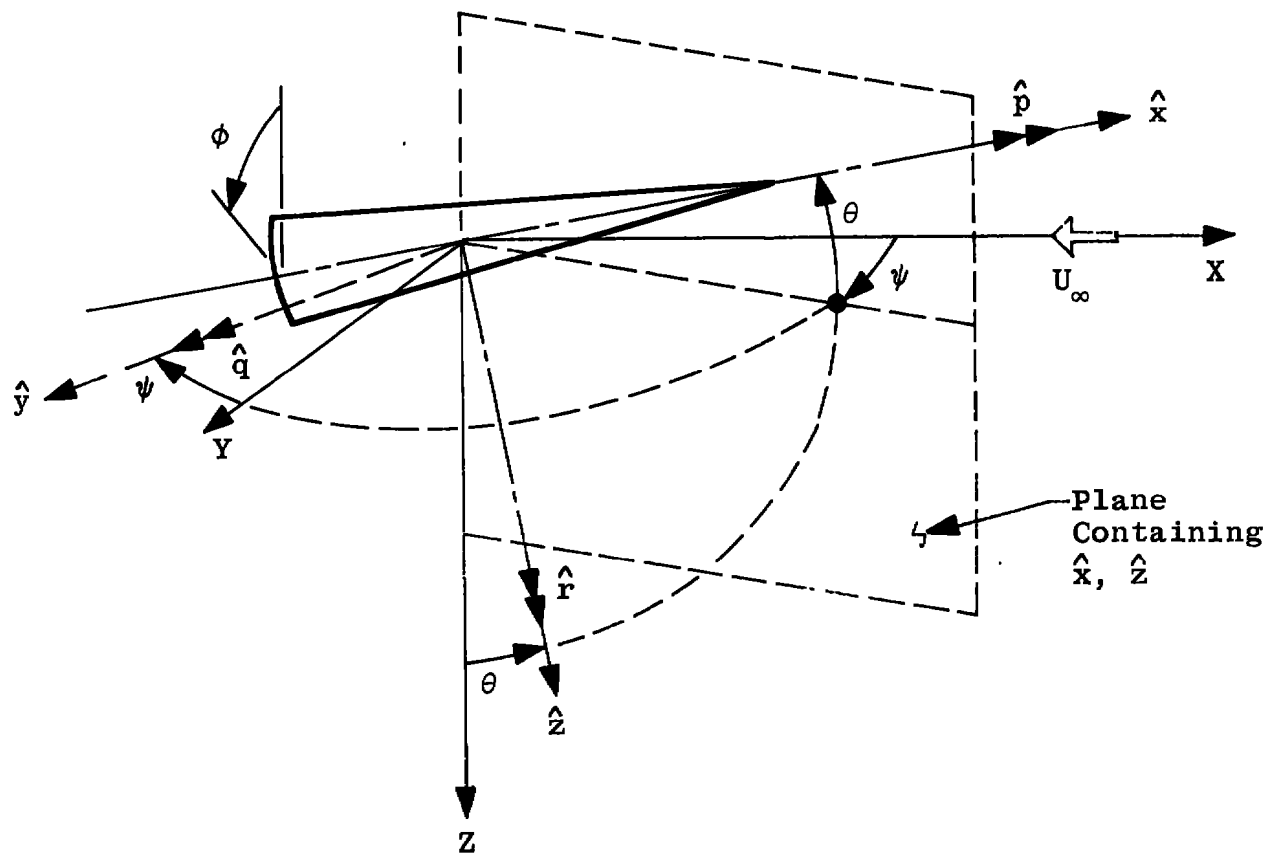
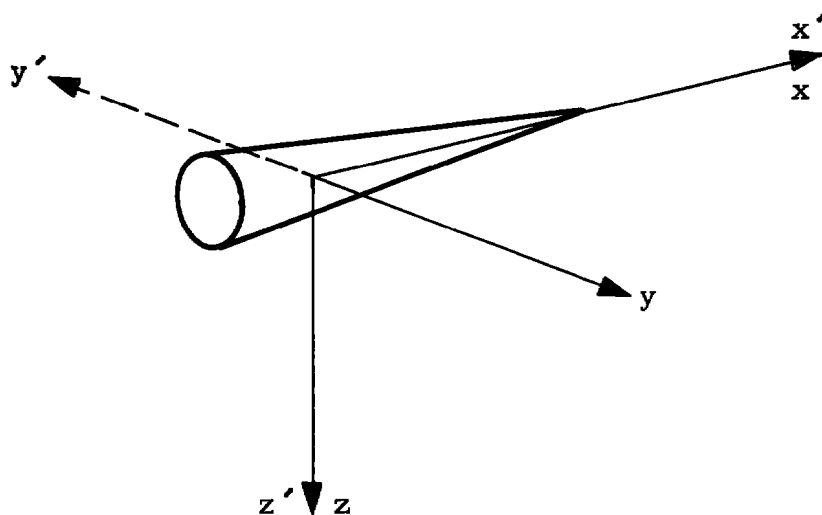
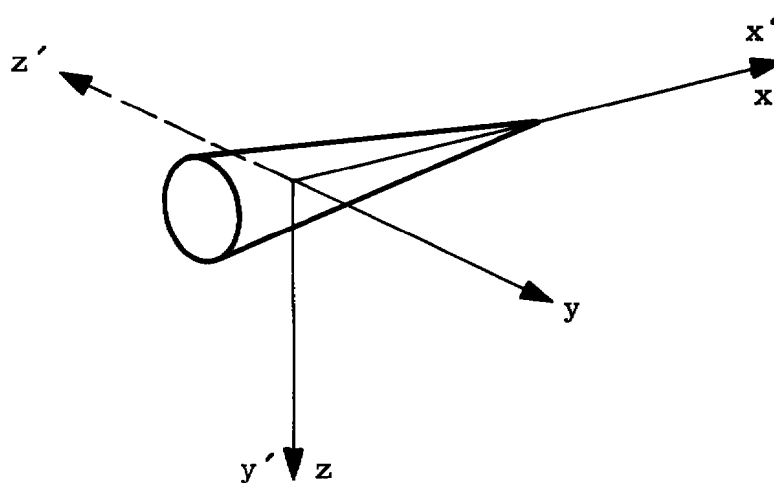


Figure 2. Plane-fixed coordinate system showing Euler angles and velocity components relative to space-fixed system.



a. Symmetry operation for mirror symmetry
in x, z plane



b. Symmetry operation for 90-deg rotational
symmetry about the x axis

Figure 3. Physical description of symmetry operations on
axis systems.

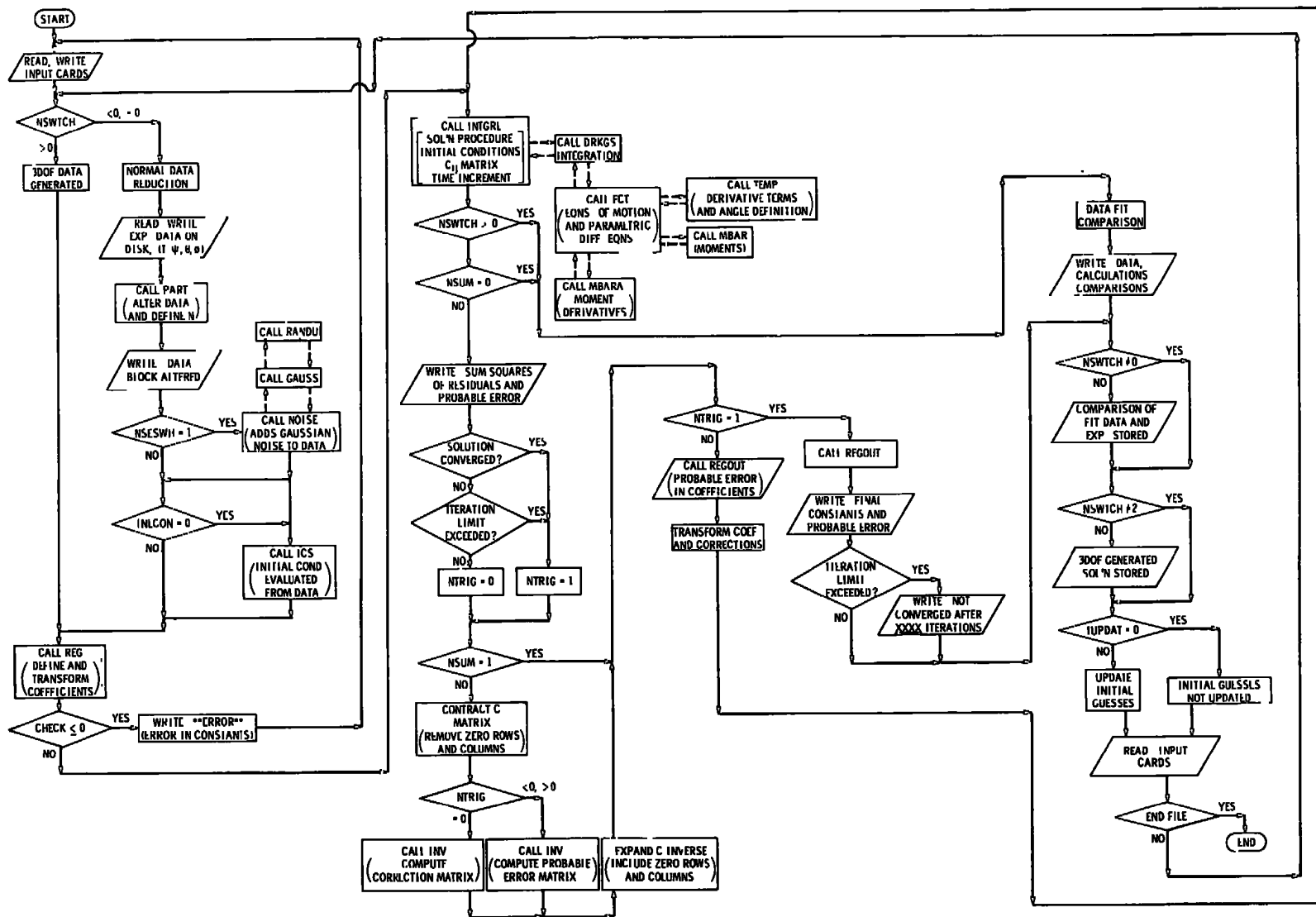
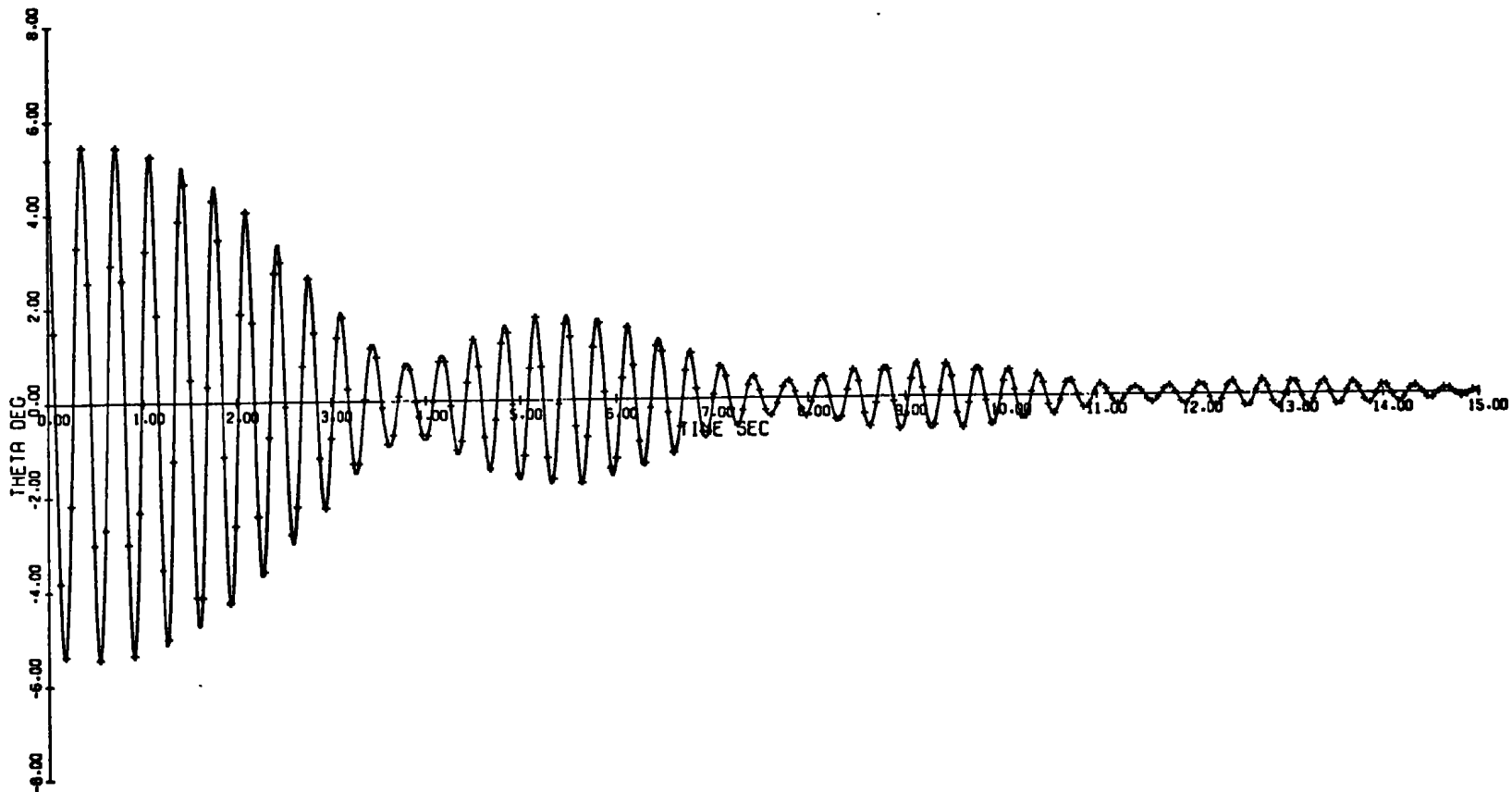
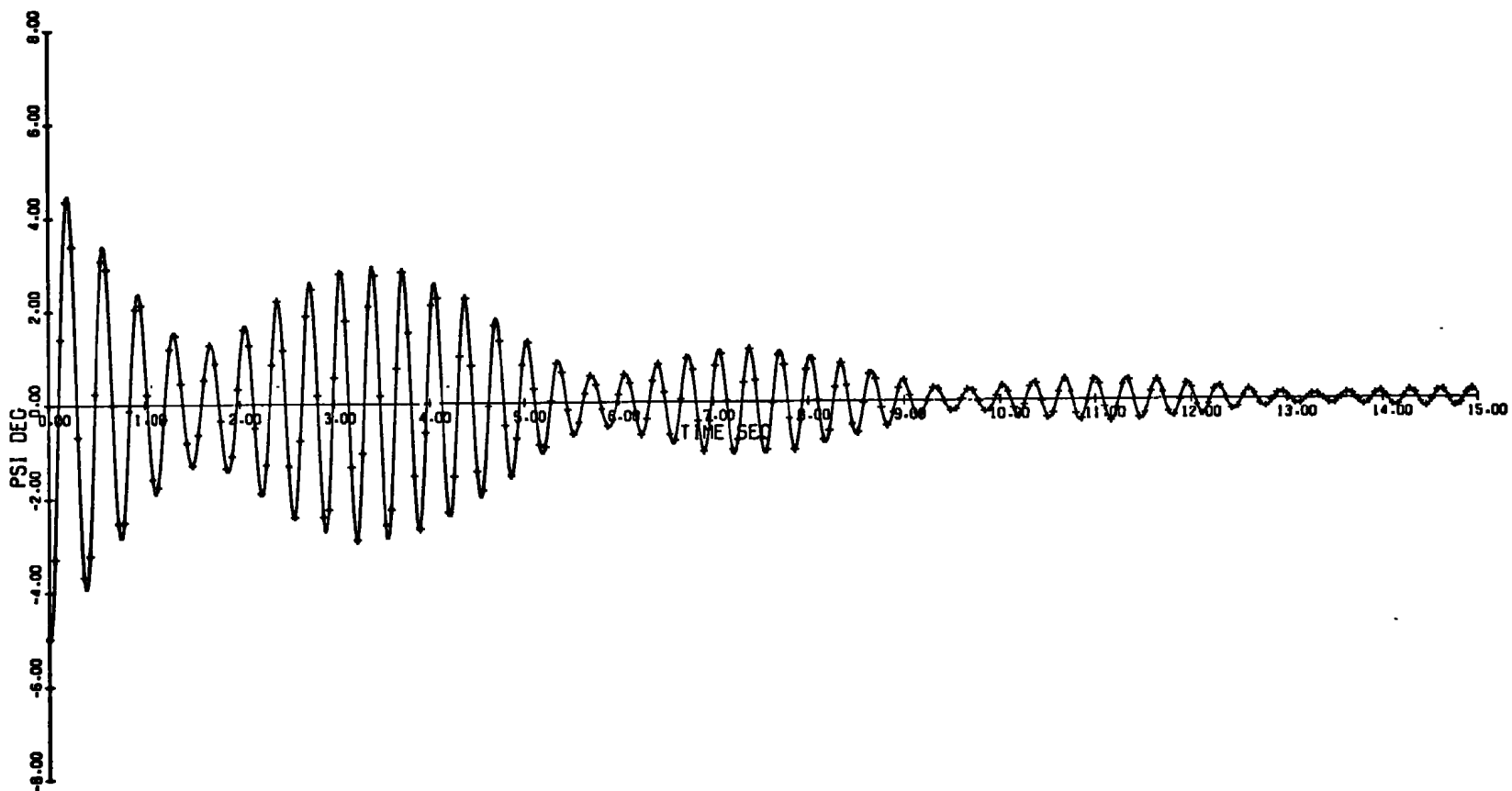


Figure 4. Flow Chart: symmetric and asymmetric parameter extraction program.

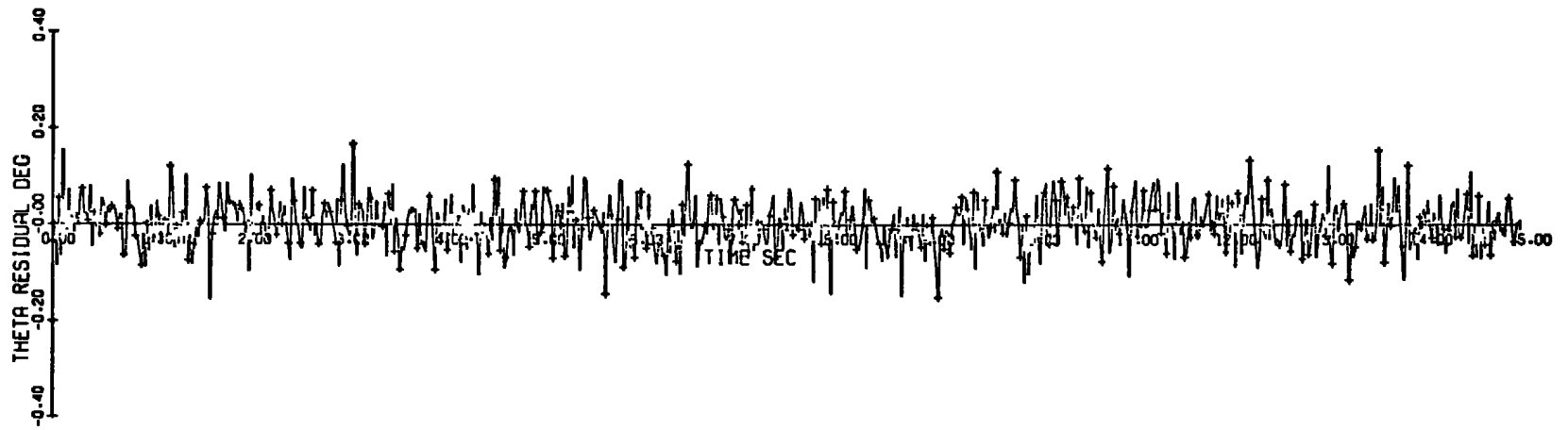


a. Computed θ versus time

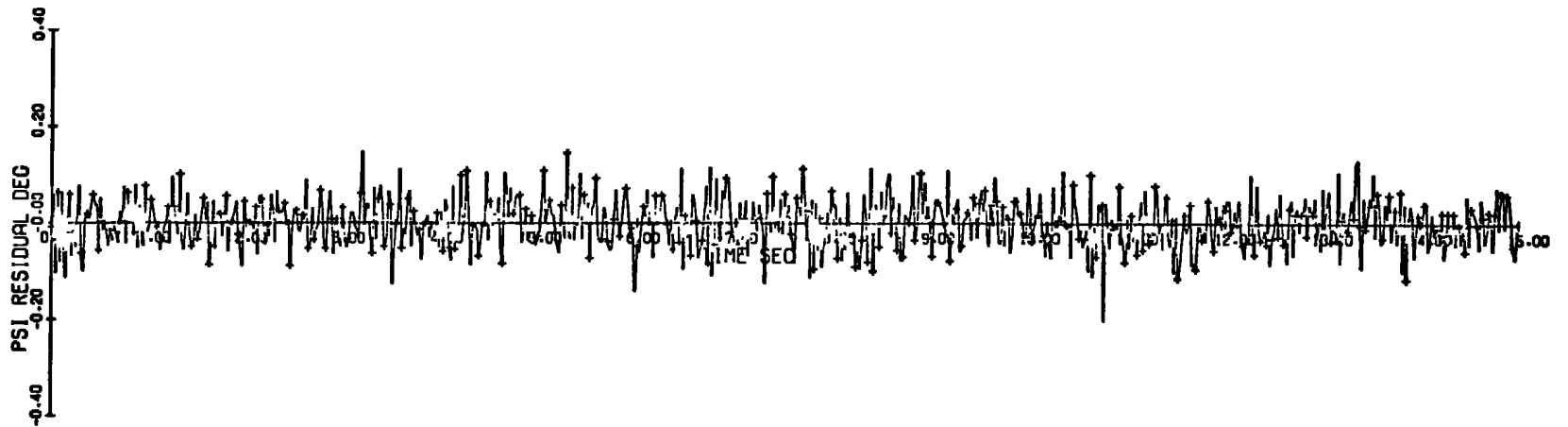
Figure 5. Graphical solution corresponding to Table 6, $\sigma = 0.05$ deg.



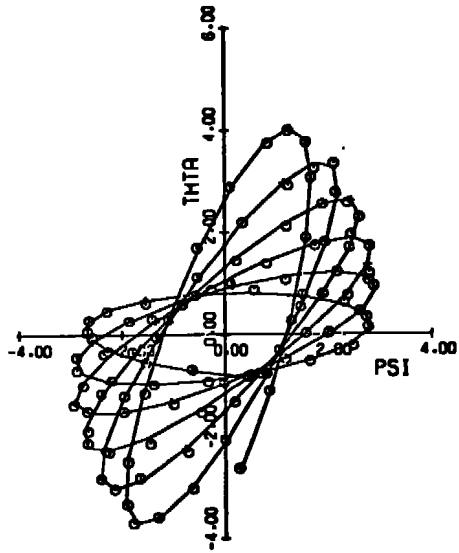
b. Computed ψ versus time
Figure 5. Continued.



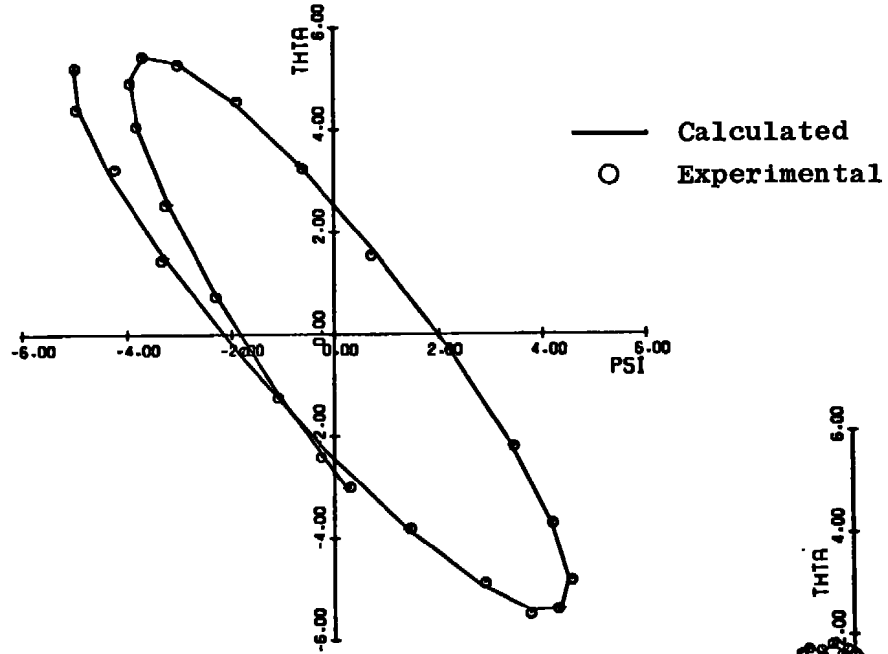
c. Residual in θ versus time



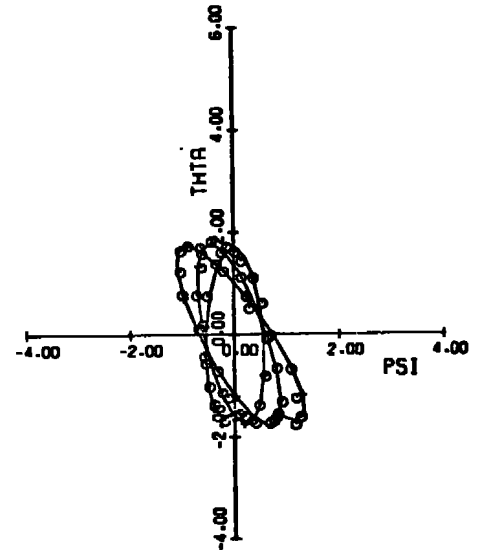
d. Residual in ψ versus time
Figure 5. Continued.



f. Fit of calculated solution to experimental data in ψ, θ plane, time increment 1.98 to 3.98 sec



e. Fit of calculated solution to experimental data in ψ, θ plane, time increment 0 to 0.48 sec



g. Fit of calculated solution to experimental data in ψ, θ plane, time increment 4.98 to 5.98 sec

Figure 5. Concluded.

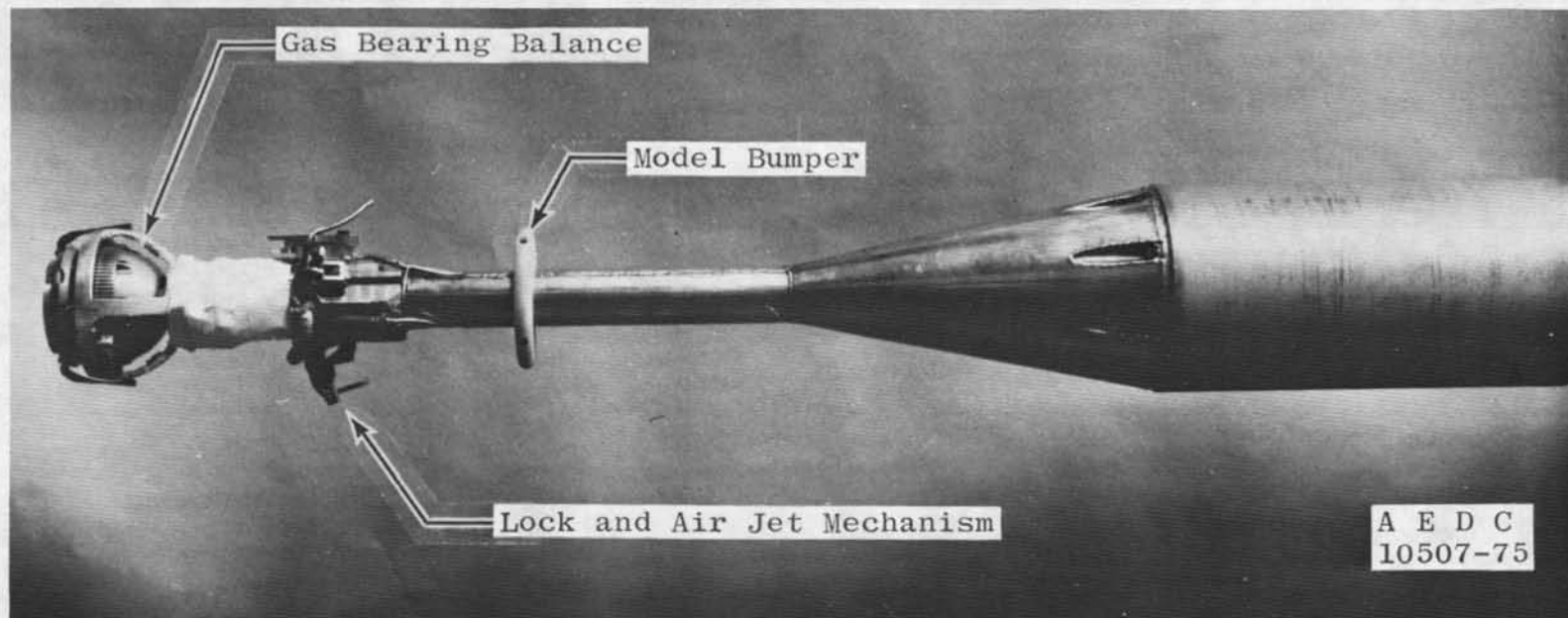


Figure 6. Photograph of 3DOF balance and sting.

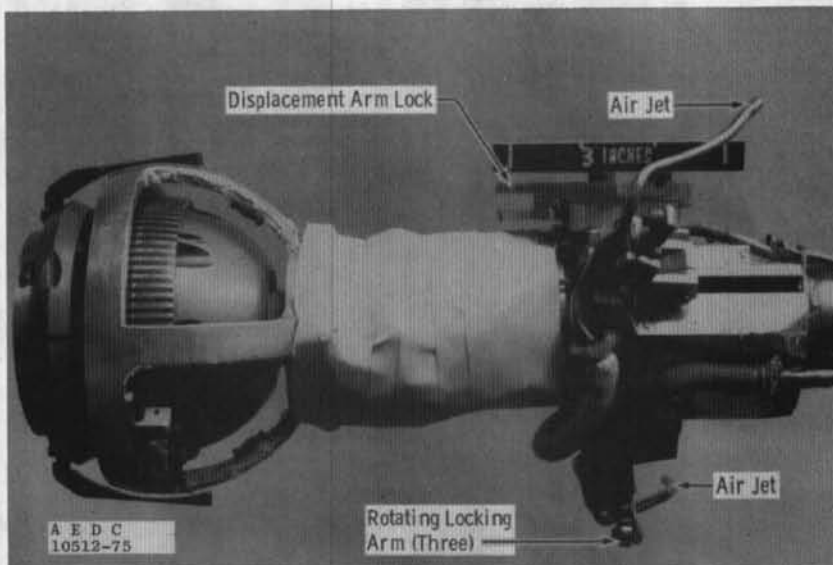
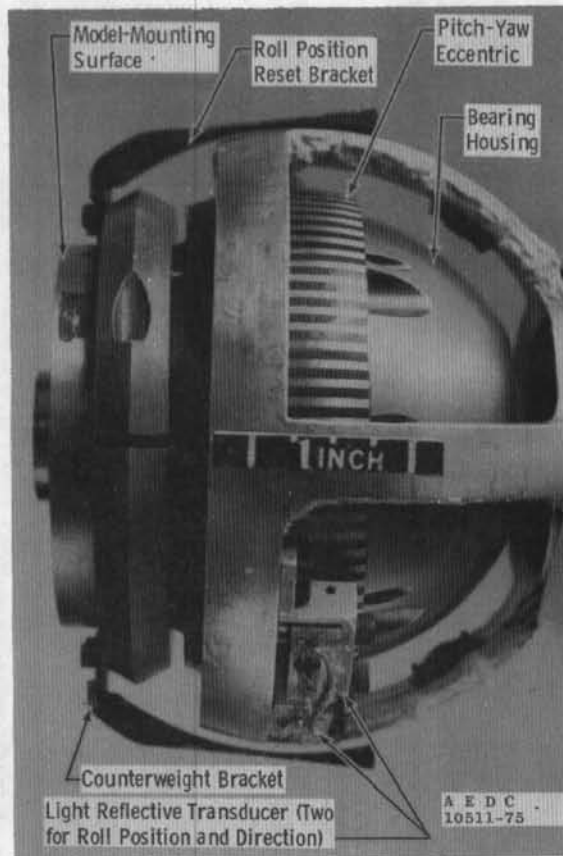


Figure 7. 3DOF balance photographs.

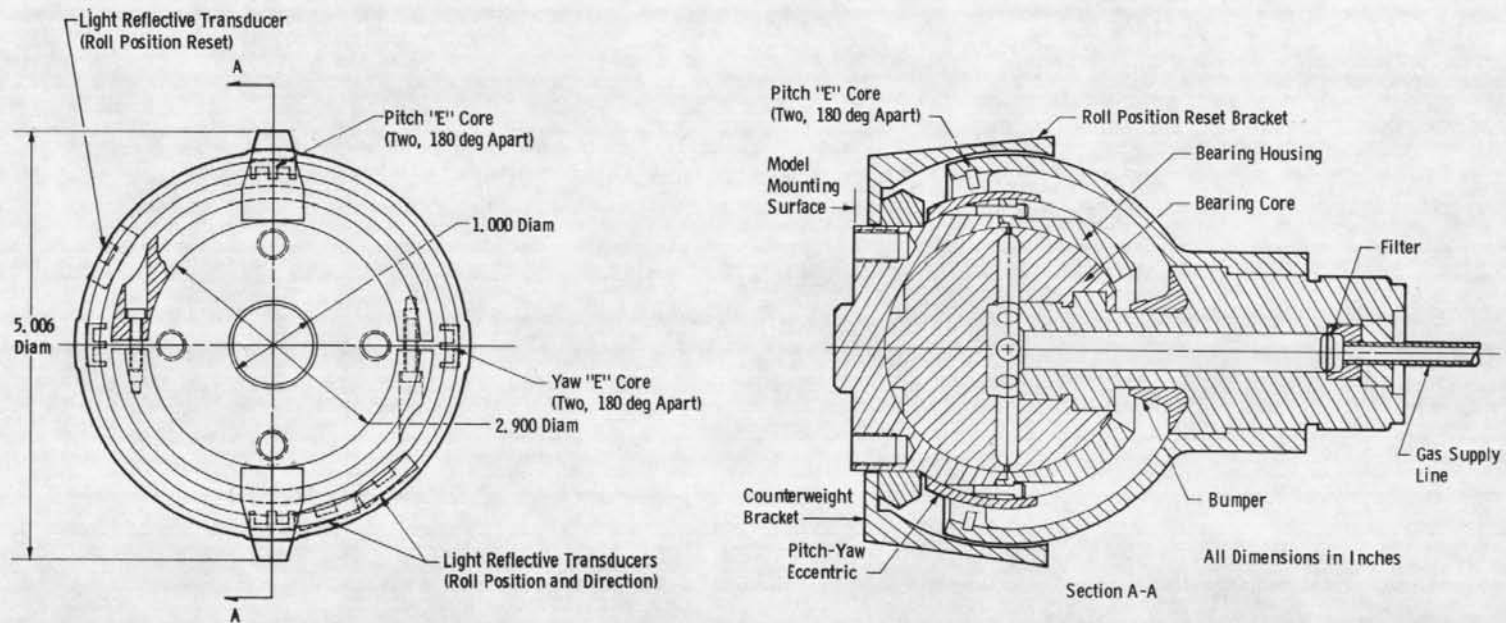
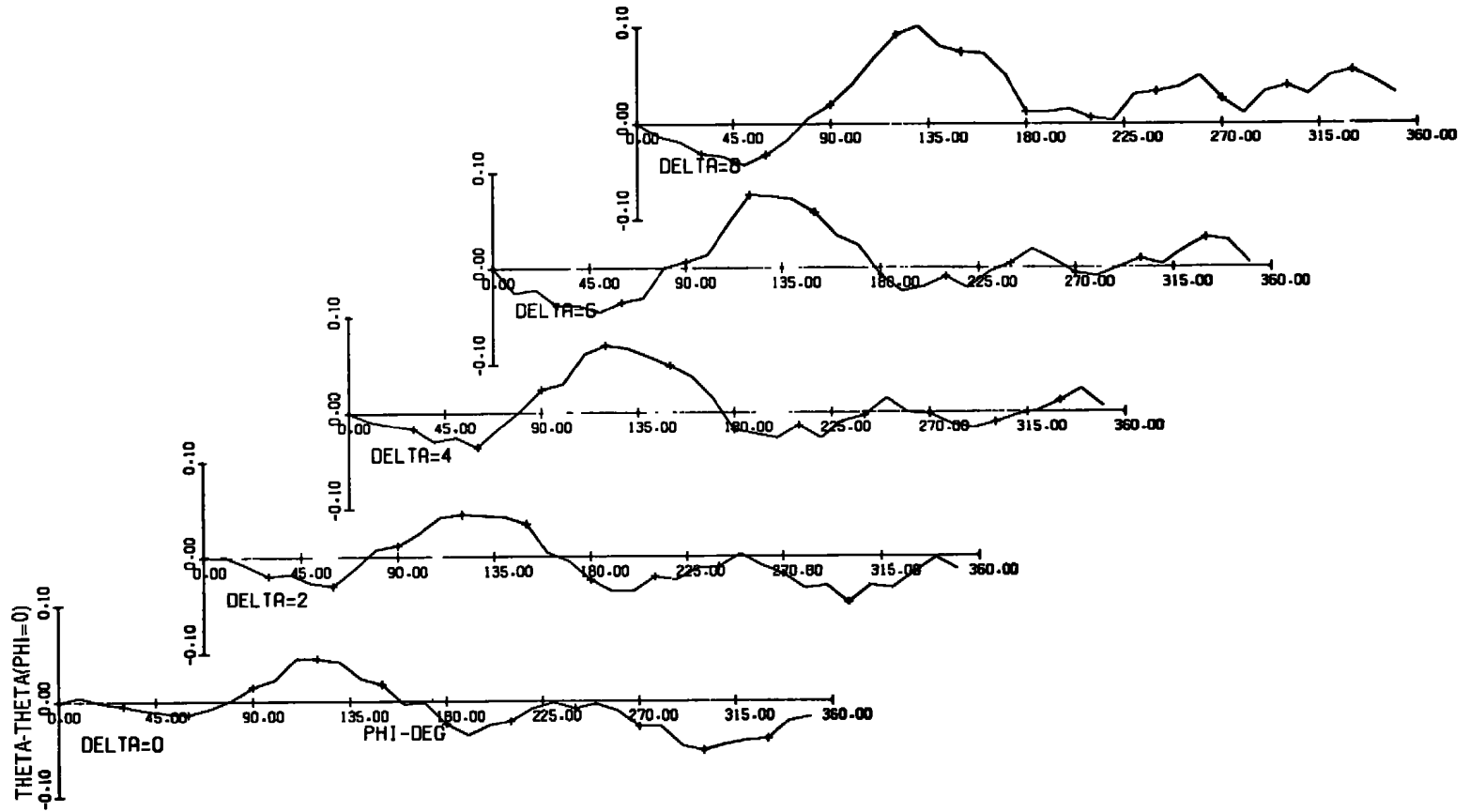
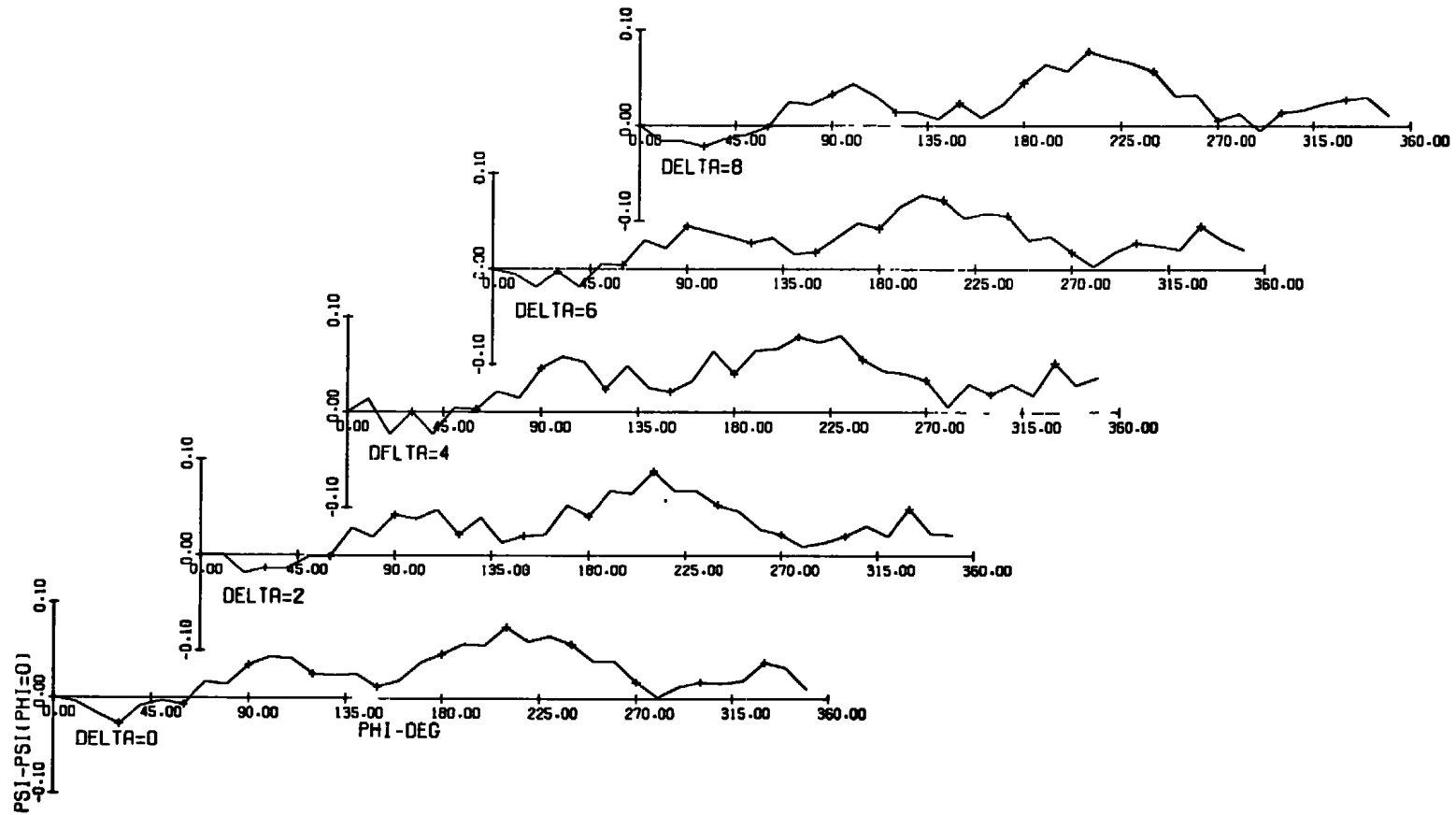
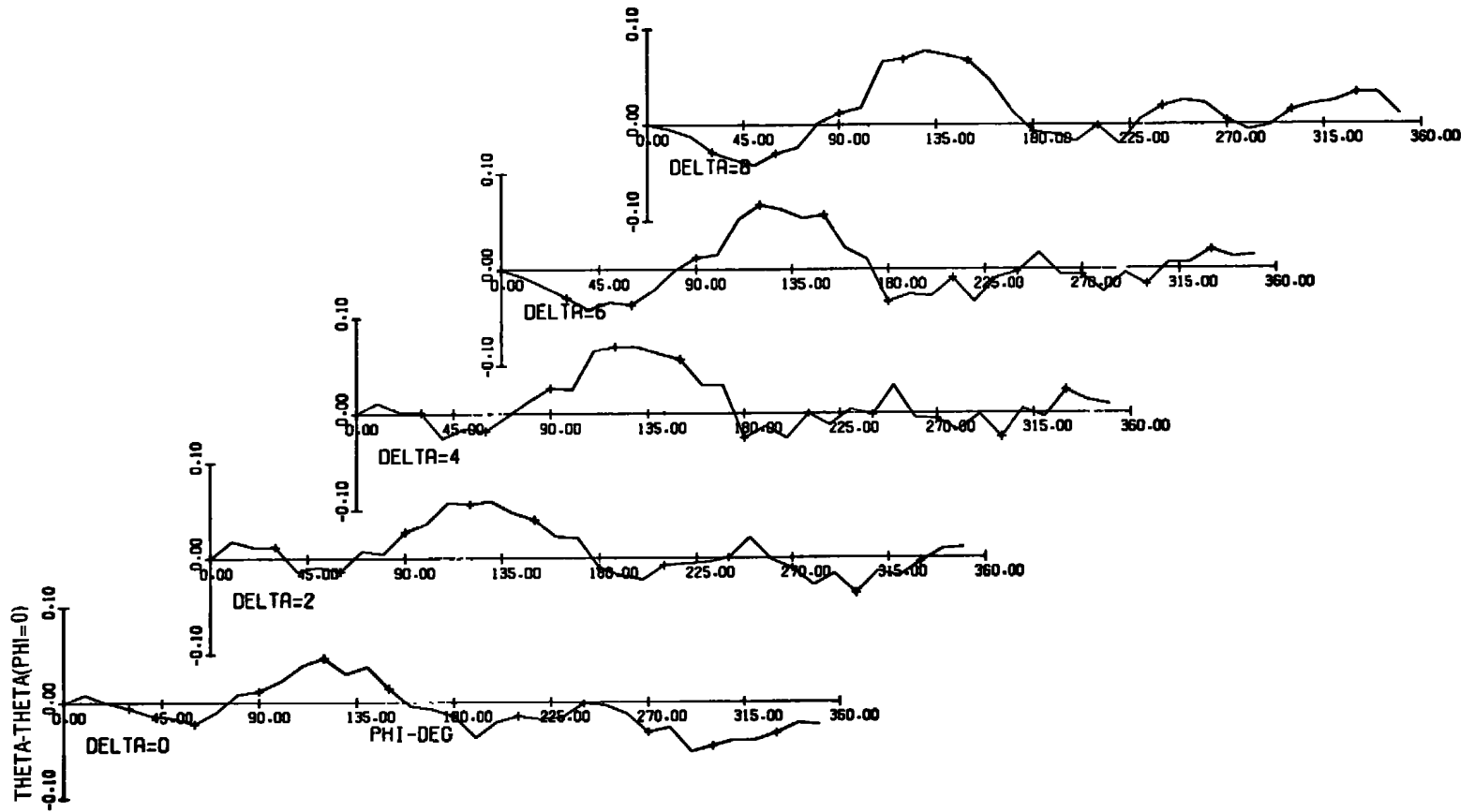


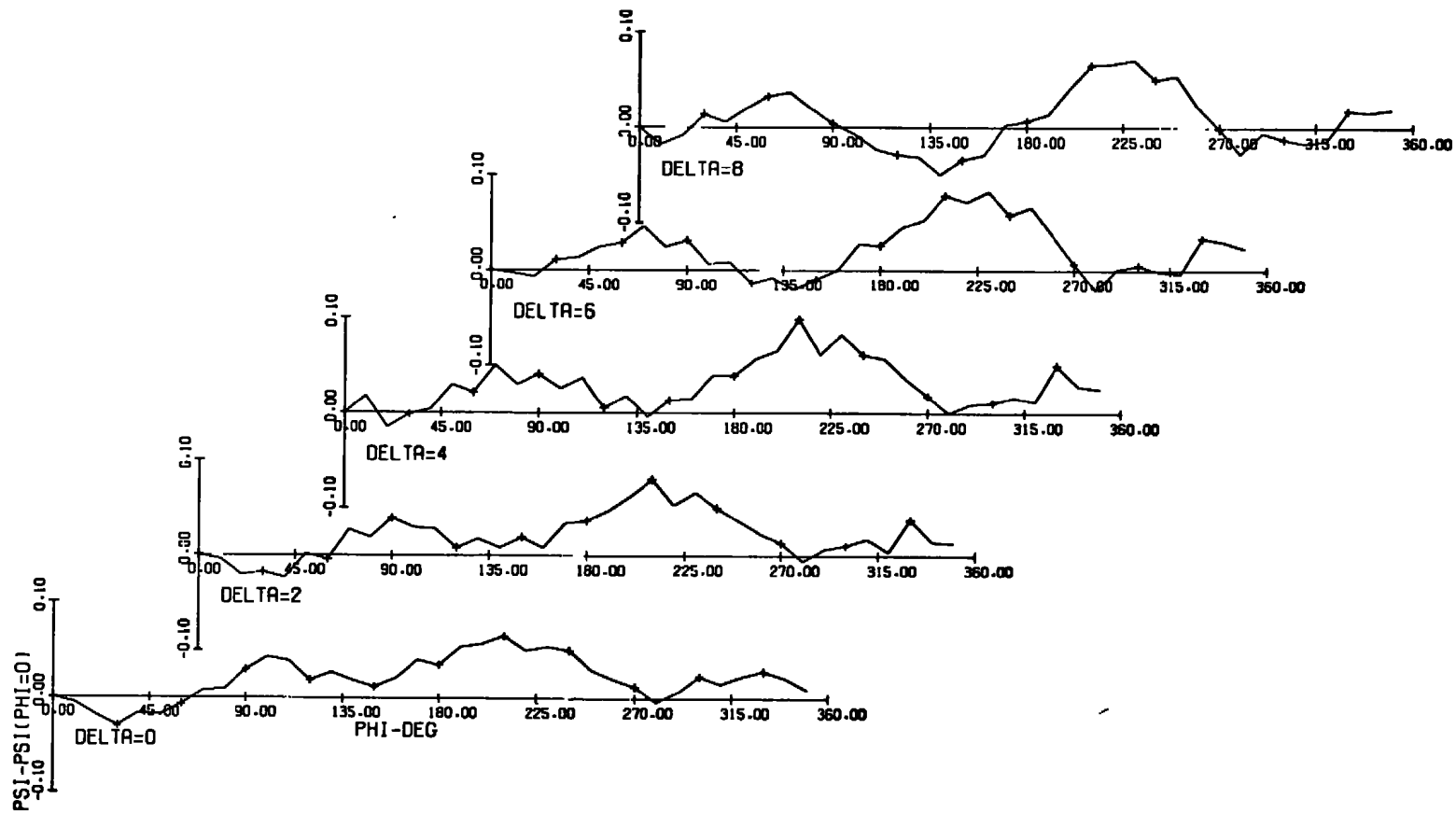
Figure 8. 3DOF balance schematic.

a. θ correction versus ϕ Figure 9. Roll interaction effect for sting roll position $\Omega = 0$ deg.

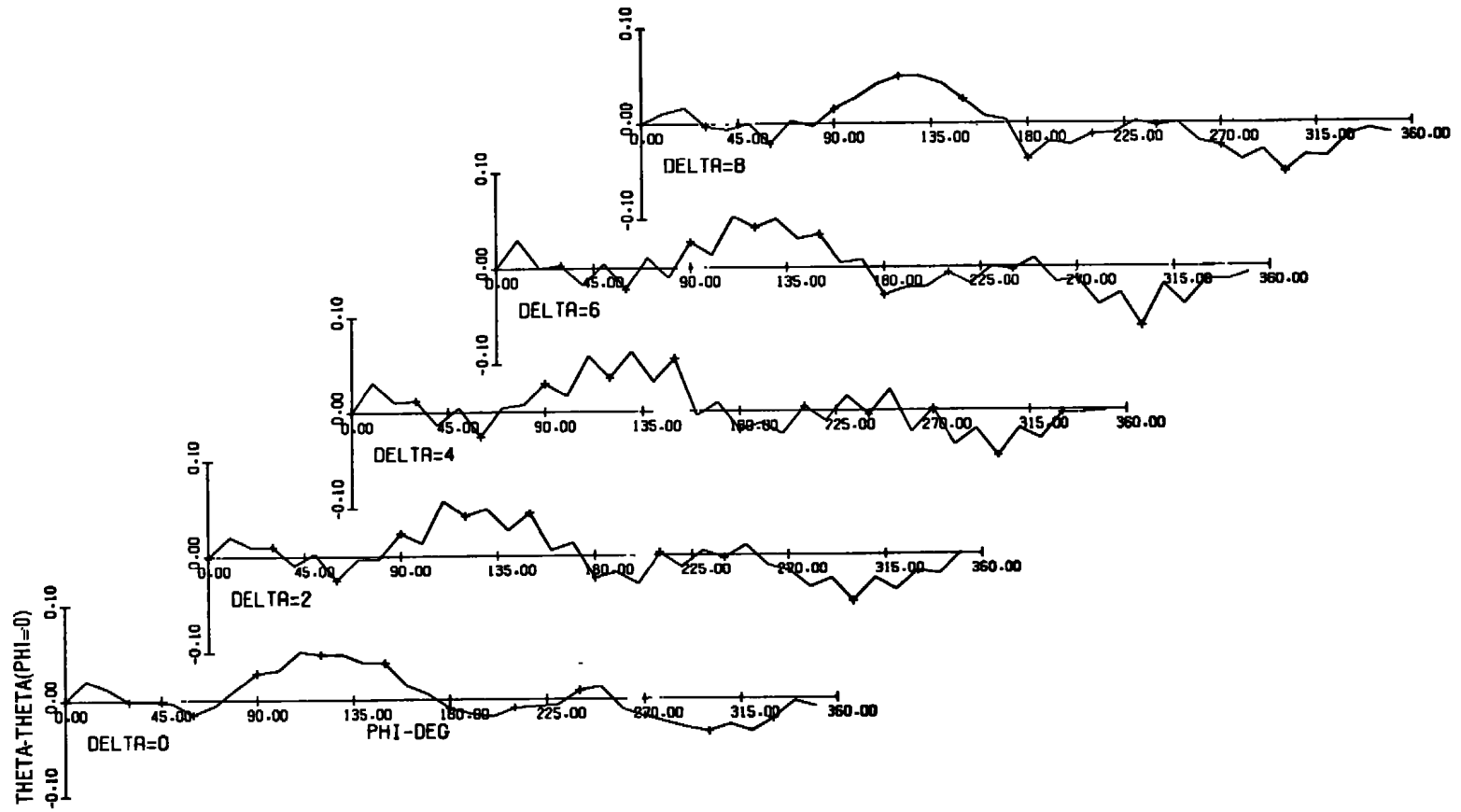


b. ψ correction versus ϕ
Figure 9. Concluded.

a. θ correction versus ϕ Figure 10. Roll interaction effect for sting roll position $\Omega = 45$ deg.

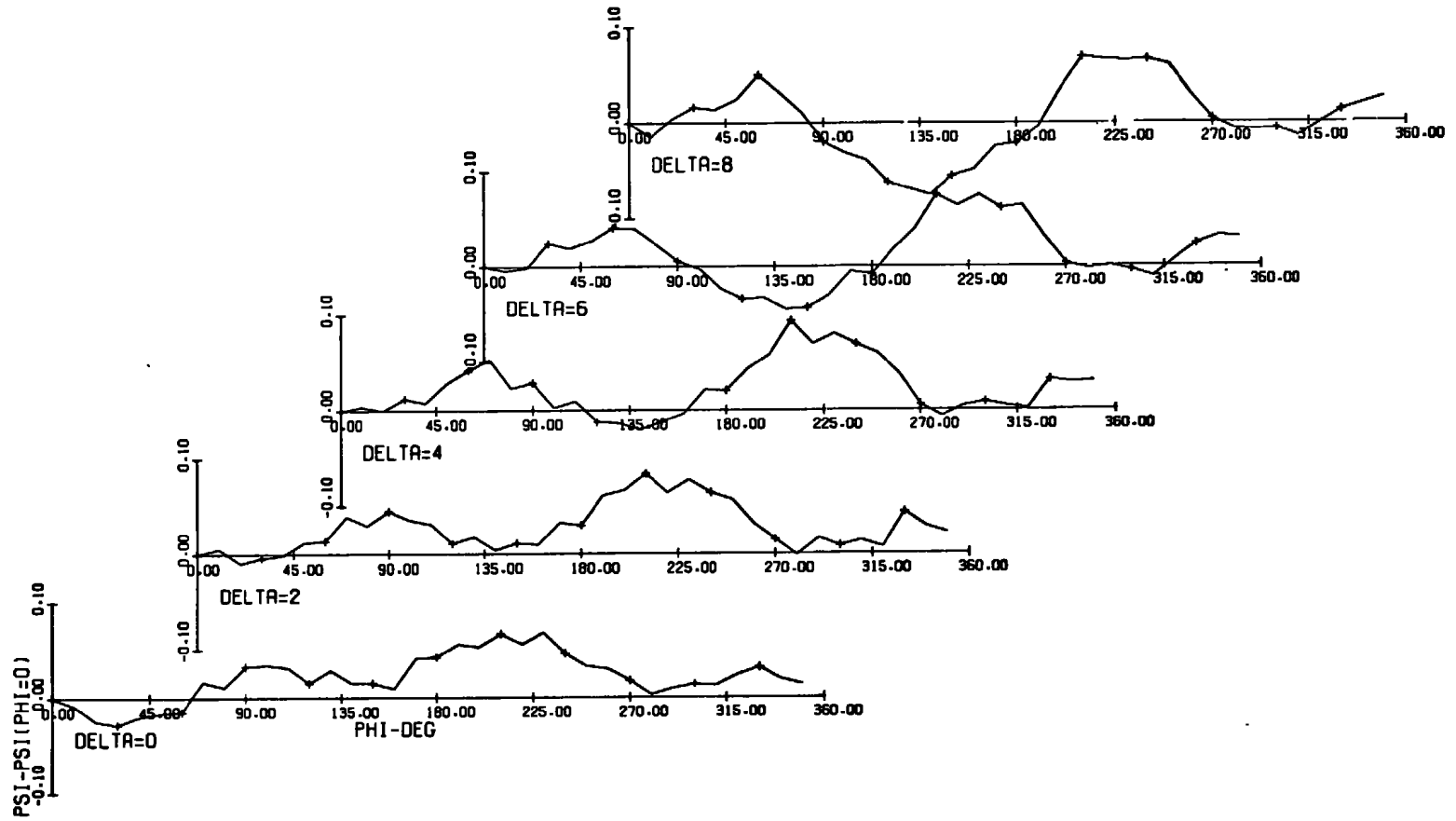


b. ψ correction versus ϕ
Figure 10. Concluded.

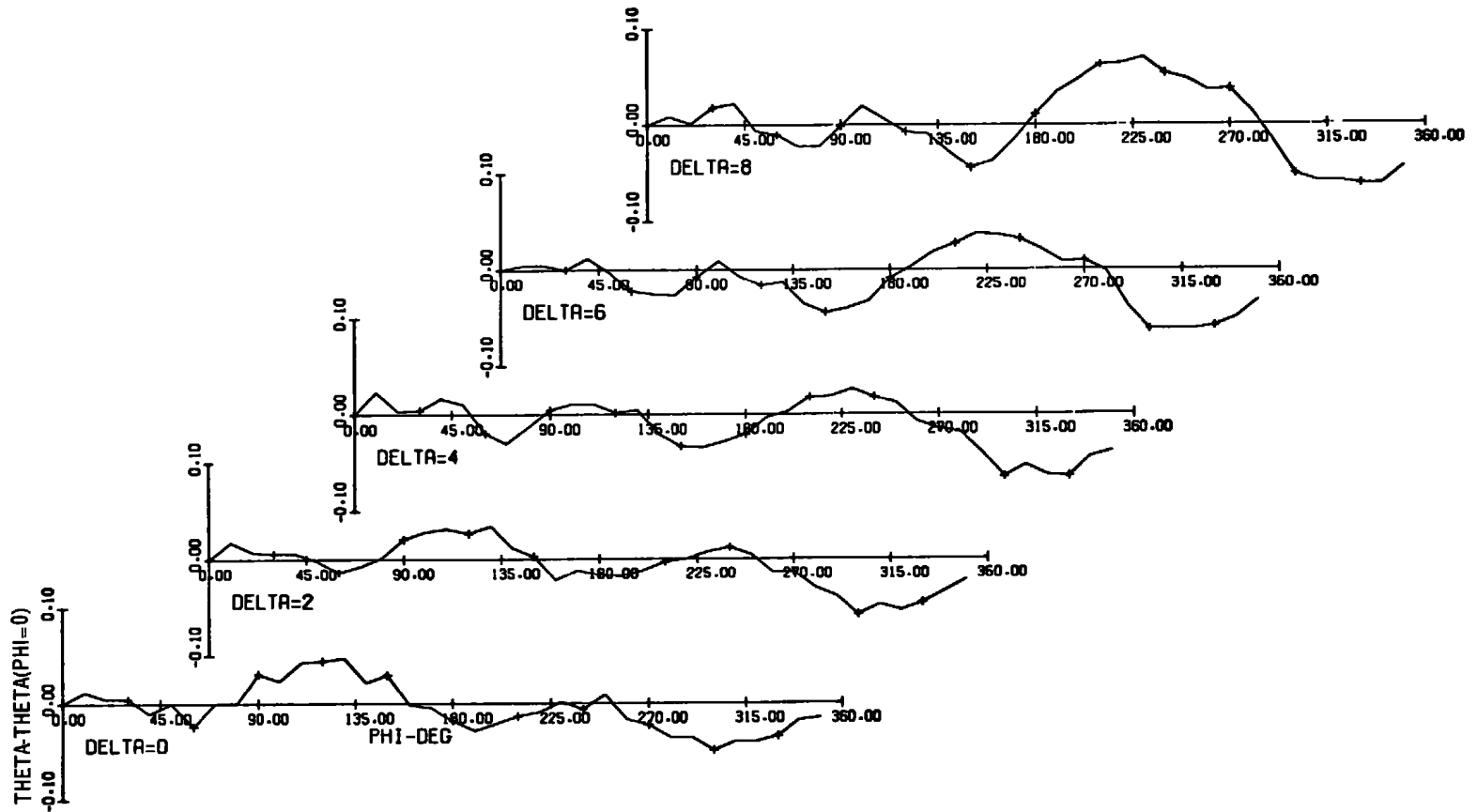


a. θ correction versus ϕ

Figure 11. Roll interaction effect for sting roll position $\Omega = 90$ deg.

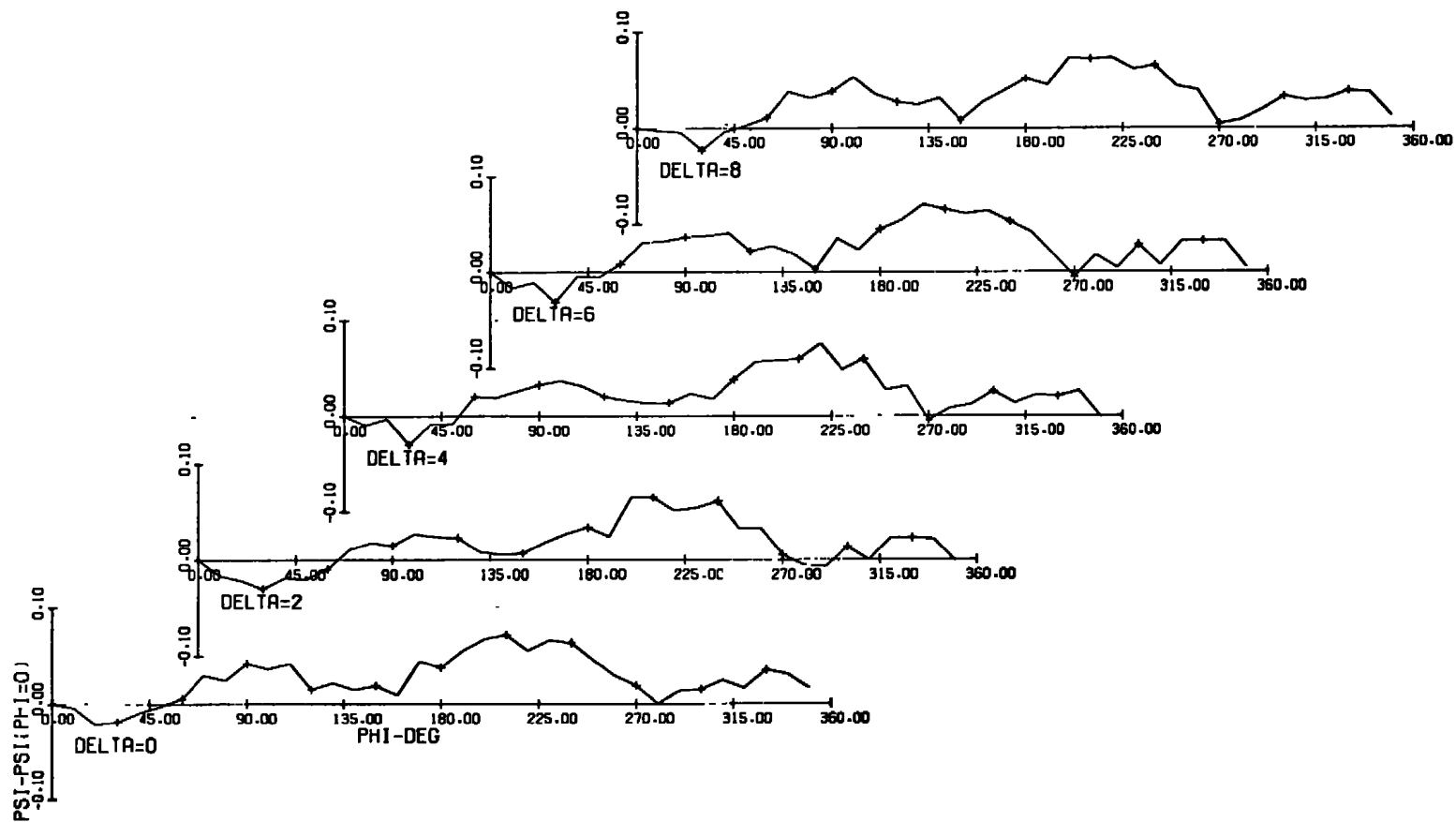


b. ψ correction versus ϕ
Figure 11. Concluded.



a. θ correction versus ϕ

Figure 12. Roll interaction effect for sting roll position $\Omega = 180$ deg.



b. ψ correction versus ϕ
Figure 12. Concluded.

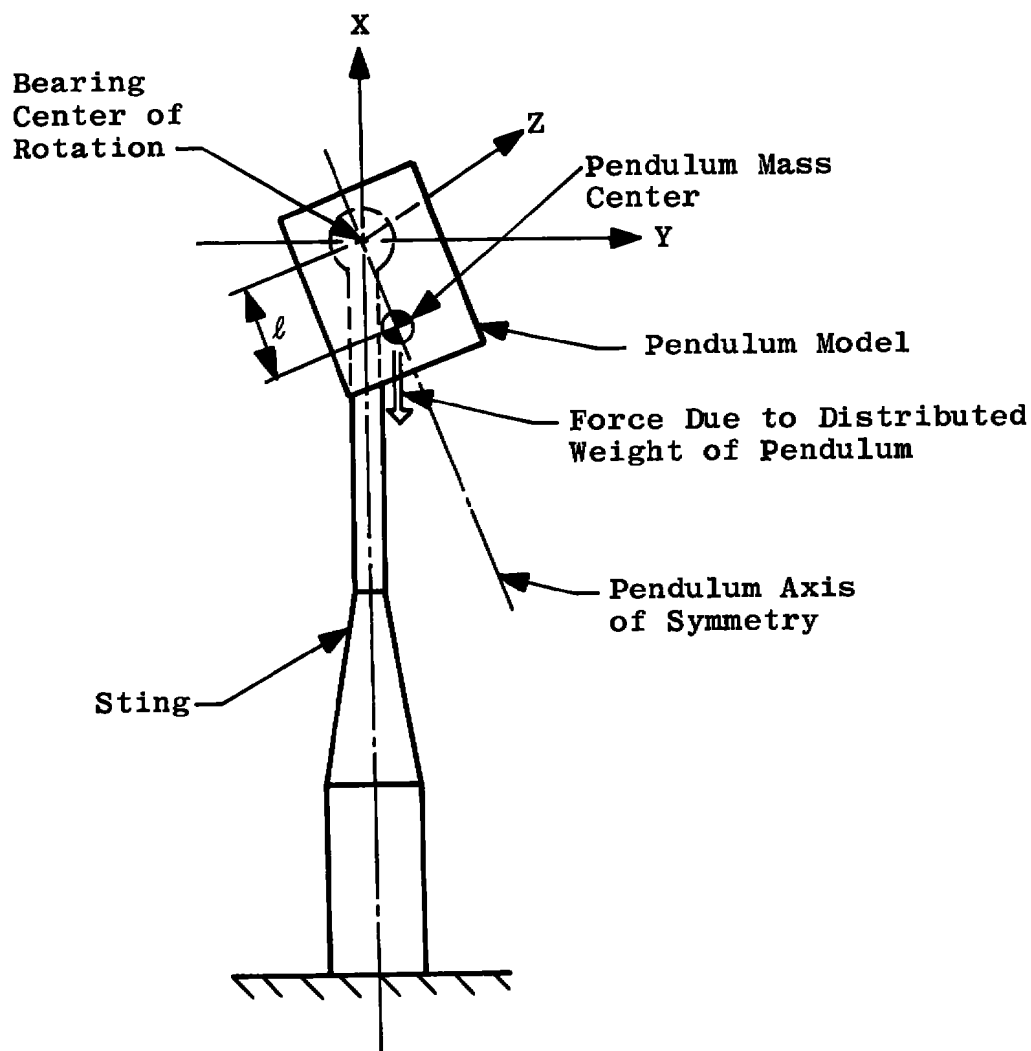
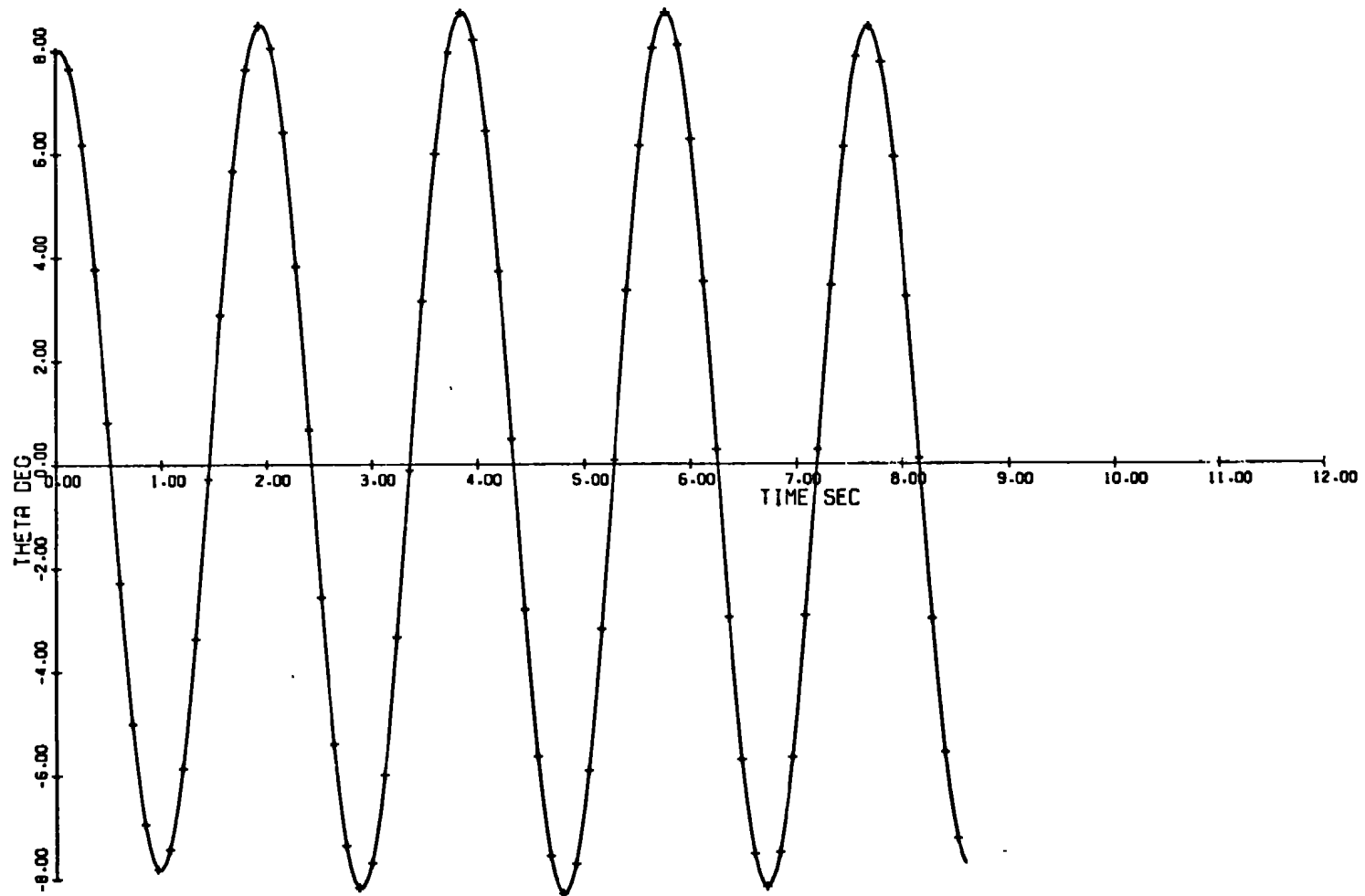
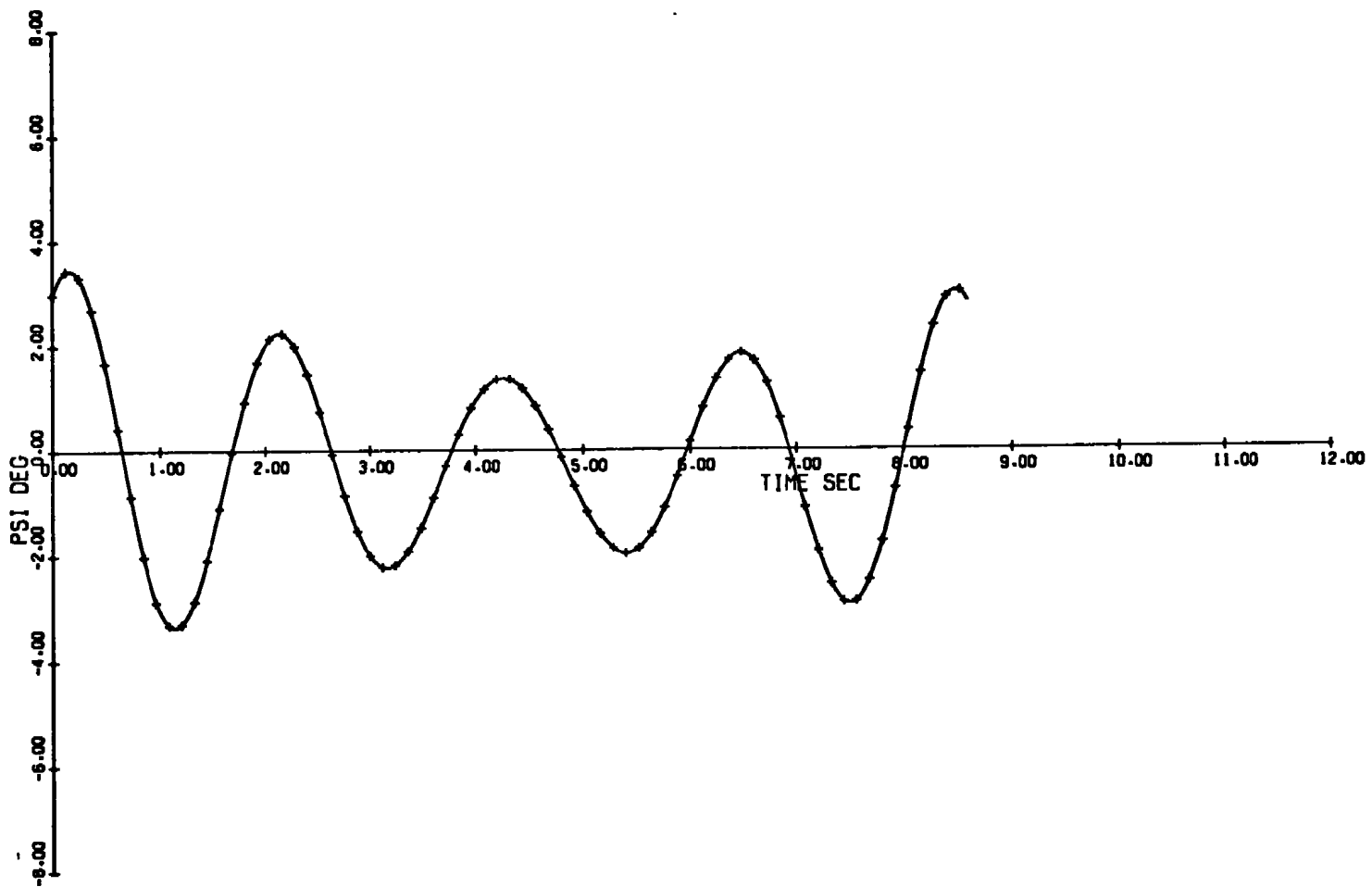


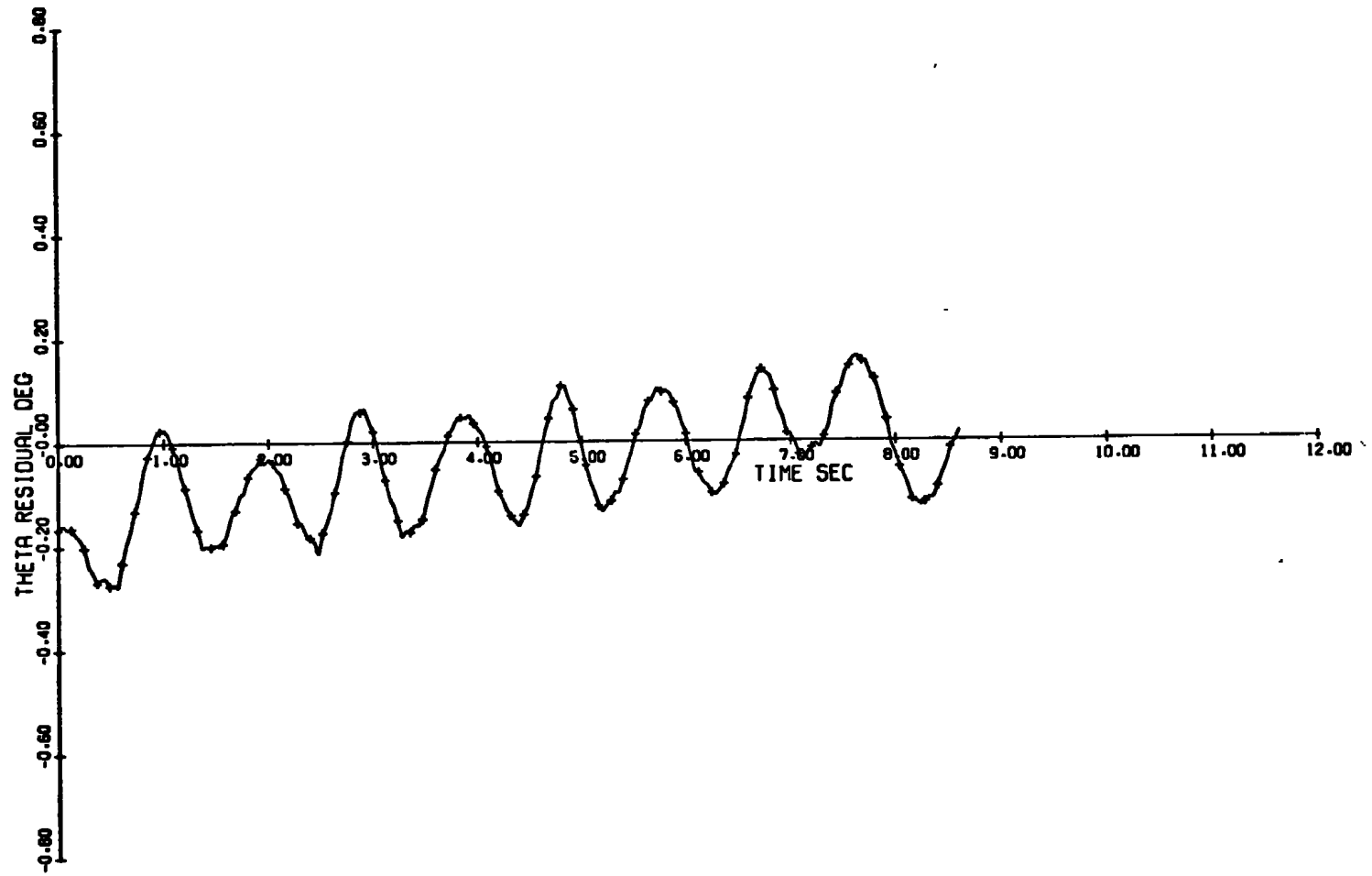
Figure 13. Schematic of bench test mechanism.



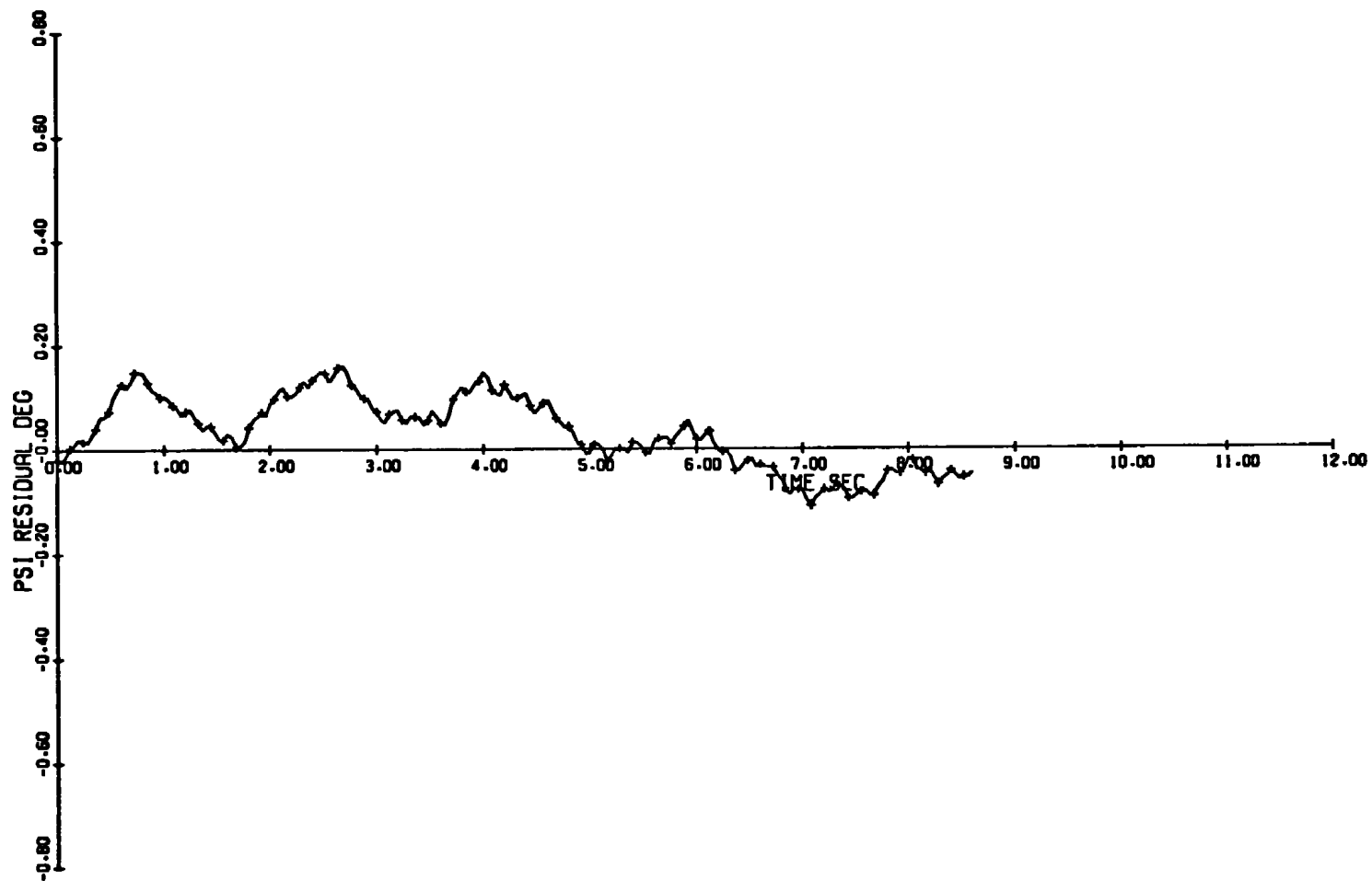
a. Computed θ versus time
Figure 14. Bench test results for 100-psi bearing pressure.



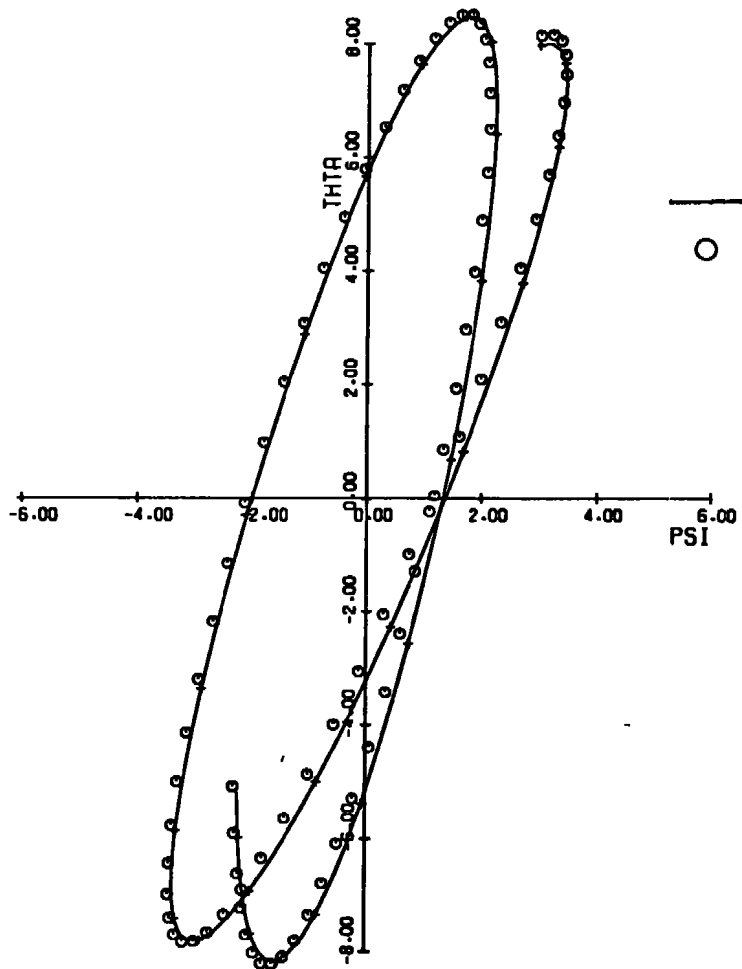
b. Computed ψ versus time
Figure 14. Continued.



c. Residual in θ versus time
Figure 14. Continued.

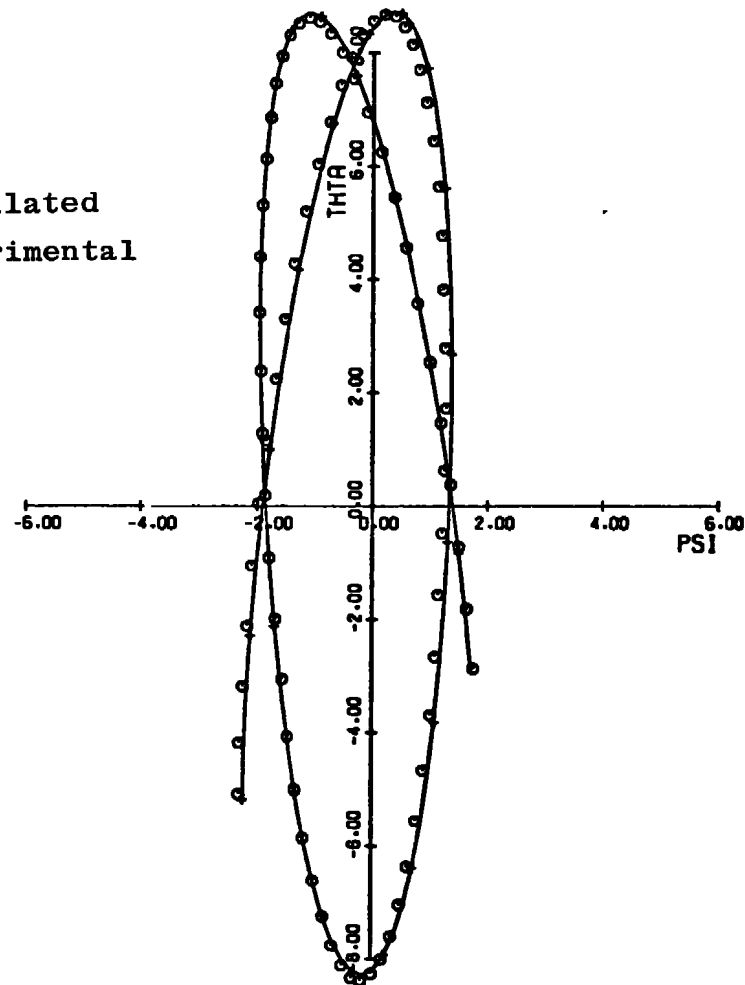


d. Residual in ψ versus time
Figure 14. Continued.



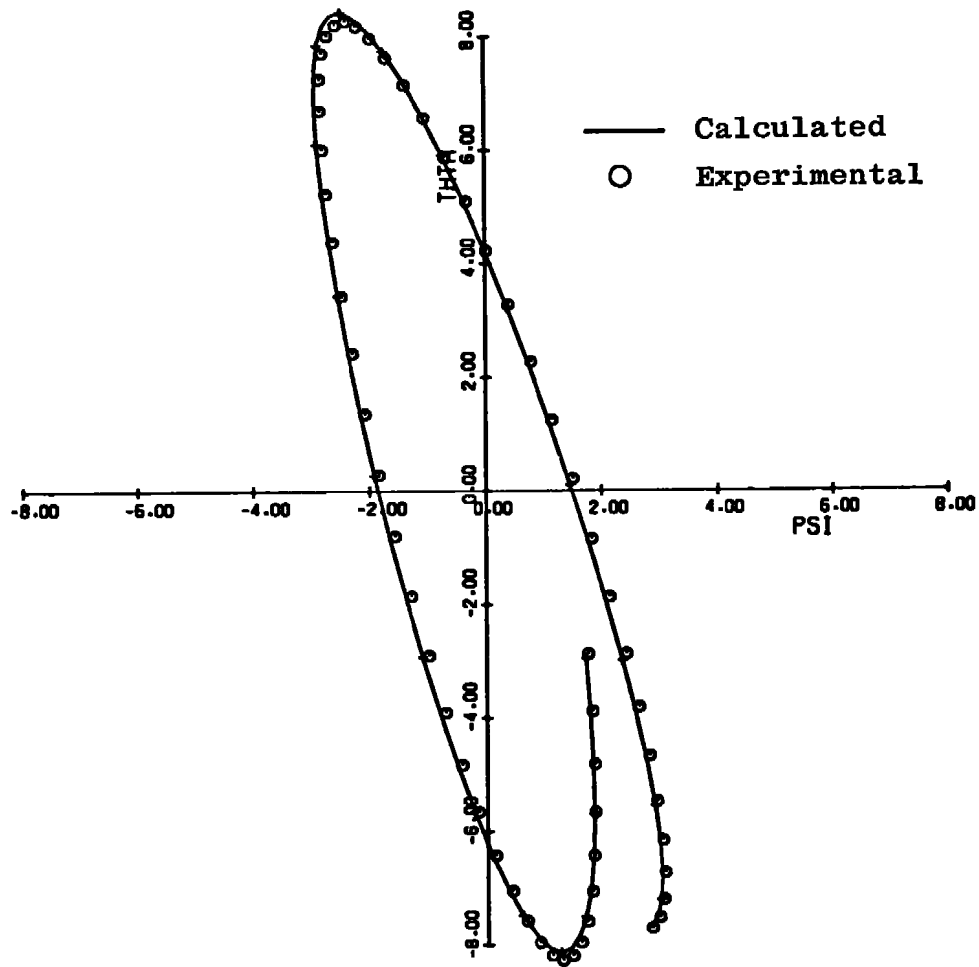
e. Fit of calculated solution to experimental data
in ψ, θ plane, time increment 0 to 3.16 sec

— Calculated
○ Experimental

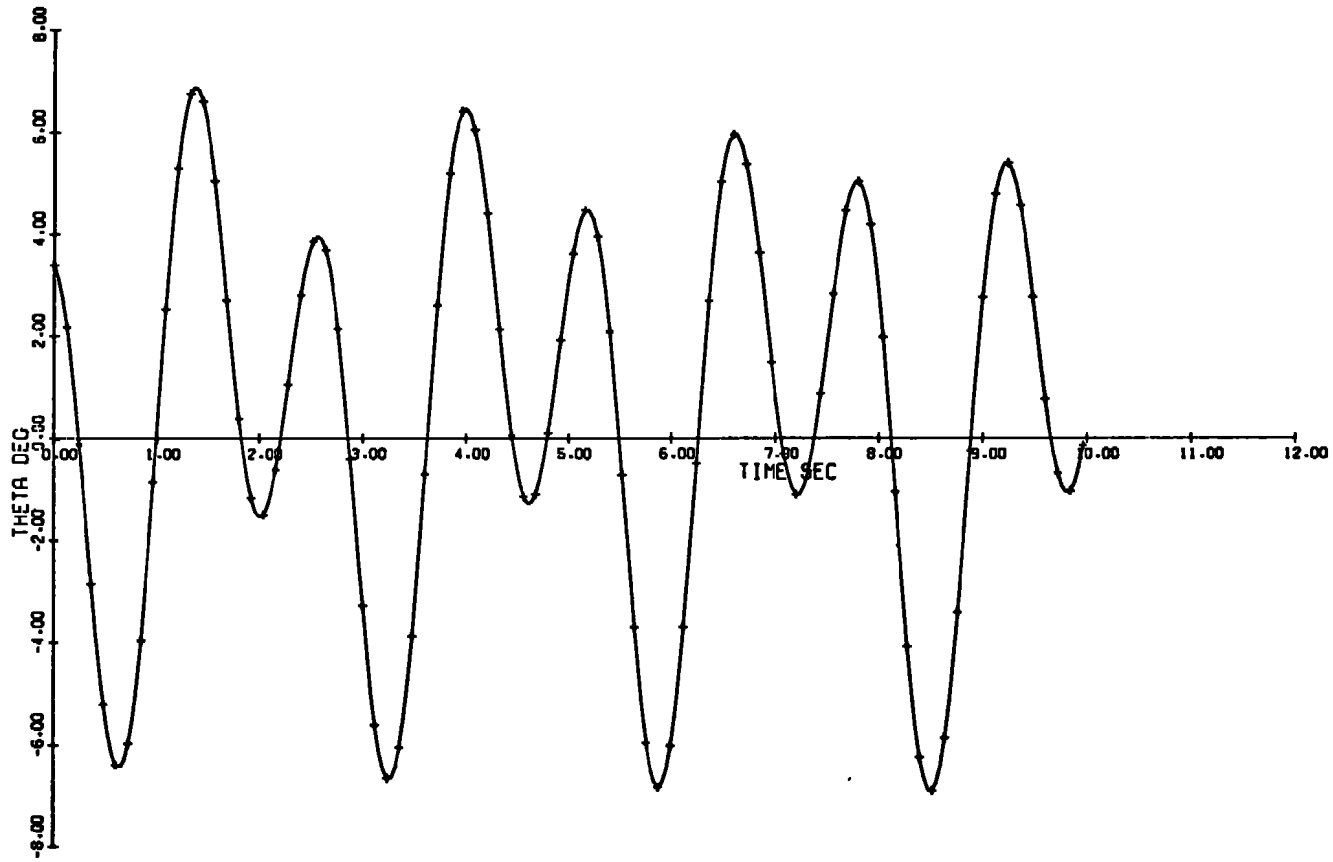


f. Fit of calculated solution to experimental data
in ψ, θ plane, time increment 3.16 to 6.36 sec

Figure 14. Continued.

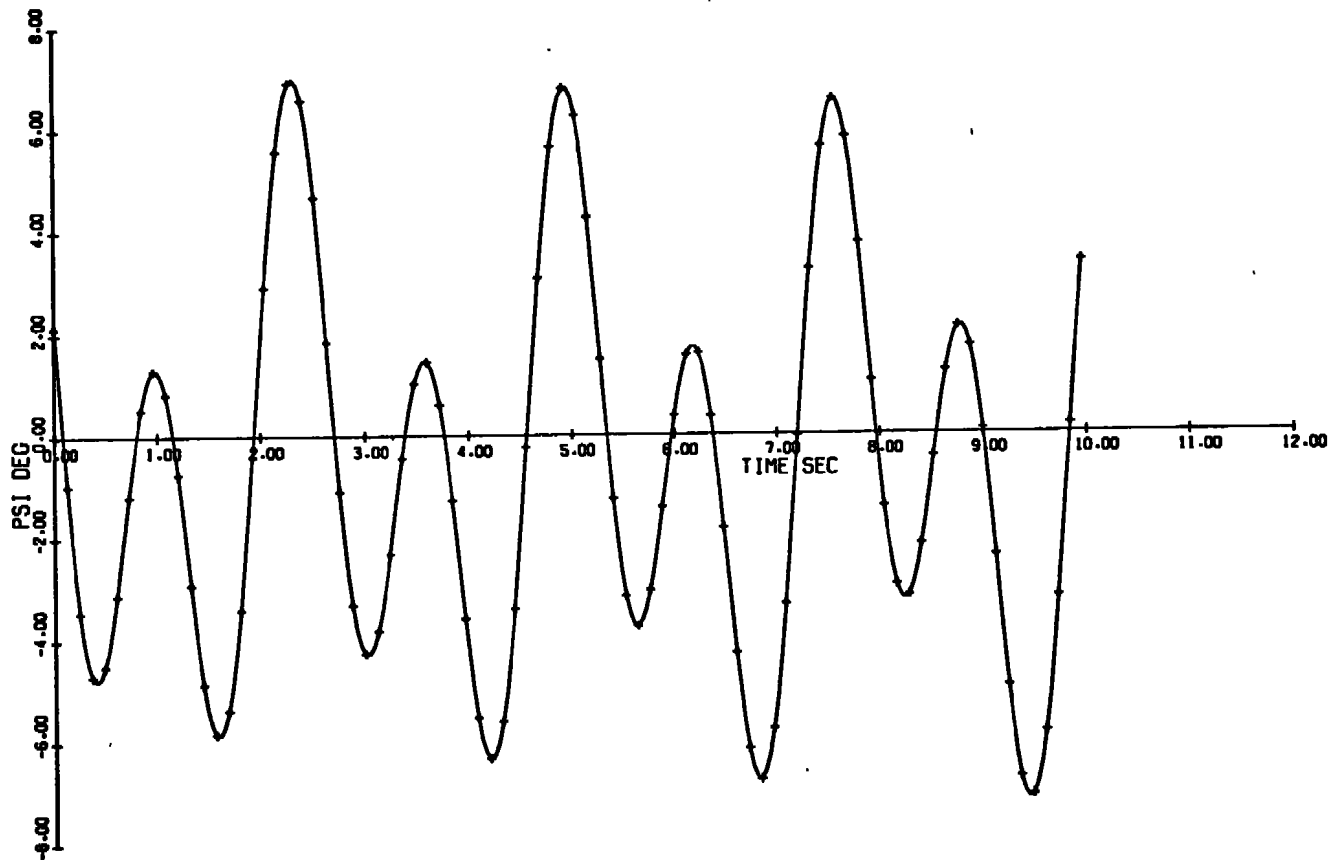


g. Fit of calculated solution to experimental data
in ψ, θ plane, time increment 6.36 to 8.6 sec
Figure 14. Concluded.

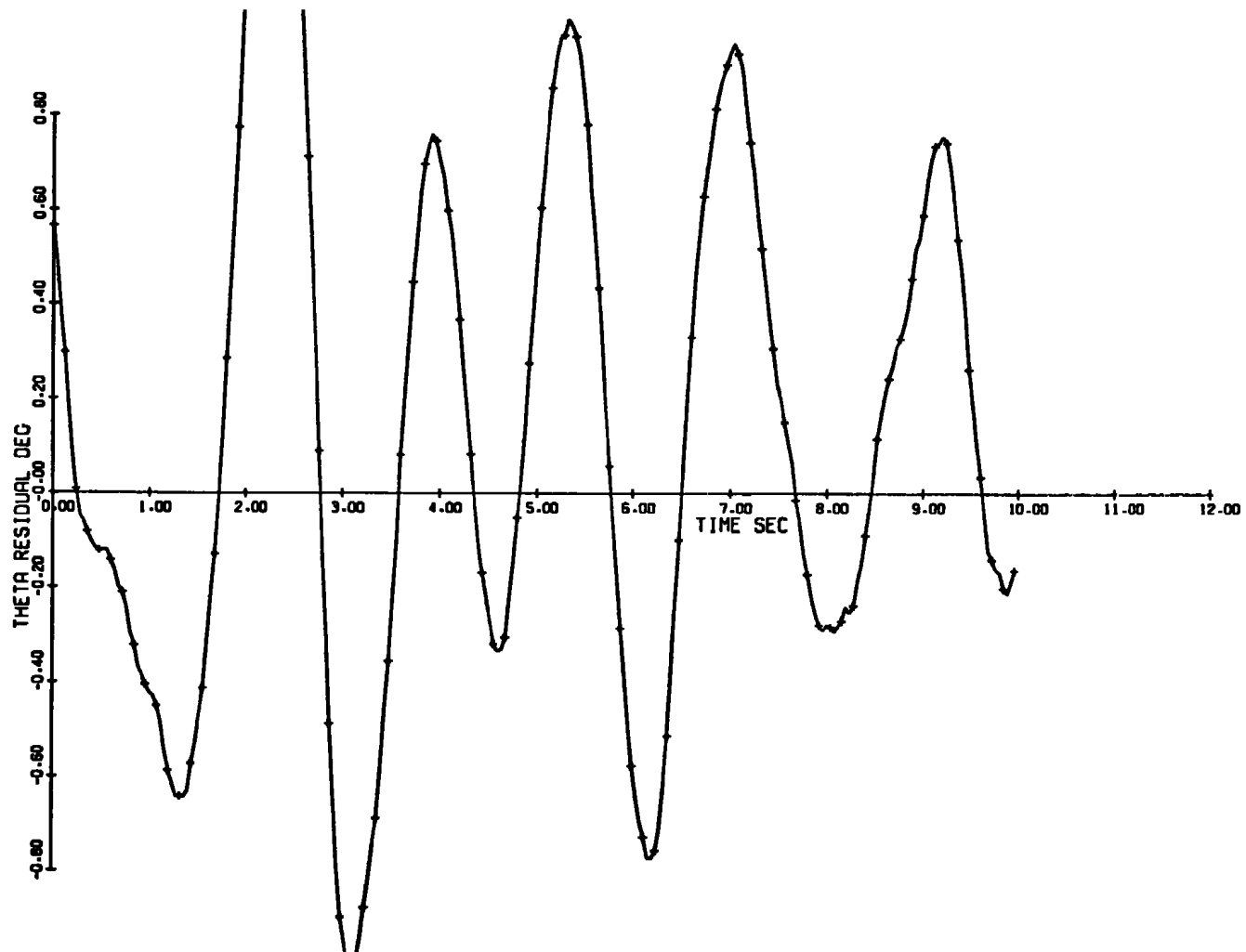


a. Computed θ versus time

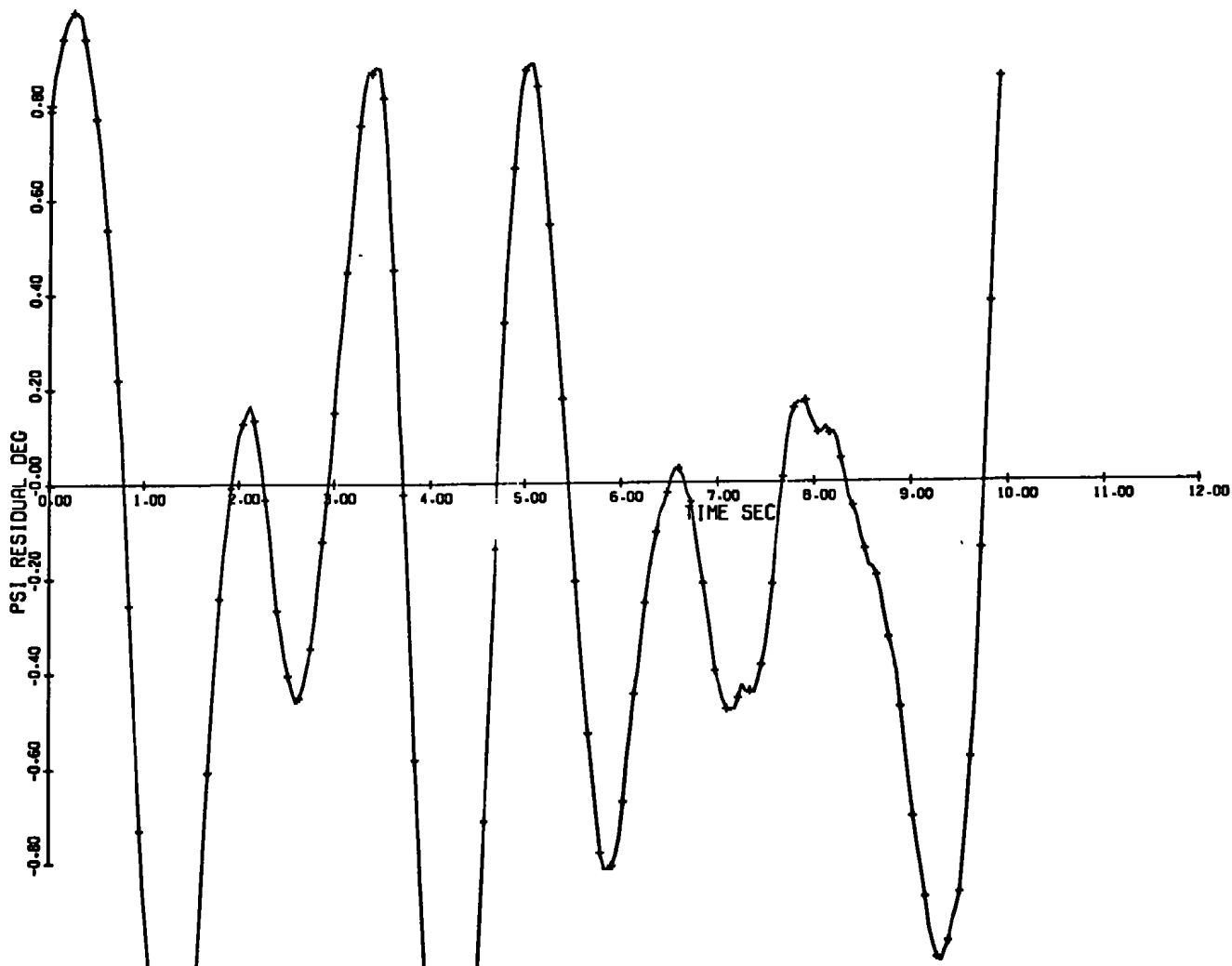
Figure 15. Bench test results for high angle of attack and 400-psi bearing pressure.



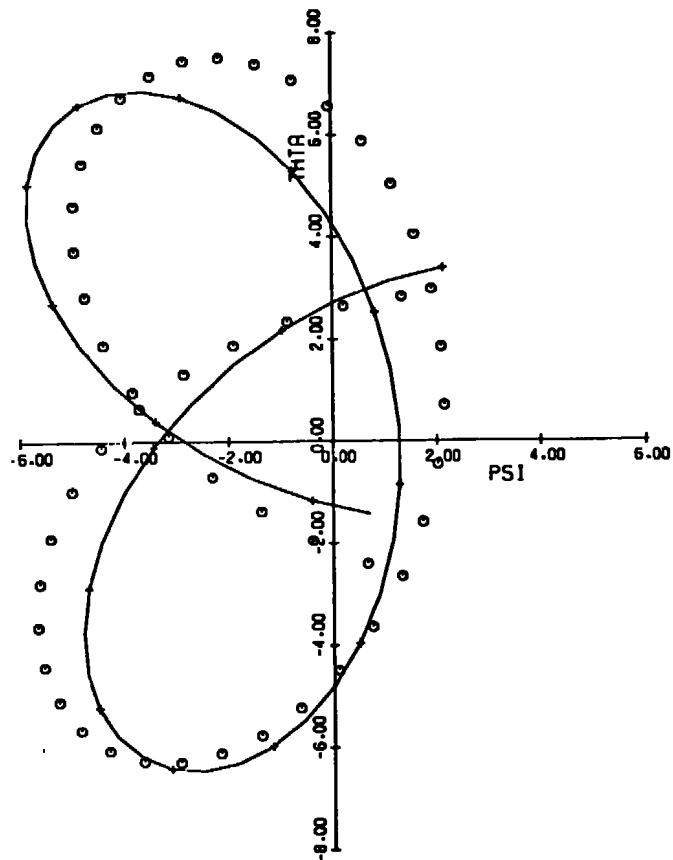
b. Computed ψ versus time
Figure 15. Continued.



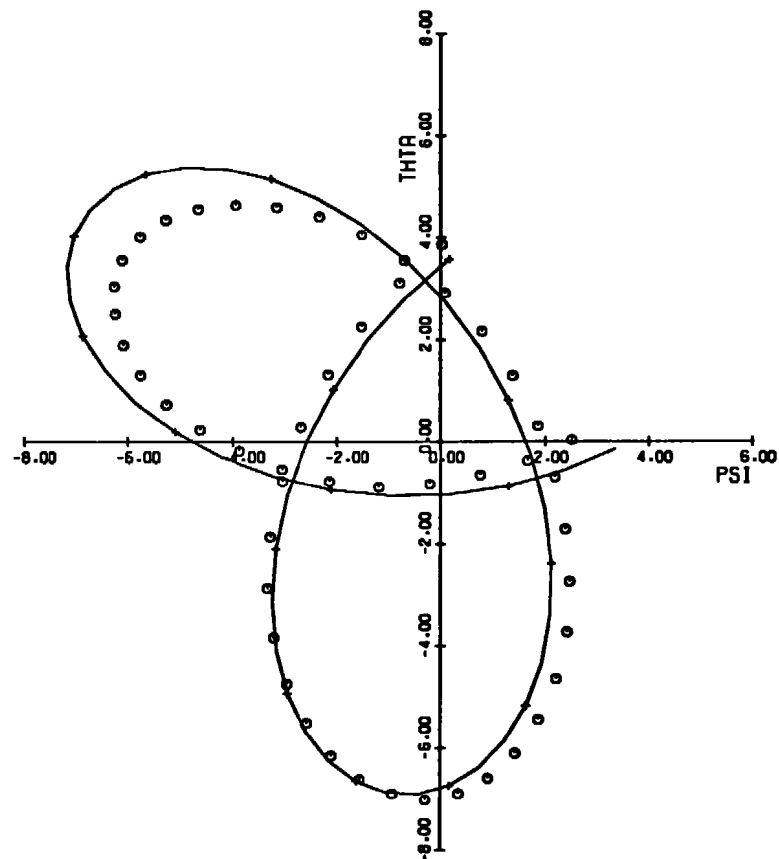
c. Residual in θ versus time
Figure 15. Continued.



d. Residual in ψ versus time
Figure 15. Continued.

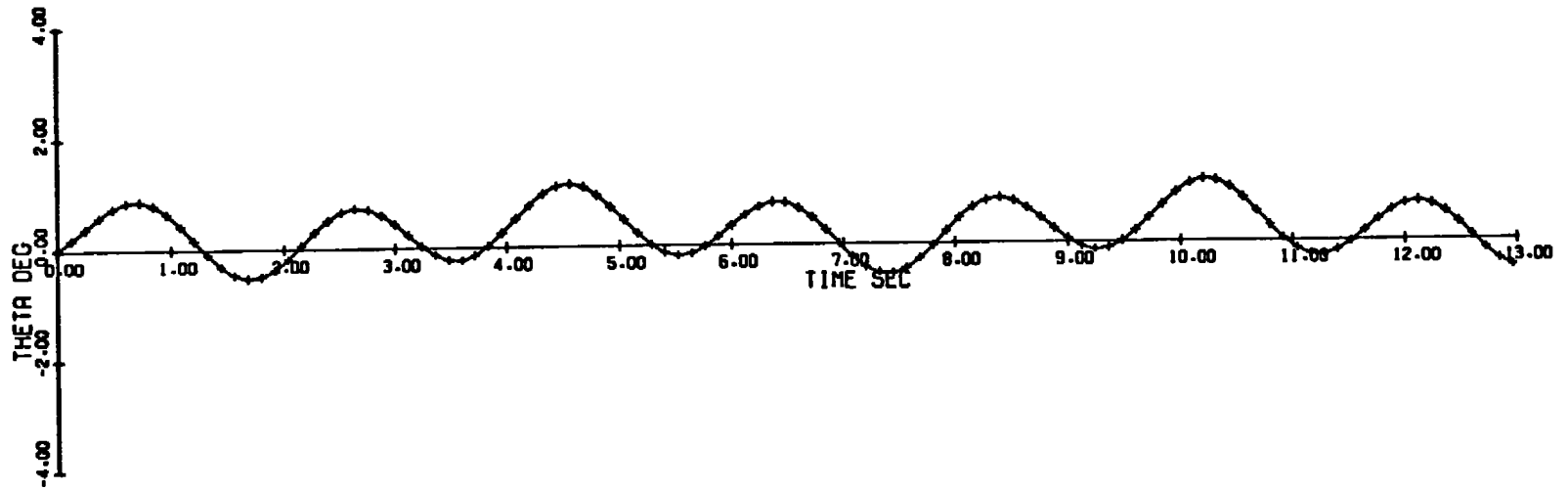


e. Fit of calculated solution to experimental data in ψ, θ plane, time increment 0 to 1.96 sec

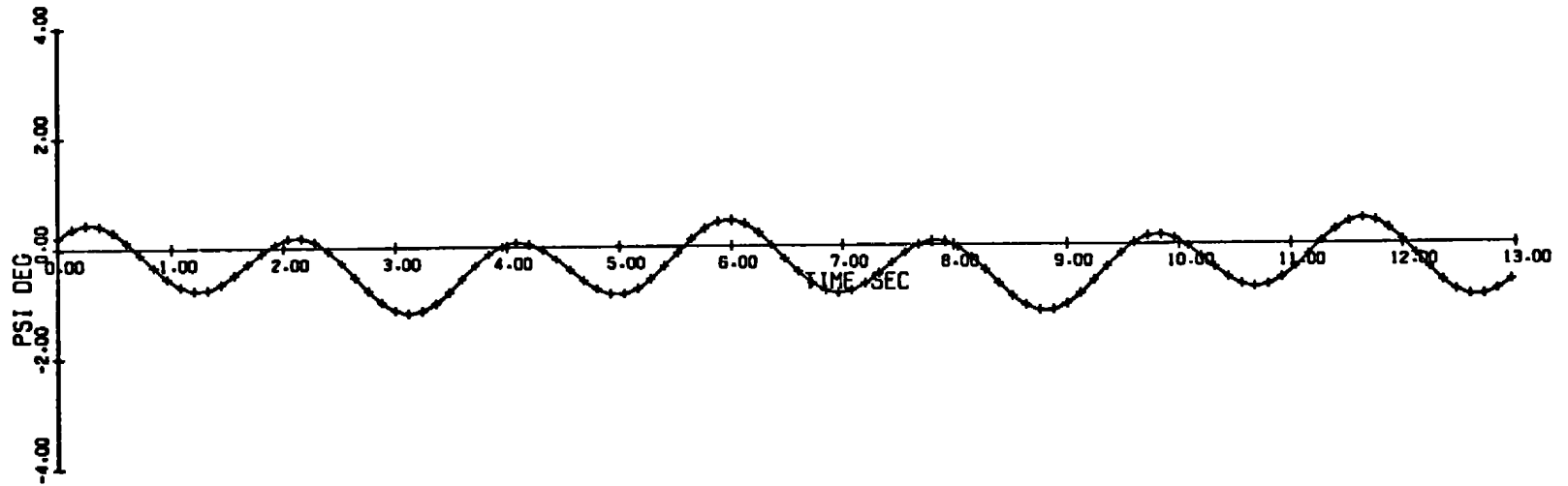


f. Fit of calculated solution to experimental data in ψ, θ plane, time increment 7.96 to 9.96 sec

Figure 15. Concluded.

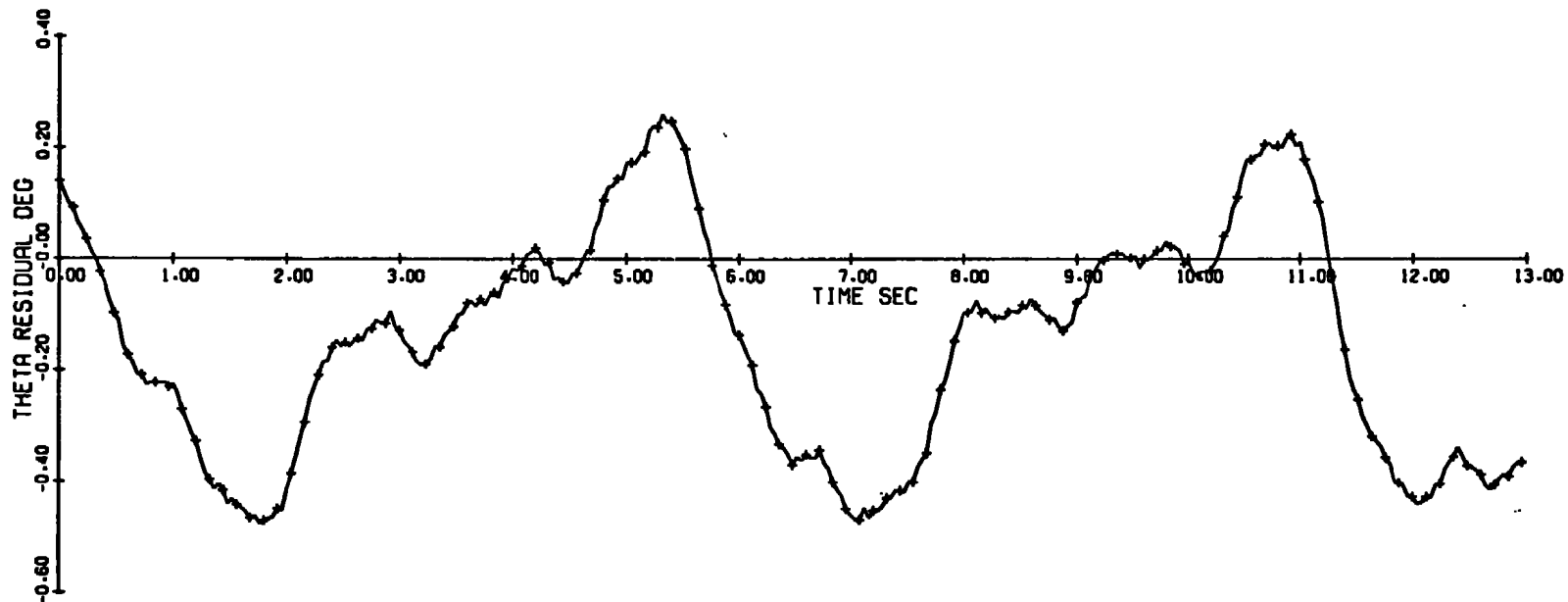


a. Computed θ versus time

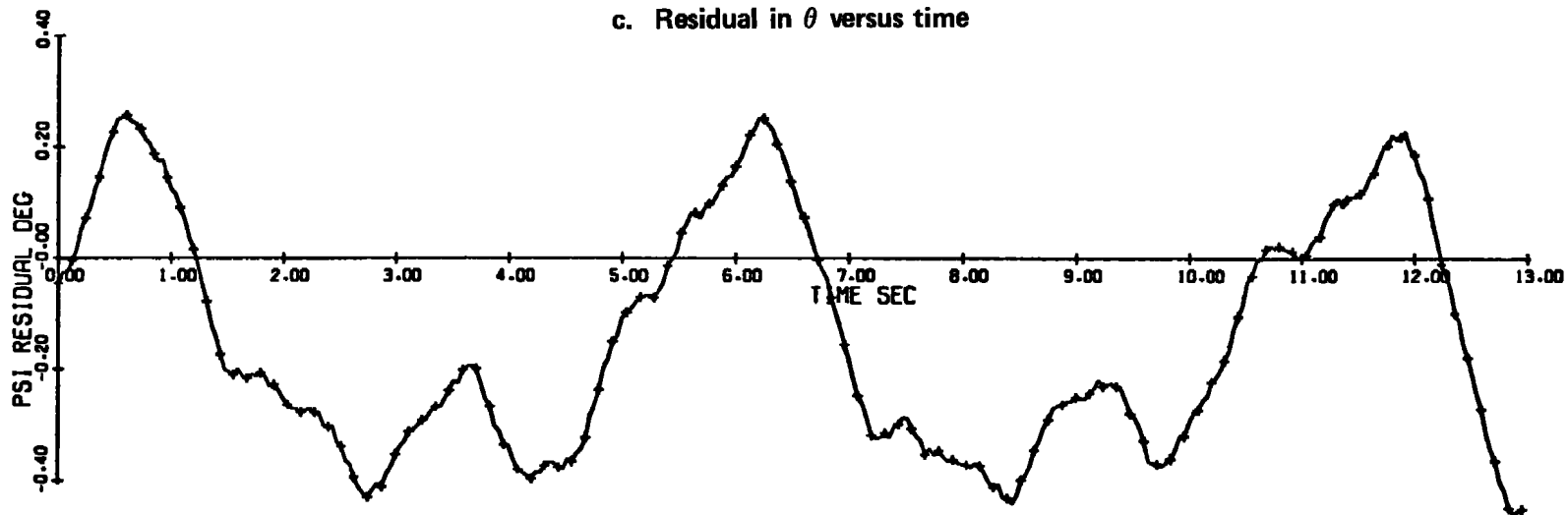


b. Computed ψ versus time

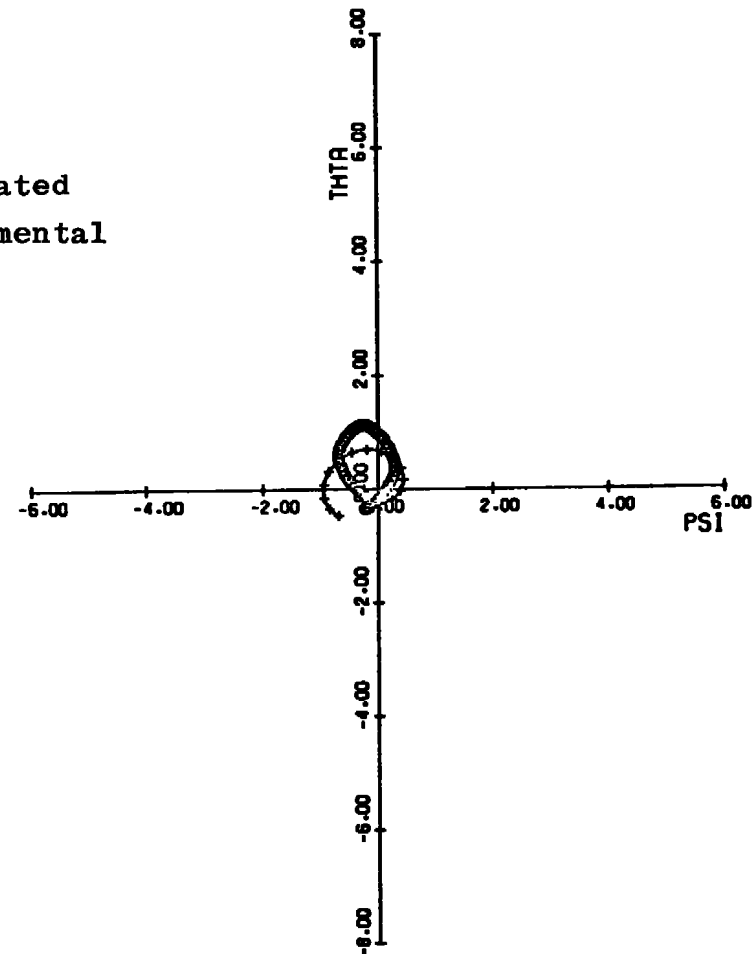
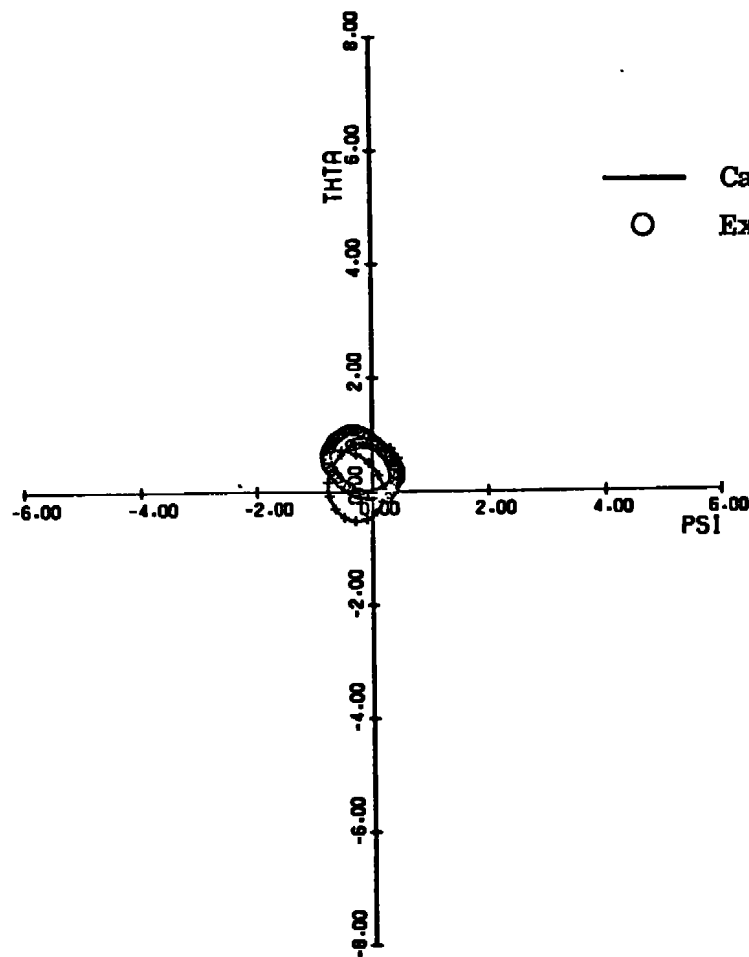
Figure 16. Bench test results for small angle of attack and 400-psi bearing pressure.



c. Residual in θ versus time



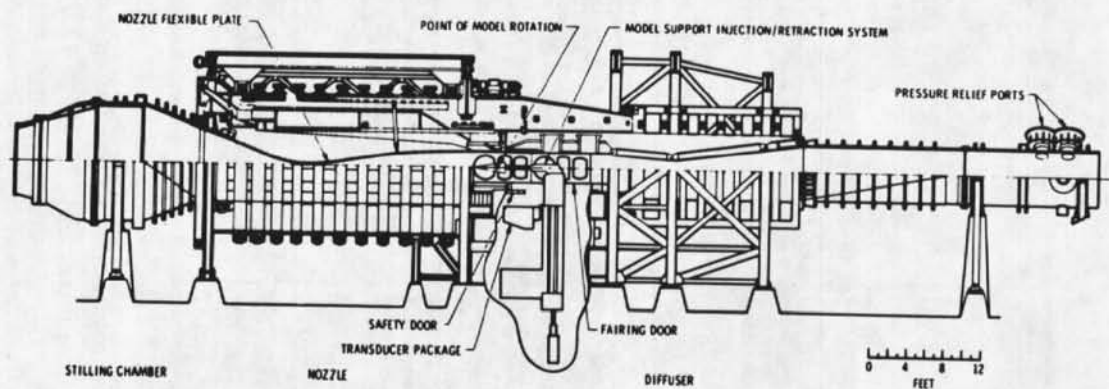
d. Residual in ψ versus time
Figure 16. Continued.



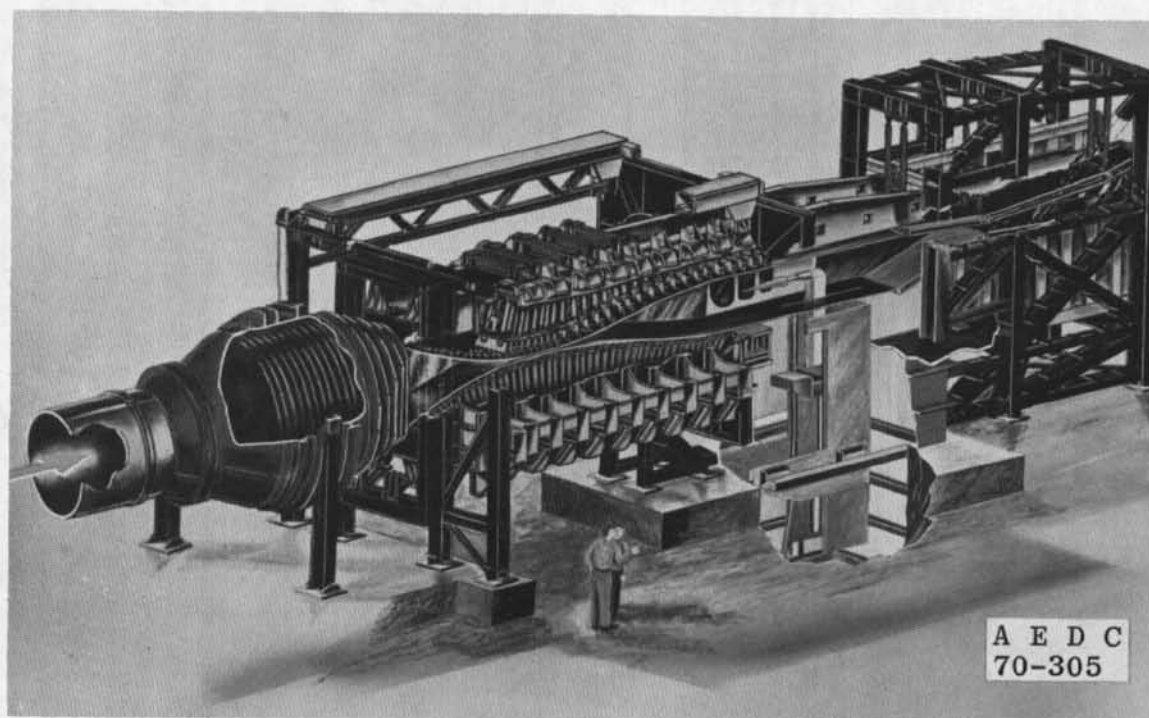
e. Fit of calculated solution to experimental data
in ψ, θ plane, time increment 0 to 2.76 sec

f. Fit of calculated solution to experimental data
in ψ, θ plane, time increment 11.16 to 12.96 sec

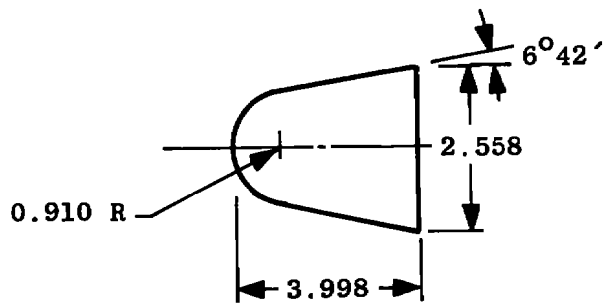
Figure 16. Concluded.



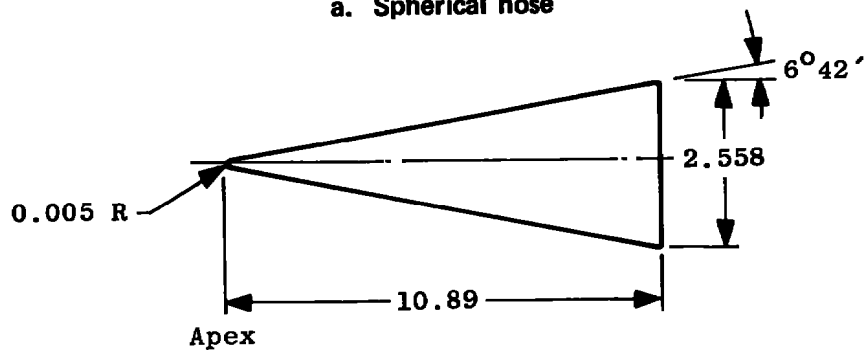
a. Tunnel assembly



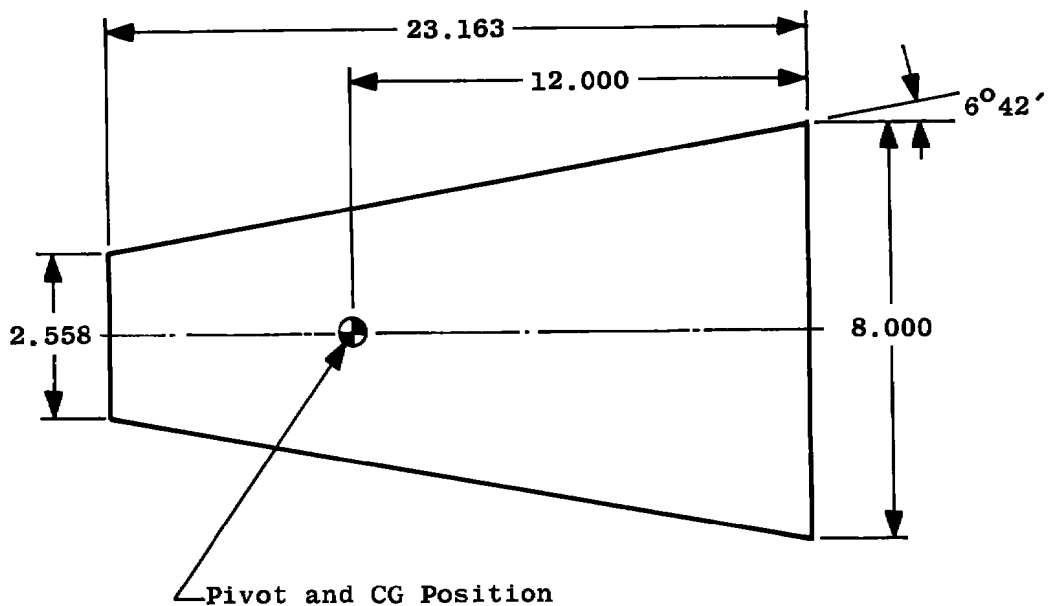
b. Tunnel test section
Figure 17. Tunnel A.



a. Spherical nose



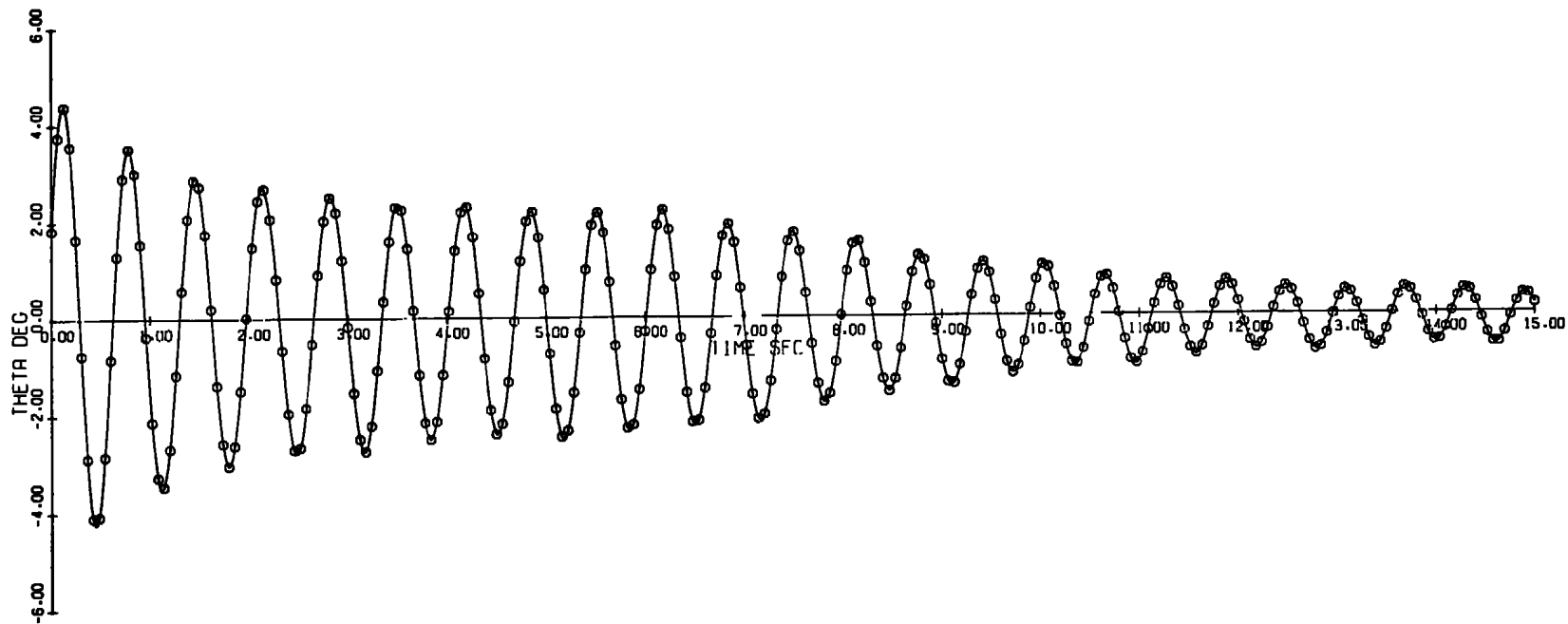
b. Sharp nose



Note: All Dimensions in Inches

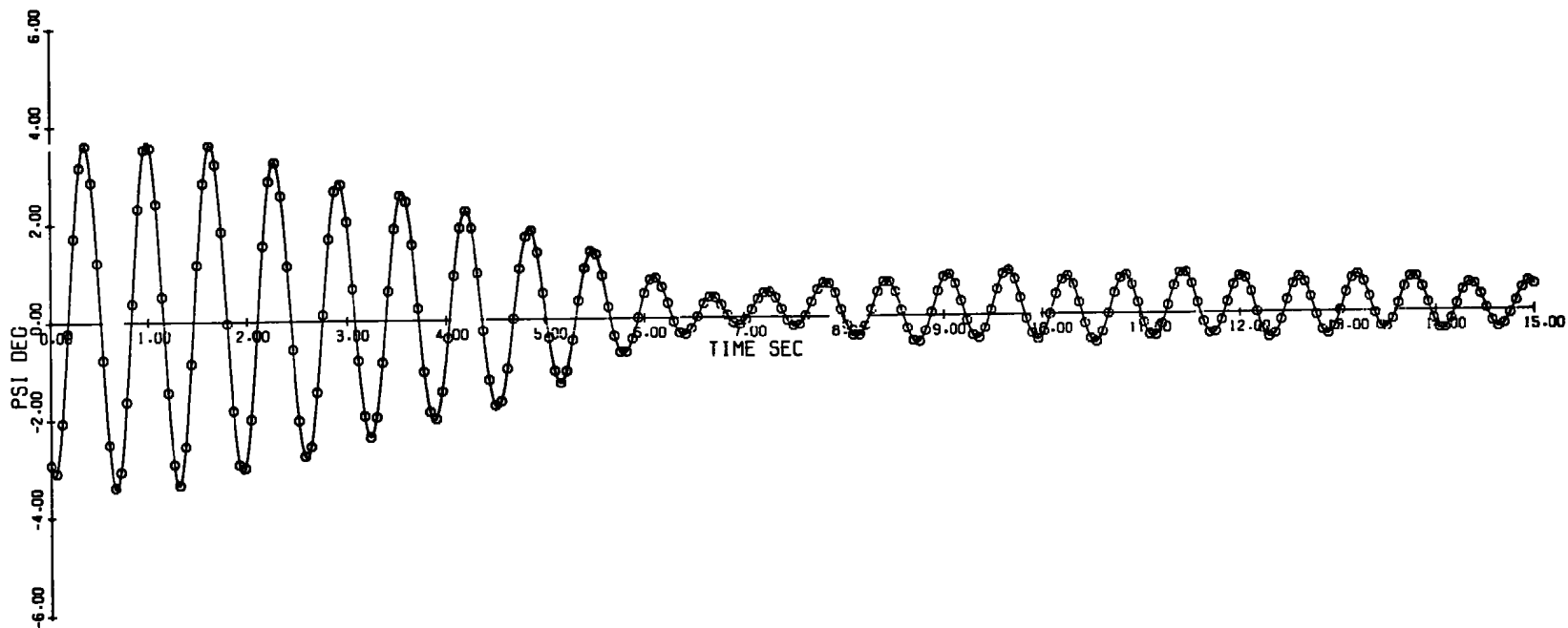
c. Aft body

Figure 18. Model schematic.

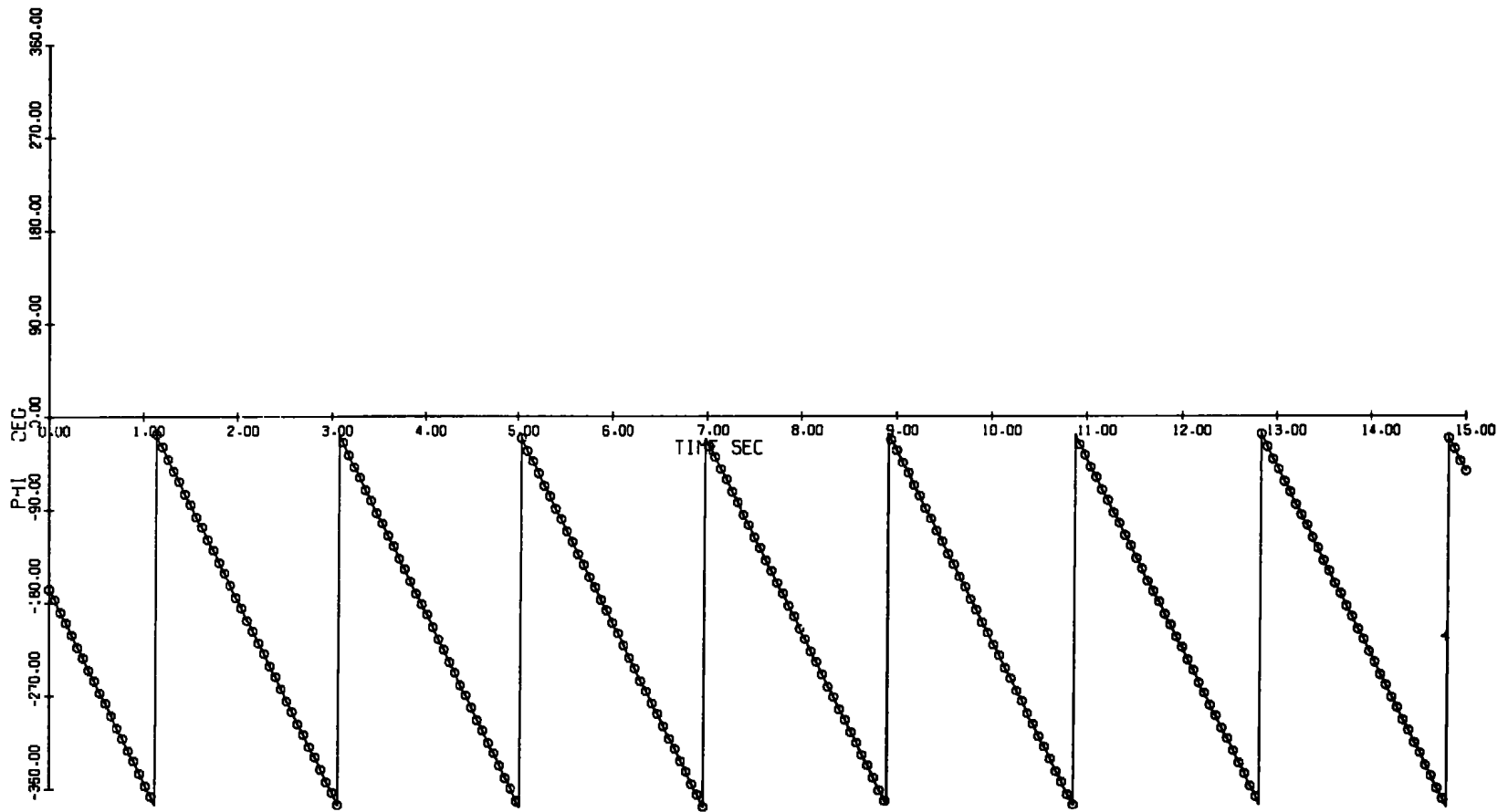


a. θ versus time

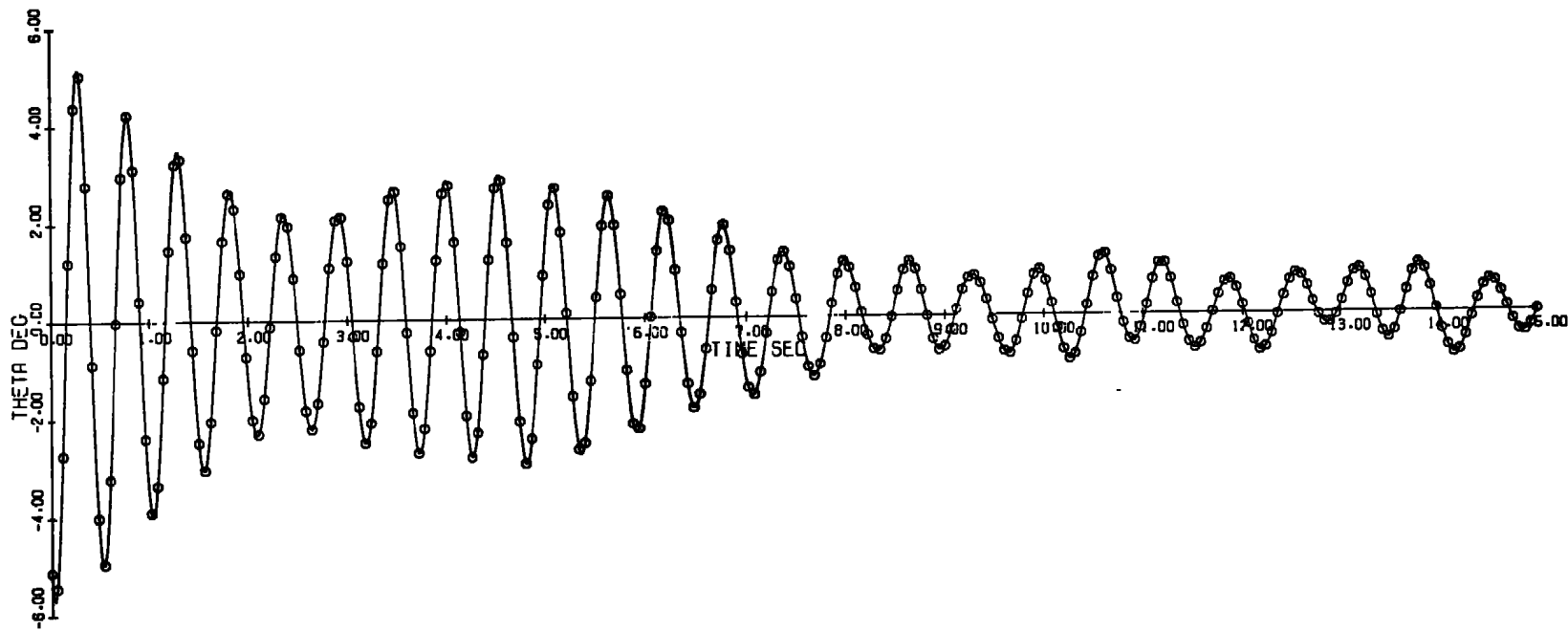
Figure 19. Experimental 6.7-deg sharp cone data taken in Tunnel A at Mach number 4.02 and 3.6 million per foot Reynolds number.



b. ψ versus time
Figure 19. Continued.

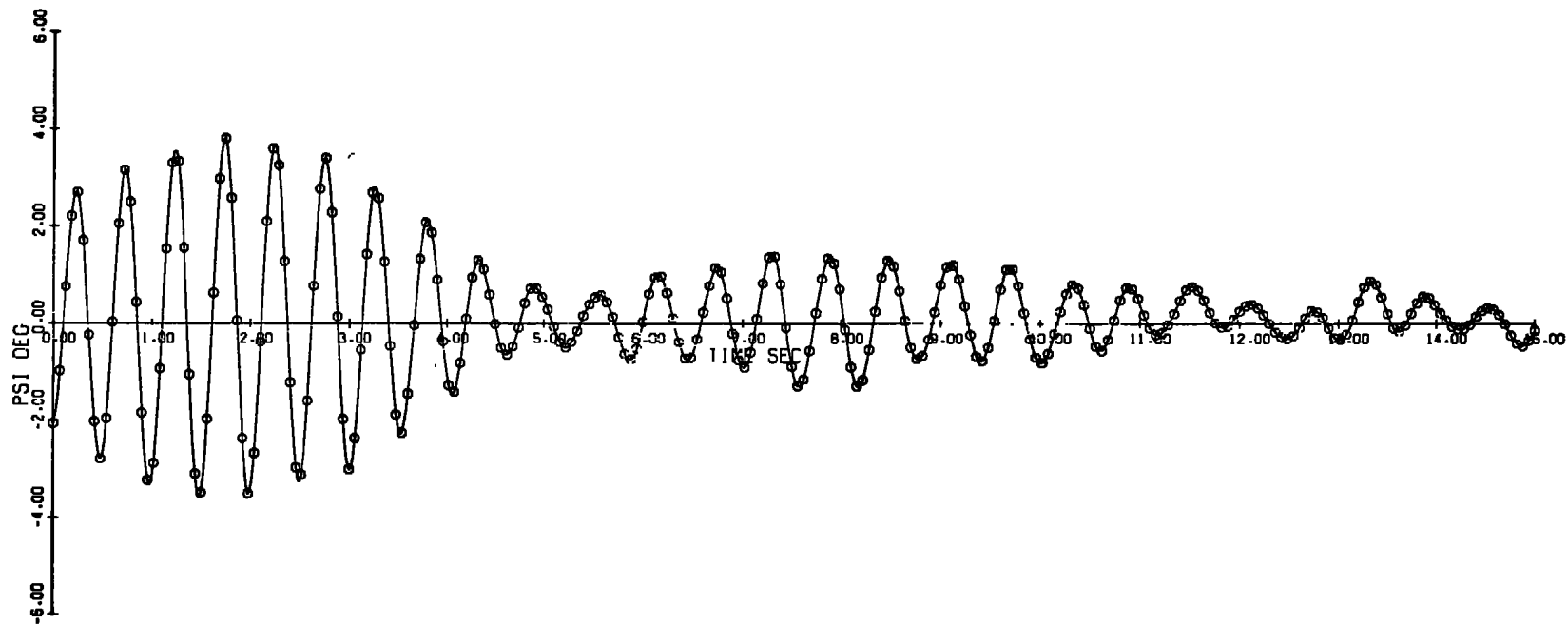


c. ϕ versus time
Figure 19. Concluded.



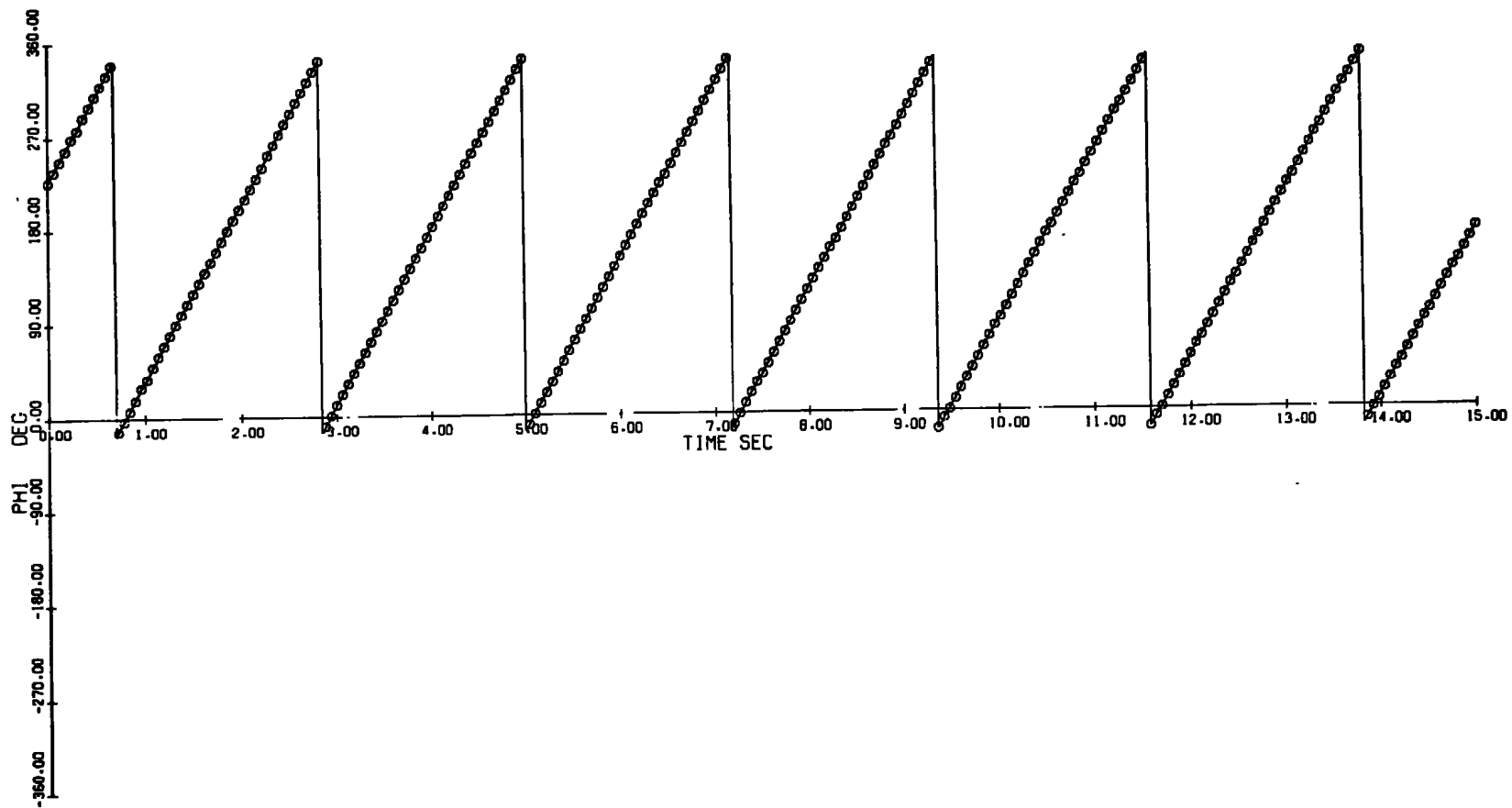
a. θ versus time

Figure 20. Experimental $d_N/d = 0.2275$, $\theta_c = 6.7$ -deg sphere cone data taken in Tunnel A at Mach number 4.02 and 3.6 million per foot Reynolds number.

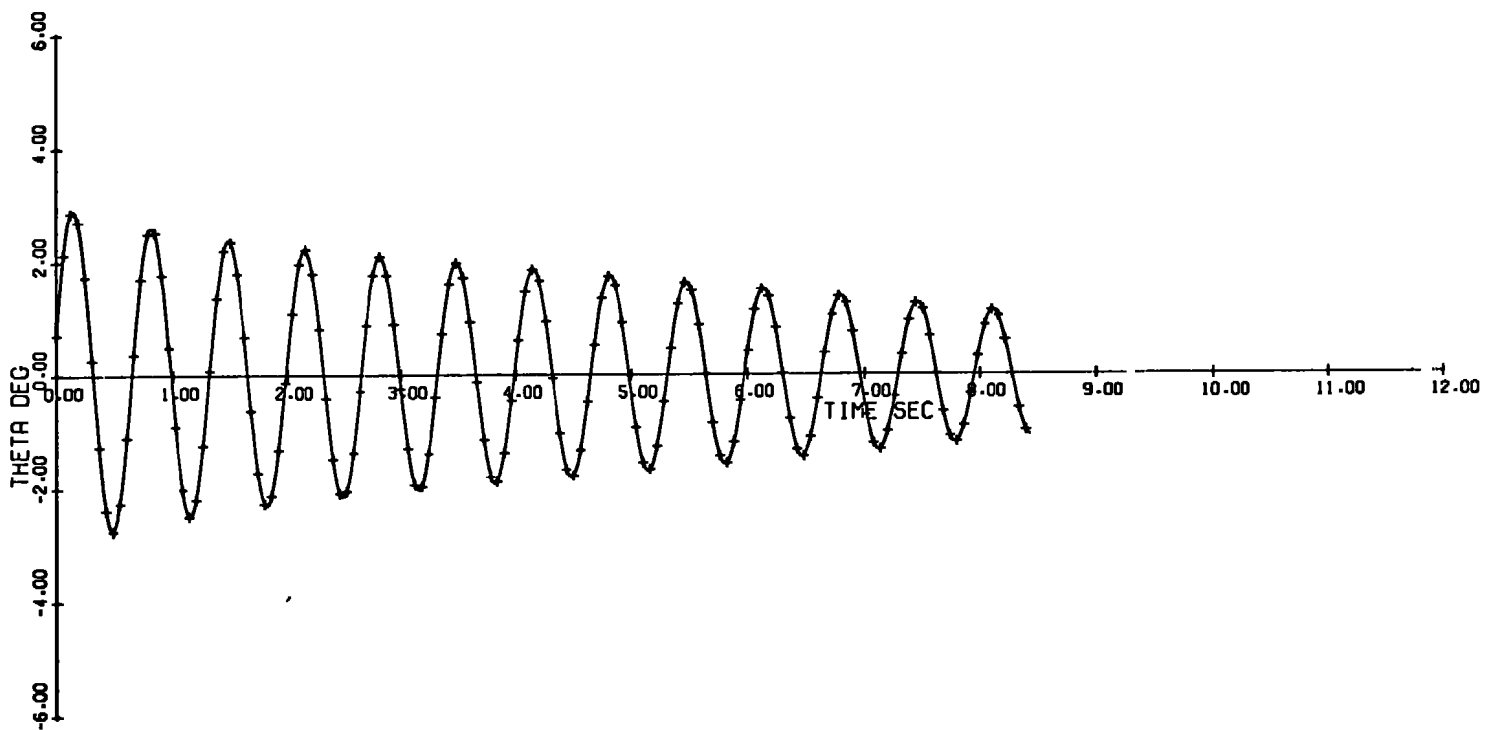


b. ψ versus time
Figure 20. Continued.

08

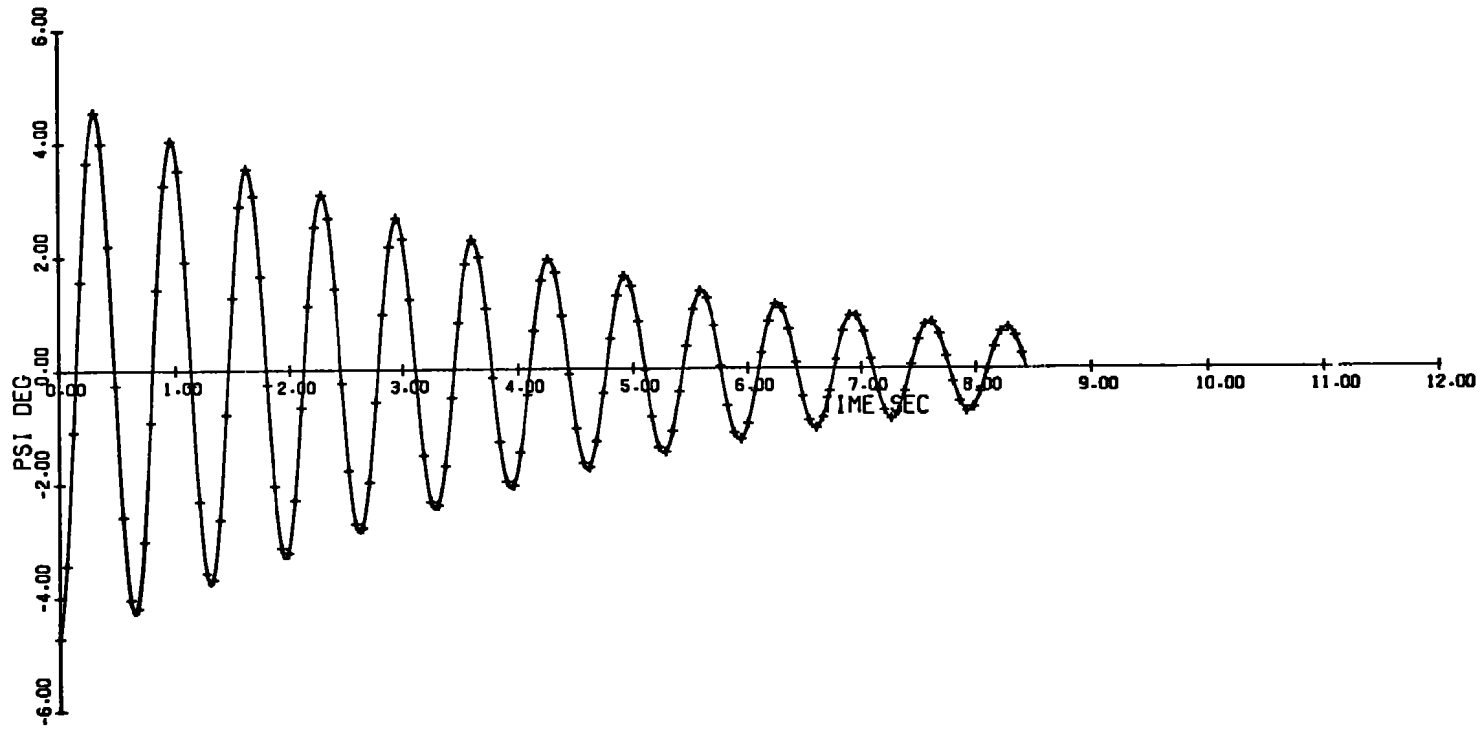


c. ϕ versus time
Figure 20. Concluded.

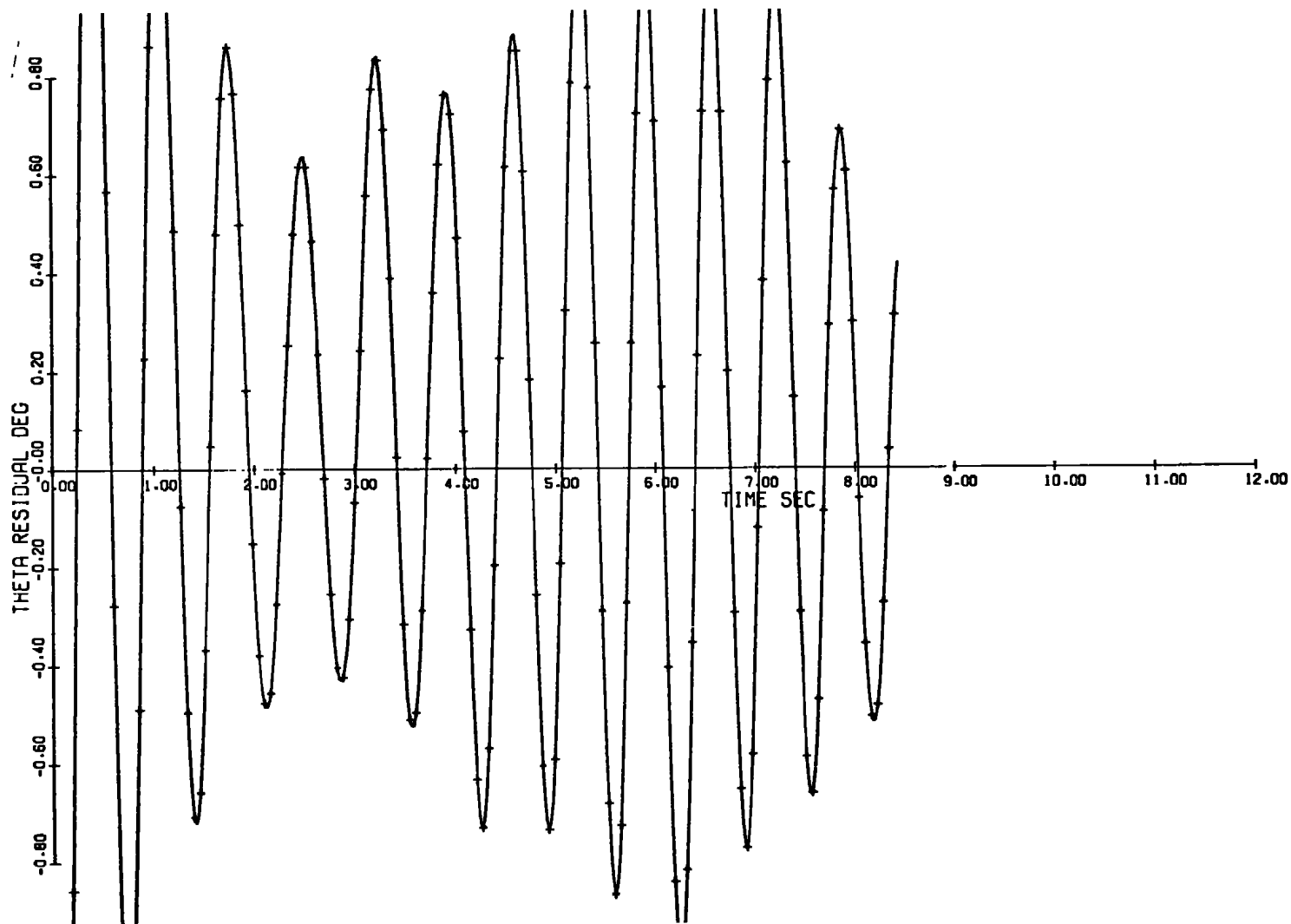


a. Computed θ versus time

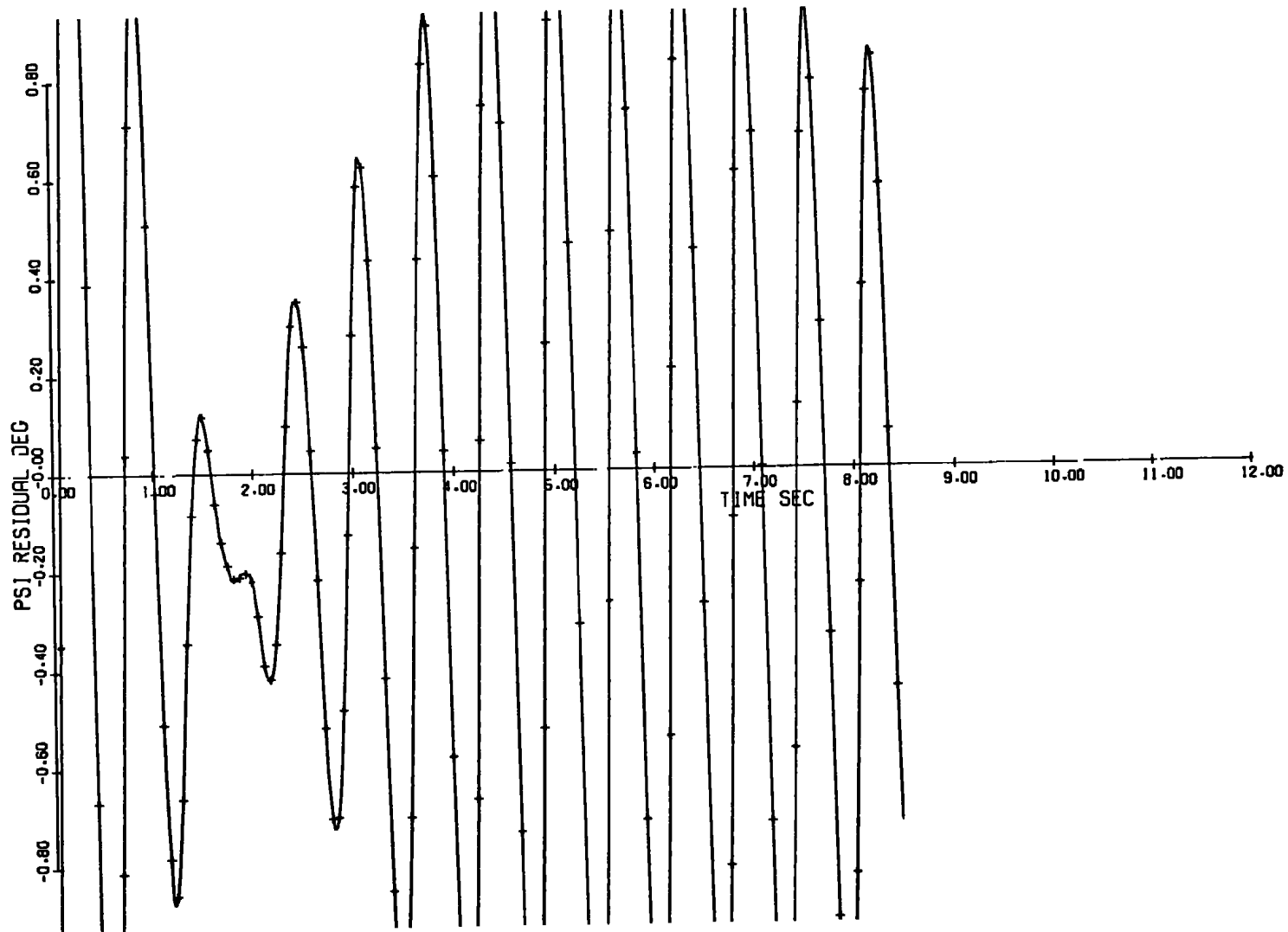
Figure 21. Graphical solution of sharp cone data given in Fig. 19 for a fit interval of 8.44 sec with no tunnel-fixed process noise.



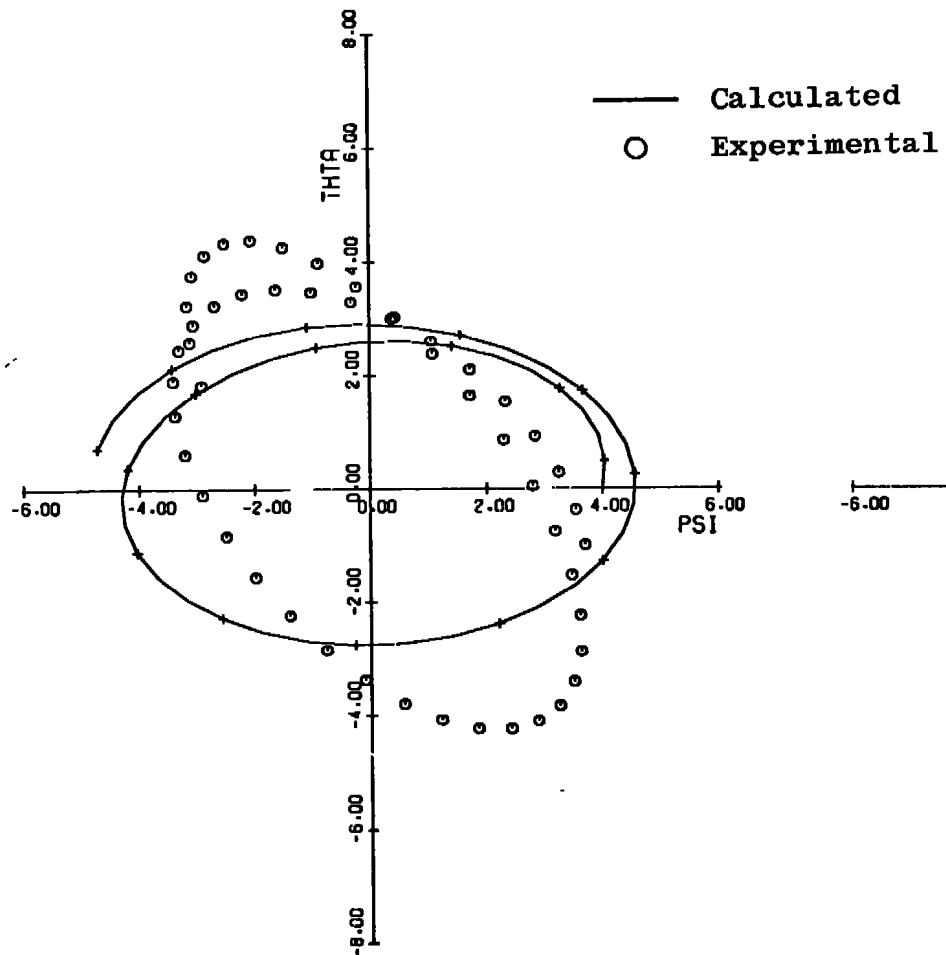
b. Computed ψ versus time
Figure 21. Continued.



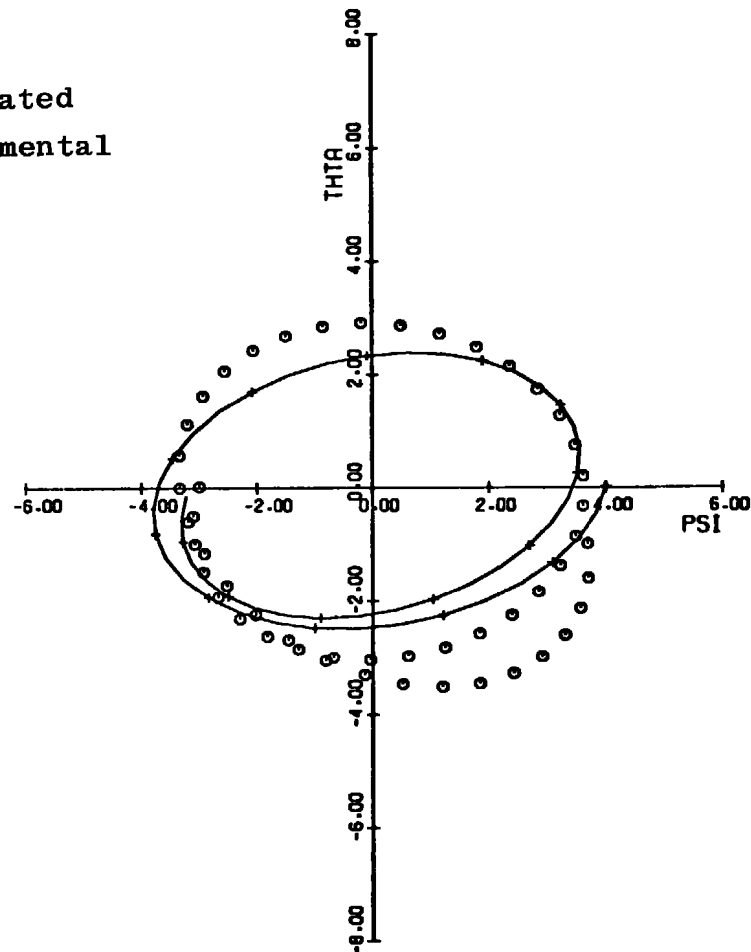
c. Residual in θ versus time
Figure 21. Continued.



d. Residual in ψ versus time
Figure 21. Continued.

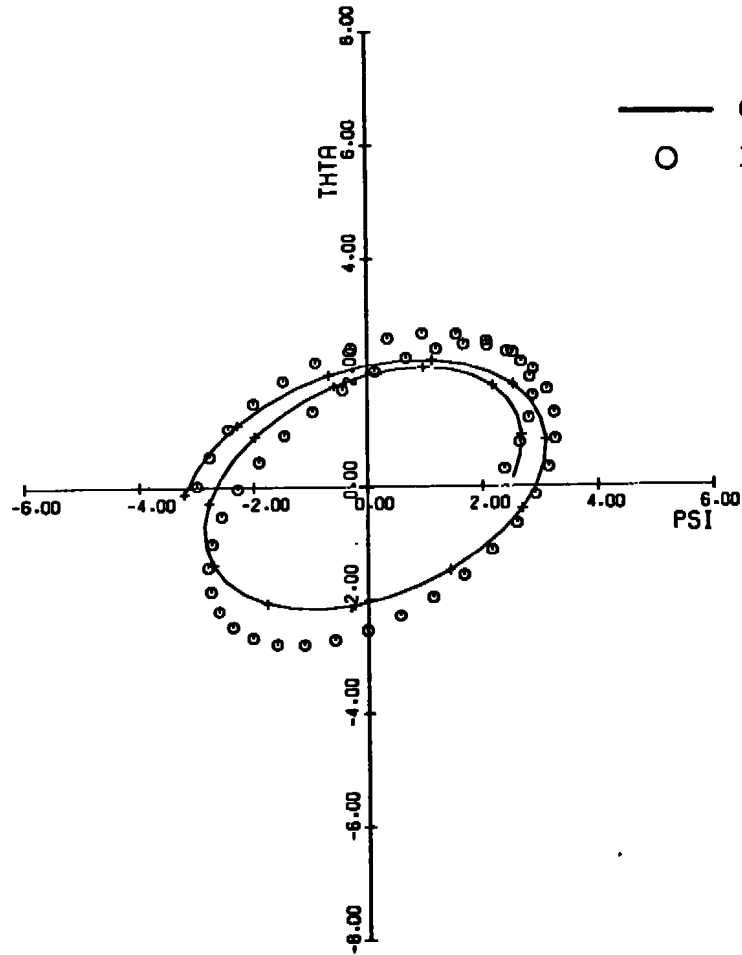


e. Fit of calculated solution to experimental data
in ψ, θ plane, time increment 0 to 0.98 sec

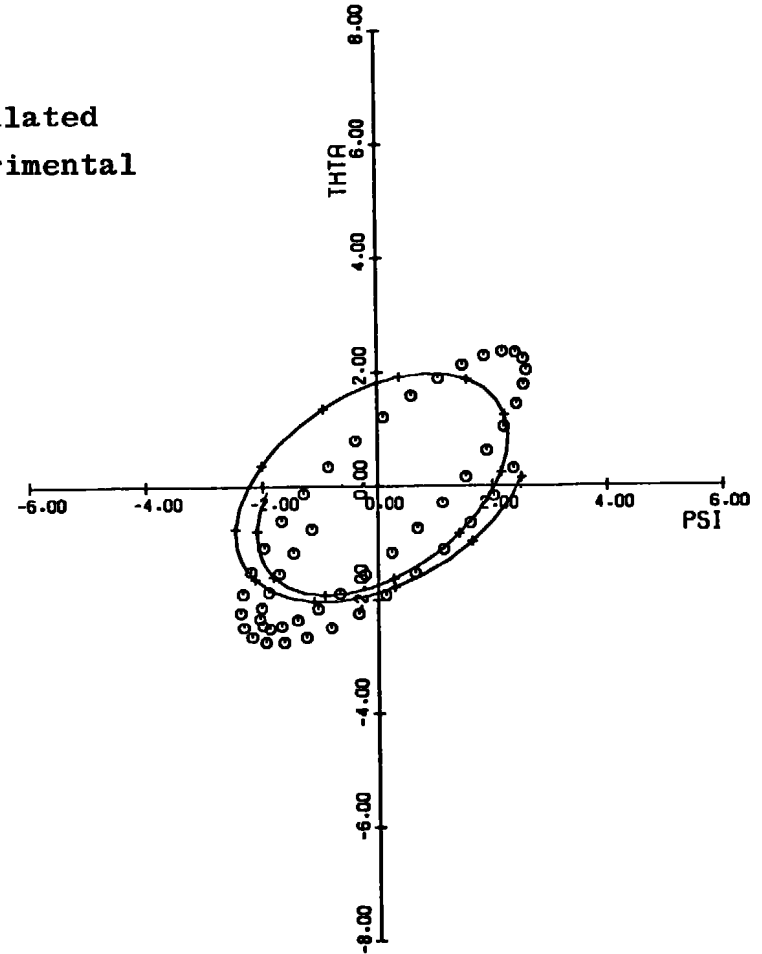


f. Fit of calculated solution to experimental data
in ψ, θ plane, time increment 0.98 to 1.98 sec

Figure 21. Continued.

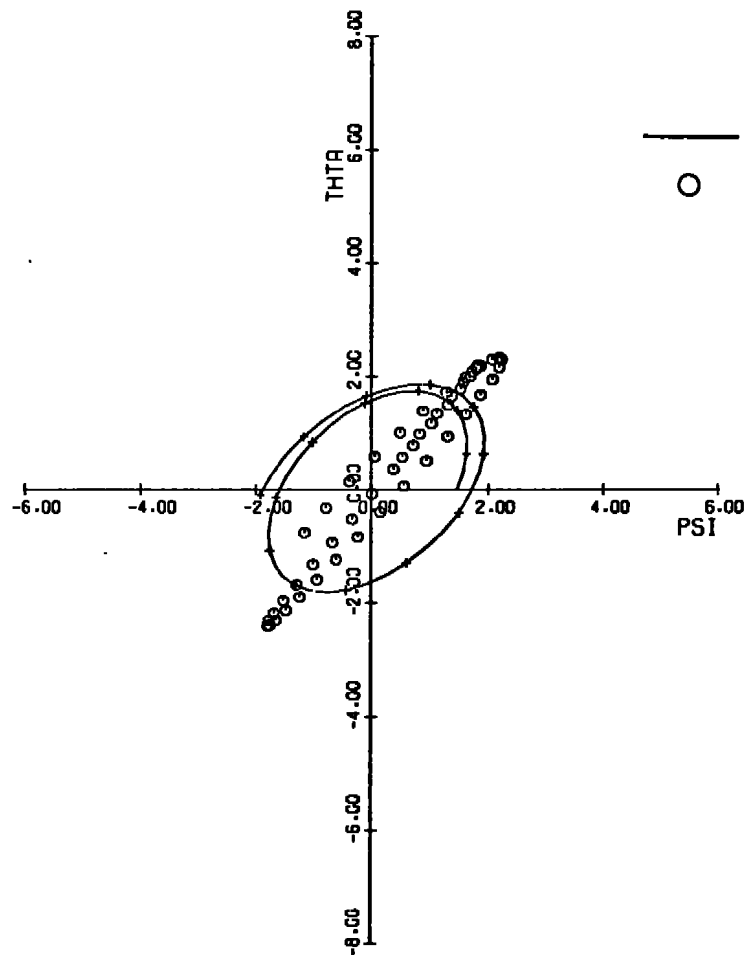


g. Fit of calculated solution to experimental data in ψ, θ plane, time increment 1.98 to 2.98 sec

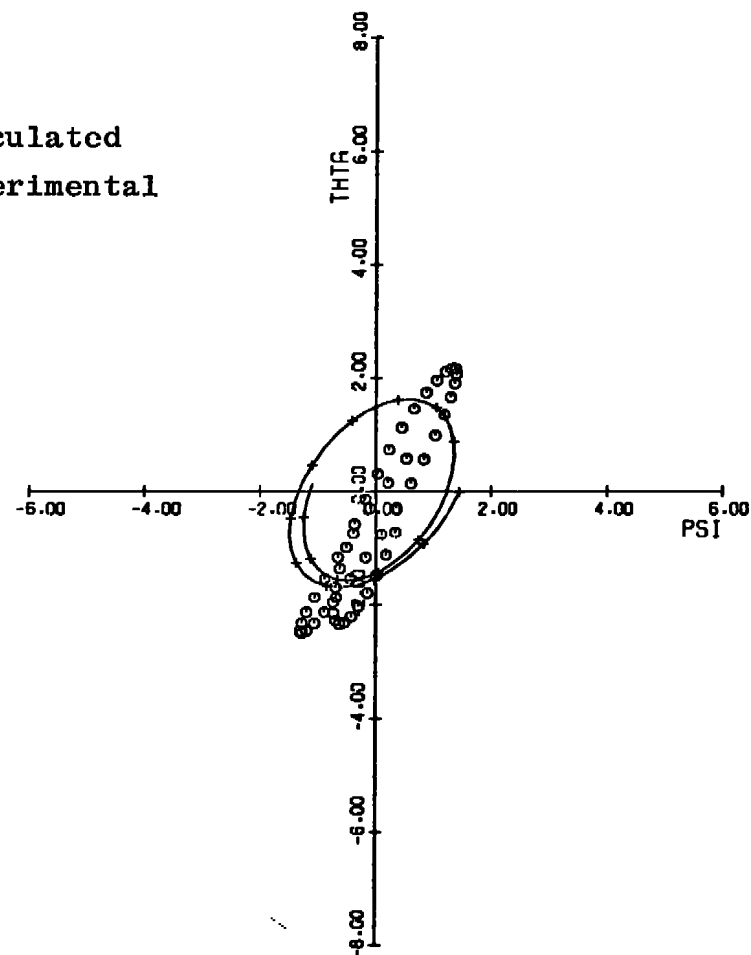


h. Fit of calculated solution to experimental data in ψ, θ plane, time increment 2.98 to 3.98 sec

Figure 21. Continued.

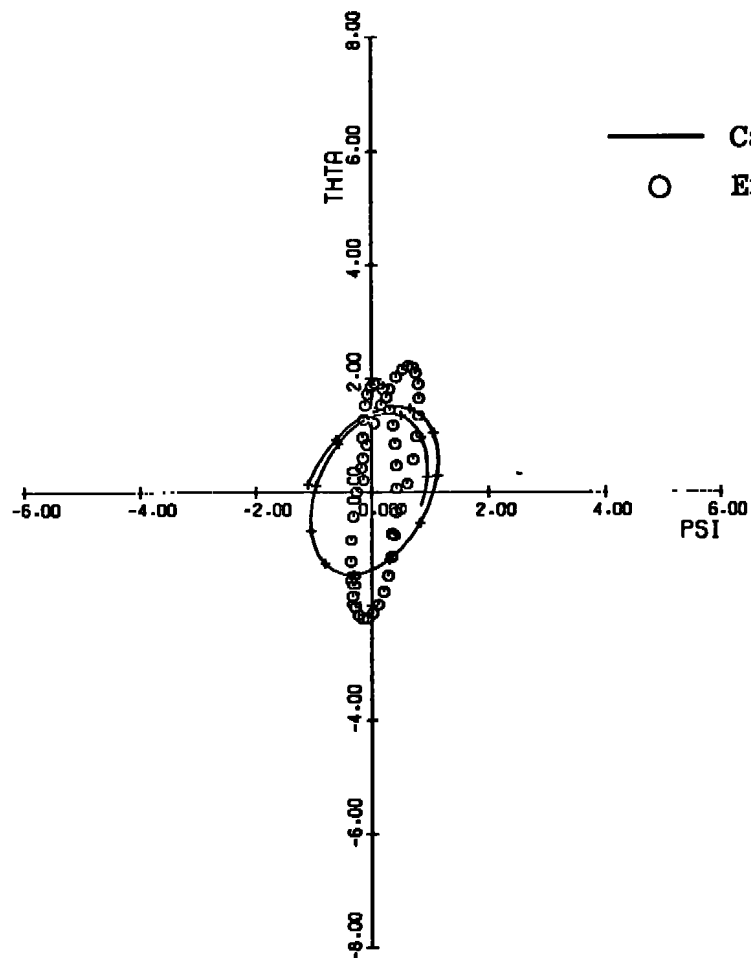


i. Fit of calculated solution to experimental data
in ψ, θ plane, time increment 3.98 to 4.98 sec

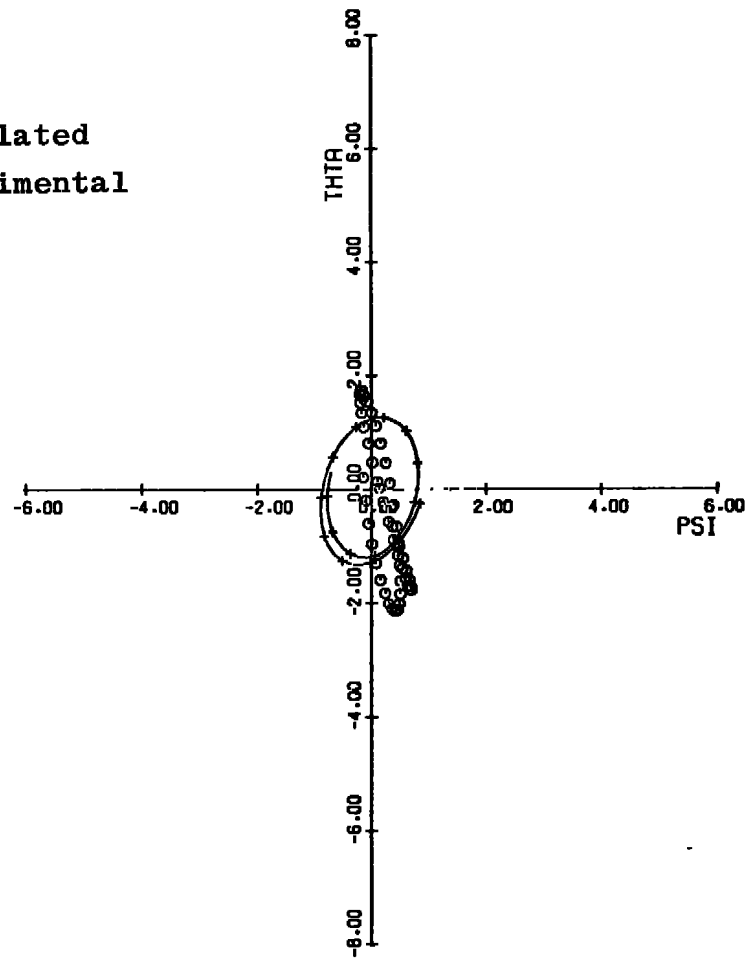


j. Fit of calculated solution to experimental data
in ψ, θ plane, time increment 4.98 to 5.98 sec

Figure 21. Continued.

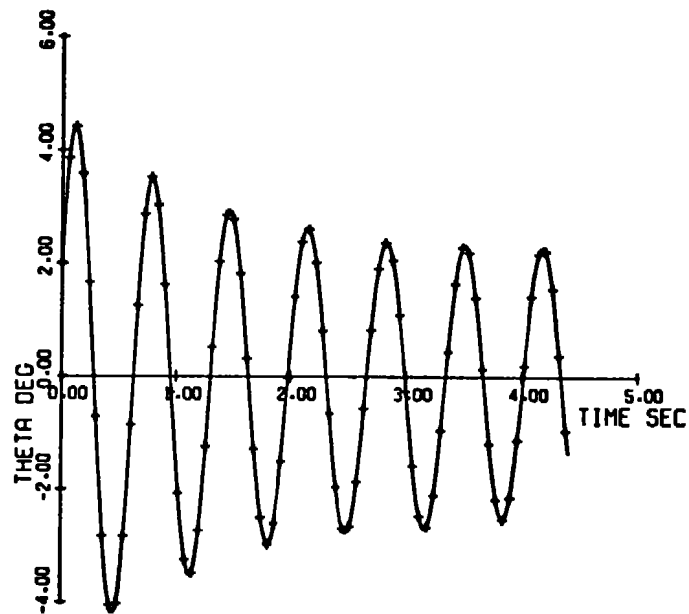


k. Fit of calculated solution to experimental data
in ψ , θ plane, time increment 5.98 to 6.98 sec

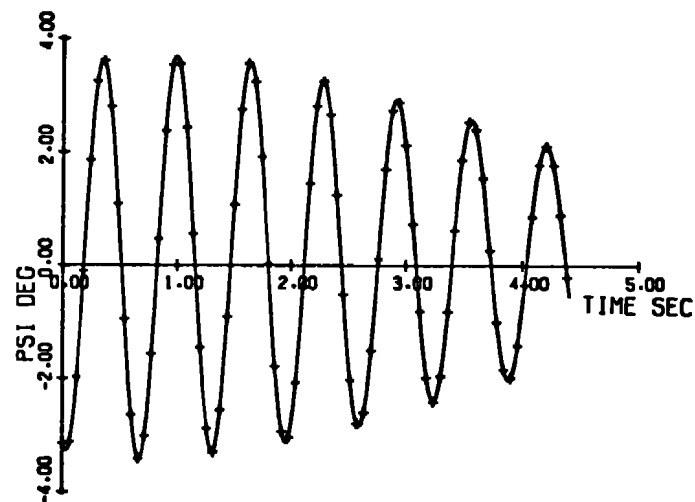


l. Fit of calculated solution to experimental data
in ψ , θ plane, time increment 6.98 to 7.98 sec

Figure 21. Concluded.

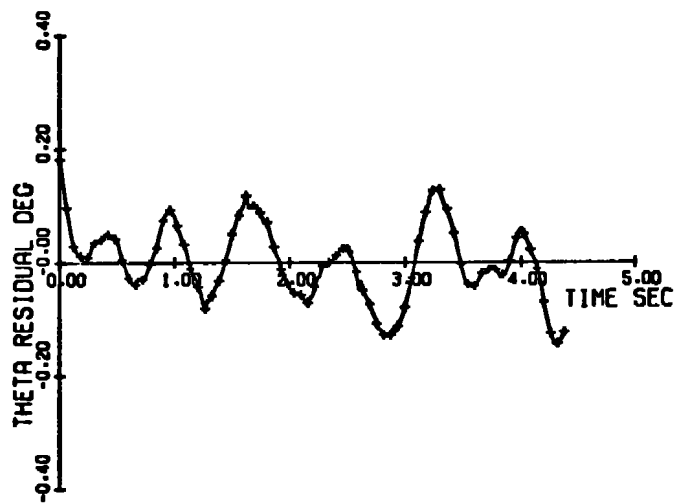


a. Computed θ versus time

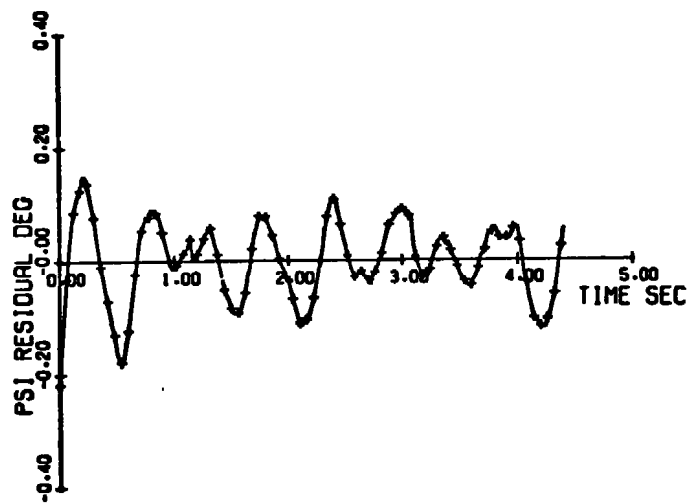


b. Computed ψ versus time

Figure 22. Graphical solution of sharp cone data given in Fig. 19 for a fit interval of 4.4 sec with fixed aerodynamics.

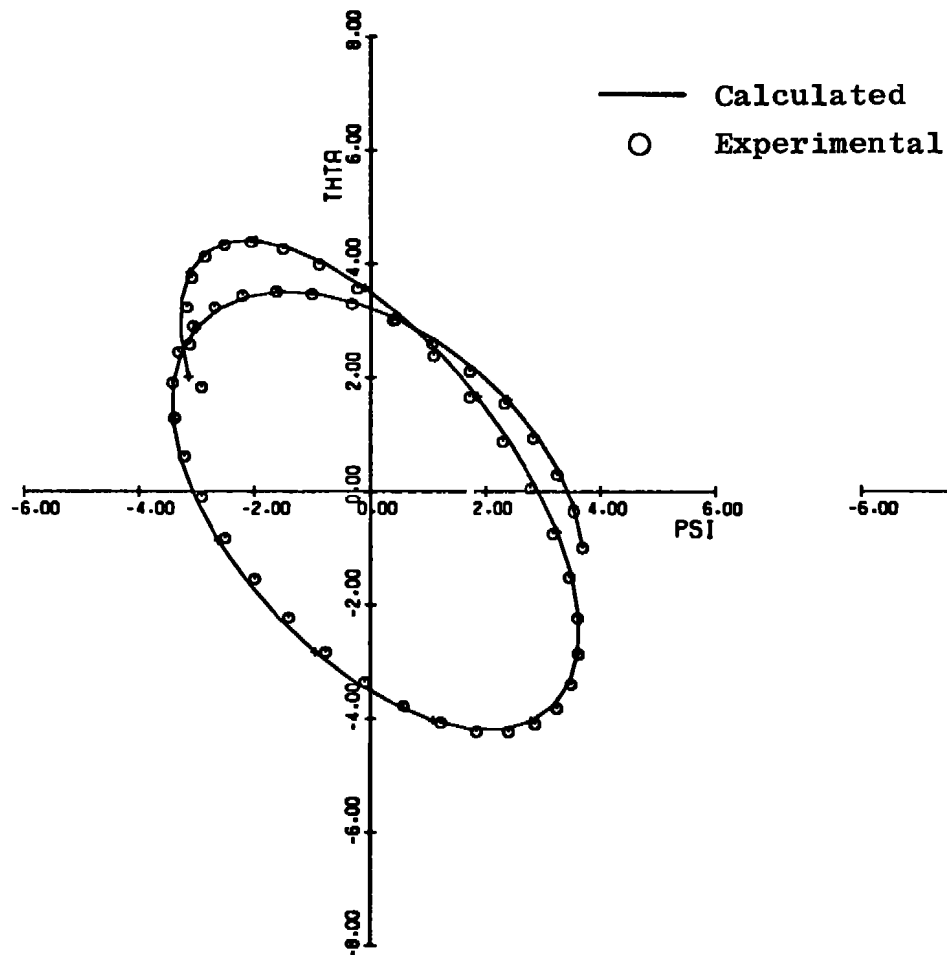


c. Residual in θ versus time

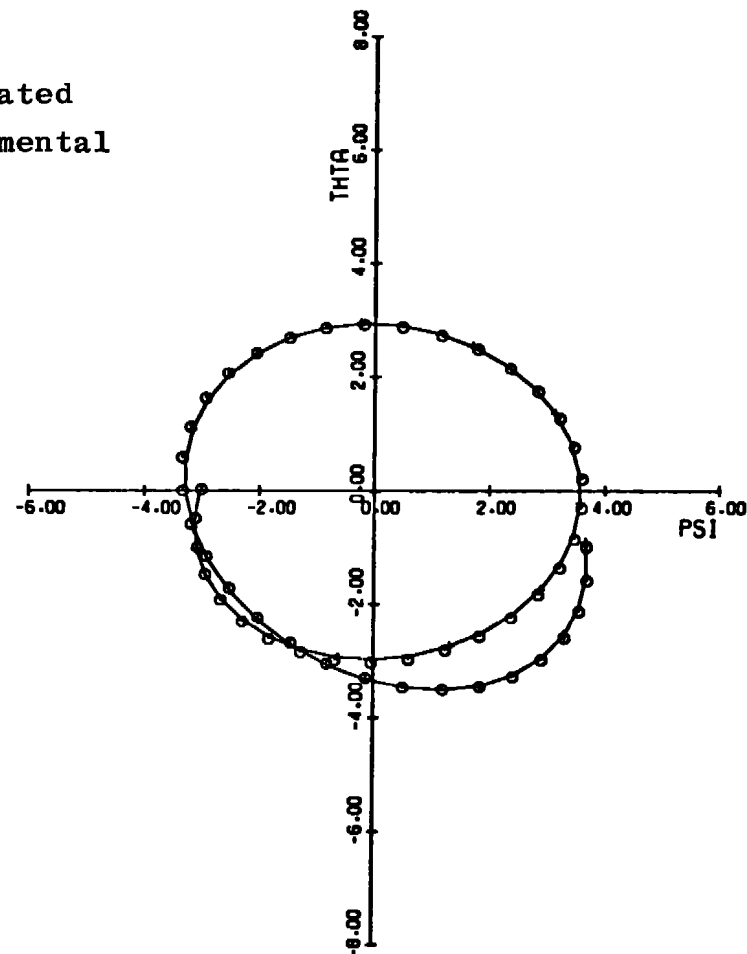


d. Residual in ψ versus time

Figure 22. Continued.

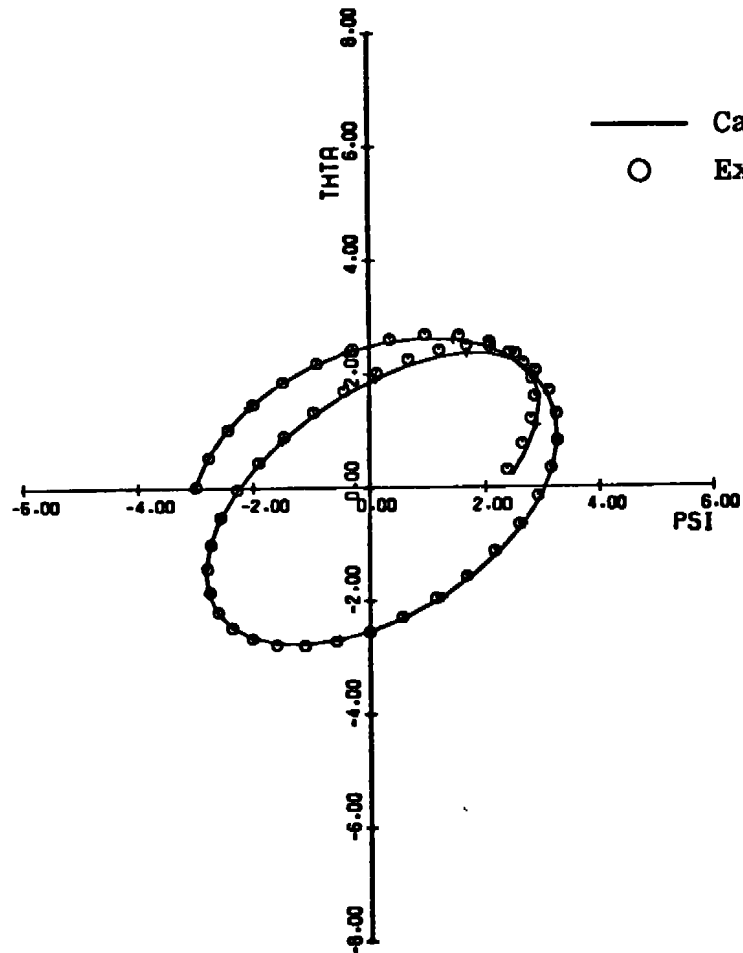


e. Fit of calculated solution to experimental data
in ψ, θ plane, time increment 0 to 0.98 sec

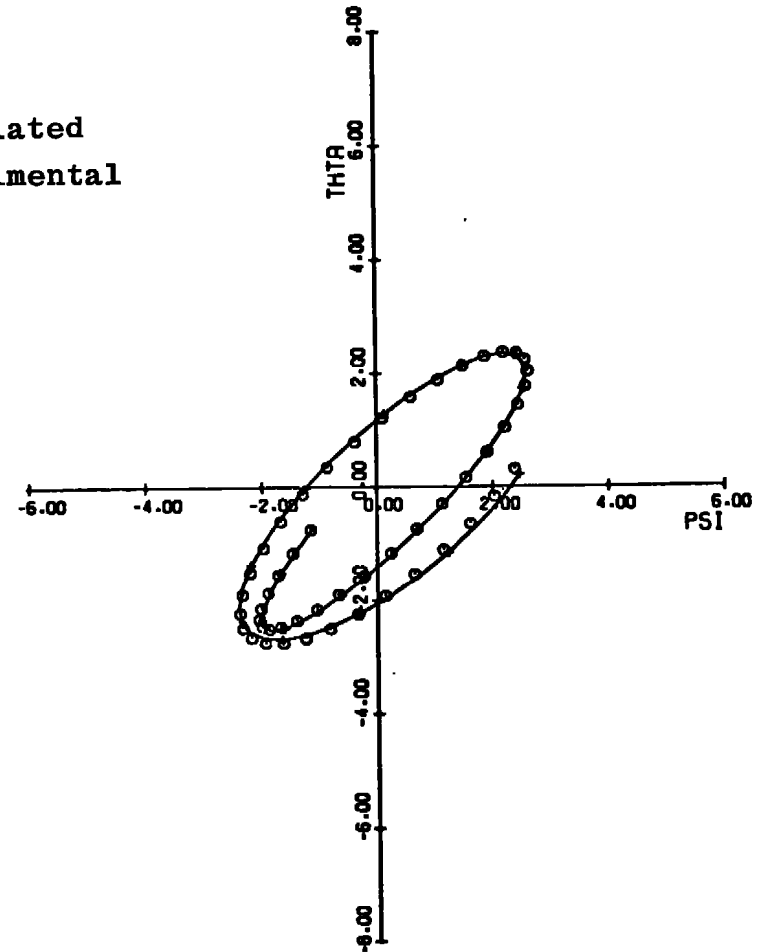


f. Fit of calculated solution to experimental data
in ψ, θ plane, time increment 0.98 to 1.98 sec

Figure 22. Continued.

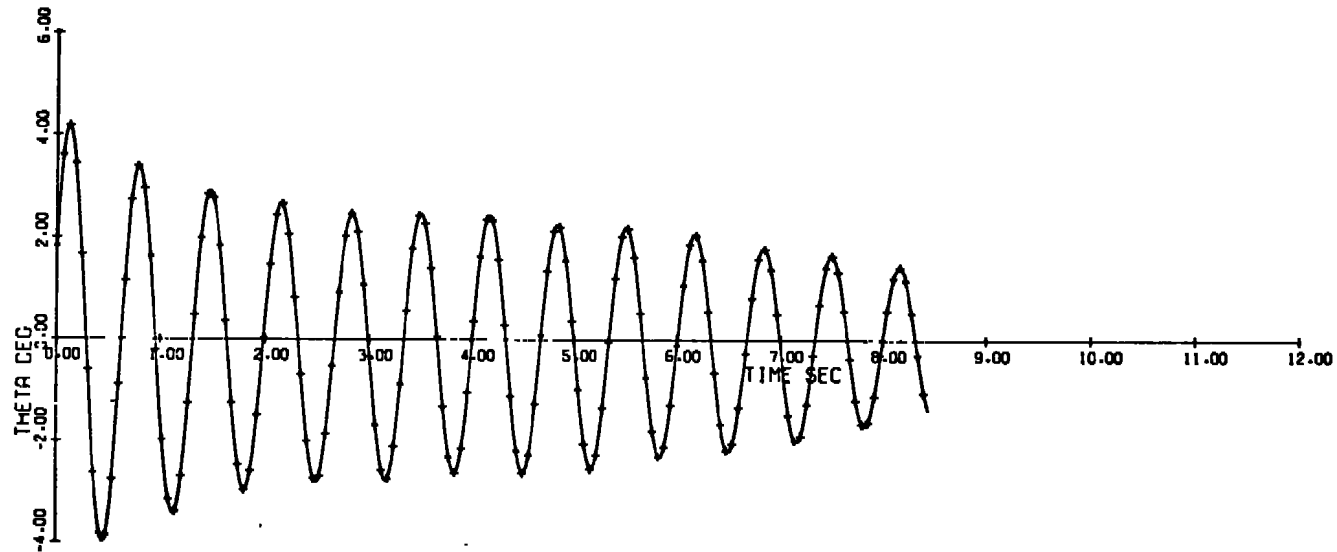


g. Fit of calculated solution to experimental data in ψ, θ plane, time increment 1.98 to 2.98 sec

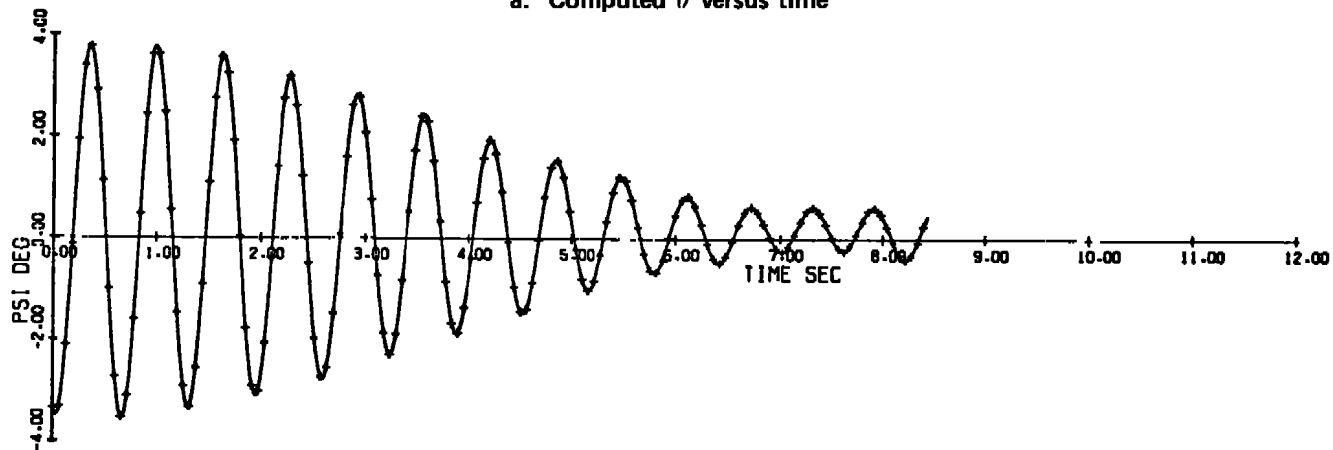


h. Fit of calculated solution to experimental data in ψ, θ plane, time increment 2.98 to 3.98 sec

Figure 22. Concluded.

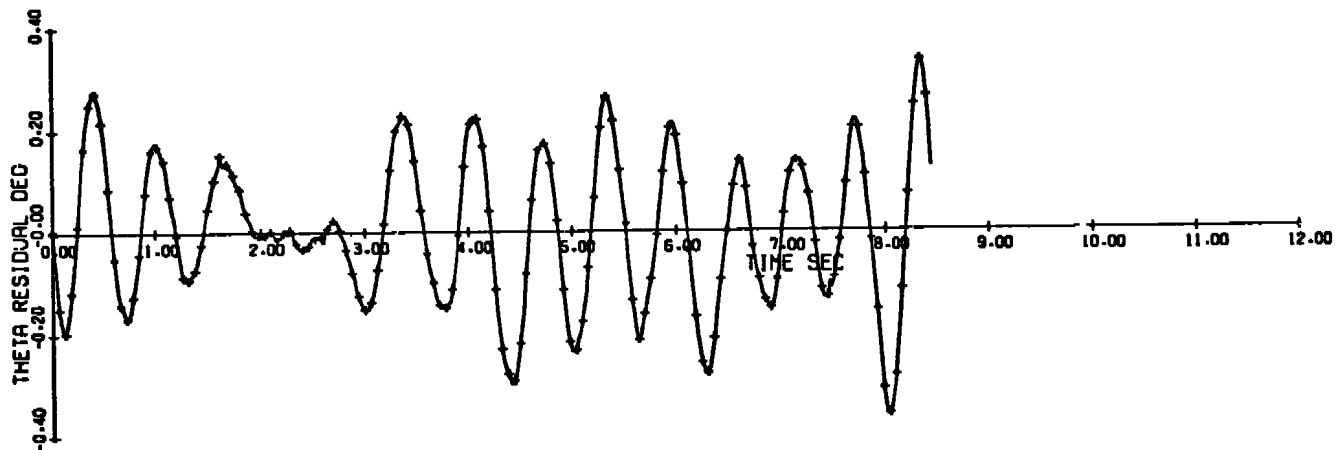


a. Computed θ versus time

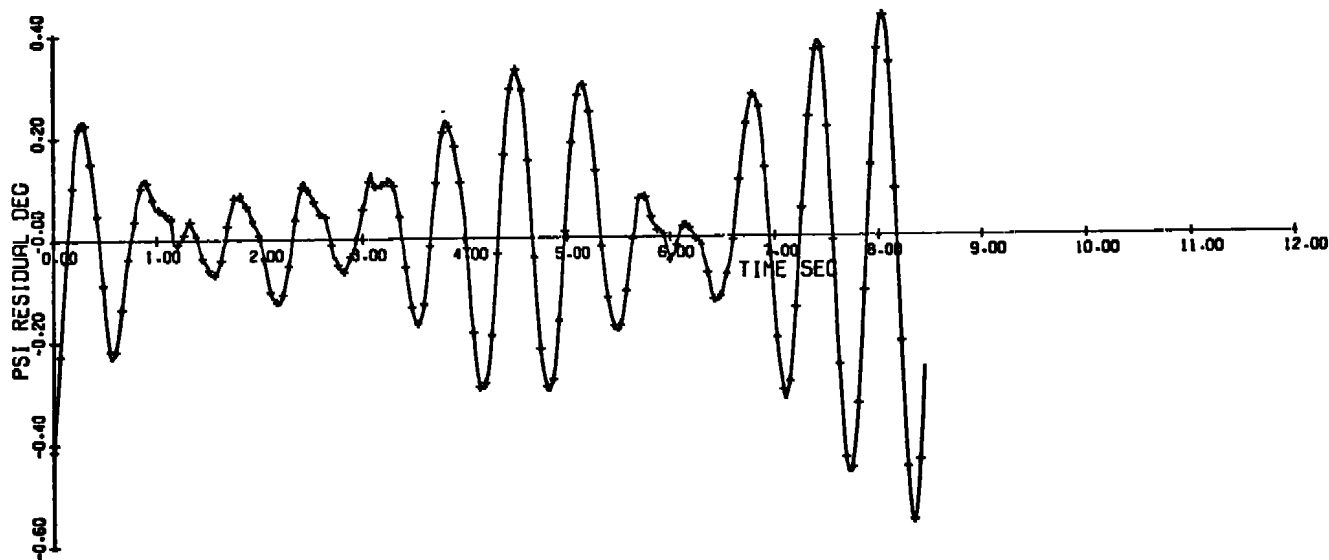


b. Computed ψ versus time

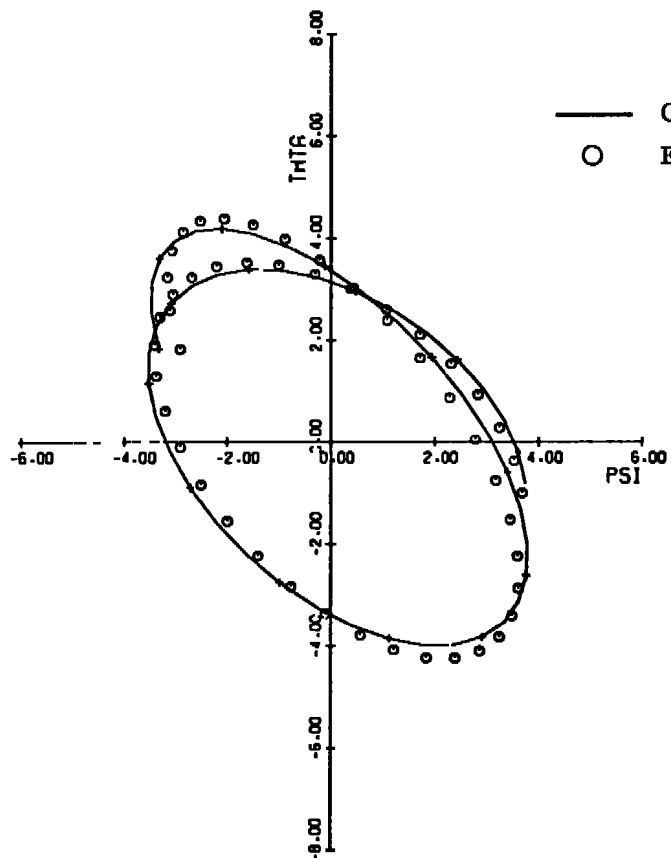
Figure 23. Graphical solution of sharp cone data given in Fig. 19 for a fit interval of 8.4 sec with fixed aerodynamics.



c. Residual in θ versus time

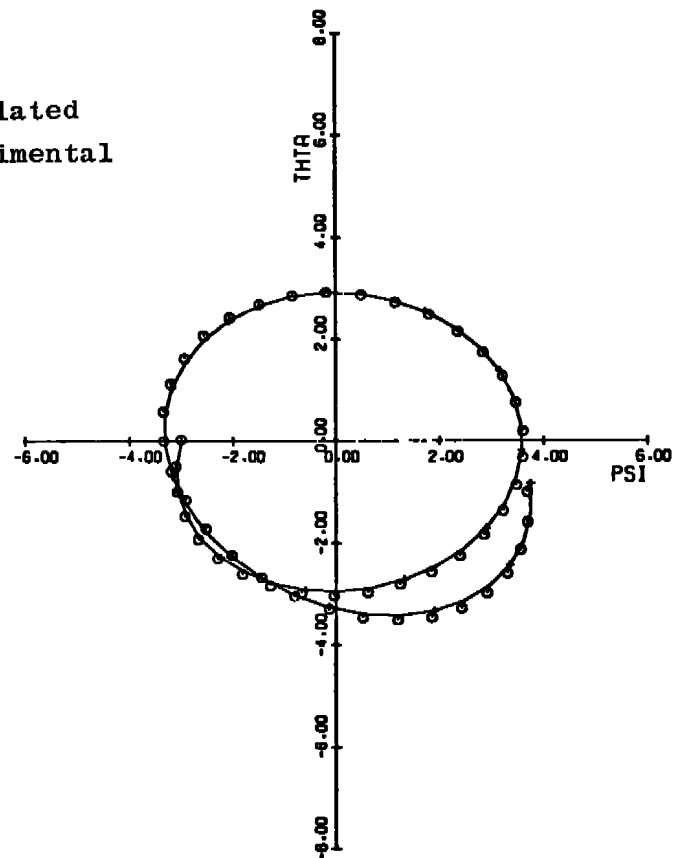


d. Residual in ψ versus time
Figure 23. Continued.



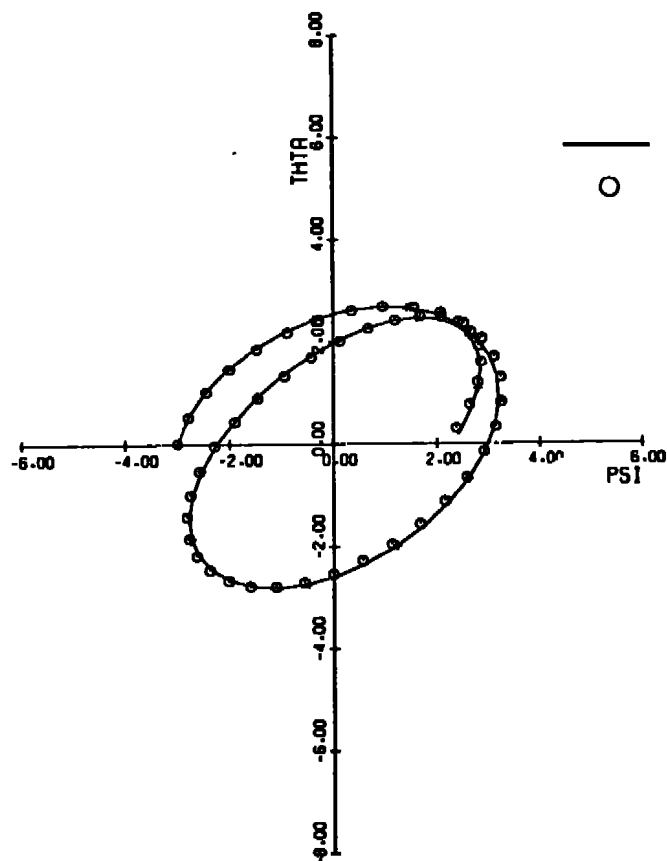
e. Fit of calculated solution to experimental data
in ψ, θ plane, time increment 0 to 0.98 sec

— Calculated
○ Experimental

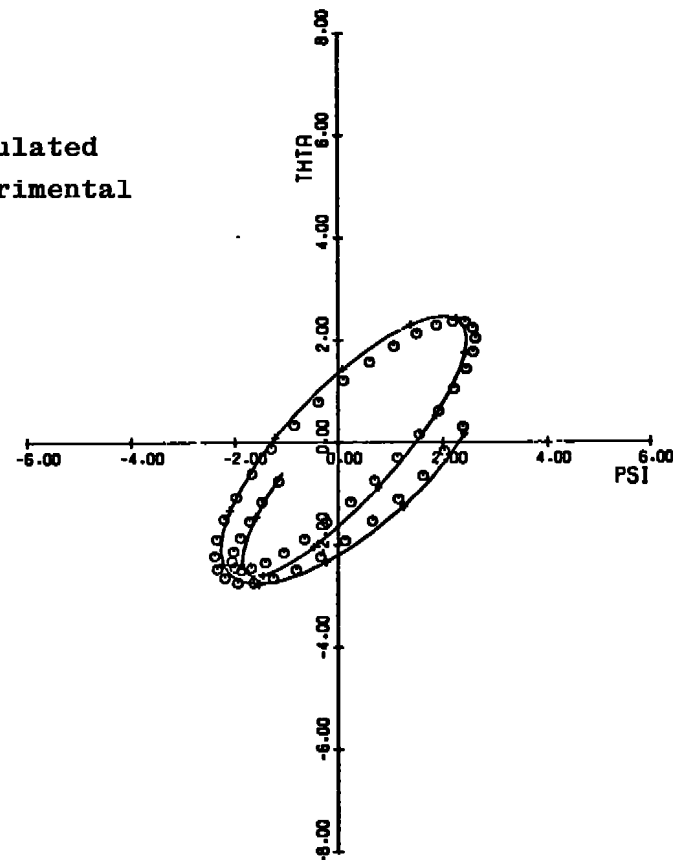


f. Fit of calculated solution to experimental data
in ψ, θ plane, time increment 0.98 to 1.98 sec

Figure 23. Continued.



g. Fit of calculated solution to experimental data
in ψ, θ plane, time increment 1.98 to 2.98 sec



h. Fit of calculated solution to experimental data
in ψ, θ plane, time increment 2.98 to 3.98 sec

Figure 23. Continued.

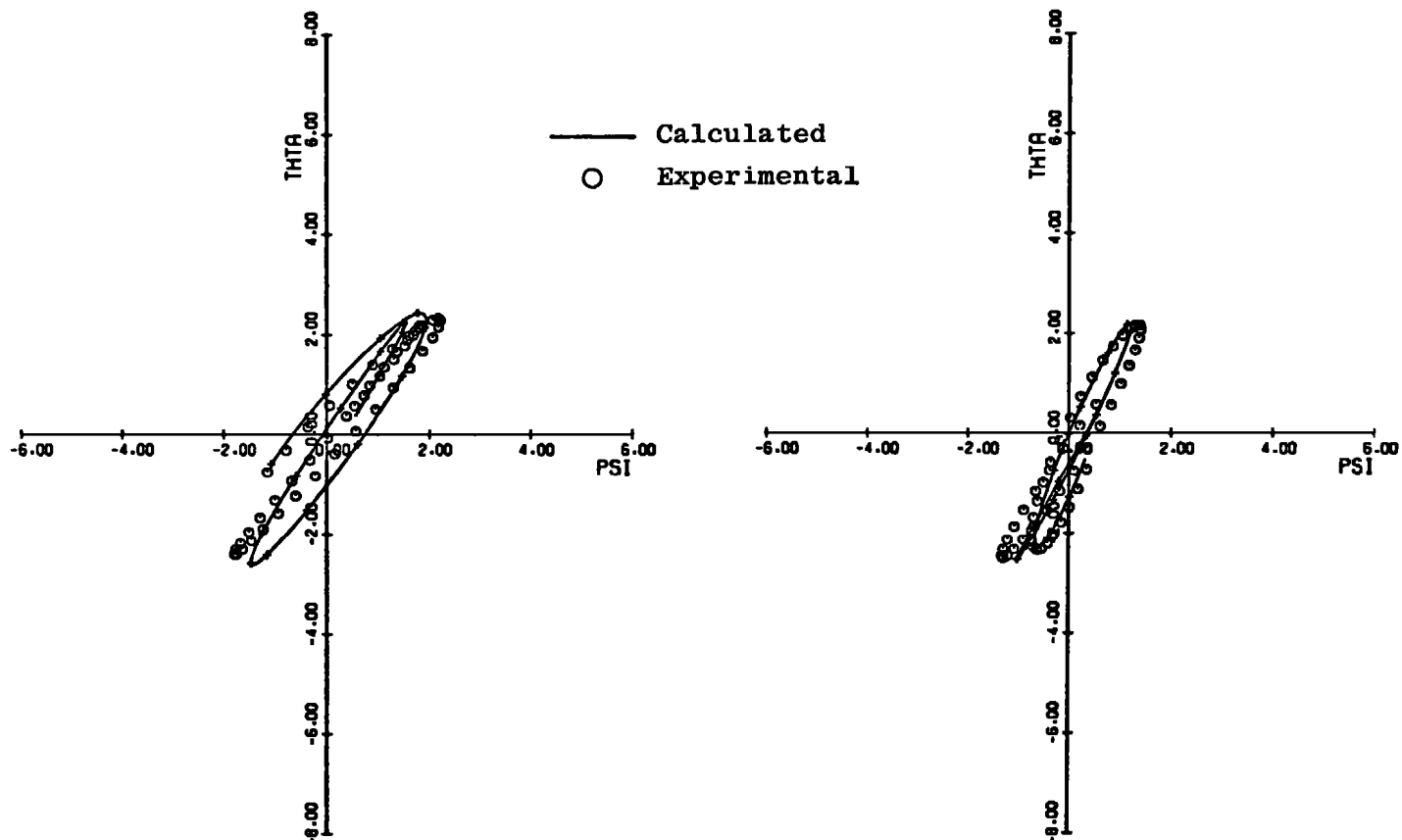
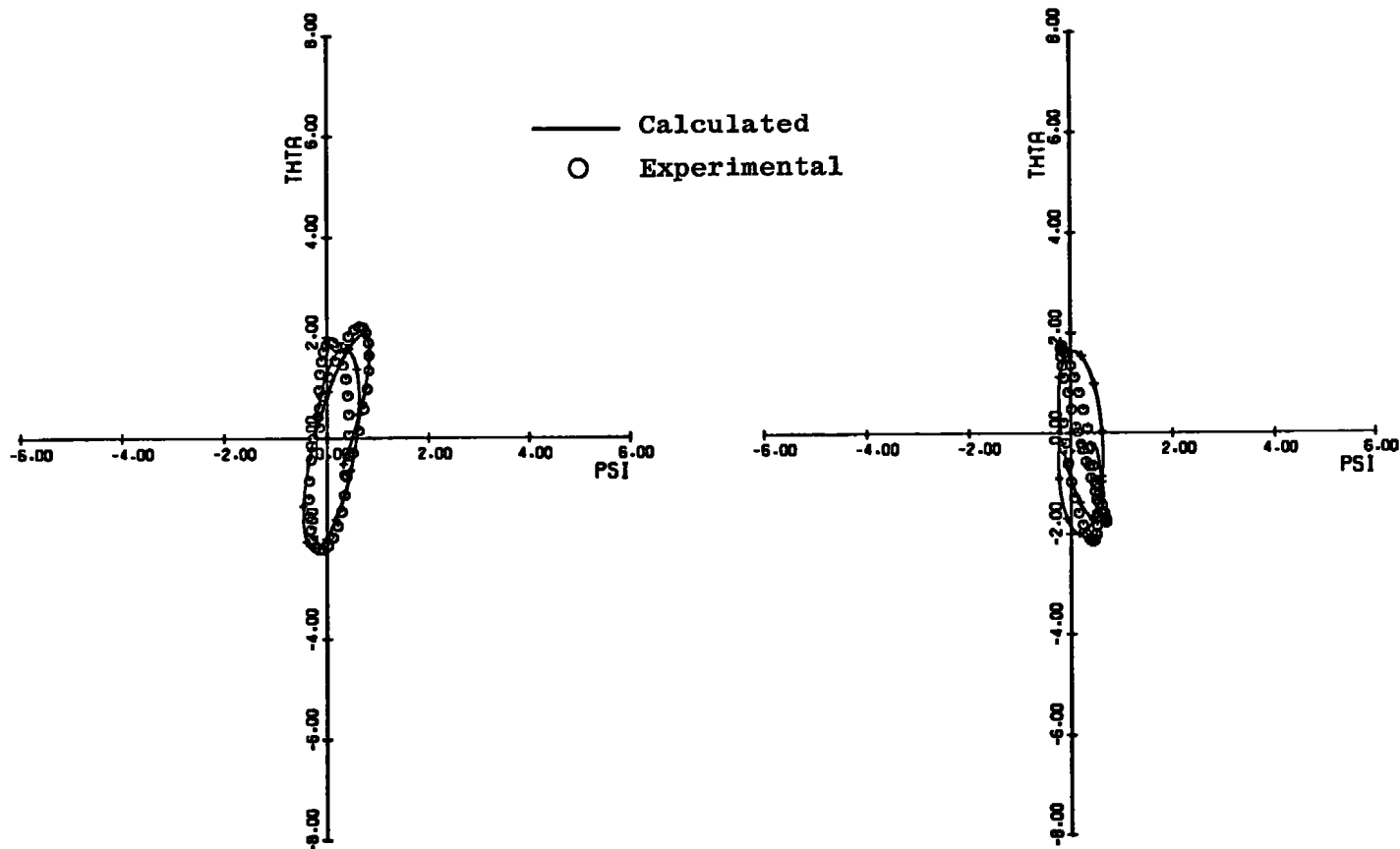


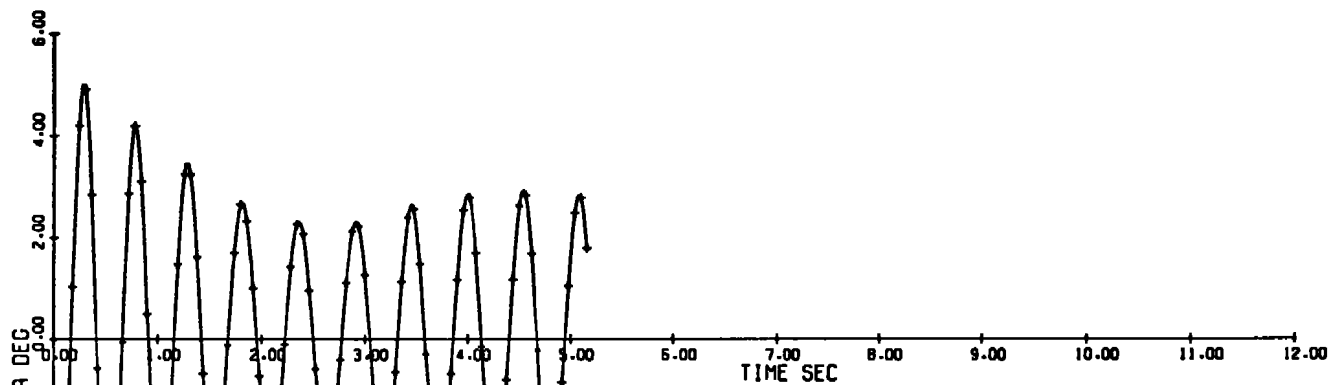
Figure 23. Continued.



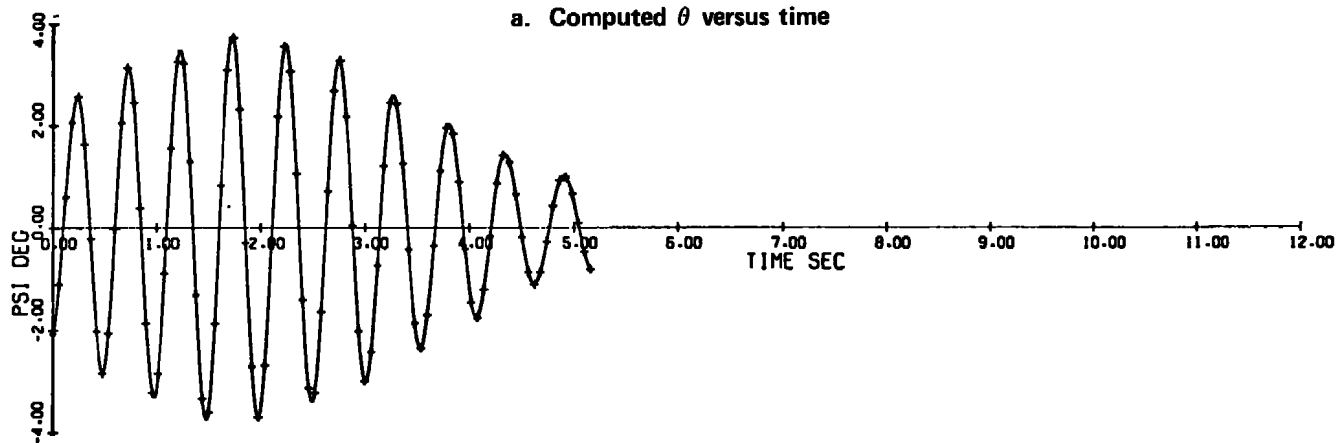
k. Fit of calculated solution to experimental data
in ψ, θ plane, time increment 5.98 to 6.98 sec

l. Fit of calculated solution to experimental data
in ψ, θ plane, time increment 6.98 to 7.98 sec

Figure 23. Concluded.

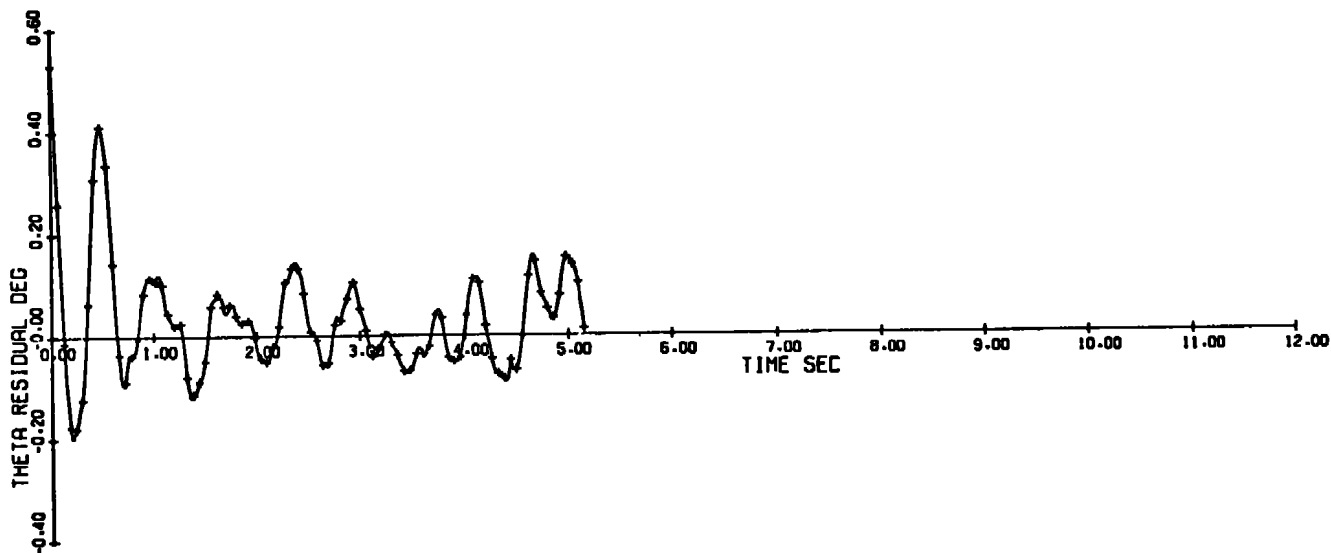


a. Computed θ versus time

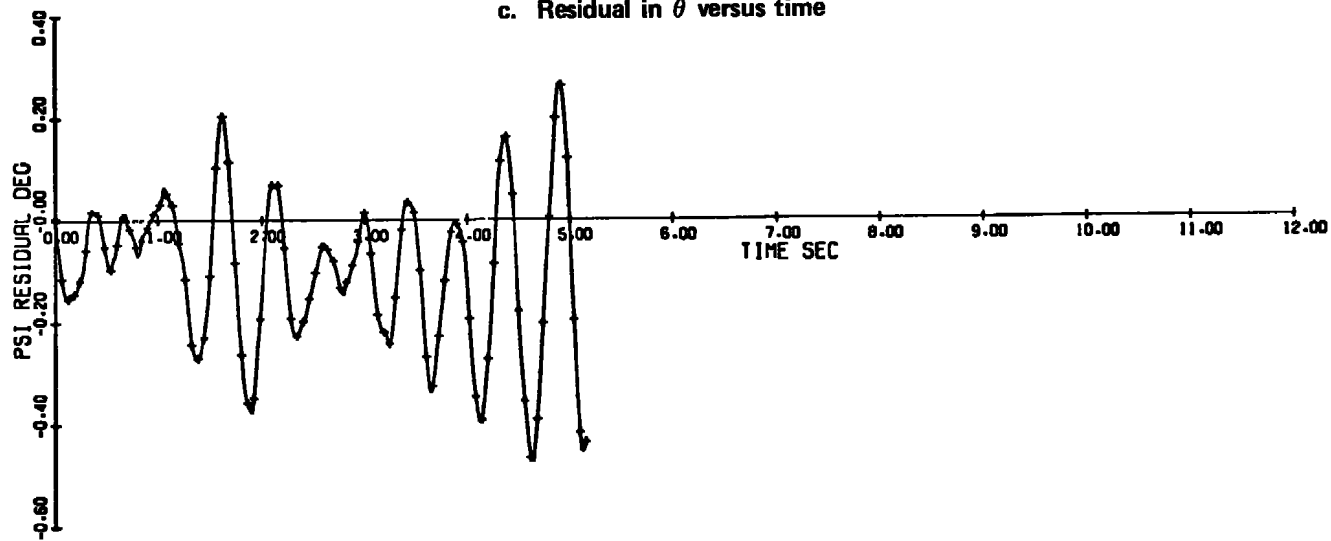


b. Computed ψ versus time

Figure 24. Graphical solution of sphere cone data given in Fig. 20 for a fit interval of 5.16 sec.



c. Residual in θ versus time



d. Residual in ψ versus time
Figure 24. Continued.

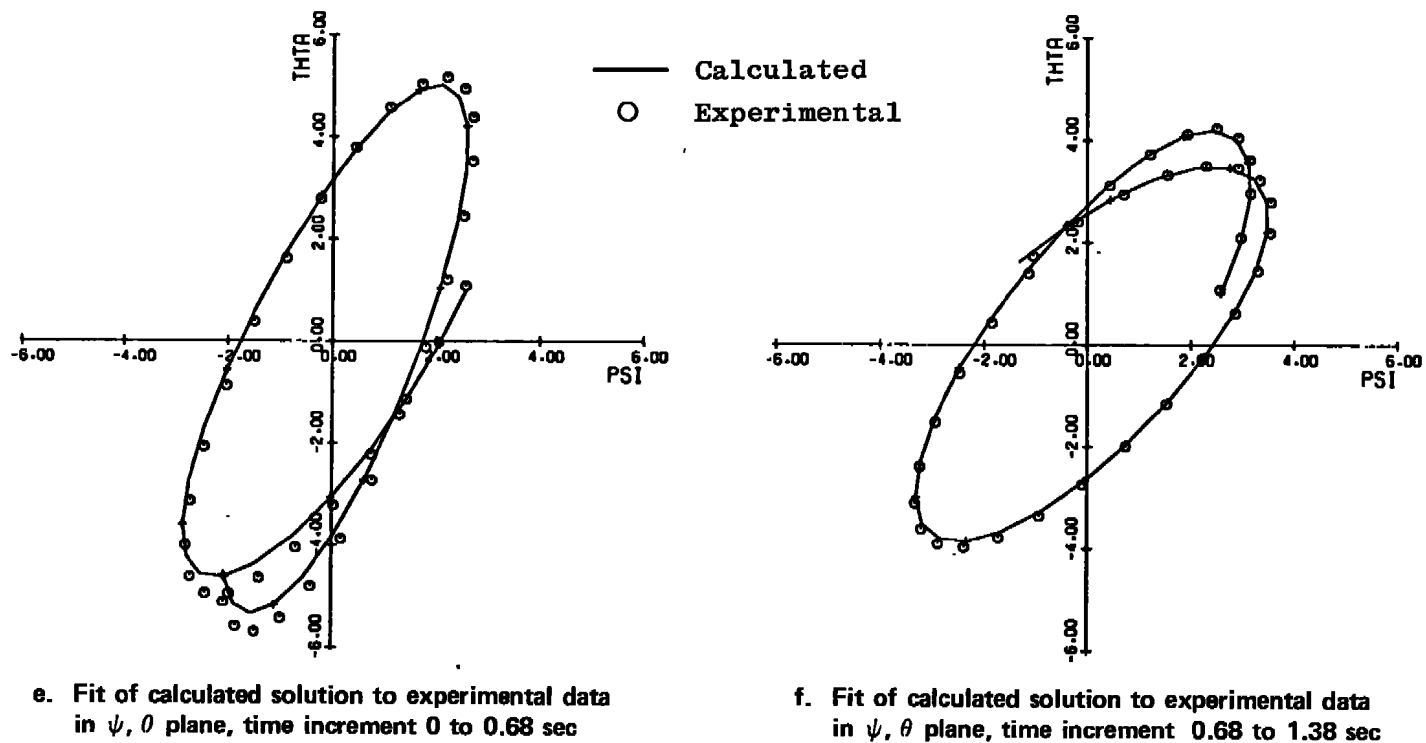
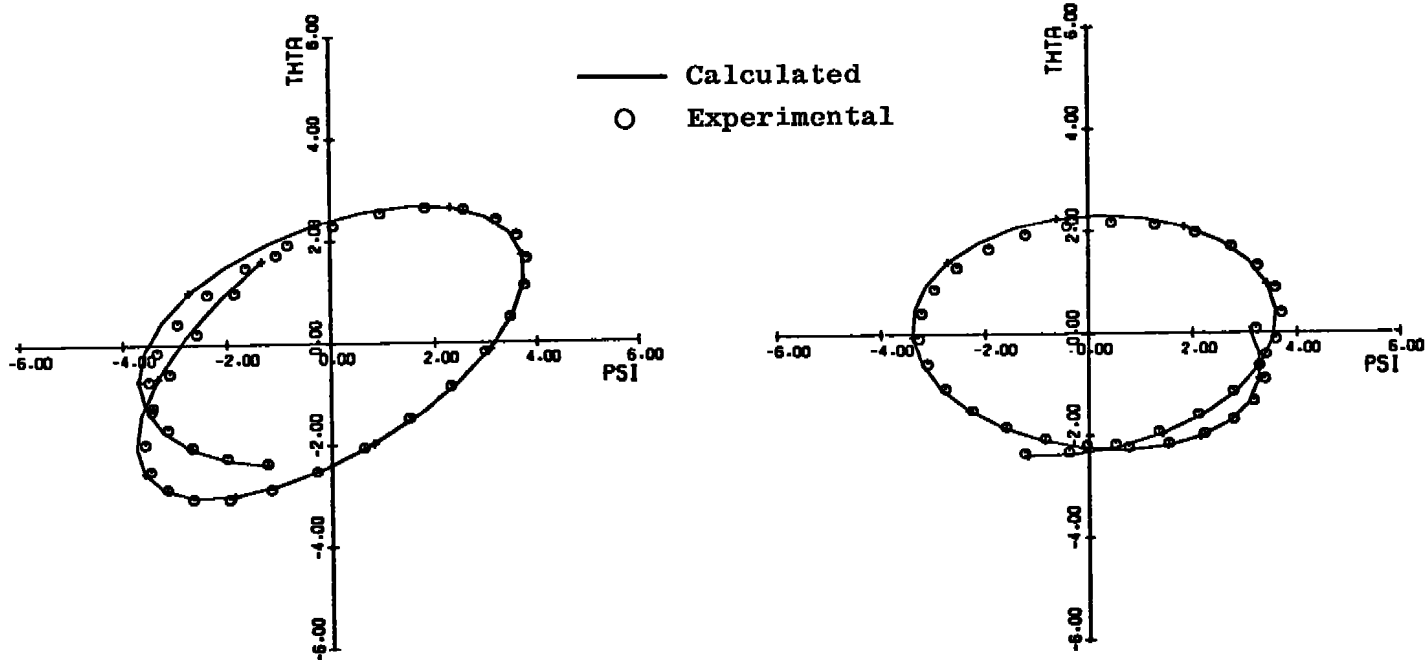


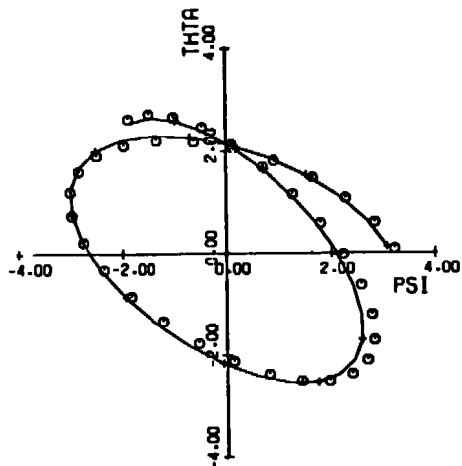
Figure 24. Continued.



g. Fit of calculated solution to experimental data
in ψ, θ plane, time increment 1.38 to 2.08 sec

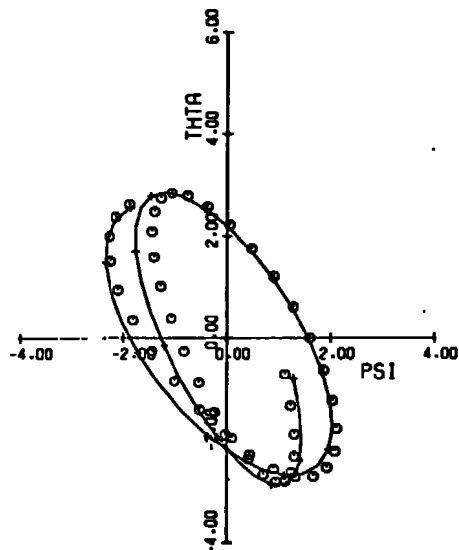
h. Fit of calculated solution to experimental data
in ψ, θ plane, time increment 2.08 to 2.78 sec

Figure 24. Continued.

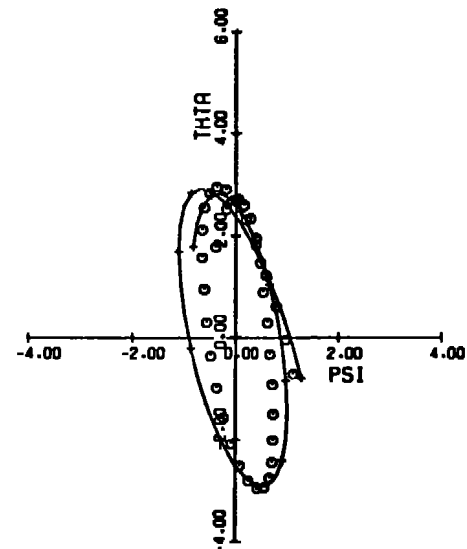


— Calculated
○ Experimental

i. Fit of calculated solution to experimental data
in ψ, θ plane, time increment 2.78 to 3.48 sec

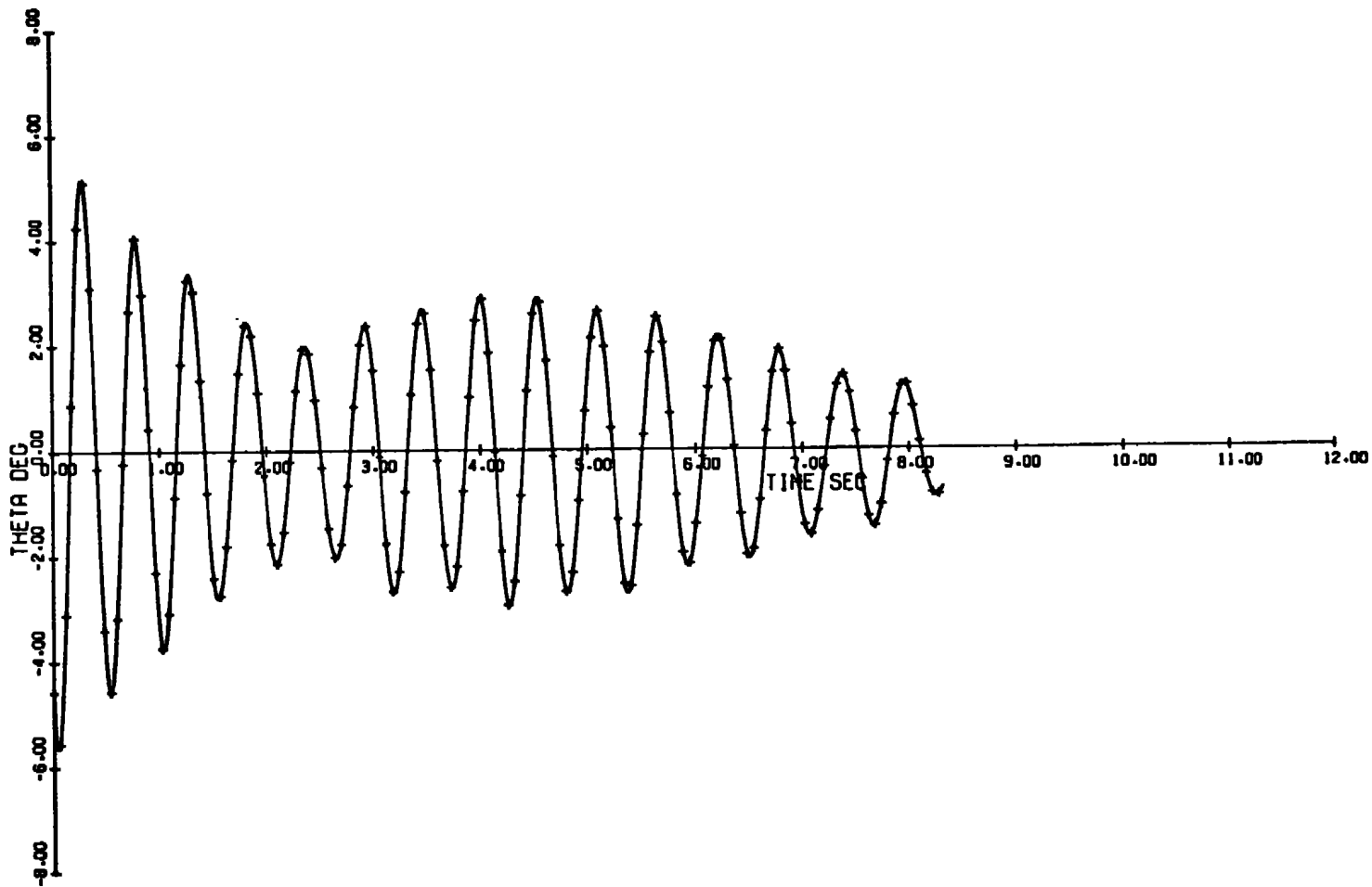


j. Fit of calculated solution to experimental data
in ψ, θ plane, time increment 3.48 to 4.38 sec



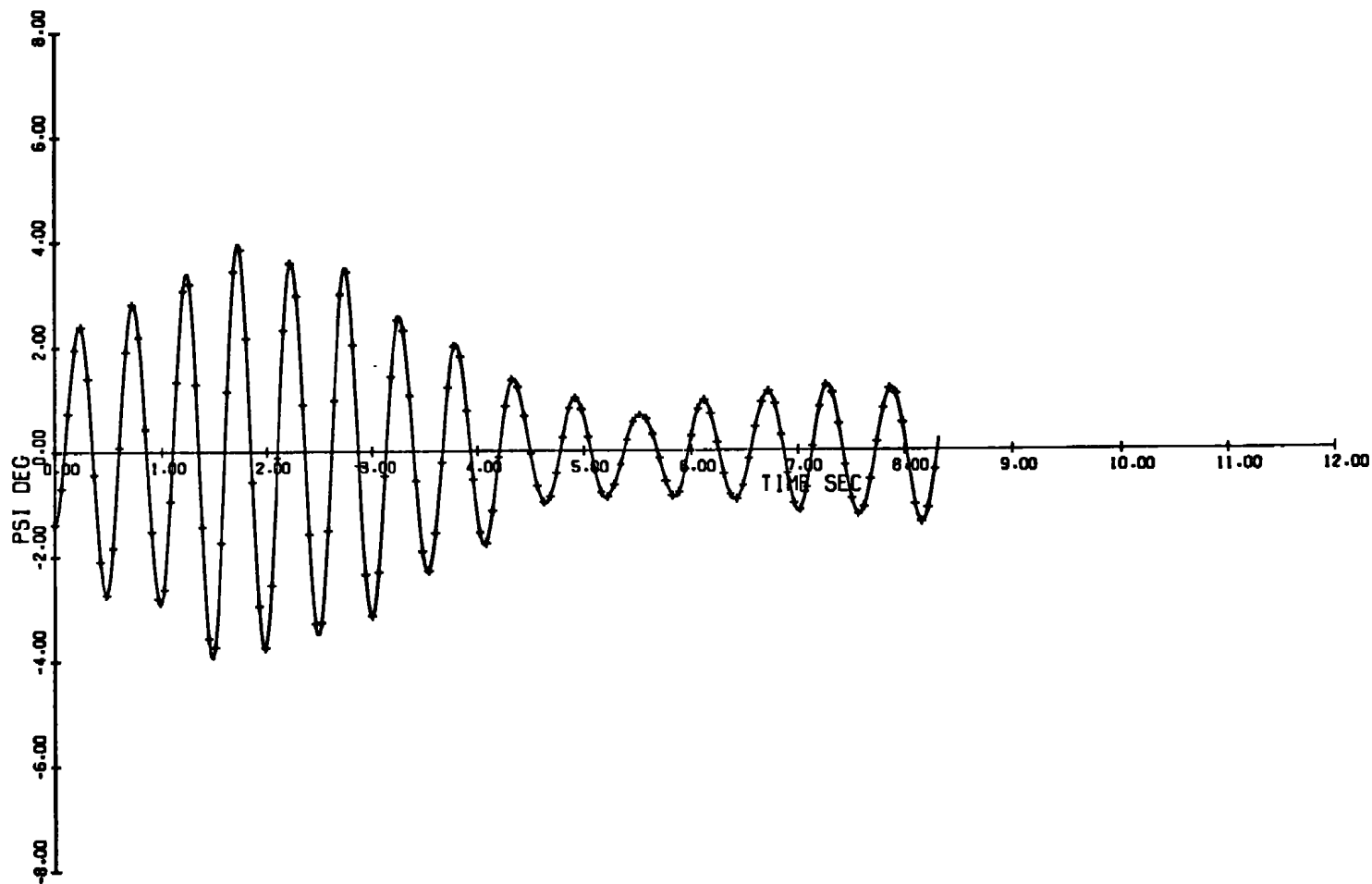
k. Fit of calculated solution to experimental data
in ψ, θ plane, time increment 4.38 to 5.16 sec

Figure 24. Concluded.

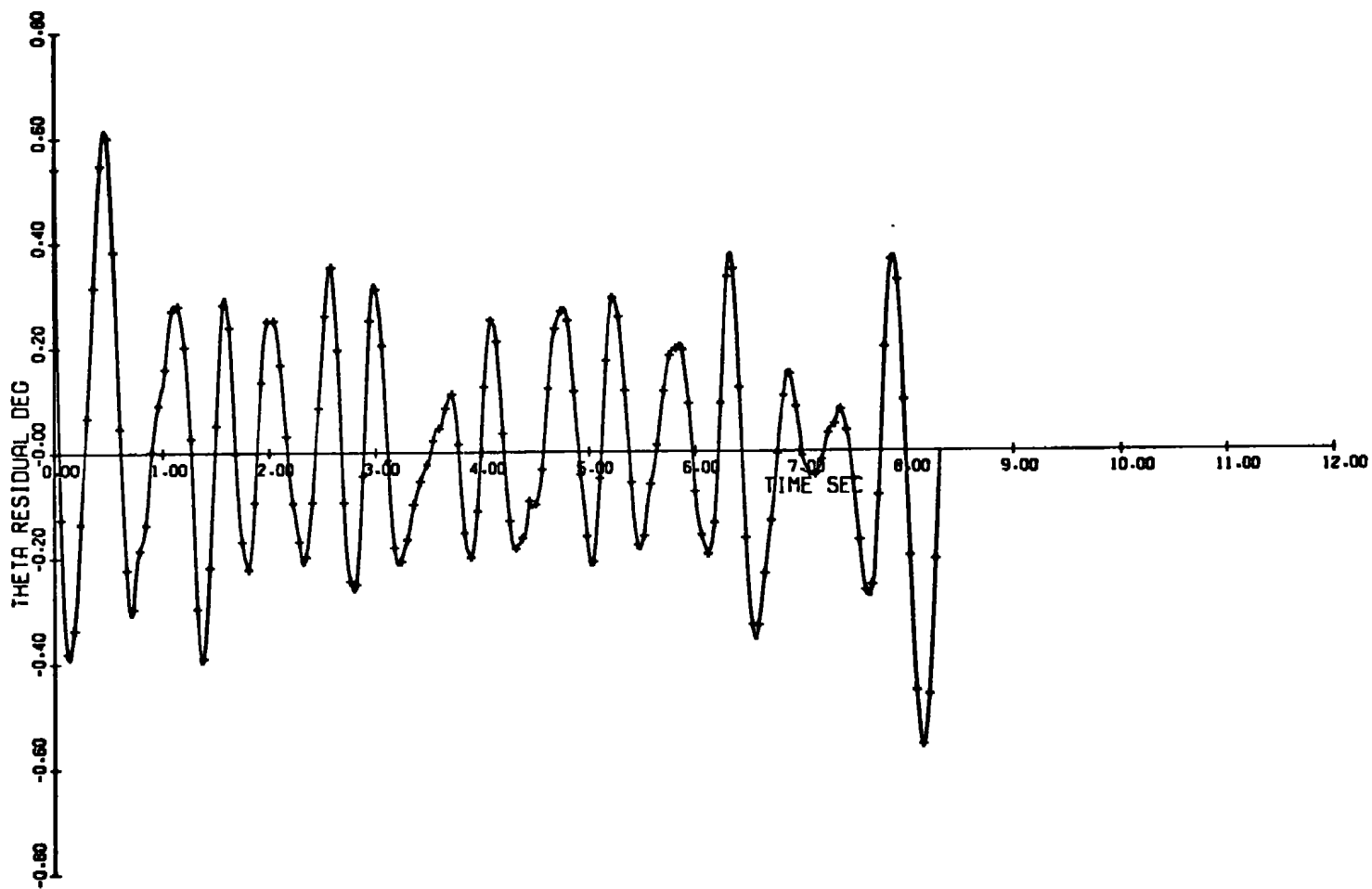


a. Computed θ versus time

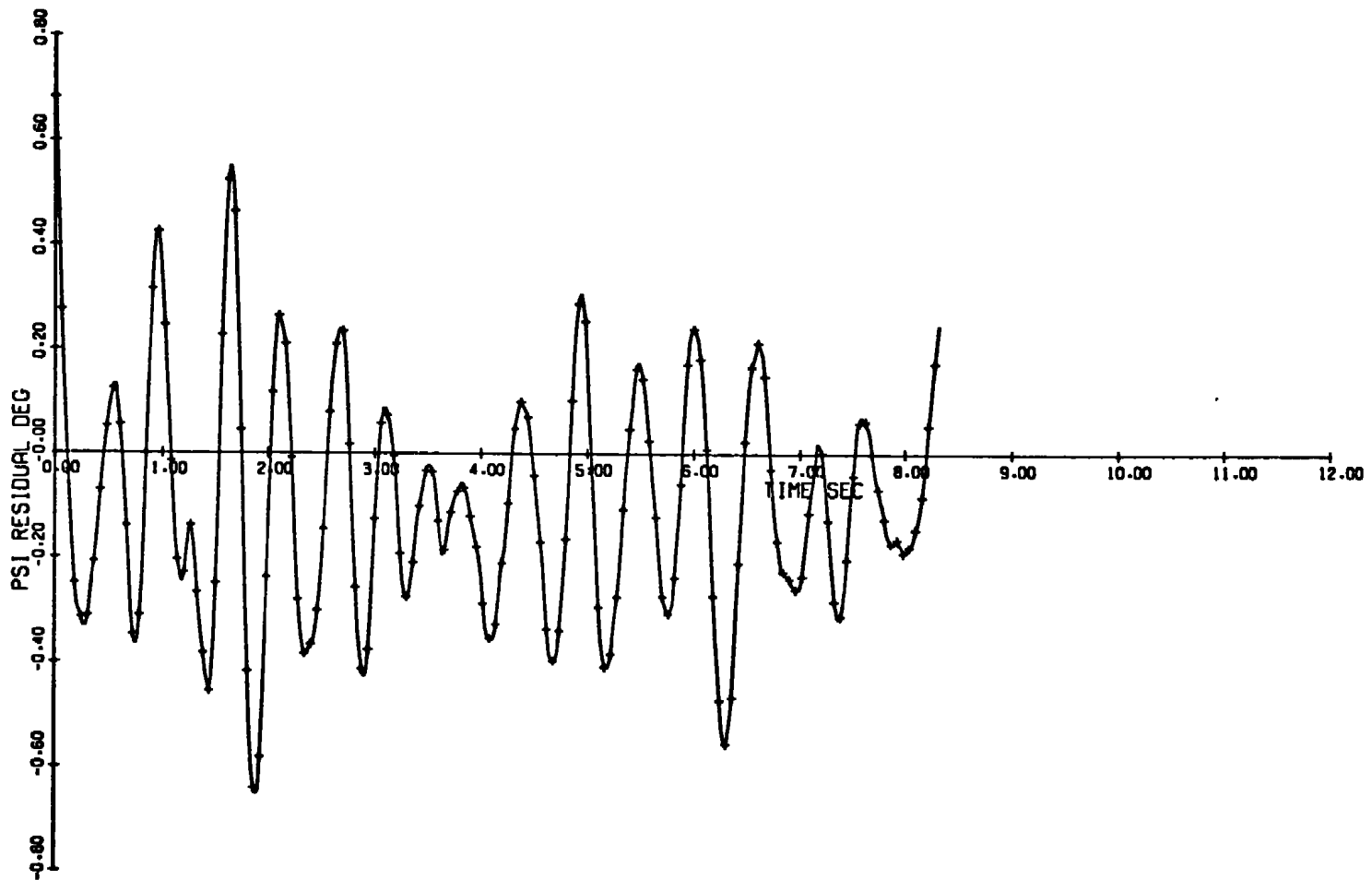
Figure 25. Graphical solution of sphere cone data given in Fig. 20 for a fit interval of 8.32 sec.



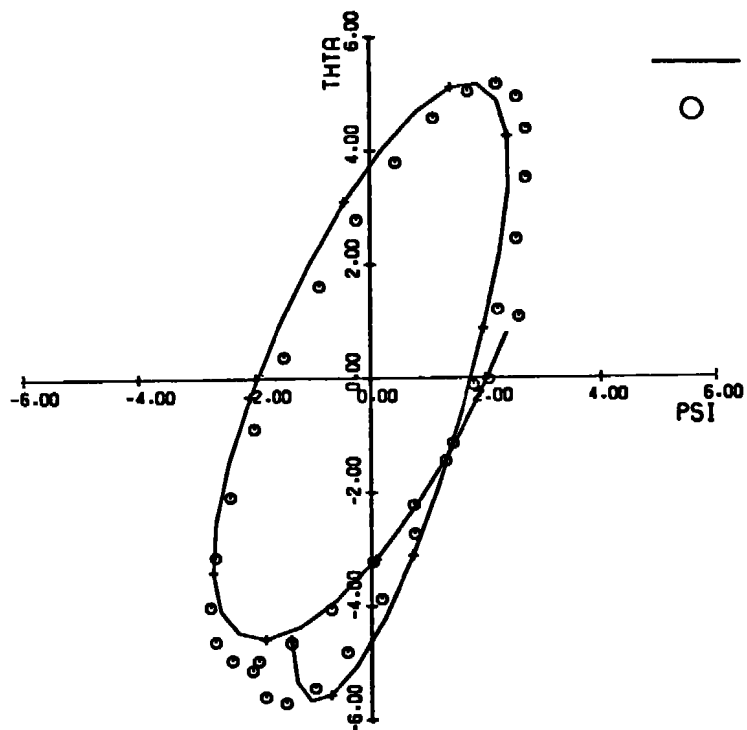
b. Computed ψ versus time
Figure 25. Continued.



c. Residual in θ versus time
Figure 25. Continued.

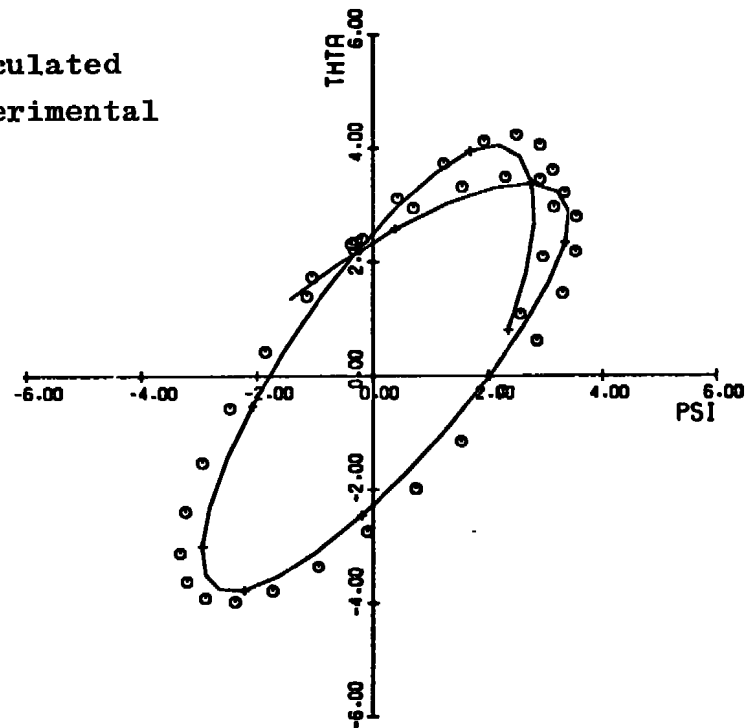


d. Residual in ψ versus time
Figure 25. Continued.



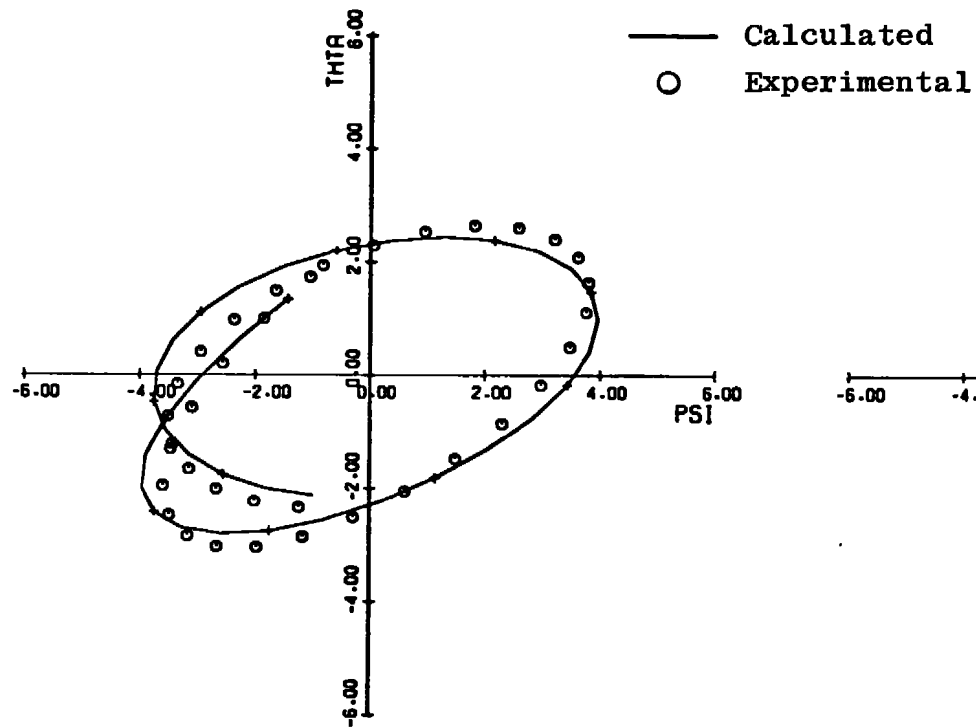
e. Fit of calculated solution to experimental data
in ψ, θ plane, time increment 0 to 0.68 sec

— Calculated
○ Experimental

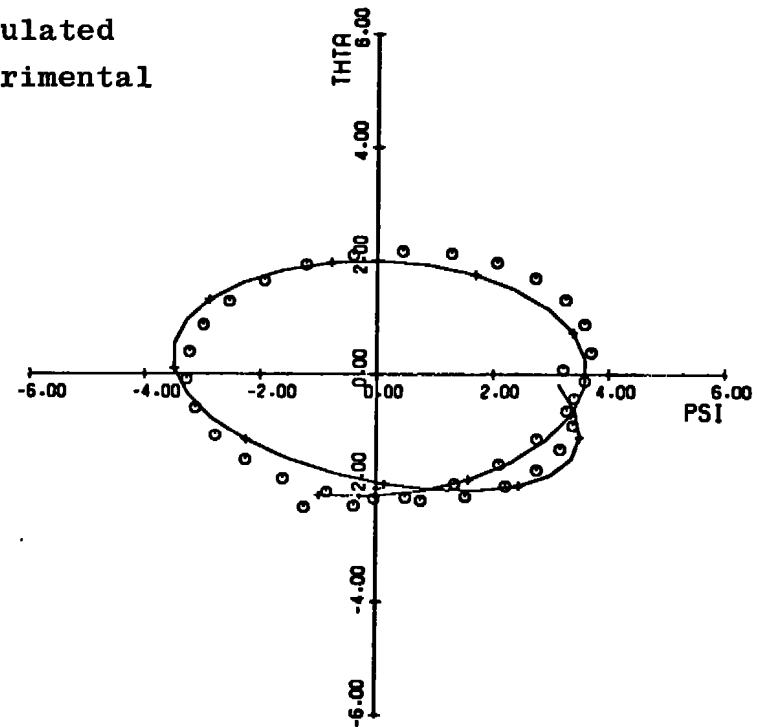


f. Fit of calculated solution to experimental data
in ψ, θ plane, time increment 0.68 to 1.38 sec

Figure 25. Continued.

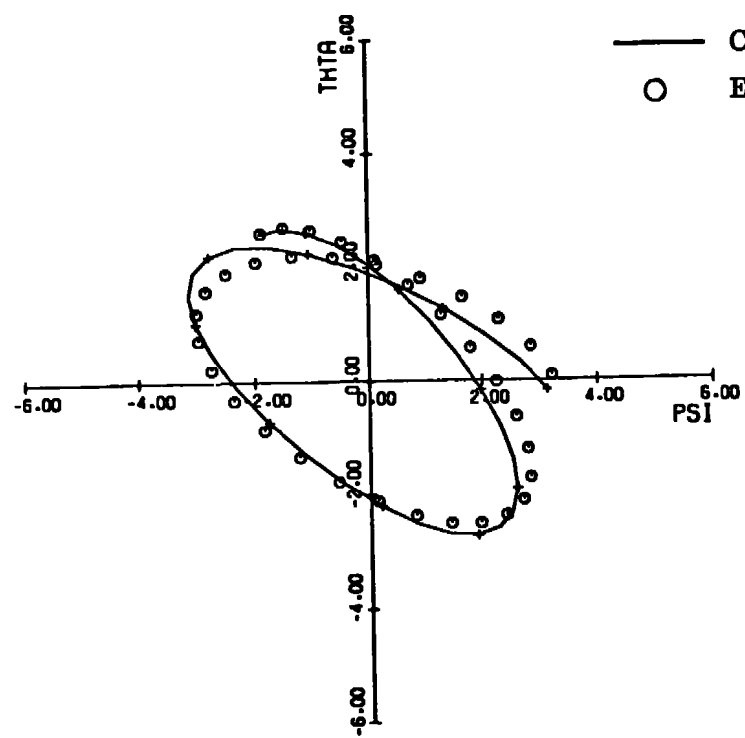


g. Fit of calculated solution to experimental data
in ψ, θ plane, time increment 1.38 to 2.08 sec

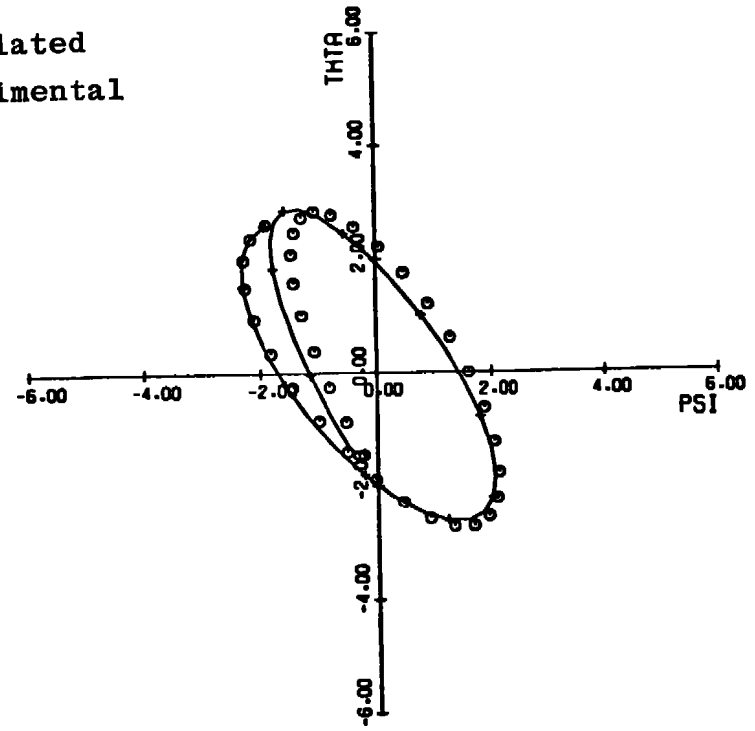


h. Fit of calculated solution to experimental data
in ψ, θ plane, time increment 2.08 to 2.78 sec

Figure 25. Continued.

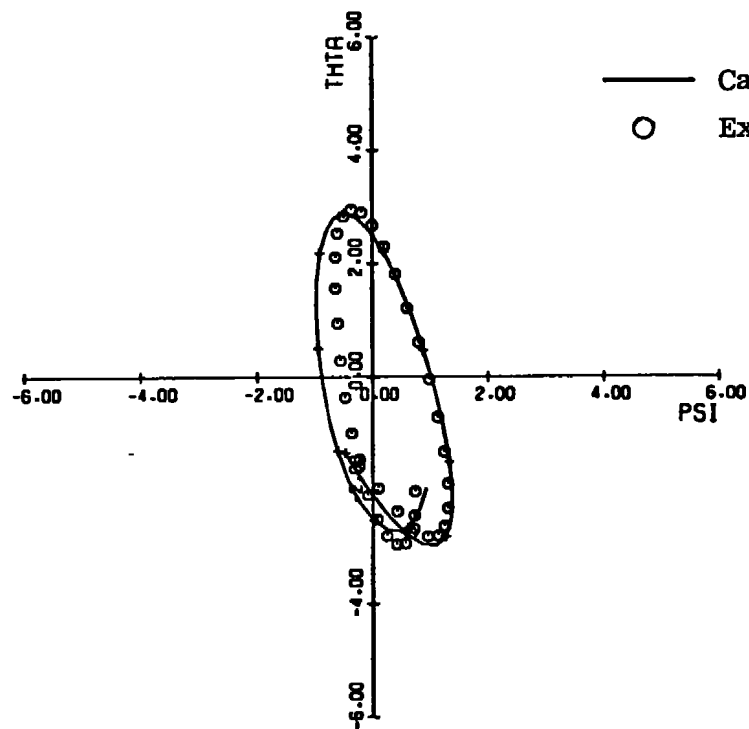


i. Fit of calculated solution to experimental data in ψ, θ plane, time increment 2.78 to 3.48 sec

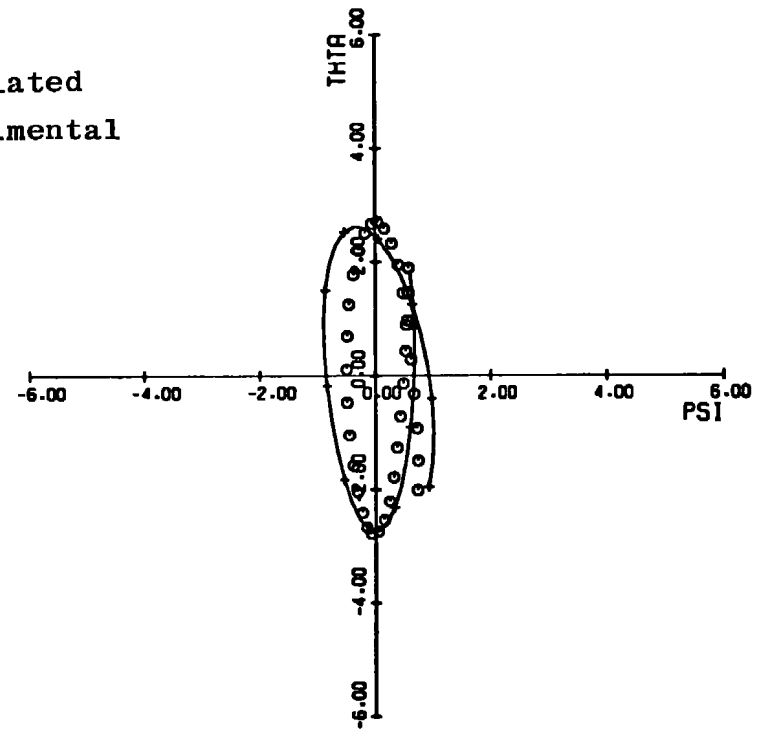


j. Fit of calculated solution to experimental data in ψ, θ plane, time increment 3.48 to 4.18 sec

Figure 25. Continued.

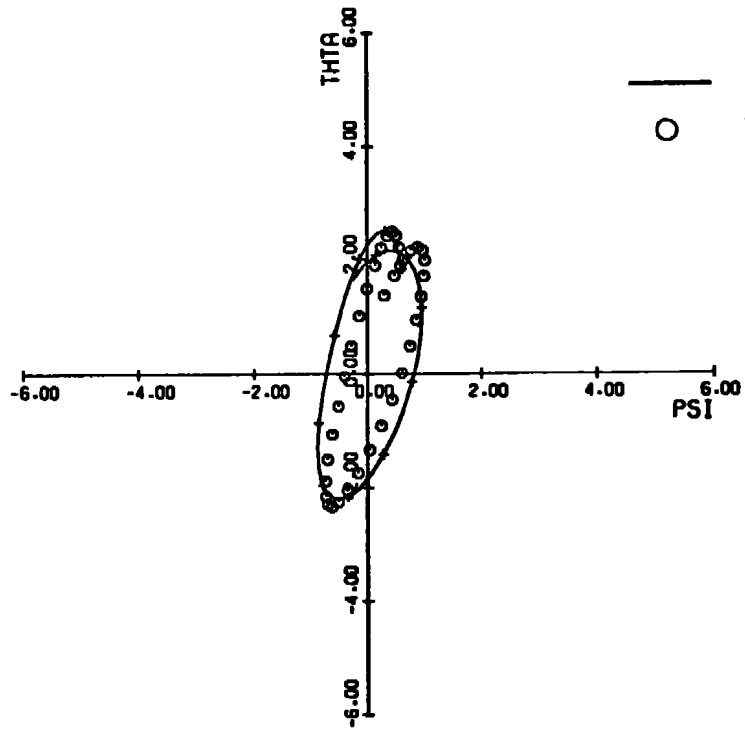


k. Fit of calculated solution to experimental data
in ψ, θ plane, time increment 4.18 to 4.88 sec

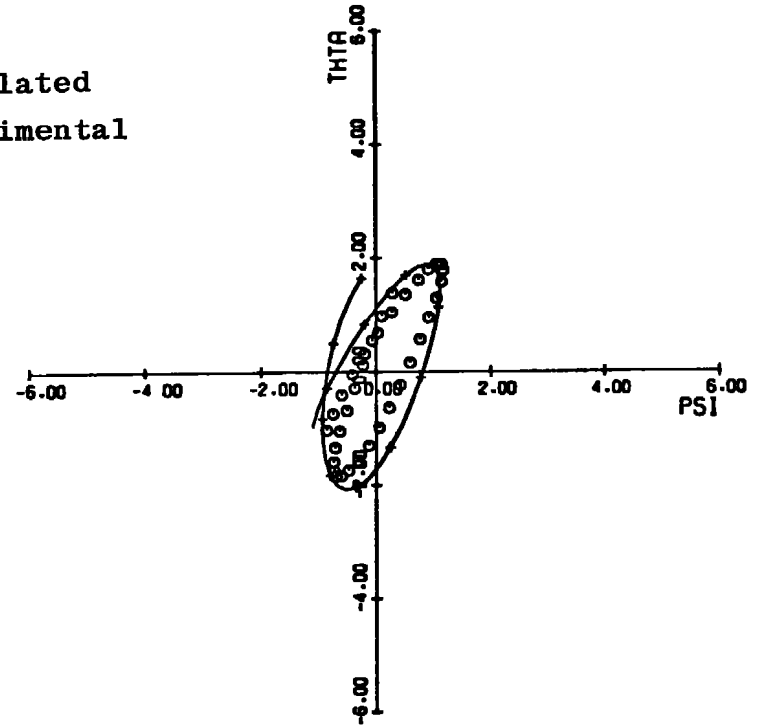


l. Fit of calculated solution to experimental data
in ψ, θ plane, time increment 4.88 to 5.58 sec

Figure 25. Continued.

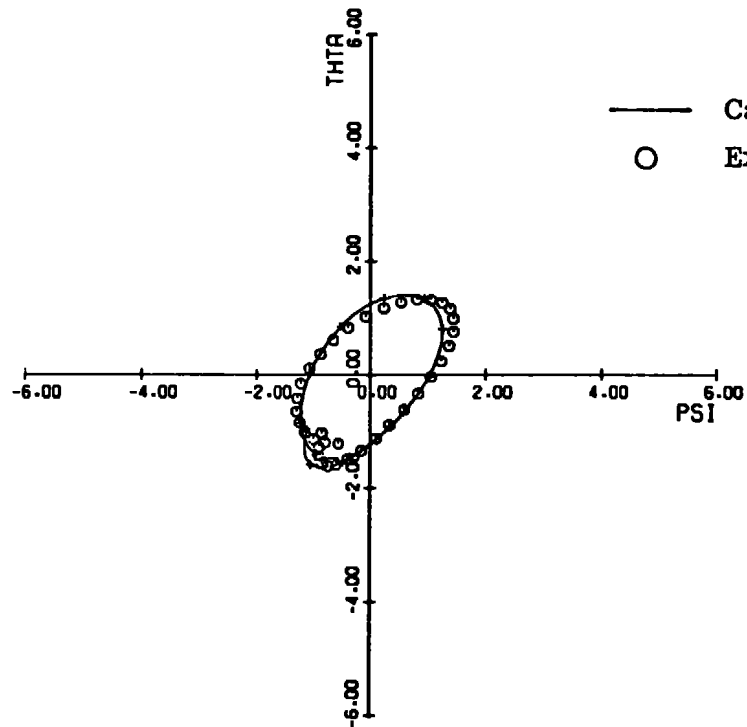


m. Fit of calculated solution to experimental data
in ψ, θ plane, time increment 5.58 to 6.28 sec

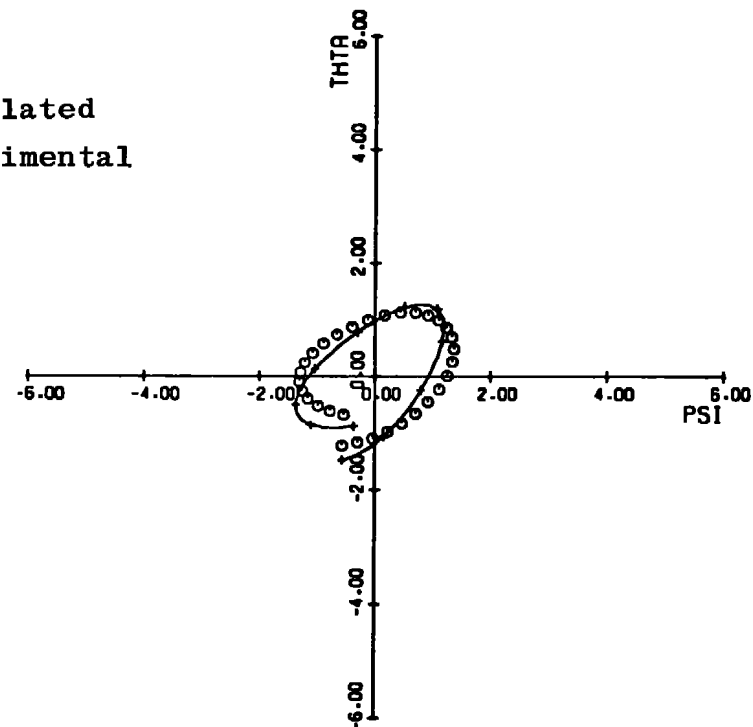


n. Fit of calculated solution to experimental data
in ψ, θ plane, time increment 6.28 to 6.98 sec

Figure 25. Continued.

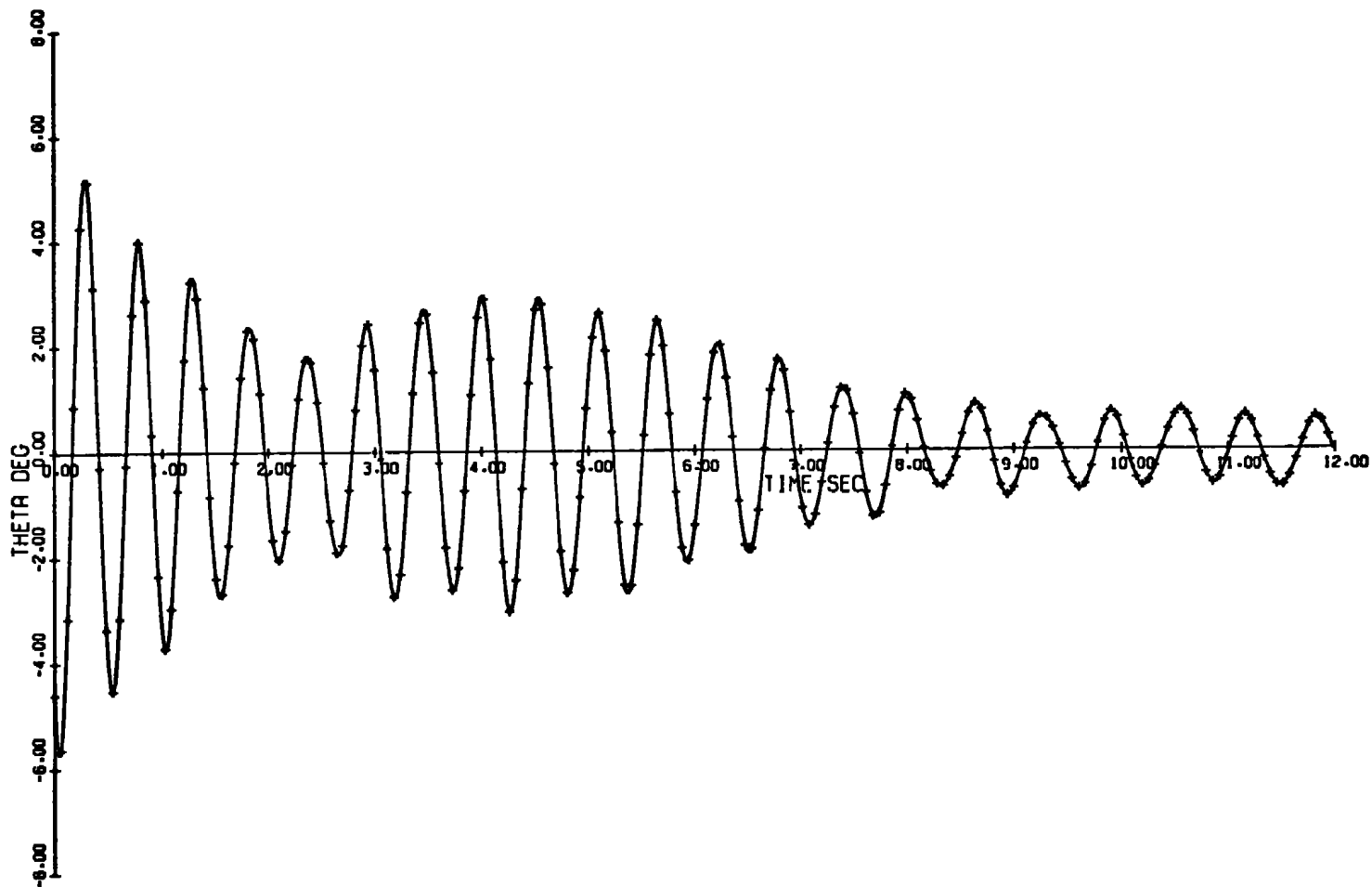


o. Fit of calculated solution to experimental data
in ψ, θ plane, time increment 6.98 to 7.68 sec



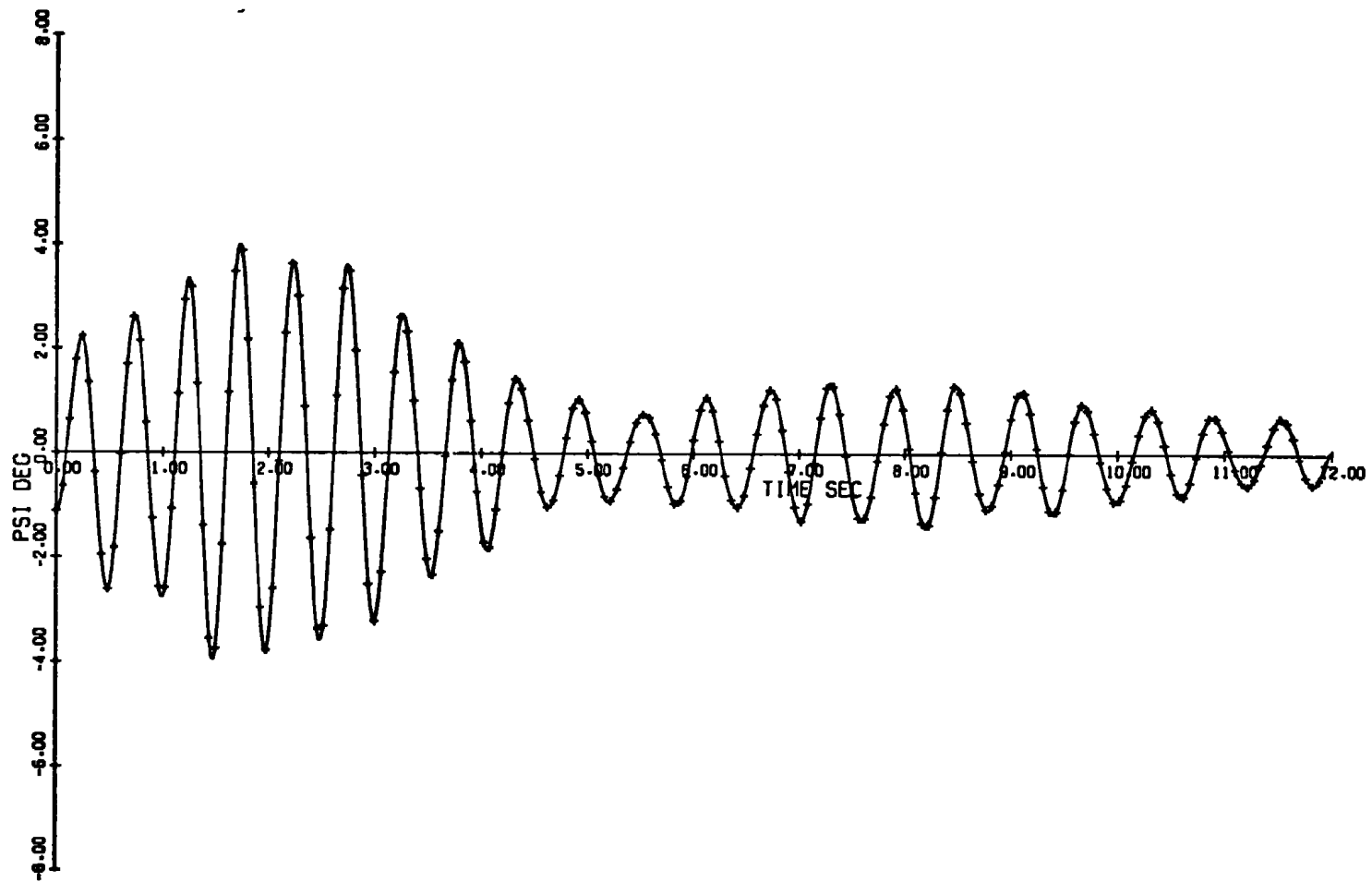
p. Fit of calculated solution to experimental data
in ψ, θ plane, time increment 7.68 to 8.28 sec

Figure 25. Concluded.

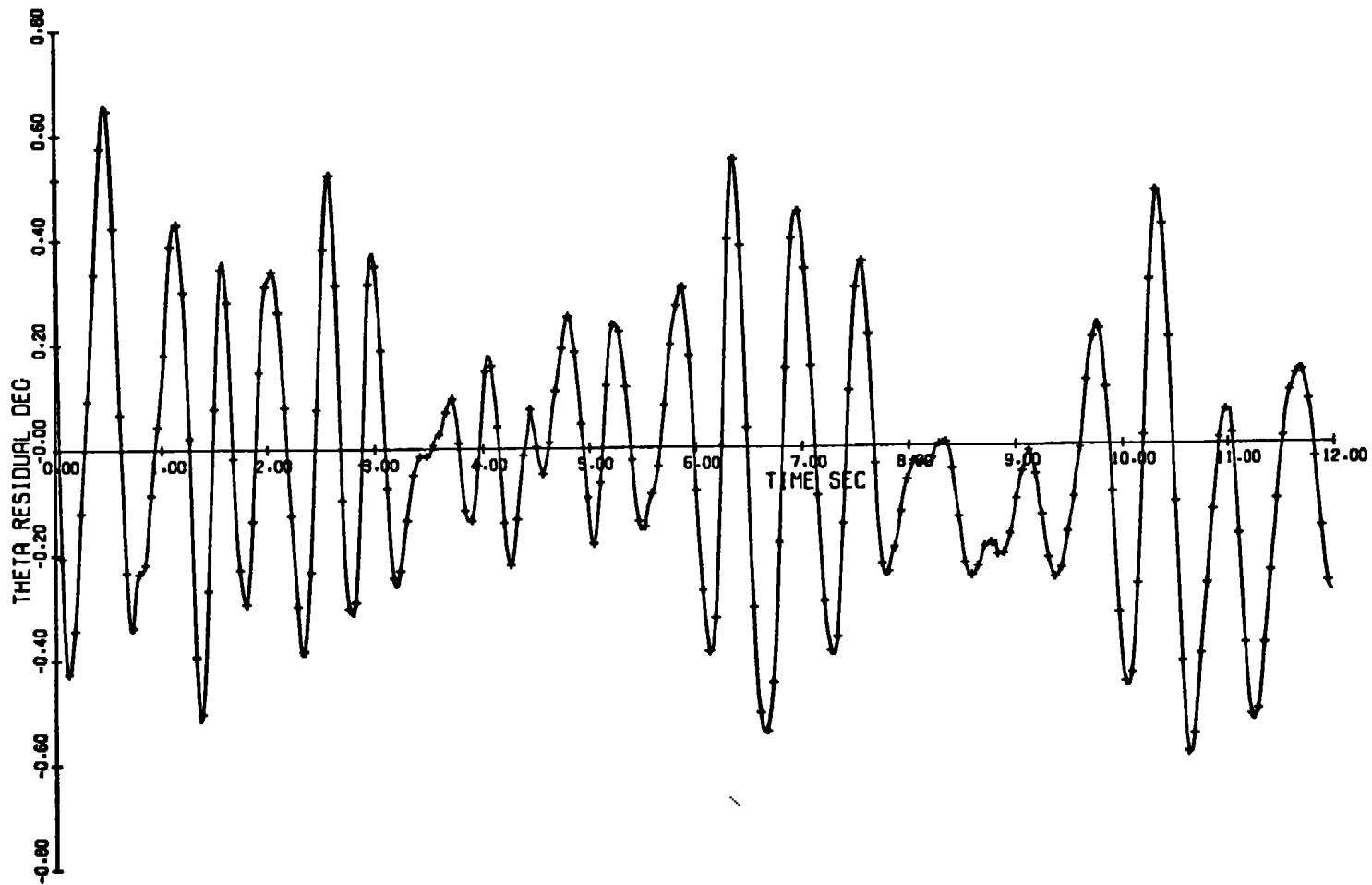


a. Computed θ versus time

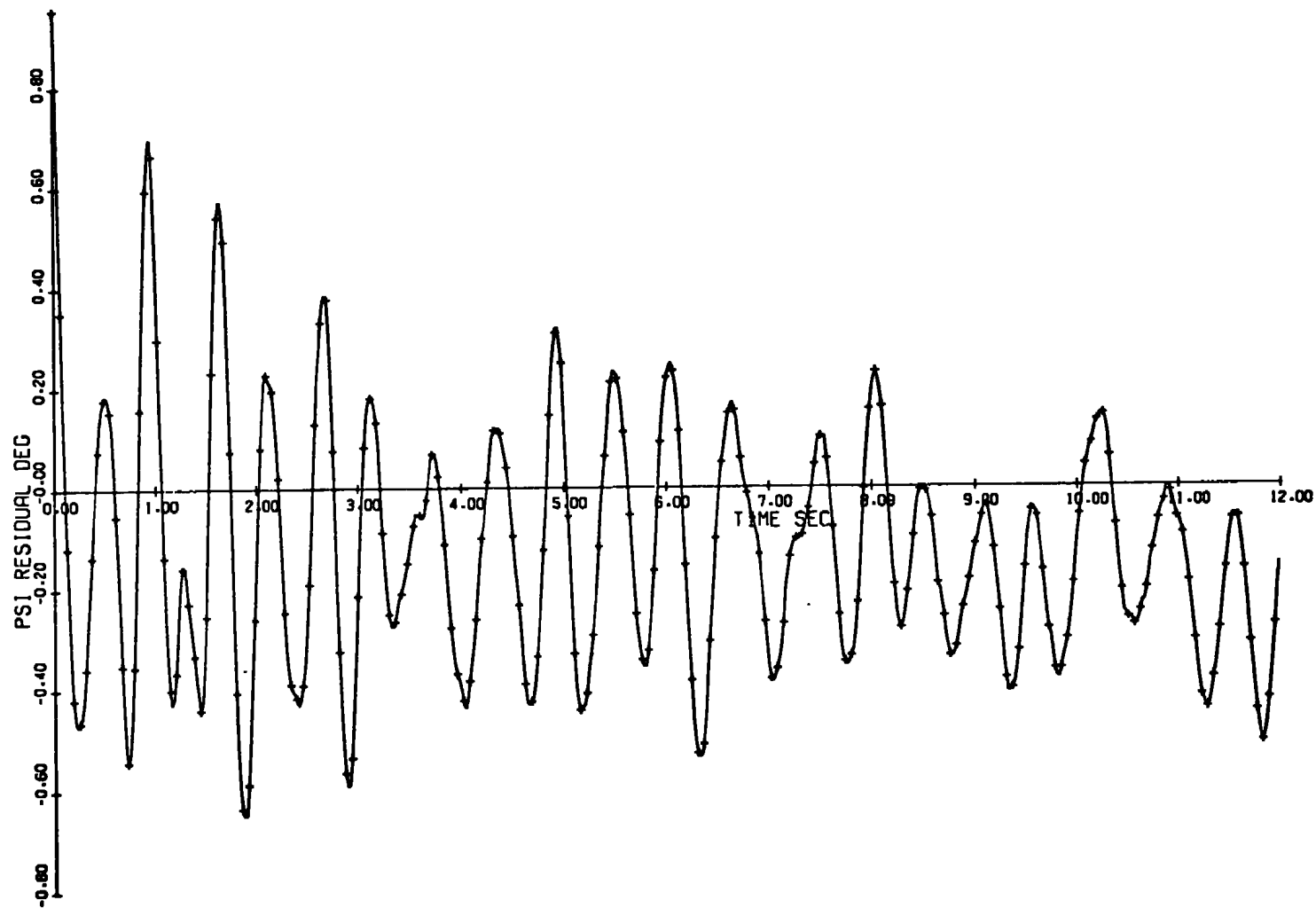
Figure 26. Graphical solution of sphere cone data given in Fig. 20 for a fit interval of 11.98 sec.



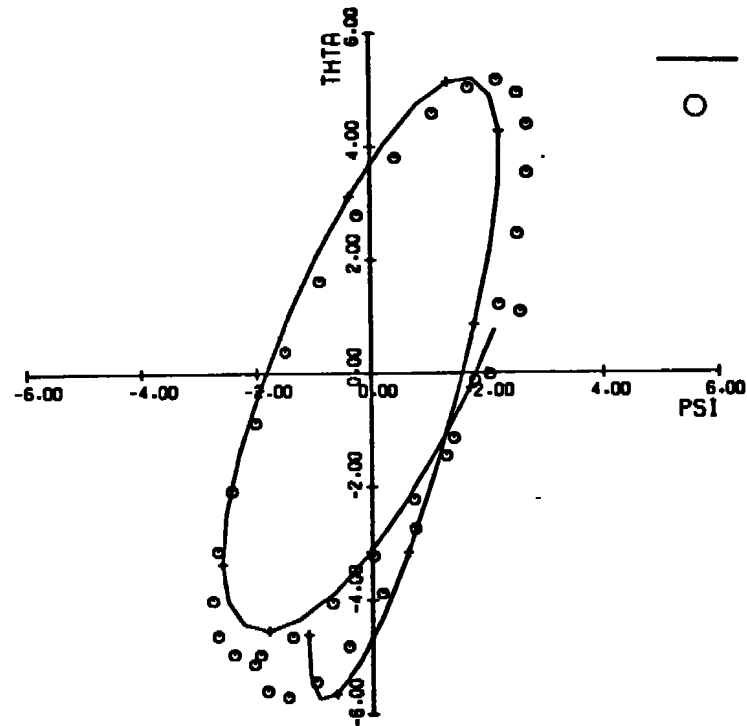
b. Computed ψ versus time
Figure 26. Continued.



c. Residual in θ versus time
Figure 26. Continued.

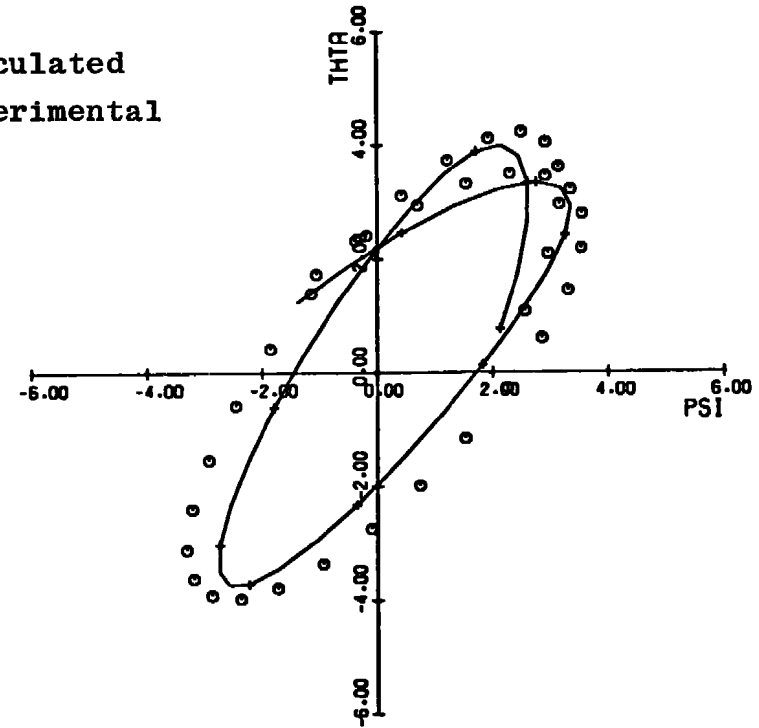


d. Residual in ψ versus time
Figure 26. Continued.



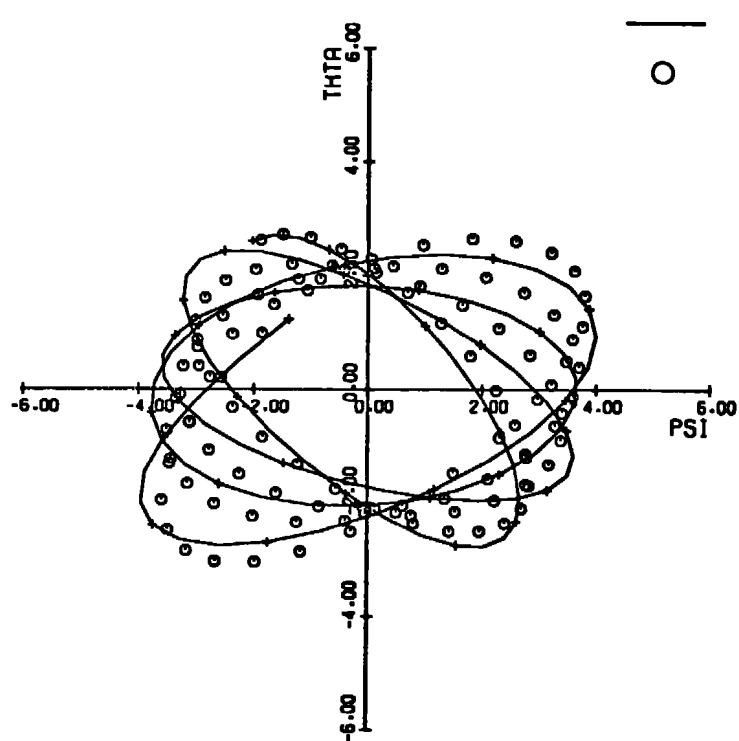
e. Fit of calculated solution to experimental data
in ψ, θ plane, time increment 0 to 0.68 sec

— Calculated
○ Experimental



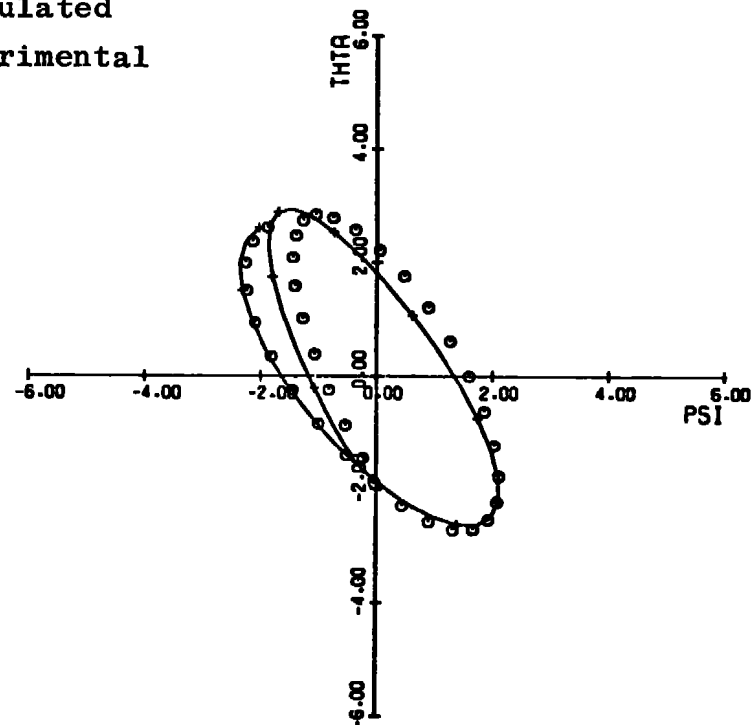
f. Fit of calculated solution to experimental data
in ψ, θ plane, time increment 0.68 to 1.38 sec

Figure 26. Continued.



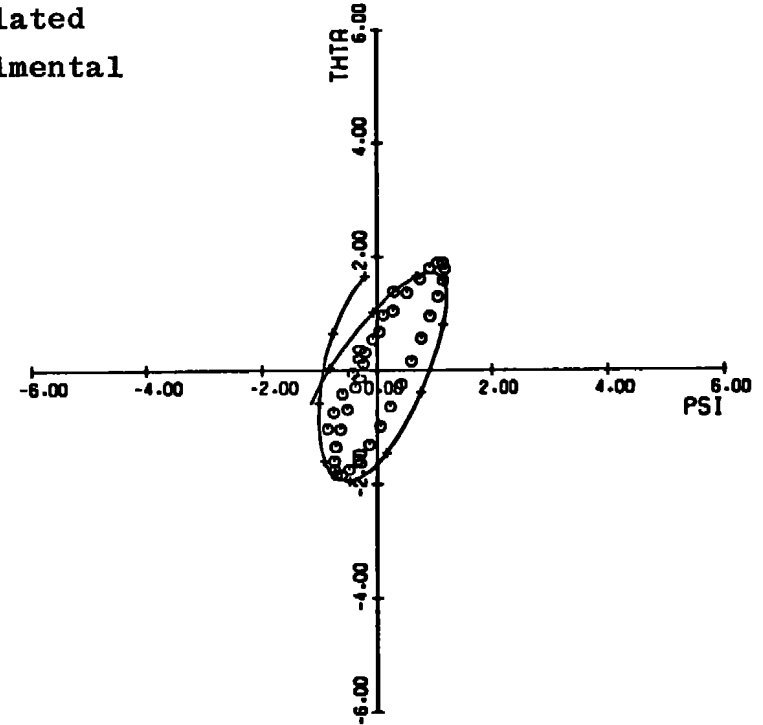
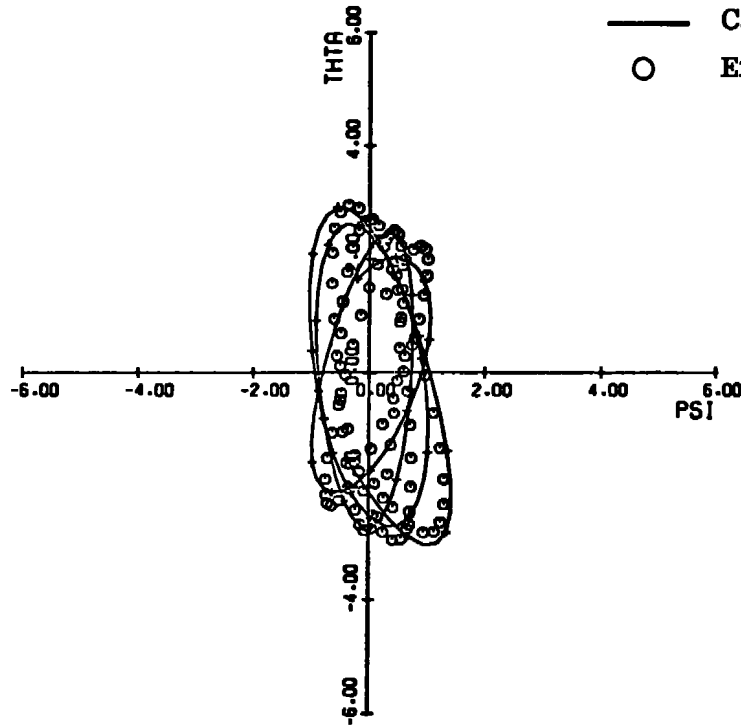
g. Fit of calculated solution to experimental data
in ψ, θ plane, time increment 1.38 to 3.48 sec

— Calculated
○ Experimental



h. Fit of calculated solution to experimental data
in ψ, θ plane, time increment 3.48 to 4.18 sec

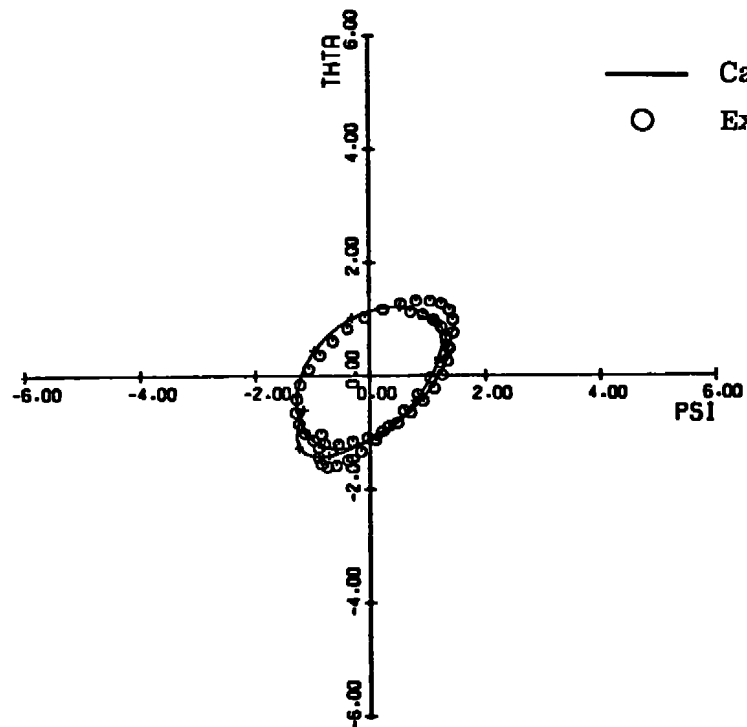
Figure 26. Continued.



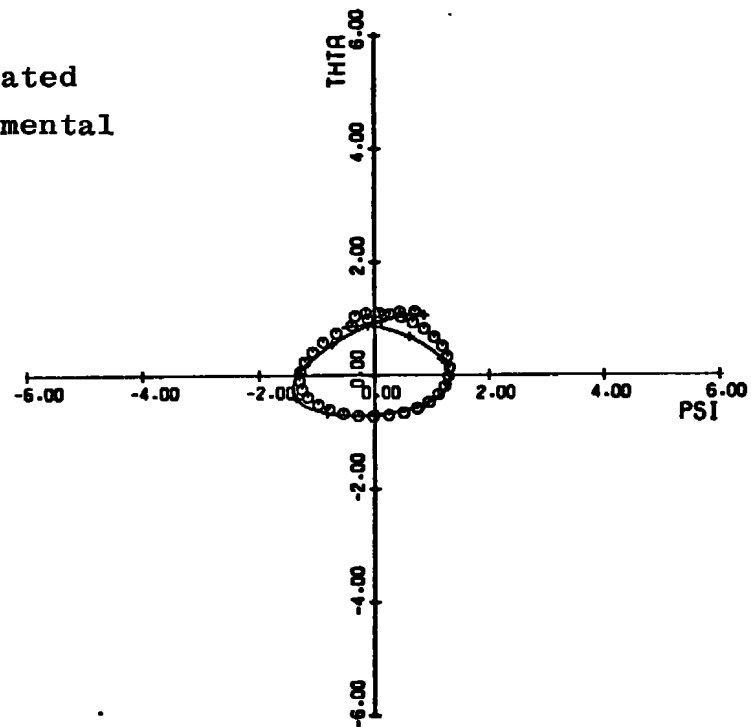
i. Fit of calculated solution to experimental data
in ψ, θ plane, time increment 4.18 to 6.28 sec

j. Fit of calculated solution to experimental data
in ψ, θ plane, time increment 6.28 to 6.98 sec

Figure 26. Continued.

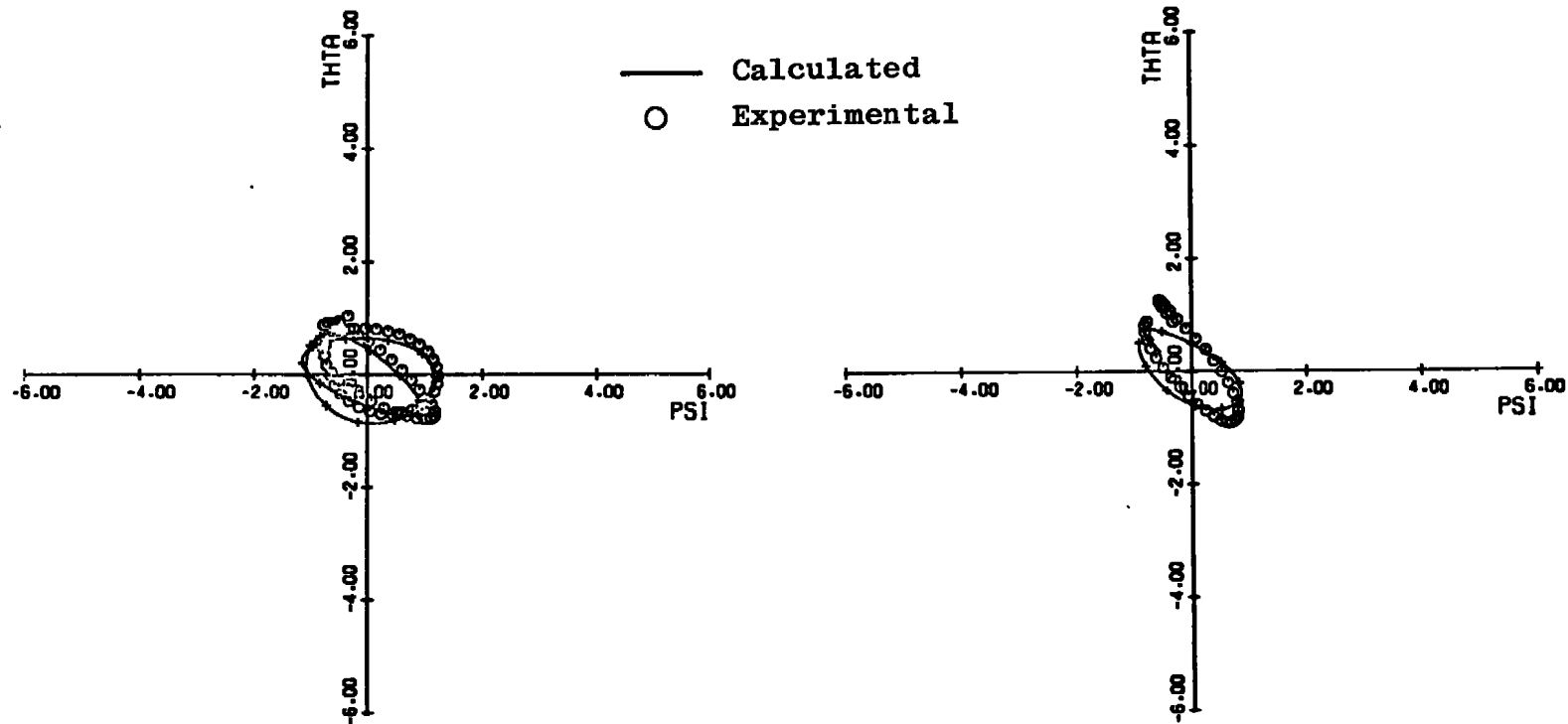


k. Fit of calculated solution to experimental data
in ψ, θ plane, time increment 6.98 to 7.98 sec



l. Fit of calculated solution to experimental data
in ψ, θ plane, time increment 7.98 to 8.68 sec

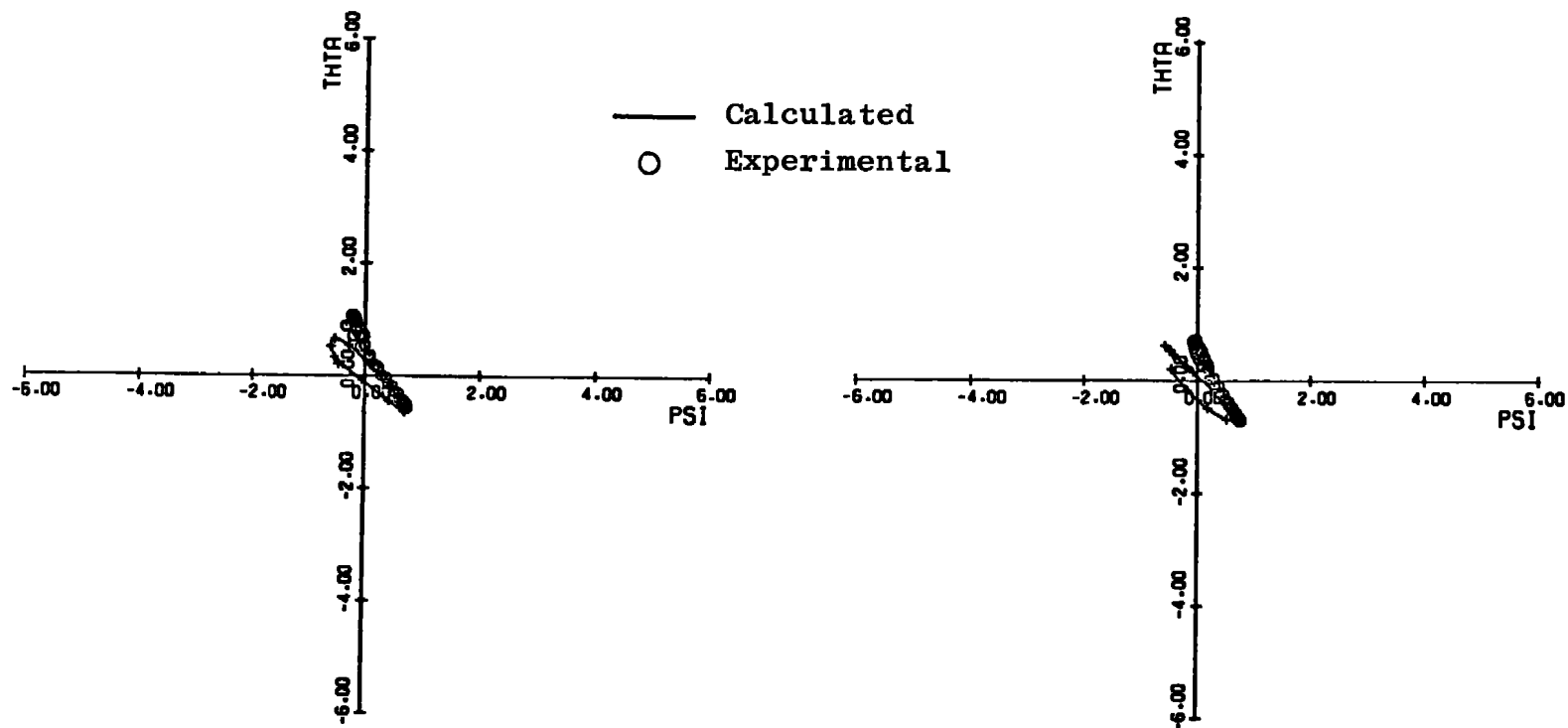
Figure 26. Continued.



m. Fit of calculated solution to experimental data
in ψ, θ plane, time increment 8.68 to 9.98 sec

n. Fit of calculated solution to experimental data
in ψ, θ plane, time increment 9.98 to 10.68 sec

Figure 26. Continued.



o. Fit of calculated solution to experimental data
in ψ, θ plane, time increment 10.68 to 11.28 sec

p. Fit of calculated solution to experimental data
in ψ, θ plane, time increment 11.28 to 11.98 sec

Figure 26. Concluded.

ANGLES

```

IMPLICIT REAL*8(A-H,O-Z)
REAL*8 IX,IY,MPRM,IPRM
REAL*8 ALIST(30)
REAL*8 CARD(10)
REAL*4 TS(1000),PHIS(1000),THTAS(1000),PSIS(1000)
DIMENSION AUX(6,186),Y(186),DERY(186),WXX(30),ACON(30),CT(30,31)
1,WX(30),AACON(30),CC(30,60)
EXTERNAL FCT,DRKGS
COMMON/MEAS/PHIM(1000),THTAM(1000),PSIM(1000)
COMMON/SOL/T(1000),PHI(1000),THTA(1000),PSI(1000)
COMMON/COEF/CON(30),CCON(30),NC,NCON(30)
COMMON/MATRIX/C(30,60),RESSUM,SIGPHI,SIGTHA,SIGPSI
COMMON/CONST/RATIO,MPRM,IPRM,A,IANGLE
EQUIVALENCE (AUX(1),CT(1)),(CC(1),C(1)),
1 (PHIS(1),PHI(1)),(THTAS(1),THTA(1)),(PSIS(1),PSI(1))
DATA ALIST/'CMA ','CMQ ','CMAD ','CMPA ','CMAD**2 ','
*CMQD**2 ','CMQB**2 ','CMRAB ','CMQD ','CLO ','CLPD ','
*CMAD**2','CLP ','CLPD**2 ','DUMMY ','DUMMY ','DUMMY ','
*DUMMY ','CNR TUN ','CMQ TUN ','CMA TUN ','CNB TUN ','FLOANG T',
*FLOANG P','PHI(0) ','PHIDOT ','THTA(0) ','THTADOT ','PSI(0) ','
*PSIDOT '/'
NAMELIST/NAM/NSWTC,NTOT,NC,NITER,DTMIN,BOUND,AREA,DIA,IX,IY,RO,U,
1AACON,NCON,NSESWH,SPHI,STHTA,SPSI,AMPHI,AMTHTA,AMPSI,
2SAMPLE,NUDELTA,IUPDAT,INLCON,IANGL,DTGEN
3,IGPNO,IBLKNO,IRCGEN,SIGPHI,SIGTHA,SIGPSI,NSTART,IRCSTR
0 FORMAT(1H1,20X,'***** INPUT DATA *****',/,
11X,'GROUP NUMBER =',I5,5X,'BLOCK NUMBER =',I5,/,
19X,'TIME',10X,'PSI',10X,'THETA',10X,'PHI',//)
1 FORMAT(7F10.0)
2 FORMAT(5X,4(E13.6,1X))
3 FORMAT(5X,A8,2X,2(E13.6,5X))
4 FORMAT(/,1X,'ITERATION NO',I5,/,19X,'CON',13X,'DELTA CON')
5 FORMAT(///,10X,'FINAL CONSTANTS AND PROBABLE ERROR',10X,/)
6 FORMAT(5X,'C(1,13)',E13.6,5X,'(1,E13.6,1)',2X,A8)
7 FORMAT(1H1,5X,'DATA FIT COMPARISON',//,11X,'TIME',
13X,'PSI/FIT',3X,'PSI/EXP',3X,'DEL PSI',2X,'THTA/FIT',2X,'THTA/EXP',
2,2X,'DEL THTA',2X,'PHI/FIT',3X,'PHI/EXP',3X,'DEL PHI',/)
8 FORMAT(5X,F10.6,9F10.3)
9 FORMAT (1X,**** CONVERGENCE CRITERIA NOT SATISFIED AFTER',I4,
11X,'ITERATIONS ****)
0 FORMAT(1H1,1X,'SUM OF RESIDUALS',E13.6,5X,'NEW PROBABLE ERROR =',
1E13.6,5X,'OLD PROBABLE ERROR =',E13.6)
1 FORMAT(7F10.4)
2 FORMAT(1X,70(' '),/,1X,'***** ERROR *****',/,1X,
1'NO OF CONSTANTS ALLOWED TO VARY EXCEEDS TOTAL NO OF DATA POINTS
2USED',/,1X,70(' '))

```

Table 1. Continued

```

200 FORMAT(1X,30('*'), ' AERODYNAMIC COEFFICIENT EXTRACTION BY CHAPMAN
      1KIRK METHOD ',30('*'),///,1X,'NSWTCH =',I5,'( =0, NORMAL DATA REDU
      2CTION',/,17X,'=1, 3DOF DATA GENERATED, NO ITERATION',/,
      317X,'=2, 3DOF DATA GENERATED AND STORED ON 7S PACK)',/,1X,'IUPDAT
      4=',I5,'(=0, INITIAL GUESSES NOT UPDATED FOR FOLLOWING SHOT',/,
      517X,'NE 0, INITIAL GUESSES UPDATED)')
201 FORMAT(/,1X,'PARAMETERS *****',/,1X,'NO OF POINTS (N) =',I5,
      1'TOTAL NO VARIABLES (NC) =',I5,5X,'TOTAL NO ITERATIONS (NITER) =',
      2I5,/,1X,'INTEGRATION STEP SIZE(DT) =',E8.2,5X,'CONVERGENCE BOUND ON
      3 ITERATION (BOUND) =',E8.2,/,1X,'BODY *****',/,1X,'AREA =',
      4F10.6,'FT**2',5X,'DIA =',F10.6,'FT',/,1X,'IX =',F12.7,'SLUGS-FT**2
      5',5X,'IY =',F12.7,'SLUGS-FT**2')
202 FORMAT(/,1X,'FREE STREAM *****',/,1X,'DENSITY (RO) =',E14.7,
      1'SLUGS/FT**3',5X,'U =',F10.4,'FT/SEC',/,1X,'COEFFICIENTS *****')
203 FORMAT(1X,'ACON(',I3,') =',E13.6,'(', 'A8,')',5X,'NCON(',I3,') =',I2)
301 FORMAT(1H1)
302 FORMAT(1X,'IANGLE =',I5,'(=0, ALPA AND BETA IN TERMS OF VELOCITY R
      1ATIOS',/,17X,'NE 0, ALPA AND BETA IN TERMS OF ANGLE OF ATTACK AND
      3 SIDESLIP)',/,1X,'INLCON =',I5,'(= 0, INITIAL CONDITIONS EVALUATED
      4 FROM DATA',/,17X,'NE 0, INPUT VALUES USED)')
303 FORMAT(1X,'BEGINNING RECORD NUMBER =',I5)
401 FORMAT(10A8)
402 FORMAT(1X,10A8)
404 FORMAT(1X,'*** INPUT CARD IMAGES ***',/)
406 FORMAT(1H1)
407 FORMAT(1X,' NOTE - ',10A8)
502 FORMAT(1X,69('*'),/,1X,'*** 3DOF GENERATED DATA STORED BEGINNING
      2ON RECORD NUMBER',I5,2X,'***',/,1X,'UNDER IGPNO =',I5,2X,
      3' AND IBLKNO =',I5,/,1X,'II=1,T',/,1X,'II=2,PHI',/,1X,
      4'II=3,THTA',/,1X,'II=4,PSI',/,1X,69('*'))
      WRITE(06,404)
405 READ(05,401,END=403)CARD
      WRITE(06,402)CARD
      GO TO 405
403 REWIND 5
      READ(05,401)CARD
      WRITE(06,406)
      DEFINE FILE 07(1140,4016,L,IREC)
C
C      INITIALIZATION
C
      NPRINT=0
      IPRINT=0
998 READ(05,NAM,END=999)
      N=NTOT
      WRITE(06,301)
      WRITE(06,200)NSWTCH,IUPDAT
      WRITE(06,302)IANGLE,INLCON
      WRITE(06,407)CARD
      WRITE(06,201)NTOT,NC,NITER,DTMIN,BOUND,AREA,DIA,IX,IY
      WRITE(06,202)RO,U
      DO 204 I=1,NC
      ACON(I)=AACON(I)
204 WRITE(06,203)I,ACON(I),ALIST(I),I,NCON(I)
      PI = 3.141592D+0

```

Table 1. Continued

```

      A = PI/180.D+0
      IF(NSWTCH)8,8,7
C
C      DATA INPUT
C
      7 CONTINUE
        T(1)=0.D+0
        DO 10 I=2,NTOT
          T(I)=T(I-1)+DTGEN
          PHIM(I)=0.D+0
          THTAM(I)=0.D+0
10      PSIM(I)=0.D+0
          PHIM(1)=0.D+0
          THTAM(1)=0.D+0
          PSIM(1)=0.D+0
          GO TO 9
      8 CONTINUE
        IREC=1
500    READ(07'IREC)IGPT,IBLK,II,TS
        IF(IGPNO.NE.IGPT) GO TO 500
        IF(IBLK.NE.IBLKNO) GO TO 500
        IF(II.NE.1) GO TO 500
        READ(07'IREC)IGPNO,IBLKNO,II,PHIS
        READ(07'IREC)IGPNO,IBLKNO,II,THTAS
        READ(07'IREC)IGPNO,IBLKNO,II,PSIS
C
C      DATA ALTERATION
C
        DO 504 I=1,NTOT
          T(I)=TS(I)
          PHIM(I)=PHIS(I)
          THTAM(I)=THTAS(I)
504    PSIM(I)=PSIS(I)
          IF(NPRINT.EQ.IGPNO.AND.IPRINT.EQ.IBLKNO) GO TO 4
          WRITE(06,100)IGPNO,IBLKNO
          IRECTMP=IREC-4
          WRITE(06,303) IRECTMP
          LOOP=0
          NLOOP=1
          DO 4 I=1,NTOT
            WRITE(06,102)T(I),PSIM(I),THTAM(I),PHIM(I)
            LOOP=LOOP+1
            KLOOP=NLOOP*50
            IF(LOOP.LT.KLOOP) GO TO 4
            NLOOP=NLOOP+1
            WRITE(06,100)IGPNO,IBLKNO
4        CONTINUE
          NPRINT=IGPNO
          IPRINT=IBLKNO
          CALL PART(SAMPLE,NDELTA,N,NTOT,NSTART)
          IF(NSEWH.EQ.1)CALL NOISE(SPHI,STHTA,SPSI,AMPHI,AMTHTA,AMPSI,
1N,SAMPLE,NDELTA,NTOT)
          IF(INLCON.EQ.0) CALL ICS(ACON)
          DO 46 I=1,N
            PSIM(I) = PSIM(I)*A

```

Table 1. Continued

```

      THTAM(I) = THTAM(I)*A
46 PHIM(I) = PHIM(I)*A
      9 CONTINUE
      NSUM=0
      DO 12 I=1,NC
12 CCON(I)=0.D+0
      DO 11 I=1,NC
      IF(NCON(I).EQ.1) CCON(I)=1.D+0
11 IF(NCON(I).EQ.1) NSUM=NSUM+1
      SUM = NSUM
C
C      DEFINE PARAMETERS AND TRANSFORM COEFFICIENTS IN SUB REG
C
      QINF = RO*(U**2)/2.D+0
      RATIO = IX/IY
      IPRM = IY/(QINF*AREA*DIA)
      MPRM = IPRM*2.D+0*U/DIA
      CALL REG(ACON)
      XN=N
      CHECK=3.D+0*XN-SUM
      IF(CHECK.LE.0.D+0) GO TO 997
      NT=NC+1
      E=0.D+0
      NR=0
C
C      INTEGRATION
C
20 CONTINUE
      CALL INTGR1(FCT,DRKGS,N,ERROR,AUX,Y,DERY,DTMIN)
      IF(NSWCH.GT.0) GO TO 47
      IF(NSUM.EQ.0) GO TO 47
C
C      CHECK FOR CONVERGENCE
C
      NR=NR+1
      E1=DSQRT(RESSUM/(3.D+0*XN-SUM))
      RESSUM=DSQRT(RESSUM)
      WRITE(06,110)RESSUM,E1,E
      IF(DABS(E1-E)=BOUND)36,36,21
21 IF(NR=NITER)22,22,36
22 NTRIG=0
38 CONTINUE
      IF(NSUM.EQ.1) GO TO 33
      E=E1
C
C      CONTRACT C MATRIX - REMOVE ZERO ROWS AND COLUMNS
C
      DO 23 I=1,NC
      DO 23 J=1,NT
23 CT(I,J)=C(I,J)
      LL=0
      DO 90 I=1,NC
92 IF((I+LL).GT.NC) GO TO 90
      IF(NCON(I+LL))91,91,93
91 LL=LL+1

```

Table 1. Continued

```

      GO TO 92
93  L=LL+1
      DO 94 K=1,NT
94  C(I,K)=CT(L,K)
90  CONTINUE
      LL=0
      LM=NSUM
      DO 80 I=1,NC
82  IF((I+LL).GT.NC) GO TO 80
      IF(NCON(I+LL))81,81,83
81  LL=LL+1
      GO TO 82
83  L=LL+1
      DO 84 K=1,LM
84  CT(K,I)=C(K,L)
80  CONTINUE
      DO 85 I=1,LM
85  CT(I,LM+1)=C(I,NT)
      L=NSUM
      LL=NSUM+1
      DO 71 I=1,L
      DO 71 J=1,L
71  C(I,J)=CT(I,J)

C
C   MATRIX INVERSION OF C
C
      IF(NTRIG)40,27,40
27  CALL INV(CT,L,LL,WX,CC)
      GO TO 41
40  CALL INV(CT,L,L,WX,CC)
41  DO 32 I=1,NC
      C(I,LL)=0.D+0
      WX(I)=CT(I,I)
32  WXX(I)=0.D+0
      LM=0

C
C   EXPAND C INVERSE TO INCLUDE ZERO ROWS AND COLUMNS
C
      DO 31 I=1,NC
      IF(NCON(I))28,28,30
28  LM=LM+1
      GO TO 31
30  IT=LM+1
      C(I,LL)=CT(IT,LL)
      WXX(I)=WXX(IT)
31  CONTINUE
      GO TO 34

C
C   SOLVE FOR CORRECTION TO COEFFICIENTS
C
33  DO 35 I=1,NC
      IF(NCON(I)-1)39,49,49
49  C(I,NT)=C(I,NT)/C(I,I)
      WXX(I)=1.D+0/C(I,I)
      GO TO 35

```

Table 1. Continued

```

39 C(I,NT)=0.D+0
   WXX(I)=0.D+0
35 CONTINUE
   LL=NT
34 IF(NTRIG.EQ.1) GO TO 42
   WRITE(06,104)NR
   DO 60 I=1,NC
60  WXX(I)=C(I,LL)

C
C   TRANSFORM COEFFICIENTS AND CORRECTIONS IN SUB REGOUT
C
   CALL REGOUT(ACON,WXX)
   DO 50 I=1,NC
50  WRITE(06,103)ALIST(I),ACON(I),WXX(I)
   DO 43 I=1,NC
43  CON(I)=CON(I)+C(I,LL)
   GO TO 20
36 CONTINUE
   NTRIG=1
37 GO TO 38
42 CONTINUE

C
C   COMPUTE PROBABLE ERROR IN COEFFICIENTS
C
   DO 44 I=1,NC
44  WXX(I)=E1*DSQRT(DABS(WXX(I)))
   CALL REGOUT(ACON,WXX)
   WRITE(06,105)
   IF(NR.GT.NITER)WRITE(06,109)NR
   DO 45 I=1,NC
45  WRITE(06,106) I,ACON(I),WXX(I),ALIST(I)
47  WRITE(06,107)
   LOOP=0
   NLOOP=1
   IREC=IRCGEN
   DTTEMP=T(2)-T(1)
   DO 48 I=1,N
   TT=T(I)
   Z1 = PSI(I)/A
   Z2 = PSIM(I)/A
   Z3 = THTA(I)/A
   Z4 = THTAM(I)/A
   Z5 = PHI(I)/A
   Z6 = PHIM(I)/A
   Z10=Z1-Z2
   Z11=Z3-Z4
   Z12=Z5-Z6
   WRITE(06,108)TT,Z1,Z2,Z10,Z3,Z4,Z11,Z5,Z6,Z12
   THTAS(I)=Z3
   PSIS(I)=Z1
   TS(I)=TT
   PHIS(I)=Z5
   IF(NSWTCH.NE.0) GO TO 597
   TS(I)=Z10
   PHIS(I)=Z11

```

Table 1. Continued

```

597 CONTINUE
  LOOP=LOOP+1
  KLOOP=NLOOP*50
  IF (LOOP.LT.KLOOP) GO TO 48
  NLOOP=NLOOP+1
  WRITE(06,107)
48 CONTINUE
  IF(NSWTCH.NE.0) GO TO 599
C
C   COMPARISON OF FIT DATA AND EXPERIMENT STORED
C
  IREC=IRCSTR
  IF(IRCSTH.GE.IRCGEN-3.AND.IRCSTR.LE.IRCGEN+3) GO TO 599
  WRITE(06,598)NSWTCH,IRCSTR,IGPNO,IBLKNO,DTTEMP
598 FORMAT(1H1,1X,'NSWTCH =',I5,/,1X,'3DOF DATA STORED BEGINNING AT RE
1CORD ',I5,2X,'UNDER IGPNO =',I5,2X,'AND IBLKNO =',I5,/,1X,'II=5,TH
2TA',/,1X,'II=6,THTA-THTAM',/,1X,'II=7,PSI',/,1X,'II=8,PSI-PSIM',
3/,1X,'DT =',F7.4,2X,'SEC',1H1)
  II=5
  WRITE(07'IREC)IGPNO,IBLKNO,II,THTAS
  II=6
  WRITE(07'IREC)IGPNO,IBLKNO,II,PHIS
  II=7
  WRITE(07'IREC)IGPNO,IBLKNO,II,PSIS
  II=8
  WRITE(07'IREC)IGPNO,IBLKNO,II,TS
599 CONTINUE
  IF(NSWTCH.NE.2) GO TO 501
C
C   3DOF GENERATED SOLUTION STORED
C
  WRITE(06,502)IRCGEN,IGPNO,IBLKNO
  II=1
  WRITE(07'IREC)IGPNO,IBLKNO,II,TS
  II=2
  WRITE(07'IREC)IGPNO,IBLKNO,II,PHIS
  II=3
  WRITE(07'IREC)IGPNO,IBLKNO,II,THTAS
  II=4
  WRITE(07'IREC)IGPNO,IBLKNO,II,PSIS
501 CONTINUE
  GO TO 996
997 WRITE(06,112)
996 CONTINUE
  IF(IUPDAT.EQ.0) GO TO 998
  DO 995 I=1,NC
995 AACON(I)=ACON(I)
  GO TO 998
999 CONTINUE
  STOP
  END
C
C   SUBROUTINE DRKGS(XI,Y,DERY,NDIM,FCT,AUX,DT,NDT)
C

```

Table 1. Continued

```

      IMPLICIT REAL*8(A-H,O-Z)
      DIMENSION Y(1),DERY(1),AUX(6,1)
      X=XI
      DO 5 J=1,NDT
      DO 1 I=1,NDIM
1    AUX(6,I)=Y(I)
      CALL FCT(X,Y,DERY)
      DO 2 I=1,NDIM
      AUX(1,I)=DERY(I)
2    Y(I)=AUX(6,I)+.5D+0*DT*AUX(1,I)
      XTEMP=X+.5D+0*DT
      CALL FCT(XTEMP,Y,DERY)
      DO 3 I=1,NDIM
      AUX(2,I)=DERY(I)
3    Y(I)=AUX(6,I)+.5D+0*DT*AUX(2,I)
      CALL FCT(XTEMP,Y,DERY)
      DO 4 I=1,NDIM
      AUX(3,I)=DERY(I)
4    Y(I)=AUX(6,I)+DT*AUX(3,I)
      X=X+DT
      CALL FCT(X,Y,DERY)
      DO 5 I=1,NDIM
      AUX(4,I)=DERY(I)
5    Y(I)=AUX(6,I)+DT*(AUX(1,I)+(AUX(2,I)+AUX(3,I))*2.D+0
      1+AUX(4,I))/6.D+0
      RETURN
      END

```

C
C

C

SUBROUTINE FCT(T,X,DERX)

```

      IMPLICIT REAL*8(A-H,O-Z)
      REAL*8 MXOIX,MYOI,MZOI,M1,M2,M3,MAG,MPRM,IPRM
      DIMENSION X(1),DERX(1)
      COMMON/COEF/CON(30),CCON(30),NC,NCON(30)
      COMMON/CONST/RATIO,MPRM,IPRM,A,K
      PSI=X(5)
      THTA=X(3)
      PHI=X(1)
      PSIP=X(6)
      THTAP=X(4)
      PHIP=X(2)
      CALL TEMP(PSI,THTA,PHI,PSIP,THTAP,PHIP,0.D+0,0.D+0,0.D+0,0.D+0,
10.D+0,0.D+0,K)
      CALL MBAR(MXOIX,MYOI,MZOI,PSI,THTA,PHI,PSIP,THTAP,PHIP)
      DERX(1) = PHIP
      DERX(2) = MXOIX + PSIP*THTAP*DCOS(THTA)+MZOI*DTAN(THTA)
1 + (2.D+0-RATIO)*PSIP*THTAP*DTAN(THTA)*DSIN(THTA)
2 + RATIO*PHIP*THTAP*DTAN(THTA)
      DERX(3) = THTAP
      DERX(4) = MYOI - (1.D+0-RATIO)*(PSIP**2)*(DSIN(THTA)*DCOS(THTA))
1 - RATIO*PHIP*PSIP*DCOS(THTA)
      DERX(5) = PSIP
      DERX(6) = MZOI/DCOS(THTA) + (2.D+0-RATIO)*PSIP*THTAP*
1 DTAN(THTA) + RATIO*PHIP*THTAP/DCOS(THTA)

```

Table 1. Continued

```

      NEQ=(NC+1)*6
      DO 5 I=7,NEQ
5     DERX(I)=0.D+0
      DO 10 I=1,NC
      IF(NCON(I).EQ.0) GO TO 10
      DERX(6+I) = X(6+NC+I)
      DERX(2*NC+6+I) = X(3*NC+6+I)
      DERX(4*NC+6+I) = X(5*NC+6+I)
      P1 = X(6+I)
      P2 = X(2*NC+6+I)
      P3 = X(4*NC+6+I)
      P1P= X(NC+6+I)
      P2P= X(3*NC+6+I)
      P3P= X(5*NC+6+I)
      CALL TEMP(PSI,THTA,PHI,PSIP,THTAP,PHIP,P1,P2,P3,P1P,P2P,P3P,K)
      CALL MBAHA(M1,M2,M3,PSI,THTA,PHI,PSIP,THTAP,PHIP,P1,P2,P3,P1P,P2P,
1     P3P,I)
      DERX(6+NC+I)=M1+THTAP*P3P*DCOS(THTA)+PSIP*P2P*DCOS(THTA)
1-PSIP*THTAP*P2*DSIN(THTA) + M3*DTAN(THTA) +
      2MZ0I*P2/(DCOS(THTA)**2) + (2.D+0-RATIO)*DTAN(THTA)*
      3DSIN(THTA)*(THTAP*P3P + PSIP*P2P)+(2.D+0-RATIO)*PSIP*THTAP
      4*P2*DSIN(THTA)*(1.D+0+1.0+0/(DCOS(THTA)**2)) +
      5RATIO*(P1P*THTAP*DTAN(THTA)+PHIP*P2P*DTAN(THTA)
      6+PHIP*THTAP*P2/(DCOS(THTA)**2))
      DERX(6+3*NC+I)=M2-(1.D+0-RATIO)*2.D+0*PSIP*P3P*DSIN(THTA)
1*DCOS(THTA)-(1.D+0-RATIO)*P2*(1.D+0-2.D+0*(DSIN(THTA)**2))*
      2PSIP**2 - RATIO*(P1P*PSIP*DCOS(THTA)+PHIP*P3P*DCOS(THTA)
      3-PHIP*PSIP*P2*DSIN(THTA))
      DERX(6+5*NC+I)=M3/DCOS(THTA)+MZ0I*P2*DTAN(THTA)/DCOS(THTA)
1+(2.D+0-RATIO)*DTAN(THTA)*(PSIP*P2P+THTAP*P3P) +
      2(2.D+0-RATIO)*PSIP*THTAP*P2/DCOS(THTA)**2 +
      3RATIO*P1P*THTAP/DCOS(THTA)+RATIO*(PHIP*THTAP*P2*DTAN(THTA)
      4/DCOS(THTA)+PHIP*P2P/DCOS(THTA))
10    CONTINUE
      RETURN
      END
C
C
C     SUBROUTINE PART(SAMPLE,NDELTA,N,NTOT,NSTART)
C
C     IMPLICIT REAL*8 (A-H,O-Z)
      COMMON/MEAS/PHIM(1000),THTAM(1000),PSIM(1000)
      COMMON/SOL/T(1000),PHI(1000),THTA(1000),PSI(1000)
      DO 13 I=2,NTOT
      IF(T(I).NE.0.D+0) NTEMP=I
13    CONTINUE
      TMAX=T(NTEMP)
      DO 11 I=NSTART,NTOT
      J=(I-1)*NDELTA+1
      IF(J.GT.NTEMP) GO TO 11
      RATIO=(T(J)-T(NSTART))/TMAX
      IF(RATIO.GT.SAMPLE) GO TO 11
      N=I
      T(I)=T(J)
      PHIM(I)=PHIM(J)

```

Table 1. Continued

```

      THTAM(I)=THTAM(J)
      PSIM(I)=PSIM(J)
11  CONTINUE
      N=N+1-NSTART
      DO 12 I=1,N
        J=I+NSTART-1
        T(I)=T(J)
        PHIM(I)=PHIM(J)
        THTAM(I)=THTAM(J)
12  PSIM(I)=PSIM(J)
      N1=N+1
      IF(NTOT.LT.N1) GO TO 14
      DO 15 I=N1,NTOT
15  T(I)=0.D+0
14  CONTINUE
      WRITE(06,10)SAMPLE,NDELTA,NSTART,N,T(1),T(N)
10  FORMAT(1H1,1X,'**** DATA BLOCK ALTERED ****',/,1X,'SAMPLE =',
1F7.4,/,1X,'NDELTA =',I5,/,1X,'NSTART =',I5,/,1X,'N =',I5,/,
21X,'T(1) = ',F7.4,5X,'T(N) = ',F7.4,/,
31X,28(' '))
      RETURN
      END
C
C
C      FUNCTION DUM(I,J)
C
C      IMPLICIT REAL*8(A-H,O-Z)
C      DUM=0.D+0
C      IF(I.EQ.J) DUM=1.D+0
C      RETURN
C      END
C
C
C      SUBROUTINE ICS(ACON)
C
C      IMPLICIT REAL*8 (A-H,O-Z)
C      DIMENSION ACON(30)
C      COMMON/MEAS/PHIM(1000),THTAM(1000),PSIM(1000)
C      COMMON/SOL/T(1000),PHI(1000),THTA(1000),PSI(1000)
C      DT=T(2)-T(1)
C      PHIO=PHIM(1)
C      THTA0=THTAM(1)
C      PSIO=PSIM(1)
C      ACON(25)=PHIO
C      ACON(27)=THTA0
C      ACON(29)=PSIO
C      ACON(26)=(PHIM(2)-PHIO)/DT
C      ACON(28)=(THTAM(2)-THTA0)/DT
C      ACON(30)=(PSIM(2)-PSIO)/DT
C      RETURN
C      END
C
C
C      SUBROUTINE INV(C,NC,NCS1,XXX,CC)
C

```

Table 1. Continued

```

      IMPLICIT REAL*8(A-H,O-Z)
      DIMENSION C(30,31),WXX(30),PIVOT(2),CC(30,60)
3000 FORMAT(/10X,'DET IS EQUAL TO ZERO')
      NCT=NC*2
      NCP1=NC+1
      DO 10 I=1,NC
      DO 10 J=1,NC
10    CC(I,J)=C(I,J)
      DO 20 I=1,NC
      DO 20 J=NCP1,NCT
20    CC(I,J)=0.D+0
      DO 30 I=1,NC
30    CC(I,NC+I)=1.D+0
      DO 205 I=1,NC
      PIVOT(1)=CC(I,I)
      DO 200 K=1,NC
      PIVOT(2)=CC(K,I)
126  IF(K-I) 135,130,140
130  DO 150 J=1,NCT
      IF(PIVOT(1)) 134,210,134
134  CC(K,J)=CC(I,J)/PIVOT(1)
150  CONTINUE
      GO TO 200
135  DO 160 J=1,NCT
      IF(PIVOT(1)) 136,160,136
136  CC(K,J)=CC(K,J)-CC(I,J)*PIVOT(2)/PIVOT(1)
160  CONTINUE
      GO TO 200
140  DO 170 J=1,NCT
      IF(PIVOT(2)) 145,170,145
145  CC(K,J)=CC(K,J)/PIVOT(2)-CC(I,J)
170  CONTINUE
200  CONTINUE
205  CONTINUE
      GO TO 250
210  WRITE (6,3000)
250  DO 300 I=1,NC
      DO 300 J=1,NC
300  C(I,J)=CC(I,J+NC)
      NCS=NCS1
350  IF(NCS=NC)500,500,400
400  DO 420 I=1,NC
      WXX(I)=C(I,NCS)
420  C(I,NCS)=0.D+0
      DO 450 I=1,NC
      DO 450 J=1,NC
450  C(I,NCS)=C(I,NCS)+C(I,J)*WXX(J)
      NCS=NCS+1
      GO TO 350
500  CONTINUE
      RETURN
      END
C
C
      SUBROUTINE NOISE(SPHI,STHTA,SPSI,AMPHI,AMTHTA,AMPSI,N,

```

Table 1. Continued

```

ISAMPLE,NDELTA,NTOT)
C
C      THIS SUBROUTINE  ADDS GAUSSIAN NOISE TO DATA
      IMPLICIT REAL*8(A-H,O-Z)
      COMMON/MEAS/PHIM(1000),THTAM(1000),PSIM(1000)
      COMMON/SOL/T(1000),PHI(1000),THTA(1000),PSI(1000)
      WRITE(06,100)SPSI,STHTA,SPHI,AMPSI,AMTHTA,AMPHI,N
      CALL TIME(IYEAR,ISEC)
7  IF(ISEC-1000) 5,5,6
6  ISEC=ISEC-1000
    GO TO 7
5  IX=(ISEC+IYEAR)*2+1
    IY=IX+2
    IZ=IX+4
    SIG1PH=0.D+0
    SIG2PH=0.D+0
    SIG3PH=0.D+0
    SIG1TH=0.D+0
    SIG2TH=0.D+0
    SIG3TH=0.D+0
    SIG1PS=0.D+0
    SIG2PS=0.D+0
    SIG3PS=0.D+0
    TOTPHI=0.D+0
    TOTTHA=0.D+0
    TOTPSI=0.D+0
    LOOP=1
    NLOOP=1
    DO 10 I=1,N
      CALL GAUSS(IX,SPHI,AMPHI,VPHI)
      CALL GAUSS(IY,STHTA,AMTHTA,VTHTA)
      CALL GAUSS(IZ,SPSI,AMPSI,VPSI)
      PHIM(I)=PHIM(I)+VPHI
      THTAM(I)=THTAM(I)+VTHTA
      PSIM(I)=PSIM(I)+VPSI
      TOTPHI=TOTPHI+VPHI
      TOTTHA=TOTTHA+VTHTA
      TOTPSI=TOTPSI+VPSI
      P=DABS(VPHI)
      Q=DABS(VTHTA)
      R=DABS(VPSI)
      IF(P.LT.SPHI)SIG1PH=SIG1PH+1.D+0
      IF(P.GE.SPHI.AND.P.LT.2.D+0*SPHI)SIG2PH=SIG2PH+1.D+0
      IF(P.GE.2.D+0*SPHI.AND.P.LE.3.D+0*SPHI)SIG3PH=SIG3PH+1.D+0
      IF(Q.LT.STHTA)SIG1TH=SIG1TH+1.D+0
      IF(Q.GE.STHTA.AND.Q.LT.2.D+0*STHTA)SIG2TH=SIG2TH+1.D+0
      IF(Q.GE.2.D+0*STHTA.AND.Q.LE.3.D+0*STHTA)SIG3TH=SIG3TH+1.D+0
      IF(R.LT.SPSI)SIG1PS=SIG1PS+1.D+0
      IF(R.GE.SPSI.AND.R.LT.2.D+0*SPSI)SIG2PS=SIG2PS+1.D+0
      IF(R.GE.2.D+0*SPSI.AND.R.LE.3.D+0*SPSI)SIG3PS=SIG3PS+1.D+0
10  CONTINUE
      WRITE(06,103)TOTPSI,TOTTHA,TOTPHI,SIG1PS,SIG1TH,SIG1PH,
1  SIG2PS,SIG2TH,SIG2PH,SIG3PS,SIG3TH,SIG3PH
100 FORMAT(1H1,1X,'*** GAUSSIAN NOISE ADDED ***',/,1X,
1  'ONE STANDARD DEVIATION = PSI =',F10.6,5X,'THETA =',F10.6,5X,

```

Table 1. Continued

```

2'PHI =',F10.6,/,1X,'CONSTANT BIAS - PSI =',F10.6,5X,
3'THETA =',F10.6,5X,'PHI =',F10.6,/,1X,'TOTAL NO OF TIME POINTS USE
4D IN FIT (N)=',I5)
103 FORMAT(1H1,1X,'SUM OF NOISE ADDED',/,6X,'PSI',6X,'THTA',7X,'PHI',
1/,1X,3F10.3,/,/,1X,'NOISE CONTRIBUTION WITHIN ONE SIGMA',/,
26X,'PSI',6X,'THTA',7X,'PHI',/,1X,3F10.3,/,/,
31X,'NOISE CONTRIBUTION BETWEEN ONE SIGMA AND TWO SIGMA',/,
46X,'PSI',6X,'THTA',7X,'PHI',/,1X,3F10.3,/,/,1X,'NOISE CONTRIBUTION
5BETWEEN TWO SIGMA AND THREE SIGMA',/,6X,'PSI',6X,'THTA',7X,'PHI',
6/,1X,3F10.3)
RETURN
END

C
C
SUBROUTINE RANDU(IX,IY,YPL)
C
IMPLICIT REAL*8(A-H,O-Z)
IY=IX*65539
IF(IY)5,6,6
5 IY=IY+2147483647+1
6 YPL=IY
YPL=YPL*.4656613D-9
RETURN
END

C
C
SUBROUTINE GAUSS(IX,S,AM,V)
C
IMPLICIT REAL*8(A-H,O-Z)
A=0.D+0
DO 50 I=1,48
CALL RANDU(IX,IY,Y)
IX=IY
50 A=A+Y
V=(A-24.D+0)/2.D+0
V=V*S+AM
RETURN
END

C
C
SUBROUTINE INTGRL(FCT,DRKGS,N,ERROR,AUX,Y,DERY,DTMIN)
C
IMPLICIT REAL*8(A-H,O-Z)
DIMENSION AUX(6,1),Y(1),DERY(1)
COMMON/MEAS/PHIM(1000),THTAM(1000),PSIM(1000)
COMMON/SOL/T(1000),PHI(1000),THTA(1000),PSI(1000)
COMMON/COEF/CON(30),CCON(30),NC,NCON(30)
COMMON/MATRIX/C(30,60),RESSUM,SPHI,STHA,SPSI
A=6.28318531D+0
NL=NC-5
DO 10 I=1,6
10 Y(I)=CON(NL+I-1)
DO 11 I=1,NC
Y(6+I)=DUM(NL,I)
DO 11 J=1,5

```

Table 1. Continued

```

11 Y(6+J*NC+I)=DUM(NL+J,I)
   NEQ=(NC+1)*6
   DNEQ=NEQ
   NL=NC+1
   K=1
   PHI(K)=Y(1)
   THTA(K)=Y(3)
   PSI(K)=Y(5)
   THTA(K)=THTA(K)+CON(23)
   PSI(K)=PSI(K)+CON(24)
   DPHI=PHIM(K)-PHI(K)
   IF(DPHI.GT.(A/2.D+0)) PHI(K)=PHI(K)+A
   IF(DPHI.LT.(-A/2.D+0)) PHI(K)=PHI(K)-A
   DO 19 I=1,NC
     Y(6+2*NC+I)=Y(6+2*NC+I)+DUM(23,I)
     Y(6+4*NC+I)=Y(6+4*NC+I)+DUM(24,I)
19 CONTINUE
   DO 12 I=1,NC
     DO 12 J=1,NC
       C(I,J)=Y(6+I)*Y(6+J)/SPHI**2 + Y(6+2*NC+I)*Y(6+2*NC+J)/STHA**2
       1+ Y(6+4*NC+I)*Y(6+4*NC+J)/SPSI**2
12 C(I,J)=C(I,J)*CCON(I)*CCON(J)
   DO 17 J=1,NC
     C(J,NL)=(PHIM(K)-PHI(K))*Y(6+J)/SPHI**2 + (THTAM(K)-THTA(K))*
       1Y(6+2*NC+J)/STHA**2 + (PSIM(K)-PSI(K))*Y(6+4*NC+J)/SPSI**2
17 C(J,NL)=C(J,NL)*CCON(J)
   RESSUM = ((PHIM(K)-PHI(K))/SPHI)**2 + ((THTAM(K)-THTA(K))/STHA)**2
   1+ ((PSIM(K)-PSI(K))/SPSI)**2
   DO 13 K=2,N
     XI=T(K-1)
     DTE=T(K)-T(K-1)
     DT=DTE
     NDT=1
     IF(DTMIN.GE.DTE) GO TO 18
     NDT=DTE/DTMIN
     UT=NDT
     DT=DTE/DT
18 CONTINUE
   CALL DRKGS(XI,Y,DERY,NEQ,FCT,AUX,DT,NDT)
   IF(Y(1).LE.(-A)) Y(1)=Y(1)+A
   IF(Y(1).GE.A) Y(1)=Y(1)-A
   PHI(K)=Y(1)
   THTA(K)=Y(3)
   PSI(K)=Y(5)
   THTA(K)=THTA(K)+CON(23)
   PSI(K)=PSI(K)+CON(24)
   DPHI=PHIM(K)-PHI(K)
   IF(DPHI.LT.(-A/2.D+0)) PHI(K)=PHI(K)-A
   IF(DPHI.GT.(A/2.D+0)) PHI(K)=PHI(K)+A
   DO 20 I=1,NC
     Y(6+2*NC+I)=Y(6+2*NC+I)+DUM(23,I)
     Y(6+4*NC+I)=Y(6+4*NC+I)+DUM(24,I)
20 CONTINUE
   DO 15 I=1,NC
     DO 15 J=1,NC

```

Table 1. Continued

```

      C(I,J)=Y(6+I)*Y(6+J)/SPHI**2 + Y(6+2*NC+I)*Y(6+2*NC+J)/STHA**2
      1+ Y(6+4*NC+I)*Y(6+4*NC+J)/SPSI**2 + C(I,J)
15  C(I,J)=C(I,J)*CCON(I)*CCON(J)
      DO 16 J=1,NC
      C(J,NL)=(PHIM(K)-PHI(K))*Y(6+J)/SPHI**2 + (THTAM(K)-THTA(K))*
      1Y(6+2*NC+J)/STHA**2 + (PSIM(K)-PSI(K))*Y(6+4*NC+J)/SPSI**2+C(J,NL)
16  C(J,NL)=C(J,NL)*CCON(J)
      RESSUM = ((PHIM(K)-PHI(K))/SPHI)**2 + ((THTAM(K)-THTA(K))/STHA)**2
      1+ ((PSIM(K)-PSI(K))/SPSI)**2 + RESSUM
13  CONTINUE
      RETURN
      END

```

C
C

```

      SUBROUTINE TEMP(PSI,THTA,PHI,PSIP,THTAP,PHIP,P1,P2,P3,P1P,P2P,P3P,
      1K)

```

C

```

      IMPLICIT REAL*8(A-H,O-Z)
      REAL*8 MAG
      COMMON/TCOEF1/SPN,A,B,MAG,QA,RA,AD,BD,ALPA,BTA,ALPAP,BTAP,DLTA2,P,
      1Q,R,SMAG,DLTA
      COMMON/COEF/CON(30),CCON(30),NC,NCON(30)
      SPN=P1P-PSIP*P2*DCOS(THTA)-P3P*DSIN(THTA)
      A=-P3*DSIN(PSI)*DSIN(THTA)+P2*DCOS(PSI)*DCOS(THTA)
      B=-P3*DCOS(PSI)
      MAG= 2.0+0*(P2*DSIN(THTA)*DCOS(PSI)
      1+ P3* DCOS(THTA)*DSIN(PSI))*DCOS(PSI)*DCOS(THTA)
      QA = P2P
      RA = P3P*DCOS(THTA)-PSIP*P2*DSIN(THTA)
      AD=-P3P*DSIN(PSI)*DSIN(THTA)-P2*(PSIP*DSIN(PSI)*DCOS(THTA)
      1+THTAP*DCOS(PSI)*DSIN(THTA))-P3*(PSIP*DCOS(PSI)*DSIN(THTA)
      2+THTAP*DSIN(PSI)*DCOS(THTA))+P2P* DCOS(PSI)*DCOS(THTA)
      BD=- P3P*DCOS(PSI)+PSIP*P3*DSIN(PSI)
      ALPA = DCOS(PSI) * DSIN(THTA)
      BTA =-DSIN(PSI)
      ALPAP = -PSIP*DSIN(PSI)*DSIN(THTA)+THTAP*DCOS(PSI)*DCOS(THTA)
      BTAP = -PSIP*DCOS(PSI)
      DLTA2 = (DCOS(PSI)*DSIN(THTA))**2 + (DSIN(PSI))**2
      P = PHIP - PSIP * DSIN(THTA)
      Q = THTAP
      R = PSIP*DCOS(THTA)
      IF(K.EQ.0) GO TO 10
      ALPA=THTA
      BTA=DATAN(-DTAN(PSI)/DCOS(THTA))
      A=P2
      B=-(P3/(DCOS(PSI)**2)+DTAN(PSI)*DTAN(THTA)*P2)*
      1(DCOS(BTA)**2)/DCOS(THTA)
      DLTA2=ALPA**2+BTA**2
      MAG=2.0+0*(ALPA*A+BTA*B)
10  CONTINUE
      DLTA=DSQRT(DLTA2)
      SMAG=0.0+0
      IF(DLTA2.EQ.0.0+0) GO TO 9
      SMAG=MAG/(2.0+0*DLTA)
9  CONTINUE

```

Table 1. Continued

```

AD=0.D+0
BD=0.D+0
ALPAP=0.D+0
BTAP=0.D+0
RETURN
END

C
C
SUBROUTINE REGOUT(ACON,WXX)
C
  IMPLICIT REAL*8(A-H,O-Z)
  REAL*8 MPRM,IPRM
  DIMENSION ACON(30),WXX(30)
  COMMON/COEF/CON(30),CCON(30),NC,NCON(30)
  COMMON/CONST/RATIO,MPRM,IPRM,A,IANGLE
  C1 = IPRM/MPRM
  DO 10 I=1,22
    ACON(I) = MPRM*CON(I)
10  WXX(I) = MPRM*WXX(I)
    ACON(1) = ACON(1)*C1
    ACON(3) = ACON(3)*C1
    ACON(5) = ACON(5)*C1
    WXX(1) = WXX(1) * C1
    WXX(3) = WXX(3)*C1
    WXX(5) = WXX(5) *C1
    ACON(21) = ACON(21)*C1
    ACON(22) = ACON(22)*C1
    WXX(21) = WXX(21)*C1
    WXX(22) = WXX(22)*C1
    ACON(10) = ACON(10)*C1*RATIO
    ACON(11) = ACON(11)*RATIO
    ACON(13) = ACON(13) * RATIO
    ACON(14) = ACON(14) * RATIO
    WXX(10) = WXX(10)*C1*RATIO
    WXX(11) = WXX(11)*RATIO
    WXX(13) = WXX(13) * RATIO
    WXX(14) = WXX(14) * RATIO
  DO 11 I=23,30
    WXX(I) = WXX(I)/A
11  ACON(I) = CON(I)/A
  RETURN
  END

C
C
SUBROUTINE REG(ACON)
C
  IMPLICIT REAL*8(A-H,O-Z)
  REAL*8 MPRM,IPRM
  DIMENSION ACON(30)
  COMMON/COEF/CON(30),CCON(30),NC,NCON(30)
  COMMON/CONST/RATIO,MPRM,IPRM,A,IANGLE
  DO 10 I=1,22
10  CON(I) = ACON(I)/MPRM
    CON(1) = ACON(1)/IPRM
    CON(3) = ACON(3)/IPRM

```

Table 1. Continued

```

CON(5) = ACON(5)/IPRM
CON(10) = ACON(10)/(IPRM*RATIO)
CON(11) = CON(11)/RATIO
CON(13) = CON(13)/RATIO
CON(14) = CON(14)/RATIO
CON(21) = ACON(21)/IPRM
CON(22) = ACON(22)/IPRM
DO 11 I=23,30
11 CON(I) = ACON(I)*A
RETURN
END

C
C
SUBROUTINE MBARA(M1,M2,M3,PSI,THTA,PHI,PSIP,THTAP,PHIP,
1P1,P2,P3,P1P,P2P,P3P,J)
C
IMPLICIT REAL*8(A-H,O-Z)
REAL*8 M1,M2,M3,MAG,MYT,MZT,MYTP,MZTP,MYTE,MZTE
COMMON/TCOE1/SPN,A,B,MAG,QA,RA,AD,BD,ALPA,BTA,
1ALPAP,BTAP,DLTA2,P,Q,R,SMAG,DLTA
COMMON/COEF/CON(30),CCON(30),NC,NCON(30)
COMMON/CONST/RATIO,Z1,Z2,Z3,I4
M1 = SPN*(CON(13)+CON(14)*DLTA2)+P*(DUM(13,J)
1+DUM(14,J)*DLTA2 + CON(14)*MAG)
M1 = M1+DUM(10,J)*SPN*CON(11)*DLTA+P*DUM(11,J)*DLTA+P*CON(11)*SMAG
TEMP1 = CON(1) + CON(5)*DLTA2
TEMP2 = DUM(1,J)+DUM(5,J)*DLTA2 + CON(5)*MAG
TEMP3Y = CON(2)+CON(6)*DLTA2-CON(7)*BTA**2
TEMP3Z = CON(2) + CON(6)*DLTA2 - CON(7)*ALPA**2
TEMP4Y = DUM(2,J)+DUM(6,J)*DLTA2 + CON(6)*MAG
1-DUM(7,J)*BTA**2-2.0+0*BTA*CON(7)*B
TEMP4Z = DUM(2,J) + DUM(6,J)*DLTA2 + CON(6)*MAG
1-DUM(7,J)*ALPA**2 - 2.0+0*ALPA*CON(7)*A
TEMP1 = TEMP1+CON(3)*DLTA
TEMP2 = TEMP2+DUM(3,J)*DLTA+CON(3)*SMAG
TEMP3Y = TEMP3Y+CON(9)*DLTA
TEMP3Z = TEMP3Z+CON(9)*DLTA
TEMP4Y = TEMP4Y+DUM(9,J)*DLTA+CON(9)*SMAG
TEMP4Z = TEMP4Z+DUM(9,J)*DLTA+CON(9)*SMAG
TEMP5Y = CON(3)+CON(9)*DLTA2-CON(10)*BTA**2
TEMP5Z = CON(3) + CON(9)*DLTA2 - CON(10)*ALPA**2
TEMP6Y = DUM(3,J)+DUM(9,J)*DLTA2 + CON(9)*MAG
1-DUM(10,J)*BTA**2 - 2.0+0*CON(10)*BTA*B
TEMP6Z = DUM(3,J)+DUM(9,J)*DLTA2 + CON(9)*MAG
1-DUM(10,J)*ALPA**2 - 2.0+0*CON(10)*ALPA*A
TEMP7 = CON(4)+CON(12)*DLTA2
TEMP8 = DUM(4,J)+DUM(12,J)*DLTA2 + CON(12)*MAG
M2 = A*TEMP1 + ALPA*TEMP2 + QA*TEMP3Y + Q*TEMP4Y
1+DUM(8,J)*R*ALPA*BTA+CON(8)*(RA*ALPA*BTA+R*A*BTA
2+R*ALPA*B)+AD*TEMP5Y + ALPAP*TEMP6Y
3+DUM(11,J)*BTAP*ALPA*BTA + CON(11)*(BD*ALPA*BTA+BTAP*A*BTA
4+BTAP*ALPA*B) + SPN*BTA *TEMP7 + B*P*TEMP7
5+P*BTA *TEMP8
M3 = -B*TEMP1-BTA*TEMP2+RA*TEMP3Z + R*TEMP4Z
1+DUM(8,J)*Q*ALPA*BTA+CON(8)*(QA*ALPA*BTA+Q*A*BTA

```

Table 1. Concluded

```

2*Q*ALPA*B)-BD*TEMP5Z - BTAP*TEMP6Z
3-DUM(11,J)*ALPAP*ALPA*BTA-CON(11)*(AD*ALPA*BTA+ALPAP*A*BTA
4*ALPAP*ALPA*B)+SPN*ALPA*TEMP7 + A*P*TEMP7
5*P*ALPA*TEMP8
MYT=CON(21)*THTA
MYT=MYT+CON(20)*THTAP
MZT=CON(22)*PSI
MZT=MZT+CON(19)*PSIP
MYTP=DUM(21,J)*THTA+CON(21)*P2
MYTP=MYTP+DUM(20,J)*THTAP+CON(20)*P2P
MZTP=DUM(22,J)*PSI+CON(22)*P3
MZTP=MZTP+DUM(19,J)*PSIP+CON(19)*P3P
MYTE=(DUM(21,J)*THTA+CON(21)*P2)/RATIO
MYTE=MYTE+(DUM(20,J)*THTAP+CON(20)*P2P)/RATIO
MZTE=(DUM(22,J)*PSI+CON(22)*P3)/RATIO
MZTE=MZTE+(DUM(19,J)*PSIP+CON(19)*P3P)/RATIO
M1=M1+MYTE*DSIN(PSI)*DCOS(THTA)+MYT*(P3*DCOS(PSI)*DCOS(THTA)
1 -P2*DSIN(PSI)*DSIN(THTA))/RATIO
2 -MZTE*DSIN(THTA)-MZT*P2*DCOS(THTA)/RATIO
M2=M2+MYTP*DCOS(PSI)-MYT*P3*DSIN(PSI)
M3=M3+MYTP*DSIN(PSI)*DSIN(THTA)+MYT*(P3*DCOS(PSI)*DSIN(THTA)
1 +P2*DSIN(PSI)*DCOS(THTA)
2 +MZTP*DCOS(THTA)-MZT*P2*DSIN(THTA)
RETURN
END

```

C
C
C

SUBROUTINE MBAR(MX0IX,MY0I,MZ0I,PSI,THTA,PHI,PSIP,THTAP,PHIP)

```

IMPLICIT REAL*8(A-H,O-Z)
REAL*8 MX0IX,MY0I,MZ0I,MAG,MYT,MZT
COMMON/TCOEF1/SPN,A,B,MAG,QA,RA,AD,BD,ALPA,BTA,ALPAP,BTAP,DLTA2,
1P,Q,R,SMAG,DLTA
COMMON/COEF/CON(30),CCON(30),NC,NCON(30)
COMMON/CONST/RATIO,Z1,Z2,Z3,I4
MX0IX= P*(CON(13)+CON(14)*DLTA2)
MY0I = ALPA*(CON(1)+CON(5)*DLTA2)+Q*(CON(2)+CON(6)*DLTA2
1-CON(7)*BTA**2)+CON(8)*R*ALPA*BTA+ALPAP*(CON(3) +
2CON(9)*DLTA2-CON(10)*BTA**2)+CON(11)*BTAP*ALPA*BTA
3+P*BTA *(CON(4)+CON(12)*DLTA2)
MZ0I = -BTA*(CON(1)+CON(5)*DLTA2)+R*(CON(2)+CON(6)*DLTA2
1-CON(7)*ALPA**2)+CON(8)*Q*ALPA*BTA-BTAP*(CON(3)+
2CON(9)*DLTA2 - CON(10)*ALPA**2)-CON(11)*ALPAP*ALPA*BTA
3+P*ALPA*(CON(4)+CON(12)*DLTA2)
MX0IX=MX0IX+CON(10)*P*CON(11)*DLTA
MY0I=MY0I+ALPA*CON(3)*DLTA+Q*CON(9)*DLTA
MZ0I=MZ0I-BTA*CON(3)*DLTA+R*CON(9)*DLTA
MYT=CON(21)*THTA
MYT=MYT+CON(20)*THTAP
MZT=CON(22)*PSI
MZT=MZT+CON(19)*PSIP
MX0IX=MX0IX+(MYT*DSIN(PSI)*DCOS(THTA)-MZT*DSIN(THTA))/RATIO
MY0I=MY0I+MYT*DCOS(PSI)
MZ0I=MZ0I+MYT*DSIN(PSI)*DSIN(THTA)+MZT*DCOS(THTA)
RETURN
END

```

Table 2. Fortran Listing: Asymmetric Parameter Extraction Program

C
C
C
C
C
C
C
C
C

A N G L E S

VARNER VERSION 1 APR. 1977
 COMPUTES AERO COEFFICIENTS FOR MIRROR SYMMETRY BODY
 BODY AXIS SYSTEM, AERODYNAMIC ASYMMETRY
 EXACT 300 EQUATIONS UTILIZED

```

  IMPLICIT REAL*8(A-H,O-Z)
  REAL*8 IX,IY,IZ,IZX,JX,JY,JZ,IXP,IYP,IZP,MX1,MX2,MY1,MY2,MZ1,MZ2
  REAL*8 ALIST(72)
  REAL*8 CARD(10)
  REAL*4 TS(1000),PHIS(1000),THTAS(1000),PSIS(1000)
  DIMENSION AUX( 5,438),Y(438),DERY(438),WXX(72),ACON(72),CT(72,73)
1  WX(72),AACON(72),CC(72,144)
  EXTERNAL FCT,DRKGS
  COMMON/MEAS/PHIM(1000),THTAM(1000),PSIM(1000)
  COMMON/SOL/T(1000),PHI(1000),THTA(1000),PSI(1000)
  COMMON/COEF/CON(72),CCON(72),NC,NCON(72)
  COMMON/MATRIX/C(72,73),RESSUM,SIGPHI,SIGTHA,SIGPSI
  COMMON/CONST/JX,JY,JZ,IXP,IYP,IZP,IANGLE,IX,IY,IZ
  COMMON/CONST2/MX1,MX2,MY1,MY2,MZ1,MZ2,A
  EQUIVALENCE (AUX(1),CT(1)),(Y(1),CT(2191)),(DERY(1),CT(2629)),
1  (CC(1),C(1))
2  , (PHIS(1),PHI(1)),(THTAS(1),THTA(1)),(PSIS(1),PSI(1))
  DATA ALIST/'CM 0 ','CM A ','CM MA ','CM A2 ','CM A MA ','
1 'CM A3 ','CM A2 MA','CM MB ','CM B2 ','CM B2 MB','CM A MB ','
2 'CM MAB ','CM A2 MB','CM MAB A','CM A B2 ','CM MA B2','CMQ 0 ','
3 'CMQ A ','CMQ MA ','CMQ A2 ','CMQ A MA','CMQ MB ','CMQ B2 ','
4 'CMQ A MB','CMQ MAB ','CMR B ','CMP B ','CN 0 ','CN B ','
5 'CN A B ','CN MA B ','CN B3 ','CN A2 B ','CN B MB ','CN B MAB','
6 'CNR 0 ','CNR A ','CNR MA ','CNR A2 ','CNR MB ','CNR B2 ','
7 'CNR A MA','CNR A MB','CNR MAB ','CNQ B ','CNP A ','CL 0 ','
8 'CL A ','CL B ','CL A B ','CL MA B ','CL B MB ','CL P ','
9 'CLP MA ','CLP MB ','CLP A2 ','CLP R2 ','DUMMY ','DUMMY ','
* IZX ','CNR TUN ','CMQ TUN ','CMA TUN ','CNB TUN ','FLOANG T',
* FLOANG P','PHI(0) ','THTA(0) ','PSI(0) ','P(0) ','Q(0) ','
* R(0) '/'
  NAMELIST/NAM/NSWTC,NTOT,NC,NITER,DTMIN,BOUND,AREA,DIA,IX,IY,RO,U,
1 AACON,NCON,NSESWH,SPHI,STHTA,SPSI,AMPHI,AMTHTA,AMPSI,
2 SAMPLE,NDELTA,IUPDAT,IZ,IZX,IANGLE,INLCON,DTGEN
3 ,IGPNO,IBLKNO,IRCGEN,SIGPHI,SIGTHA,SIGPSI,NSTART,IRCSTR
100 FORMAT(1H1,20X,'***** INPUT DATA *****',/,
11X,'GROUP NUMBER =',I5,5X,'BLOCK NUMBER =',I5,/,
19X,'TIME',10X,'PSI',10X,'THETA',10X,'PHI',//)
101 FORMAT(7F10.0)
102 FORMAT(5,4(E13.6,1X))
103 FORMAT(5X,2(A8,2X,2(E13.6,5X)))
104 FORMAT(/,1X,'ITERATION NO',I5,/,2(21X,'CON',11X,'DELTA CON'))
105 FORMAT(2(11X,'FINAL CONSTANTS AND PROBABLE ERROR',10X),/)
106 FORMAT(2(5X,'C(',I3,')=',E13.6,5X,'(',E13.6,')',2X,A8))
107 FORMAT(1H1,5X,'DATA FIT COMPARISON',//,11X,'TIME',
13X,'PSI/FIT',3X,'PSI/EXP',3X,'DEL PSI',2X,'THTA/FIT',2X,'THTA/EXP'

```

Table 2. Continued

```

      2,2X,'DEL THTA',2X,'PHI/FIT',3X,'PHI/EXP',3X,'DEL PHI',/)
108 FORMAT(5X,F10.6,9F10.3)
109 FORMAT (1X,'**** CONVERGENCE CRITERIA NOT SATISFIED AFTER',I4,
      11X,'ITERATIONS ****')
110 FORMAT(1H1,1X,'SUM OF RESIDUALS',E13.6,5X,'NEW PROBABLE ERROR=',
      1E13.6,5X,'OLD PROBABLE ERROR =',E13.6)
111 FORMAT(4F10.4)
112 FORMAT(1X,70(' '),/,1X,'***** ERROR *****',/,1X,
      1'NO OF CONSTANTS ALLOWED TO VARY EXCEEDS TOTAL NO OF DATA POINTS
      2USED',/,1X,70(' '))
200 FORMAT(1X,30(' '), ' AERODYNAMIC COEFFICIENT EXTRACTION BY CHAPMAN
      1KIRK METHOD ',30(' '),/ ,1X,'NSWTC =',I5,'( =0, NORMAL DATA REDU
      2CTION',/,17X,'=1, 3DOF DATA GENERATED, NO ITERATION',/,
      317X,'=2, 3DOF DATA GENERATED AND STORED ON 75 PACK)',/,1X,'IUPDAT
      4=',I5,'(=0, INITIAL GUESSES NOT UPDATED FOR FOLLOWING SHOT',/,
      517X,'=1, INITIAL GUESSES UPDATED)')
302 FORMAT(1X,'IANGLE =',I5,'(=0, ALPA AND BETA IN TERMS OF VELOCITY R
      1ATIOS',/,17X,'=1, ALPA AND BETA IN TERMS OF ANGLE OF ATTACK AND
      3 SIDESLIP)',/,1X,'INLCON =',I5,'(= 0, INITIAL CONDITIONS EVALUATED
      4 FROM DATA',/,17X,'=1, INPUT VALUES USED)')
201 FORMAT( /,1X,'PARAMETERS *****',/,1X,'NO OF POINTS (N) =',I5,
      1'TOTAL NO VARIABLES (NC) =',I5,5X,'TOTAL NO ITERATIONS (NITER)=',
      2I5,/,1X,'INTEGRATION STEP SIZE(DT)=',E8.2,5X,'CONVERGENCE BOUND ON
      3 ITERATION (BOUND)=',E8.2,/,1X,'BODY *****',/,1X,'AREA =',
      4F10.6,'FT**2',5X,'DIA =',F10.6,'FT',/,1X,'IX =',F12.7,'SLUGS-FT**2
      5',5X,'IY =',F12.7,'SLUGS-FT**2',/,1X,'IZ =',F12.7,'SLUGS-FT**2',
      65X,'IZX =',F12.7,'SLUGS-FT**2')
202 FORMAT(/,1X,'FREE STREAM *****',/,1X,'DENSITY (RO) =',E14.7,
      1'SLUGS/FT**3',5X,'U =',F10.4,'FT/SEC',/ ,1X,'COEFFICIENTS *****')
203 FORMAT(1X,2('ACON(',I3,') =',E13.6,2X,'(',A8,')',5X,'NCON(',I3,
      1') =',I2,5X,))
301 FORMAT(1H1)
303 FORMAT(1X,'BEGINNING RECORD NUMBER =',I5)
401 FORMAT(10A8)
402 FORMAT(1X,10A8)
404 FORMAT(1X,40(' '), ' INPUT CARD IMAGES ',40(' '),/)
406 FORMAT(1H1)
407 FORMAT(1X,'NOTE - ',10A8)
502 FORMAT(1X,69(' '),/,1X,'**** 3DOF GENERATED DATA STORED BEGINNING
      2ON RECORU NUMBER',I5,2X,'*****',/,1X,'UNDER IGPNO =',I5,2X,
      3' AND IBLKNO =',I5,/,1X,'II=1,T',/,1X,'II=2,PHI',/,1X,
      4'II=3,THTA',/,1X,'II=4,PSI',/,1X,69(' '))
      WRITE(06,404)
405 READ(05,401,END=403)CARD
      WRITE(06,402)CARD
      GO TO 405
403 REWIND 5
      READ(05,401)CARD
      WRITE(06,406)
      DEFINE FILE 07(1140,4016,L,IREC)
C
C
C
      INITIALIZATION
      IPRINT=0
      NPRINT=0

```

Table 2. Continued

```

998 READ(05,NAM,END=999)
   AACON(60)=IZX
   N=NTOT
   WRITE(06,301)
   WRITE(06,200)NSWTCH,IUPOAT
   WRITE(06,302) IANGLE,INLCON
   WRITE(06,407)CARD
   WRITE(06,201)NTOT,NC,NITER,DTMIN,BOUND,AREA,DIA,IX,IY,IZ,IZX
   WRITE(06,202)RO,U
   NCO2=NC/2
   DO 204 I=1,NCO2
     IT=I+NCO2
     ACON(IT)=AACON(IT)
     ACON(I)=AACON(I)
204  WRITE(06,203)I,ACON(I),ALIST(I),I,NCON(I),IT,ACON(IT),
     1ALIST(IT),IT,NCON(IT)
     PI = 3.141592D+0
     A = PI/180.D+0
     IF(NSWTCH)8,8,7
C
C   DATA INPUT
C
7  CONTINUE
   T(1)=0.D+0
   DO 10 I=2,NTOT
     T(I)=T(I-1)*DTGEN
     PHIM(I)=0.D+0
     THTAM(I)=0.D+0
10  PSIM(I)=0.D+0
     PHIM(1)=0.D+0
     THTAM(1)=0.D+0
     PSIM(1)=0.D+0
     GO TO 9
8  CONTINUE
   IREC=1
500 READ(07'IREC)IGPT,IBLK,II,TS
     IF(IGPNO.NE.IGPT) GO TO 500
     IF(IBLK.NE.IBLKNO) GO TO 500
     IF(II.NE.1) GO TO 500
     READ(07'IREC)IGPNO,IBLKNO,II,PHIS
     READ(07'IREC)IGPNO,IBLKNO,II,THTAS
     READ(07'IREC)IGPNO,IBLKNO,II,PSIS
C
C   DATA ALTERATION
C
   DO 504 I=1,NTOT
     T(I)=TS(I)
     PHIM(I)=PHIS(I)
     THTAM(I)=THTAS(I)
504  PSIM(I)=PSIS(I)
     IF(NPRINT.EQ.IGPNO.AND.IPRINT.EQ.IBLKNO) GO TO 4
     WRITE(06,100)IGPNO,IBLKNO
     IRECTMP=IREC-4
     WRITE(06,303) IRECTMP
     LOOP=0

```

Table 2. Continued

```

NLOOP=1
DO 4 I=1,NTOT
WRITE(06,102) T(I),PSIM(I),THTAM(I),PHIM(I)
LOOP=LOOP+1
KLOOP=NLOOP*50
IF (LOOP.LT.KLOOP) GO TO 4
NLOOP=NLOOP+1
WRITE(06,100) IGPNO,IBLKNO
4 CONTINUE
NPRINT=IGPNO
IPRINT=IBLKNO
CALL PART(SAMPLE,NDELTA,N,NTOT,NSTART)
IF (NSESWH.EQ.1) CALL NOISE(SPHI,STHTA,SPSI,AMPHI,AMHTA,AMPSI,
IN,SAMPLE,NDELTA,NTOT)
IF (INLCON.EQ.0) CALL ICS(ACON)
DO 46 I=1,N
PSIM(I) = PSIM(I)*A
THTAM(I) = THTAM(I)*A
46 PHIM(I) = PHIM(I)*A
9 CONTINUE
NSUM=0
DO 11 I=1,NC
11 IF (NCON(I).EQ.1) NSUM=NSUM+1
SUM = NSUM
C
C   DEFINE PARAMETERS AND TRANSFORM COEFFICIENTS IN SUB REG
C
DO 12 I=1,NC
12 CCON(I)=NCON(I)
QINF = R0*(U**2)/2.D+0
JX=IZX/IX
JY=IZX/IY
JZ=IZX/IZ
IXP=(IZ-IY)/IX
IYP=(IX-IZ)/IY
IZP=(IY-IX)/IZ
SQTT=DIA/(2.D+0*U)
SQT=QINF*AREA*DIA
MX1=SQT/IX
MX2=MX1*SQTT
MY1=SQT/IY
MY2=MY1*SQTT
MZ1=SQT/IZ
MZ2=MZ1*SQTT
CALL REG(ACON)
XN=N
CHECK=3.U+0*XN-SUM
IF (CHECK.LE.0.D+0) GO TO 997
NT=NC+1
E=0.D+0
NR=0
20 CONTINUE
JX=CON(60)/IX
JY=CON(60)/IY
JZ=CON(60)/IZ

```

Table 2. Continued

```

C
C      INTEGRATION
C
      CALL INTGRL(FCT,DRKGS,N,ERROR,AUX,Y,DERY,DTMIN)
      IF(NSWTC.HGT.0) GO TO 47
      IF(NSUM.EQ.0) GO TO 47
      NR=NR+1

C
C      CHECK FOR CONVERGENCE
C
      E1=DSQRT(RESSUM/(3.D+0*XN-SUM))
      RESSUM=DSQRT(RESSUM)
      WRITE(06,110)RESSUM,E1,E
      IF(DABS(E1-E)-BOUND)36,36,21
21  IF(NR-NITER)22,22,36
22  NTRIG=0
38  CONTINUE
      IF(NSUM.EQ.1) GO TO 33
      E=E1

C
C      CONTRACT C MATRIX - REMOVE ZERO ROWS AND COLUMNS
C
      DO 23 I=1,NC
      DO 23 J=1,NT
23  CT(I,J)=C(I,J)
      LL=0
      DO 90 I=1,NC
92  IF((I+LL).GT.NC) GO TO 90
      IF(NCON(I+LL))91,91,93
91  LL=LL+1
      GO TO 92
93  L=LL+I
      DO 94 K=1,NT
94  C(I,K)=CT(L,K)
90  CONTINUE
      LL=0
      LM=NSUM
      DO 80 I=1,NC
82  IF((I+LL).GT.NC) GO TO 80
      IF(NCON(I+LL))81,81,83
81  LL=LL+1
      GO TO 82
83  L=LL+I
      DO 84 K=1,LM
84  CT(K,I)=C(K,L)
80  CONTINUE
      DO 85 I=1,LM
85  CT(I,LM+1)=C(I,NT)
      L=NSUM
      LL=NSUM+1
      DO 71 I=1,L
      DO 71 J=1,L
71  C(I,J)=CT(I,J)

C
C      MATRIX INVERSION OF C

```

Table 2. Continued

```

C      IF(NTRIG)40,27,40
27 CALL INV(CT,L,LL,WX,CC)
   GO TO 41
40 CALL INV(CT,L,L,WX,CC)
41 DO 32 I=1,NC
   C(I,LL)=0.0+0
   WX(I)=CT(I,I)
32 WXX(I)=0.0+0
   LM=0

C
C      EXPAND C INVERSE TO INCLUDE ZERO ROWS AND COLUMNS
C
   DO 31 I=1,NC
   IF(NCON(I))28,28,30
28 LM=LM+1
   GO TO 31
30 IT=LM+I
   C(I,LL)=CT(IT,LL)
   WXX(I)=WX(IT)
31 CONTINUE
   GO TO 34

C
C      SOLVE FOR CORRECTION TO COEFFICIENTS
C
33 DO 35 I=1,NC
   IF(NCON(I)-1)39,49,49
49 C(I,NT)=C(I,NT)/C(I,I)
   WXX(I)=1.0+0/C(I,I)
   GO TO 35
39 C(I,NT)=0.0+0
   WXX(I)=0.0+0
35 CONTINUE
   LL=NT
34 IF(NTRIG.EQ.1) GO TO 42
   WRITE(06,104)NR
   DO 60 I=1,NC
- 60 WXX(I)=C(I,LL)

C
C      TRANSFORM COEFFICIENTS AND CORRECTIONS IN SUB REGOUT
C
   CALL REGOUT(ACON,WXX)
   DO 50 I=1,NC02
   IT=I+NC02
50 WRITE(06,103)ALIST(I),ACON(I),WXX(I),ALIST(IT),ACON(IT),WXX(IT)
   DO 43 I=1,NC
43 CON(I)=CON(I)+C(I,LL)
   GO TO 20
36 CONTINUE
   NTRIG=1
37 GO TO 38
42 CONTINUE

C
C      COMPUTE PROBABLE ERROR IN COEFFICIENTS
C

```

Table 2. Continued

```

DO 44 I=1,NC
44 WXX(I)=E1*DSQRT(DABS(WXX(I)))
   CALL REGOUT(ACON,WXX)
   WRITE(06,105)
   IF(NR.GT.NITER)WRITE(06,109)NR
   DO 45 I=1,NC02
     IT=I+NC02
45 WRITE(06,106) I,ACON(I),WXX(I),ALIST(I),IT,ACON(IT),WXX(IT)
     1,ALIST(IT)
47 WRITE(06,107)
   LOOP=0
   NLOOP=1
   IREC=IRCGEN
   DTTEMP=T(2)-T(1)
   DO 48 I=1,N
     TT=T(I)
     Z1 = PSI(I)/A
     Z2 = PSIM(I)/A
     Z3 = THTA(I)/A
     Z4 = THTAM(I)/A
     Z5 = PHI(I)/A
     Z6 = PHIM(I)/A
     Z10=Z1-Z2
     Z11=Z3-Z4
     Z12=Z5-Z6
     WRITE(06,108)TT,Z1,Z2,Z10,Z3,Z4,Z11,Z5,Z6,Z12
     THTAS(I)=Z3
     PSIS(I)=Z1
     TS(I)=TT
     PHIS(I)=Z5
     IF(NSWTCH,NE,0) GO TO 597
     TS(I)=Z10
     PHIS(I)=Z11
597 CONTINUE
     LOOP=LOOP+1
     KLOOP=NLOOP*50
     IF(LOOP.LT.KLOOP) GO TO 48
     NLOOP=NLOOP+1
     WRITE(06,107)
48 CONTINUE
     IF(NSWTCH,NE,0) GO TO 599
C
C   COMPARISON OF FIT DATA AND EXPERIMENT STORED
C
   IREC=IRCSTR
   IF(IRCSTR.GE.IRCGEN-3.AND.IRCSTR.LE.IRCGEN+3) GO TO 599
   WRITE(06,598)NSWTCH,IRCSTR,IGPNO,IBLKNO,DTTEMP
598 FORMAT(1H1,1X,'NSWTCH =',I5,/,1X,'3DOF DATA STORED BEGINNING AT RE
1CORD ',I5,2X,'UNDER IGPNO =',I5,2X,'AND IBLKNO =',I5,/,1X,'II=5,THT
2TA',/,1X,'II=6,THTA-THTAM',/,1X,'II=7,PSI',/,1X,'II=8,PSI-PSIM',
3/,1X,'DT =',F7.4,2X,'SEC',1H1)
   II=5
   WRITE(07,IREC)IGPNO,IBLKNO,II,THTAS
   II=6
   WRITE(07,IREC)IGPNO,IBLKNO,II,PHIS

```

Table 2. Continued

```

      II=7
      WRITE(07'IREC) IGPNO,IBLKNO,II,PSIS
      II=8
      WRITE(07'IREC) IGPNO,IBLKNO,II,TS
599  CONTINUE
      IF(NSWTCH.NE.2) GO TO 501
C
C      3DOF GENERATED SOLUTION STORED
C
      WRITE(06,502) IRCGEN,IGPNO,IBLKNO
      II=1
      WRITE(07'IREC) IGPNO,IBLKNO,II,TS
      II=2
      WRITE(07'IREC) IGPNO,IBLKNO,II,PHIS
      II=3
      WRITE(07'IREC) IGPNO,IBLKNO,II,THTAS
      II=4
      WRITE(07'IREC) IGPNO,IBLKNO,II,PSIS
501  CONTINUE
      GO TO 996
997  WRITE(06,112)
996  CONTINUE
      IF(IUPDAT.EQ.0) GO TO 998
      DO 995 I=1,NC
995  AACON(I)=ACON(I)
      IZX=AACON(60)
      GO TO 998
999  CONTINUE
      STOP
      END
C
C      SUBROUTINE NOISE(SPHI,STHTA,SPSI,AMPHI,AMTHTA,AMPSI,N,
C      ISAMPLE,NDELTA,NTOT)
C
C      THIS SUBROUTINE ADDS GAUSSIAN NOISE TO DATA
      IMPLICIT REAL*8(A-H,O-Z)
      COMMON/MEAS/PHIM(1000),THTAM(1000),PSIM(1000)
      COMMON/SOL/T(1000),PHI(1000),THTA(1000),PSI(1000)
      WRITE(06,100)SPSI,STHTA,SPHI,AMPSI,AMTHTA,AMPHI,N
      CALL TIME(IYEAR,ISEC)
7    IF(ISEC-1000) 5,5,6
6    ISEC=ISEC-1000
      GO TO 7
5    IX=(ISEC+IYEAR)*2+1
      IY=IX+2
      IZ=IX+4
      SIG1PH=0.0+0
      SIG2PH=0.0+0
      SIG3PH=0.0+0
      SIG1TH=0.0+0
      SIG2TH=0.0+0
      SIG3TH=0.0+0
      SIG1PS=0.0+0
      SIG2PS=0.0+0

```

Table 2. Continued

```

SIG3PS=0.D+0
TOTPHI=0.D+0
TOTTHA=0.D+0
TOTPSI=0.D+0
LOOP=1
NLOOP=1
DO 10 I=1,N
CALL GAUSS(IX,SPHI,AMPHI,VPHI)
CALL GAUSS(IY,STHTA,AMTHTA,VTHTA)
CALL GAUSS(IZ,SPSI,AMPSI,VPSI)
PHIM(I)=PHIM(I)+VPHI
THTAM(I)=THTAM(I)+VTHTA
PSIM(I)=PSIM(I)+VPSI
TOTPHI=TOTPHI+VPHI
TOTTHA=TOTTHA+VTHTA
TOTPSI=TOTPSI+VPSI
P=DABS(VPHI)
Q=DABS(VTHTA)
R=DABS(VPSI)
IF(P.LT.SPHI)SIG1PH=SIG1PH+1.D+0
IF(P.GE.SPHI.AND.P.LT.2.D+0*SPHI)SIG2PH=SIG2PH+1.D+0
IF(P.GE.2.D+0*SPHI.AND.P.LE.3.D+0*SPHI)SIG3PH=SIG3PH+1.D+0
IF(Q.LT.STHTA)SIG1TH=SIG1TH+1.D+0
IF(Q.GE.STHTA.AND.Q.LT.2.D+0*STHTA)SIG2TH=SIG2TH+1.D+0
IF(Q.GE.2.D+0*STHTA.AND.Q.LE.3.D+0*STHTA)SIG3TH=SIG3TH+1.D+0
IF(R.LT.SPSI)SIG1PS=SIG1PS+1.D+0
IF(R.GE.SPSI.AND.R.LT.2.D+0*SPSI)SIG2PS=SIG2PS+1.D+0
IF(R.GE.2.D+0*SPSI.AND.R.LE.3.D+0*SPSI)SIG3PS=SIG3PS+1.D+0
10 CONTINUE
WRITE(06,103)TOTPSI,TOTTHA,TOTPHI,SIG1PS,SIG1TH,SIG1PH,
1SIG2PS,SIG2TH,SIG2PH,SIG3PS,SIG3TH,SIG3PH
100 FORMAT(1H1,1X,'*** GAUSSIAN NOISE ADDED ***',/,1X,
1'ONE STANDARD DEVIATION - PSI =',F10.6,5X,'THETA =',F10.6,5X,
2'PHI =',F10.6,/,1X,'CONSTANT BIAS - PSI =',F10.6,5X,
3'THETA =',F10.6,5X,'PHI =',F10.6,/,1X,'TOTAL NO OF TIME POINTS USE
4D IN FIT (N) =',I5)
103 FORMAT(1H1,1X,'SUM OF NOISE ADDED',/,6X,'PSI',6X,'THTA',7X,'PHI',
1/,1X,3F10.3,/,1X,'NOISE CONTRIBUTION WITHIN ONE SIGMA',/,
26X,'PSI',6X,'THTA',7X,'PHI',/,1X,3F10.3,/,
31X,'NOISE CONTRIBUTION BETWEEN ONE SIGMA AND TWO SIGMA',/,
46X,'PSI',6X,'THTA',7X,'PHI',/,1X,3F10.3,/,1X,'NOISE CONTRIBUTION
5BETWEEN TWO SIGMA AND THREE SIGMA',/,6X,'PSI',6X,'THTA',7X,'PHI',
6/,1X,3F10.3)
RETURN
END
C
C
C
SUBROUTINE RANDU(IX,IY,YPL)
IMPLICIT REAL*8(A-H,O-Z)
IY=IX*65539
IF(IY)5,6,6
5 IY=IY+2147483647+1
6 YPL=IY
YPL=YPL*.4656613D-9

```

Table 2. Continued

```

      RETURN
      END
C
C
      SUBROUTINE GAUSS(IX,S,AM,V)
C
      IMPLICIT REAL*8 (A-H,O-Z)
      A=0.D+0
      DO 50 I=1,48
      CALL RANDU(IX,IY,Y)
      IX=IY
50  A=A+Y
      V=(A-24.D+0)/2.D+0
      V=V*S+AM
      RETURN
      END
C
C
      SUBROUTINE ICS(ACON)
C
      IMPLICIT REAL*8 (A-H,O-Z)
      DIMENSION ACON(72)
      COMMON/MEAS/PHIM(1000),THTAM(1000),PSIM(1000)
      COMMON/SOL/T(1000),PHI(1000),THTA(1000),PSI(1000)
      DT=T(2)-T(1)
      PHIO=PHIM(1)
      THTAO=THTAM(1)
      PSIO=PSIM(1)
      PHIP = (PHIM(2)-PHIO)/DT
      THTAP = (THTAM(2)-THTAO)/DT
      PSIP=(PSIM(2)-PSIO)/DT
      ACON(70)=PHIP-PSIP*DSIN(THTAO)
      ACON(71)=THTAP*DCOS(PHIO)+PSIP*DCOS(THTAO)*DSIN(PHIO)
      ACON(72)=PSIP*DCOS(THTAO)*DCOS(PHIO)-THTAP*DSIN(PHIO)
      ACON(67)=PHIO
      ACON(68)=THTAO
      ACON(69)=PSIO
      RETURN
      END
C
C
      SUBROUTINE PART(SAMPLE,NDELTA,N,NTOT,NSTART)
C
      IMPLICIT REAL*8 (A-H,O-Z)
      COMMON/MEAS/PHIM(1000),THTAM(1000),PSIM(1000)
      COMMON/SOL/T(1000),PHI(1000),THTA(1000),PSI(1000)
      DO 13 I=2,NTOT
      IF (T(I).NE.0.D+0) NTEMP=I
13  CONTINUE
      TMAX=T(NTEMP)
      DO 11 I=NSTART,NTOT
      J=(I-1)*NDELTA+1
      IF (J.GT.NTEMP) GO TO 11
      RATIO=(T(J)-T(NSTART))/TMAX
      IF (RATIO.GT.SAMPLE) GO TO 11

```

Table 2. Continued

```

N=I
T(I)=T(J)
PHIM(I)=PHIM(J)
THTAM(I)=THTAM(J)
PSIM(I)=PSIM(J)
11 CONTINUE
N=N+1=NSTART
DO 12 I=1,N
J=I+NSTART-1
T(I)=T(J)
PHIM(I)=PHIM(J)
THTAM(I)=THTAM(J)
12 PSIM(I)=PSIM(J)
N1=N+1
IF (NTOT.LT.N1) GO TO 14
DO 15 I=N1,NTOT
15 T(I)=0.0+0
14 CONTINUE
WRITE(06,10)SAMPLE,NDELTA,NSTART,N,T(1),T(N)
10 FORMAT(1H1,1X, '**** DATA BLOCK ALTERED ****',/,1X, 'SAMPLE =',
1F7.4,/,1X, 'NDELTA =',I5,/,1X, 'NSTART =',I5,/,1X, 'N =',I5,/,
21X, 'T(1) = ',F7.4,5X, 'T(N) = ',F7.4,/,
31X,28(' '))
RETURN
END

```

C
C
C

```

SUBROUTINE ORKGS(XI,Y,DERY,NDIM,FCT,AUX,DT,NDT)

IMPLICIT REAL*8(A-H,O-Z)
DIMENSION Y(1),DERY(1),AUX( 5,1)
X=XI
DO 5 J=1,NDT
DO 1 I=1,NDIM
1 AUX(5,I)=Y(I)
CALL FCT(X,Y,DERY)
DO 2 I=1,NDIM
AUX(1,I)=DERY(I)
2 Y(I)=AUX(5,I)+.5D+0*DT*AUX(1,I)
XTEMP=X+.5D+0*DT
CALL FCT(XTEMP,Y,DERY)
DO 3 I=1,NDIM
AUX(2,I)=DERY(I)
3 Y(I)=AUX(5,I)+.5D+0*DT*AUX(2,I)
CALL FCT(XTEMP,Y,DERY)
DO 4 I=1,NDIM
AUX(3,I)=DERY(I)
4 Y(I)=AUX(5,I)+DT*AUX(3,I)
X=X+DT
CALL FCT(X,Y,DERY)
DO 5 I=1,NDIM
AUX(4,I)=DERY(I)
5 Y(I)=AUX(5,I)+DT*(AUX(1,I)+(AUX(2,I)+AUX(3,I))*2.D+0
1+AUX(4,I))/6.D+0
RETURN

```

Table 2. Continued

```

      END
C
C
      FUNCTION DUM(I,J)
C
      IMPLICIT REAL*8(A-H,O-Z)
      DUM=0.D+0
      IF(I.EQ.J) DUM=1.D+0
      RETURN
      END
C
C
      SUBROUTINE INV(C,NC,NCS1,WXX,CC)
C
      IMPLICIT REAL*8(A-H,O-Z)
      DIMENSION C(72,73),WXX(72),PIVOT(2),CC(72,144)
3000 FORMAT(/10X,'DET IS EQUAL TO ZERO')
      NCT=NC*2
      NCP1=NC+1
      DO 10 I=1,NC
      DO 10 J=1,NC
10    CC(I,J)=C(I,J)
      DO 20 I=1,NC
      DO 20 J=NCP1,NCT
20    CC(I,J)=0.D+0
      DO 30 I=1,NC
30    CC(I,NC+1)=1.D+0
      DO 205 I=1,NC
      PIVOT(1)=CC(I,1)
      DO 200 K=1,NC
      PIVOT(2)=CC(K,1)
126  IF(K=1) 135,130,140
130  DO 150 J=1,NCT
      IF(PIVOT(1)) 134,210,134
134  CC(K,J)=CC(I,J)/PIVOT(1)
150  CONTINUE
      GO TO 200
135  DO 160 J=1,NCT
      IF(PIVOT(1)) 136,160,136
136  CC(K,J)=CC(K,J)-CC(I,J)*PIVOT(2)/PIVOT(1)
160  CONTINUE
      GO TO 200
140  DO 170 J=1,NCT
      IF(PIVOT(2)) 145,170,145
145  CC(K,J)=CC(K,J)/PIVOT(2)-CC(I,J)
170  CONTINUE
200  CONTINUE
205  CONTINUE
      GO TO 250
210  WRITE (6,3000)
250  DO 300 I=1,NC
      DO 300 J=1,NC
300  C(I,J)=CC(I,J+NC)
      NCS=NCS1
350  IF(NCS-NC)500,500,400

```

Table 2. Continued

```

400 DO 420 I=1,NC
    WXX(I)=C(I,NCS)
420 C(I,NCS)=0.D+0
    DO 450 I=1,NC
    DO 450 J=1,NC
450 C(I,NCS)=C(I,NCS)+C(I,J)*WXX(J)
    NCS=NCS+1
    GO TO 350
500 CONTINUE
    RETURN
    END

```

C
C
C

```

SUBROUTINE INTGRL(FCT,DRKGS,N,ERROR,AUX,Y,DERY,DTMIN)

IMPLICIT REAL*8(A-H,O-Z)
DIMENSION AUX( 5,1),Y(1),DERY(1)
COMMON/MEAS/PHIM(1000),THTAM(1000),PSIM(1000)
COMMON/SOL/T(1000),PHI(1000),THTA(1000),PSI(1000)
COMMON/COEF/CON(72),CCON(72),NC,NCON(72)
COMMON/MATRIX/C(72,73),RESSUM,SPHI,STHA,SPSI
A=6.28318531D+0
NL=NC-5
DO 10 I=1,6
10 Y(I)=CON(NL+I-1)
    DO 11 I=1,NC
    Y(6+I)=DUM(NL,I)
    DO 11 J=1,5
11 Y(6+J*NC+I)=DUM(NL+J,I)
    NEQ=(NC+1)*6
    DNEQ=NEQ
    NL=NC+1
    K=1
    PHI(K)=Y(1)
    THTA(K)=Y(2)
    PSI(K)=Y(3)
    THTA(K)=THTA(K)+CON(65)
    PSI(K)=PSI(K)+CON(66)
    DPHI=PHIM(K)-PHI(K)
    IF(DPHI.LT.(-A/2.D+0)) PHI(K)=PHI(K)-A
    IF(DPHI.GT.(A/2.D+0)) PHI(K)=PHI(K)+A
    DO 19 I=1,NC
    Y(6+NC+I)=Y(6+NC+I)+DUM(65,I)
    Y(6+2*NC+I)=Y(6+2*NC+I)+DUM(66,I)
19 CONTINUE
    DO 12 I=1,NC
    DO 12 J=1,NC
    C(I,J)=Y(6+I)*Y(6+J)/SPHI**2 + Y(6+NC+I)*Y(6+NC+J)/STHA**2
    1+ Y(6+2*NC+I)*Y(6+2*NC+J)/SPSI**2
12 C(I,J)=C(I,J)*CCON(I)*CCON(J)
    DO 17 J=1,NC
    C(J,NL)=(PHIM(K)-PHI(K))*Y(6+J)/SPHI**2 + (THTAM(K)-THTA(K))*
    1Y(6+NC+J)/STHA**2 + (PSIM(K)-PSI(K))*Y(6+2*NC+J)/SPSI**2
17 C(J,NL)=C(J,NL)*CCON(J)
    RESSUM = ((PHIM(K)-PHI(K))/SPHI)**2 + ((THTAM(K)-THTA(K))/STHA)**2

```

Table 2. Continued

```

1* ((PSIM(K)-PSI(K))/SPSI)**2
DO 13 K=2,N
  XI=T(K-1)
  DTE=T(K)-T(K-1)
  DT=DTE
  NDT=1
  IF(UTMIN.GE.DTE) GO TO 18
  NDT=DTE/UTMIN
  DT=NDT
  DT=DTE/DT
18 CONTINUE
  CALL DRKGS(XI,Y,DERY,NEQ,FCT,AUX,DT,NDT)
  IF(Y(1).LE.(-A))Y(1)=Y(1)+A
  IF(Y(1).GE.A)Y(1)=Y(1)-A
  PHI(K)=Y(1)
  THTA(K)=Y(2)
  PSI(K)=Y(3)
  THTA(K)=THTA(K)+CON(65)
  PSI(K)=PSI(K)+CON(66)
  DPHI=PHIM(K)-PHI(K)
  IF(DPHI.LT.(-A/2.D+0)) PHI(K)=PHI(K)-A
  IF(DPHI.GT.(A/2.D+0)) PHI(K)=PHI(K)+A
  DO 20 I=1,NC
    Y(6+NC+I)=Y(6+NC+I)+DUM(65,I)
    Y(6+2*NC+I)=Y(6+2*NC+I)+DUM(66,I)
20 CONTINUE
  DO 15 I=1,NC
    DO 15 J=1,NC
      C(I,J)=Y(6+I)*Y(6+J)/SPHI**2 + Y(6+NC+I)*Y(6+NC+J)/STHA**2
      1+ Y(6+2*NC+I)*Y(6+2*NC+J)/SPSI**2 + C(I,J)
15 C(I,J)=C(I,J)*CCON(I)*CCON(J)
  DO 16 J=1,NC
    C(J,NL)=(PHIM(K)-PHI(K))*Y(6+J)/SPHI**2 + (THTAM(K)-THTA(K))*
    1Y(6+NC+J)/STHA**2 + (PSIM(K)-PSI(K))*Y(6+2*NC+J)/SPSI**2 + C(J,NL)
16 C(J,NL)=C(J,NL)*CCON(J)
  RESSUM = ((PHIM(K)-PHI(K))/SPHI)**2 + ((THTAM(K)-THTA(K))/STHA)**2
  1+ ((PSIM(K)-PSI(K))/SPSI)**2 + RESSUM
13 CONTINUE
  RETURN
  END
C
C
SUBROUTINE MBARA(M1,M2,M3,PSI,THTA,PHI,P,Q,R,P1,P2,P3,
1 Q1,Q2,Q3,J)
C
  IMPLICIT REAL*8(A-H,O-Z)
  REAL*8 MAG,M1,M2,M3,MYPX,MYPZ,MYTP,MZPX,MZPY,MZTP,
1 MYT,MZT,MX,MY,MYZ,MZ,MZY,MXP,MYP,MZP,MYHZ,MZHY
  COMMON/TCOEF/A,B,MAG,ALPA,BTA,DLTA2,RMA,DMA,RMB,DMB,RMAB,DMAB
  COMMON/COEF/CON(72),CCON(72),NC,NCON(72)
  COMMON/CONST2/RX1,RX2,RY1,RY2,RZ1,RZ2,AA
  TEMPY1=CUN(17)+CON(18)*ALPA+CON(19)*RMA+CON(20)*ALPA**2+CON(21)*AL
1PA+RMA+CON(22)*RMB+CON(23)*BTA**2+CON(24)*ALPA*RMB+CON(25)*RMAB
  TEMPY2=DUM(17,J)+DUM(18,J)*ALPA+CON(18)*A+DUM(19,J)*RMA+CON(19)*DM
1A +DUM(20,J)*ALPA**2+2.D+0*CON(20)*ALPA*A+DUM(21,J)*ALPA*RMA

```

Table 2. Continued

```

2      +CON(21)*(ALPA*DMA+RMA*A)+DUM(22,J)*RMB+CON(22)*DMB
3      +DUM(23,J)*BTA**2+2.D+0*CON(23)*BTA*B+DUM(24,J)*ALPA*RMB
4      +CON(24)*(ALPA*DMB+RMB*A)+DUM(25,J)*RMAB+CON(25)*DMAB
TEMPY=DUM(1,J)+DUM(2,J)*ALPA+CON(2)*A+DUM(3,J)*RMA+CON(3)*DMA
1      +DUM(4,J)*ALPA**2+2.D+0*CON(4)*ALPA*A+DUM(5,J)*ALPA*RMA
2      +CON(5)*(ALPA*DMA+RMA*A)+DUM(6,J)*ALPA**3+3.D+0*CON(6)*A
3      +ALPA**2+DUM(7,J)*RMA*ALPA**2+CON(7)*(DMA*ALPA**2
4      +2.D+0*A*ALPA*RMA)+DUM(8,J)*RMB+CON(8)*DMB+DUM(9,J)*
5      BTA**2+2.D+0*CON(9)*BTA*B+DUM(10,J)*RMB*BTA**2
6      +CON(10)*(DMB*BTA**2+2.D+0*BTA*RMB*B)+DUM(11,J)*ALPA*RMB
M2=TEMPY+CON(11)*(ALPA*DMB+A*RMB)+DUM(12,J)*RMAB+CON(12)*DMAB
1      +DUM(13,J)*RMB*ALPA**2+CON(13)*(DMB*ALPA**2+2.D+0*ALPA*A*RMB)
2      +DUM(14,J)*RMAB*ALPA+CON(14)*(ALPA*DMAB+RMAB*A)+DUM(15,J)*ALPA
3      *BTA**2+CON(15)*(2.D+0*ALPA*BTA*B+A*BTA**2)+DUM(16,J)*RMA*BTA**
42     +CON(16)*(DMA*BTA**2+2.D+0*BTA*RMA*B)+Q2*TEMPY1+Q*TEMPY2
5      +Q3*CON(26)*BTA*R+DUM(26,J)*BTA*R+CON(26)*B+Q1*CON(27)*BTA
6      +P*DUM(27,J)*BTA+P*CON(27)*B
TEMPZ1=CON(36)+CON(37)*ALPA+CON(38)*RMA+CON(39)*ALPA**2+CON(40)*
1RMB+CON(41)*BTA**2+CON(42)*ALPA*RMA+CON(43)*ALPA*RMB+CON(44)*RMAB
TEMPZ2=DUM(36,J)+DUM(37,J)*ALPA+CON(37)*A+DUM(38,J)*RMA+CON(38)*DM
1A+DUM(39,J)*ALPA**2+2.D+0*CON(39)*ALPA*A+DUM(40,J)*RMB
2      +CON(40)*DMB+DUM(41,J)*BTA**2+2.D+0*CON(41)*BTA*B
3      +DUM(42,J)*ALPA*RMA+CON(42)*(ALPA*DMA+RMA*A)+DUM(43,J)
4      *ALPA*RMB+CON(43)*(ALPA*DMB+RMB*A)+DUM(44,J)*RMAB
5      +CON(44)*DMAB
TEMPZ=DUM(28,J)+DUM(29,J)*BTA+CON(29)*B+DUM(30,J)*ALPA*BTA
1      +CON(30)*(ALPA*B+BTA*A)+DUM(31,J)*RMA*BTA+CON(31)*(BTA*DMA
2      +RMA*B)+DUM(32,J)*BTA**3+3.D+0*CON(32)*B*BTA**2
3      +DUM(33,J)*BTA*ALPA**2+2.D+0*CON(33)*ALPA*BTA*A+CON(33)*B
4      *ALPA**2+DUM(34,J)*BTA*RMB+CON(34)*(BTA*DMB+RMB*B)
5      +DUM(35,J)*BTA*RMAB+CON(35)*(BTA*DMAB+RMAB*B)
M3=TEMPZ+Q3*TEMPZ1+R*TEMPZ2+Q*BTA*DUM(45,J)+CON(45)*(Q2*BTA
1      +Q*B)+DUM(46,J)*P*ALPA+CON(46)*(Q1*ALPA+P*A)
M1=DUM(47,J)+DUM(48,J)*ALPA+CON(48)*A+DUM(49,J)*BTA+CON(49)*B
1      +DUM(50,J)*ALPA*BTA+CON(50)*(A*BTA+ALPA*B)+DUM(51,J)*RMA*BTA
2      +CON(51)*(BTA*DMA+RMA*B)+DUM(52,J)*BTA*RMB+CON(52)
3      *(BTA*DMB+RMB*B)+DUM(53,J)*P+CON(53)*Q1
THTAP=Q*DCOS(PHI)-R*DSIN(PHI)
PSIP=(R*DCOS(PHI)+Q*DSIN(PHI))/DCOS(THTA)
THTAPA=Q2*DCOS(PHI)-Q*P1*DSIN(PHI)
1      -Q3*DSIN(PHI)-R*P1*DCOS(PHI)
PSIPA=PSIP*DTAN(THTA)*P2+(Q3*DCOS(PHI)-R*P1*DSIN(PHI)+
1      Q2*DSIN(PHI)+Q*P1*DCOS(PHI))/DCOS(THTA)
MYTP=DUM(63,J)*THTA+CON(63)*P2
MYTP=MYTP+DUM(62,J)*THTAP+CON(62)*THTAPA
MZTP=DUM(64,J)*PSI+CON(64)*P3
MZTP=MZTP+DUM(61,J)*PSIP+CON(61)*PSIPA
MYT=CON(63)*THTA
MYT=MYT+CON(62)*THTAP
MZT=CON(64)*PSI
MZT=MZT+CON(61)*PSIP
MYPX=MYTP*RX1/RX1
MYPZ=MYTP*RZ1/RZ1
MZPX=MZTP*RX1/RZ1
MZPY=MZTP*RY1/RZ1

```

Table 2. Continued

```

MX=MYT*DSIN(PSI)*DCOS(THTA)*RX1/RY1-MZT*DSIN(THTA)*RX1/RZ1
MY=MYT*DCOS(PSI)
MYZ=MY*RZ1/RY1
MZ=MYT*DSIN(PSI)*DSIN(THTA)*RZ1/RY1+MZT*DCOS(THTA)
MZY=MYT*DSIN(PSI)*DSIN(THTA)+MZT*DCOS(THTA)*RY1/RZ1
MXP=MYPX*DSIN(PSI)*DCOS(THTA)+MYT*(P3*DCOS(PSI)*DCOS(THTA)-
1 P2*DSIN(PSI)*DSIN(THTA))*RX1/RY1-MZPX*DSIN(THTA)
2-MZT*P2*DCOS(THTA)*RX1/RZ1
MYP=MYTP*DCOS(PSI)-MYT*P3*DSIN(PSI)
MZP=MYPZ*DSIN(PSI)*DSIN(THTA)+
1 MYT*(P3*DCOS(PSI)*DSIN(THTA)+P2*DSIN(PSI)*DCOS(THTA))
2 *RZ1/RY1+MZTP*DCOS(THTA)-MZT*P2*DSIN(THTA)
MYHZ=MYPZ*DCOS(PSI)-MYT*P3*DSIN(PSI)*RZ1/RY1
MZHY=MYTP*DSIN(PSI)*DSIN(THTA)+
1 MYT*(P3*DCOS(PSI)*DSIN(THTA)+P2*DSIN(PSI)*DCOS(THTA))
2 +MZPY*DCOS(THTA)-MZT*P2*DSIN(THTA)*RY1/RZ1
M1=M1+MXP
M2=M2-P1*MY*DSIN(PHI)+MYP*DCOS(PHI)
1 +MZY*P1*DCOS(PHI)+MZHY*DSIN(PHI)
M3=M3-MY*Z*P1*DCOS(PHI)-MYHZ*DSIN(PHI)
1 -MZ*P1*DSIN(PHI)+MZP*DCOS(PHI)
M1=M1+Q1*(CON(54)*RMA+CON(55)*RMB+CON(56)*ALPA**2+CON(57)*BTA**2)
1 +P*(RMA*DUM(54,J)+DMA*CON(54)+RMB*DUM(55,J)+DMB*CON(55)
2 +DUM(56,J)*ALPA**2+2.D+0*CON(56)*ALPA*A
3 +DUM(57,J)*BTA**2+2.D+0*CON(57)*BTA*B)
RETURN
END

```

C
C
C

```

SUBROUTINE MBAR(MXOI,MYOI,MZOI,PSI,THTA,PHI,P,Q,R)

IMPLICIT REAL*8(A-H,O-Z)
REAL*8 MXOI,MYOI,MZOI,MAG,MYT,MZT
COMMON/TCOEF/A,B,MAG,ALPA,BTA,DLTA2,RMA,OMA,RMB,OMB,RMAB,DMAB
COMMON/COEF/CON(72),CCON(72),NC,NCON(72)
COMMON/CONST2/RX1,RX2,RY1,RY2,RZ1,RZ2,AA
MXOI=CON(47)+CON(48)*ALPA+CON(49)*BTA
1 +CON(50)*ALPA*BTA+CON(51)*RMA*BTA
2 +CON(52)*BTA*RMB+CON(53)*P
3 +P*(CON(54)*RMA+CON(55)*RMB+CON(56)*ALPA**2+CON(57)*BTA**2)
TEMPY=CON(17)+CON(18)*ALPA+CON(19)*RMA+CON(20)*ALPA**2+CON(21)*
1 ALPA*RMA+CON(22)*RMB+CON(23)*BTA**2+CON(24)*ALPA*RMB+CON(25)*
2 RMAB
MYOI = CON(1)+CON(2)*ALPA+CON(3)*RMA+CON(4)*ALPA**2+CON(5)*ALPA
1 *RMA+CON(6)*ALPA**3+CON(7)*RMA*ALPA**2+CON(8)*RMB*CON(9)
2 *BTA**2+CON(10)*RMB*BTA**2 + CON(11)*ALPA*RMB+CON(12)*RMAB +
3 CON(13)*RMB*ALPA**2+CON(14)*ALPA*RMAB+CON(15)*ALPA*BTA**2+
4 CON(16)*RMA*BTA**2 + Q*TEMPY + CON(26)*R*BTA*CON(27)*P*BTA
TEMPZ=CON(36)+CON(37)*ALPA+CON(38)*RMA+CON(39)*ALPA**2+CON(40)*RMB
1 +CON(41)*BTA**2+CON(42)*ALPA*RMA+CON(43)*ALPA*RMB+CON(44)*RMAB
MZOI=CON(28)+CON(29)*BTA+CON(30)*ALPA*BTA+CON(31)*BTA*RMA+CON(32)*
1 BTA**3+CON(33)*BTA*ALPA**2+CON(34)*BTA*RMB+CON(35)*BTA*RMAB
2 +R*(EMPZ+CON(45)*Q*BTA+CON(46)*P*ALPA
THTAP=Q*DCOS(PHI)-R*DSIN(PHI)
PSIP=(R*UCOS(PHI)+Q*DSIN(PHI))/DCOS(THTA)

```

Table 2. Continued

```

MYT=CON(63)*THTA
MYT=MYT+CON(62)*THTAP
MZT=CON(64)*PSI
MZT=MZT+CON(61)*PSIP
MXOI=MXOI+MYT*DSIN(PSI)*DCOS(THTA)*RX1/RY1-MZT*DSIN(THTA)*RX1/RZ1
MYOI=MYOI+MYT*DCOS(PSI)*DCOS(PHI)+(MYT*DSIN(PSI)*DSIN(THTA)+
1 MZT*DCOS(THTA)*RY1/RZ1)*DSIN(PHI)
MZOI=MZOI-MYT*DCOS(PSI)*DSIN(PHI)*RZ1/RY1+(MYT*DSIN(PSI)*
1 DSIN(THTA)*RZ1/RY1+MZT*DCOS(THTA))*DCOS(PHI)
RETURN
END

```

```

SUBROUTINE TEMP(PSI,THTA,PHI,P1,P2,P3,K)

```

```

IMPLICIT REAL*8(A-H,O-Z)
REAL*8 MAG
COMMON/TCOEF/A,B,MAG,ALPA,BTA,DLTA2,RMA,DMA,RMB,DMB,RMAB,DMAB
GAMA=DCOS(PSI)*DCOS(THTA)
BTA=-DSIN(PSI)*DCOS(PHI)+DCOS(PSI)*DSIN(THTA)*DSIN(PHI)
ALPA=DSIN(PSI)*DSIN(PHI)+DCOS(PSI)*DSIN(THTA)*DCOS(PHI)
DLTA2=(DSIN(PSI))**2+(DCOS(PSI)*DSIN(THTA))**2
A=(P3-P1*DSIN(THTA))*DCOS(PSI)*DSIN(PHI)+(P1-P3*DSIN(THTA))
1 *DSIN(PSI)*DCOS(PHI)+P2*DCOS(PSI)*DCOS(THTA)*DCOS(PHI)
B=(P1*DSIN(THTA)-P3)*DCOS(PSI)*DCOS(PHI)+(P1-P3*DSIN(THTA))
1 *DSIN(PSI)*DSIN(PHI)+P2*DCOS(PSI)*DCOS(THTA)*DSIN(PHI)
MAG=2.0+0*(P2*DCOS(PSI)*DSIN(THTA)+P3*DCOS(THTA)*DSIN(PSI))*
1 DCOS(PSI)*DCOS(THTA)
G=-P3*DSIN(PSI)*DCOS(THTA)-P2*DCOS(PSI)*DSIN(THTA)
IF(K.EQ.0) GO TO 10
A1=ALPA
B1=BTA
ALPA=DATAN(A1/GAMA)
BTA=DATAN(B1/GAMA)
A=((DCOS(ALPA))**2)*(A-A1*G/GAMA)/GAMA
B=((DCOS(BTA))**2)*(B-B1*G/GAMA)/GAMA
DLTA2=ALPA**2 + BTA**2
MAG=2.0+0*(ALPA*A+BTA*B)
10 CONTINUE
RMA=DABS(ALPA)
RMB=DABS(BTA)
RMAB=DABS(ALPA*BTA)
DMA=0.0+0
DMB=0.0+0
DMAB=0.0+0
IF(ALPA.NE.0.0+0)DMA=ALPA*A/RMA
IF(ALPA.NE.0.0+0.AND.BTA.NE.0.0+0)DMAB = ALPA*BTA*(BTA*A+ALPA*A)
1/RMAB
IF(BTA.NE.0.0+0)DMB=BTA*B/RMB
RETURN
END

```

```

SUBROUTINE FCT(T,X,DERX)

```

Table 2. Continued

```

      IMPLICIT REAL*8(A-H,O-Z)
      REAL*8 MXOI,MYOI,MZOI,M1,M2,M3,JX,JY,JZ,IXP,IYP,IZP,MPM,IPM
1     I,IX,IY,IZ
      DIMENSION X(1),DERX(1)
      COMMON/COEF/CON(72),CCON(72),NC,NCON(72)
      COMMON/CONST/JX,JY,JZ,IXP,IYP,IZP,K,IX,IY,IZ
      PHI=X(1)
      THTA=X(2)
      PSI=X(3)
      P=X(4)
      Q=X(5)
      R=X(6)
      CALL TEMP(PSI,THTA,PHI,0.0+0.0,0.0+0.0,0.0+0.0,K)
      CALL MBAR(MXOI,MYOI,MZOI,PSI,THTA,PHI,P,Q,R)
      RJ=1.0+0-JX*JZ
      DERX(1)=P*DTAN(THTA)*(Q*DSIN(PHI)+R*DCOS(PHI))
      DERX(2)=Q*DCOS(PHI)-R*DSIN(PHI)
      DERX(3)=(R*DCOS(PHI)+Q*DSIN(PHI))/DCOS(THTA)
      DERX(4)=(MXOI+MZOI*JX-Q*R*(JZ*JX+IXP)+
1     P*Q*(1.0+0-IZP)*JX)/RJ
      DERX(5)=MYOI-(P**2-R**2)*JY-R*P*IYP
      DERX(6)=(MZOI+MXOI*JZ-P*Q*(IZP-JX*JZ)-
1     Q*R*(1.0+0+IXP)*JZ)/RJ
      NEQ=(NC+1)*6
      DO 5 I=7,NEQ
5     DERX(I)=0.0+0
      DO 10 I=1,NC
      IF(NCON(I).EQ.0)GO TO 10
      P1=X(6+I)
      P2=X(NC+6+I)
      P3=X(2*NC+6+I)
      Q1=X(3*NC+6+I)
      Q2=X(4*NC+6+I)
      Q3=X(5*NC+6+I)
      CALL TEMP(PSI,THTA,PHI,P1,P2,P3,K)
      CALL MBAHA(M1,M2,M3,PSI,THTA,PHI,P,Q,R,P1,P2,P3,
1     Q1,Q2,Q3,I)
      DERX(6+I)=Q1+P2*(Q*DSIN(PHI)+R*DCOS(PHI))/(DCOS(THTA))*2
1     +DTAN(THTA)*(Q*DSIN(PHI)+P1*Q*DCOS(PHI)
2     +Q3*DCOS(PHI)-P1*R*DSIN(PHI))
      DERX(6+NC+I)=Q2*DCOS(PHI)-P1*Q*DSIN(PHI)-Q3*DSIN(PHI)
1     -P1*R*DCOS(PHI)
      DERX(6+2*NC+I)=(Q3*DCOS(PHI)-P1*R*DSIN(PHI)+Q2*DSIN(PHI)
1     +P1*Q*DCOS(PHI))/DCOS(THTA)+(R*DCOS(PHI)
2     +Q*DSIN(PHI))*P2*DTAN(THTA)/DCOS(THTA)
      DERX(6+3*NC+I)=(M1+M3*JX-(JZ*JX+IXP)*(Q*Q3+R*Q2)
1     +(1.0+0-IZP)*JX*(P*Q2+Q*Q1))/RJ
      DERX(6+4*NC+I)=M2-2.0+0*JY*(P*Q1-R*Q3)-
1     IYP*(R*Q1+P*Q3)
      DERX(6+5*NC+I)=(M3+M1*JZ-(IZP-JX*JZ)*(P*Q2+Q*Q1)
1     -(1.0+0+IXP)*JZ*(Q*Q3+R*Q2))/RJ
      DERX(6+3*NC+I)=DERX(6+3*NC+I)+((DERX(4)-Q*R)*
1     2.0+0*CON(60)/(IX*IZ)+MZOI/IX+P*Q*(1.0+0-IZP)/IX)
2     *DUM(60,I)/RJ
      DERX(6+4*NC+I)=DERX(6+4*NC+I)-(P**2-R**2)*DUM(60,I)/IY

```

Table 2. Continued

```

      DERX(6+5*NC+I)=DERX(6+5*NC+I)+((DERX(6)+P*Q)*
1  2.0+0*CON(60)/(IX*IZ)+MXOI/IZ-Q*R*(1.0+0*IXP)/IZ)
2  *DUM(60,I)/RJ
10 CONTINUE
   RETURN
   END

```

C
C

```

SUBROUTINE REGOUT(ACON,WXX)

```

C

```

   IMPLICIT REAL*8(A-H,O-Z)
   REAL*8 MX1,MX2,MY1,MY2,MZ1,MZ2
   DIMENSION ACON(72),WXX(72)
   COMMON/COEF/CON(72),CCON(72),NC,NCON(72)
   COMMON/CONST2/MX1,MX2,MY1,MY2,MZ1,MZ2,A
   DO 10 I=1,16
      ACON(I)=CON(I)/MY1
10  WXX(I)=WXX(I)/MY1
      DO 12 I=28,35
         ACON(I)=CON(I)/MZ1
12  WXX(I)=WXX(I)/MZ1
      DO 14 I=47,52
         ACON(I)=CON(I)/MX1
14  WXX(I)=WXX(I)/MX1
      DO 15 I=17,27
         ACON(I)=CON(I)/MY2
15  WXX(I)=WXX(I)/MY2
      DO 16 I=36,46
         ACON(I)=CON(I)/MZ2
16  WXX(I)=WXX(I)/MZ2
      DO 17 I=65,72
         WXX(I)=WXX(I)/A
17  ACON(I)=CON(I)/A
      DO 18 I=53,57
         WXX(I)=WXX(I)/MX2
18  ACON(I)=CON(I)/MX2
      ACON(58)=CON(58)
      WXX(58)=WXX(58)
      ACON(59)=CON(59)
      WXX(59)=WXX(59)
      ACON(60)=CON(60)
      WXX(60)=WXX(60)
      ACON(61)=CON(61)/MZ2
      WXX(61)=WXX(61)/MZ2
      ACON(63)=CON(63)/MY1
      ACON(64)=CON(64)/MZ1
      WXX(63)=WXX(63)/MY1
      WXX(64)=WXX(64)/MZ1
      ACON(62)=CON(62)/MY2
      WXX(62)=WXX(62)/MY2
   RETURN
   END

```

C
C

```

SUBROUTINE REG(ACON)

```

Table 2. Concluded

C

```

      IMPLICIT REAL*8(A-H,O-Z)
      DIMENSION ACON(72)
      REAL*8 MX1,MX2,MY1,MY2,MZ1,MZ2
      COMMON/COEF/CON(72),CCON(72),NC,NCON(72)
      COMMON/CONST2/MX1,MX2,MY1,MY2,MZ1,MZ2,A
      DO 10 I=1,16
10    CON(I)=ACON(I)*MY1
      DO 12 I=28,35
12    CON(I)=ACON(I)*MZ1
      DO 14 I=47,52
14    CON(I)=ACON(I)*MX1
      DO 15 I=17,27
15    CON(I)=ACON(I)*MY2
      DO 16 I=36,46
16    CON(I)=ACON(I)*MZ2
      DO 17 I=65,72
17    CON(I)=ACON(I)*A
      DO 18 I=53,57
18    CON(I)=ACON(I)*MX2
      CON(58)=ACON(58)
      CON(59)=ACON(59)
      CON(60)=ACON(60)
      CON(61)=ACON(61)*MZ2
      CON(62)=ACON(62)*MY2
      CON(63)=ACON(63)*MY1
      CON(64)=ACON(64)*MZ1
      RETURN
      END

```

C

Table 3. Subroutine Descriptions for Both Asymmetric and Symmetric Programs

Name	Description
NOISE	Adds noise to generated 3DOF motion or to experimental 3DOF motion data. Input values to the subroutine specify the standard deviation and bias to be added to ϕ_m , ϵ_m , ψ_m .
RANDU	Random number generator.
GAUSS	Gaussian noise evaluated.
ICS	Computes approximate boundary conditions from the input 3DOF data to be used in place of initial guesses.
PART	Alters data set to be used in extraction technique.
DRKGS	Runge-Kutta fourth-order integration scheme for NDIM simultaneous differential equations.
DUM	Equivalent to the Kroneker-Delta function.
INV	Provides solution to a set of simultaneous linear equations. Also used to define inverse of a matrix.
INTGRL	Calling subprogram for integration of parametric, kinematic, and dynamic equations. Evaluates influence coefficient matrix, residual influence matrix, and total residual.
MBARA	Defines the values of the partial derivatives of the moment coefficients with respect to the parameters.
MBAR	Defines the moment coefficients.
TEMP	Defines variables required in moment coefficients and derivatives of moments with respect to the parameters.
FCT	Values of derivatives as used in DRKGS.
REGOUT	Conversion of parameters to output form.
REG	Conversion of input parameters to internal code dimensions.

Table 4. Input Variable Definitions for Symmetric and Asymmetric Programs
a. Namelist Input Common to Both Symmetric and Asymmetric Programs for Namelist/NAM/

Namelist Variable	Type	Input Values	Meaning	Units
NSWCH	Integer	0, 1, 2	Switch indicating type of analysis: - 0, normal data reduction by Chapman-Kirk method as outlined in Section 3.2; - 1, 3DOF data generated from initial values of coefficients; - 2, 3DOF data generated and stored on disk for later analysis.	
NTOT	Integer	1,000	Maximum array size of input and output variables: time, ϕ , θ , ψ .	
NC	Integer	30 symmetric 72 asymmetric	Maximum number of coefficients allowed to vary.	
NITER	Integer	>1	Maximum number of iterations allowed to reach a converged solution.	
DTMIN	Real	>0	Integration time step (DTMIN must also be less than or equal to the minimum time step of the input data to be analyzed).	
BOUND	Real	>0	Convergence bound on iteration; convergence is assumed when difference in RMS deviation [Eq. (26)] for two consecutive iterations is less than or equal to value of BOUND.	
AREA	Real	>0	Reference aerodynamic area.	ft ²
DIA	Real	>0	Reference aerodynamic length.	ft
IX	Real	>0	Axial moment of inertia.	slugs-ft ²
IY	Real	>0	Transverse moment of inertia in body-fixed y direction.	slugs-ft ²
RO	Real	>0	Free-stream density.	slugs/ft ³
U	Real	>0	Free-stream velocity.	ft/sec

Table 4. Continued
a. Continued

Namelist Variable	Type	Input Values	Meaning	Units
AACON	Real	($a_1, a_2, \dots, a_{Nc-1}, a_{Nc}$)	Initial values of parameters which include both aerodynamic coefficients and boundary conditions on kinematic and dynamic equations. ^a	
NCON	Integer	(0 or 1 for each a_i)	Array of integers corresponding to AACON, indicating which parameters are allowed to change: = 0, parameter is constant; = 1, parameter is varied.	
NSESWH	Integer	0 or 1	Switch allowing Gaussian noise to be added to input data: = 1, noise added; = 0, no noise added.	
SPHI	Real	>0	One standard deviation of Gaussian noise added to the Euler angle ϕ for NSESWH = 1.	deg
STHA	Real	>0	One standard deviation of Gaussian noise added to the Euler angle θ for NSESWH = 1.	deg
SPSI	Real	>0	One standard deviation of Gaussian noise added to the Euler angle ψ for NSESWH = 1.	deg
AMPHI	Real		Constant bias in noise added to Euler angle ϕ for NSESWH = 1.	deg
AMTHA	Real		Constant bias in noise added to Euler angle θ for NSESWH = 1.	deg
AMPSI	Real		Constant bias in noise added to Euler angle ψ for NSESWH = 1.	deg
SAMPLE	Real	>0 ≤ 1	Fraction of data sample to be fitted.	
NDELTA	Integer	>1	Only every NDELTA points of SAMPLE data are used in fit.	

^aSee Tables 4b and c for definitions of AACON for symmetric and asymmetric versions, respectively.

Table 4. Continued
a. Concluded

Namelist Variable	Type	Input Values	Meaning	Units
IUPDAT	Integer	0 or 1	Switch for update of initial values of parameters: = 0, initial values not updated for following shot; = 1, initial values updated.	
INLCON	Integer	0 or $\neq 0$	Switch defining conditions of input data: = 0, initial conditions evaluated from data; $\neq 0$, input values of initial conditions used as given in AACON.	
IANGLE	Integer	0 or $\neq 0$	Switch giving meaning of α and β : = 0, α and β in terms of velocity ratios; $\neq 0$, α and β assumed in terms of angle of attack and sideslip.	
DTGEN	Real	>0	Time step of generated 3DOF data.	sec
IGPNO	Integer		Group number of generated or input data.	
IBLKNO	Integer		Block number of generated or input data.	
IRCGEN	Integer		Beginning record number of stored, generated 3DOF data for NSWCH = 2.	
IRCSTR	Integer		Beginning record number of stored data for NSWCH = 0 where IRCSTR < IRCGEN - 3 or IRCSTR > IRCGEN - 3.	
SIGPHI	Real	>0	Relative uncertainty in ϕ .	deg
SIGTHA	Real	>0	Relative uncertainty in θ .	deg
SIGPSI	Real	>0	Relative uncertainty in ψ .	deg
NSTART	Integer	≥ 1	Starting point of input to be fitted.	
IZ	Real	>0	Transverse moment of inertia in body-fixed z direction (<u>asymmetric program only</u>).	slugs-ft ²
IZX	Real	≥ 0	Product of inertia for asymmetric body with mirror symmetry about the body-fixed xz plane (<u>asymmetric program only</u>).	slugs-ft ²

Table 4. Continued

b. Namelist Input for AACON in Symmetric Program

Parameter Number	Meaning	Units	Namelist Variable	Meaning	Units
1	$\partial C_M / \partial \alpha$	1/rad	16	Extra	
2	$\partial C_M / \partial \left(\frac{qd}{2U_\infty} \right)$	1/rad	17	Extra	
3 ^b	$\partial C_M / \partial (\alpha \delta)$	1/rad ²	18	Extra	
4	$\partial C_M / \partial \left(\frac{pad}{2U_\infty} \right)$	1/rad ²	19 ^c	$\partial C_M / \partial \left(\frac{\psi d}{2U_\infty} \right)_T$	1/rad
5	$\partial C_M / \partial (\alpha \delta^2)$	1/rad ³	20 ^c	$\partial C_M / \partial \left(\frac{\theta d}{2U_\infty} \right)_T$	1/rad
6	$\partial C_M / \partial \left(\frac{q\delta^2 d}{2U_\infty} \right)$	1/rad ³	21 ^c	$\partial C_M / \partial \varepsilon _T$	1/rad
7	$\partial C_M / \partial \left(\frac{q\delta^2 d}{2U_\infty} \right)$	1/rad ³	22 ^c	$\partial C_M / \partial \nu _T$	1/rad
8	$\partial C_M / \partial \left(\frac{r\alpha\beta d}{2U_\infty} \right)$	1/rad ³	23 ^c	θ_T	deg
9	$\partial C_M / \partial \left(\frac{q\delta d}{2U_\infty} \right)$	1/rad ²	24 ^c	ψ_T	deg
10 ^d	C_{L0}		25	$\epsilon(0)$	deg
11	$\partial C_L / \partial \left(\frac{p\delta d}{2U_\infty} \right)$	1/rad ²	26	$\dot{\phi}(0)$	deg/sec
12	$\partial C_M / \partial \left(\frac{p\alpha\delta^2 d}{2U_\infty} \right)$	1/rad ⁴	27	$e(0)$	deg
13	$\partial C_L / \partial \left(\frac{pd}{2U_\infty} \right)$	1/rad	28	$\dot{\theta}(0)$	deg/sec
14	$\partial C_L / \partial \left(\frac{p\delta^2 d}{2U_\infty} \right)$	1/rad ³	29	$\psi(0)$	deg
15	Extra		30	$\dot{\psi}(0)$	deg/sec

^bAs used here, δ is defined as $\delta = \sqrt{\alpha^2 + \beta^2}$.

^cThese coefficients define the effects of tunnel flow nonuniformities on the body motion and are discussed in Section 5.3.

^dThis coefficient is a roll torque produced by the gas bearing and is discussed in Section 5.2.

Table 4. Continued

c. Namelist Input for AACON in Asymmetric Program

Parameter Number	Meaning	Units	Namelist Variable	Meaning	Units
1	C_{m0}		19	$\partial C_m / \partial \left(\frac{q a d}{2U_\infty} \right)$	$1/\text{rad}^2$
2	$\partial C_m / \partial \alpha$	$1/\text{rad}$	20	$\partial C_m / \partial \left(\frac{q \alpha^2 d}{2U_\infty} \right)$	$1/\text{rad}^3$
3	$\partial C_m / \partial a $	$1/\text{rad}$	21	$\partial C_m / \partial \left(\frac{q \alpha a }{2U_\infty} \right)$	$1/\text{rad}^3$
4	$\partial C_m / \partial \alpha^2$	$1/\text{rad}^2$	22	$\partial C_m / \partial \left(\frac{q a d}{2U_\infty} \right)$	$1/\text{rad}^2$
5	$\partial C_m / \partial \alpha a $	$1/\text{rad}^2$	23	$\partial C_m / \partial \left(\frac{q \beta^2 d}{2U_\infty} \right)$	$1/\text{rad}^3$
6	$\partial C_m / \partial \alpha^3$	$1/\text{rad}^3$	24	$\partial C_m / \partial \left(\frac{q \alpha a d}{2U_\infty} \right)$	$1/\text{rad}^3$
7	$\partial C_m / \partial \alpha^2 a $	$1/\text{rad}^3$	25	$\partial C_m / \partial \left(\frac{q a \alpha d}{2U_\infty} \right)$	$1/\text{rad}^3$
8	$\partial C_m / \partial a ^2$	$1/\text{rad}^2$	26	$\partial C_m / \partial \left(\frac{r \beta d}{2U_\infty} \right)$	$1/\text{rad}^2$
9	$\partial C_m / \partial \beta^2$	$1/\text{rad}^2$	27	$\partial C_m / \partial \left(\frac{p \beta d}{2U_\infty} \right)$	$1/\text{rad}^2$
10	$\partial C_m / \partial \beta^2 a $	$1/\text{rad}^3$	28	C_{n0}	
11	$\partial C_m / \partial \alpha a ^2$	$1/\text{rad}^2$	29	$\partial C_n / \partial \beta$	$1/\text{rad}$
12	$\partial C_m / \partial a \beta$	$1/\text{rad}^2$	30	$\partial C_n / \partial \alpha \beta$	$1/\text{rad}^2$
13	$\partial C_m / \partial \alpha^2 a ^2$	$1/\text{rad}^3$	31	$\partial C_n / \partial \beta a $	$1/\text{rad}^2$
14	$\partial C_m / \partial \alpha a \beta$	$1/\text{rad}^3$	32	$\partial C_n / \partial \beta^3$	$1/\text{rad}^3$
15	$\partial C_m / \partial \alpha \beta^2$	$1/\text{rad}^3$	33	$\partial C_n / \partial \alpha^2 \beta$	$1/\text{rad}^3$
16	$\partial C_m / \partial \beta^2 a ^2$	$1/\text{rad}^3$	34	$\partial C_n / \partial \beta a \beta$	$1/\text{rad}^2$
17	$\partial C_m / \partial \left(\frac{q d}{2U_\infty} \right)$	$1/\text{rad}^2$	35	$\partial C_n / \partial \beta a \beta$	$1/\text{rad}^3$
18	$\partial C_m / \partial \left(\frac{q \alpha d}{2U_\infty} \right)$	$1/\text{rad}^2$	36	$\partial C_n / \partial \left(\frac{r d}{2U_\infty} \right)$	$1/\text{rad}$

Table 4. Concluded

c. Concluded

Parameter Number	Meaning	Units	Parameter Number	Meaning	Units
37	$\partial C_n / \partial \left(\frac{r \alpha}{2U_\infty} \right)$	1/rad ²	55	$\partial C_{\ell} / \partial \left(\frac{p \beta d}{2U_\infty} \right)$	1/rad ²
38	$\partial C_n / \partial \left(\frac{r \alpha d}{2U_\infty} \right)$	1/rad ²	56	$\partial C_{\ell} / \partial \left(\frac{p \alpha^2 d}{2U_\infty} \right)$	1/rad ³
39	$\partial C_n / \partial \left(\frac{r \alpha^2 d}{2U_\infty} \right)$	1/rad ³	57	$\partial C_{\ell} / \partial \left(\frac{p \beta^2 d}{2U_\infty} \right)$	1/rad ³
40	$\partial C_n / \partial \left(\frac{r \beta d}{2U_\infty} \right)$	1/rad ²	58	Extra	
41	$\partial C_n / \partial \left(\frac{r \beta^2 d}{2U_\infty} \right)$	1/rad ³	59	Extra	
42	$\partial C_n / \partial \left(\frac{r \alpha \alpha d}{2U_\infty} \right)$	1/rad ³	60	I_{zx}	slugs-ft ²
43	$\partial C_n / \partial \left(\frac{r \alpha \beta d}{2U_\infty} \right)$	1/rad ³	61 ^c	$\partial C_n / \partial \left(\frac{\dot{y} d}{2U_\infty} \right)_T$	1/rad
44	$\partial C_n / \partial \left(\frac{r \alpha \beta d}{2U_\infty} \right)$	1/rad ³	62 ^c	$\partial C_m / \partial \left(\frac{\dot{\theta} d}{2U_\infty} \right)_T$	1/rad
45	$\partial C_n / \partial \left(\frac{q \beta d}{2U_\infty} \right)$	1/rad ²	63 ^c	$\partial C_m / \partial \theta _T$	1/rad
46	$\partial C_n / \partial \left(\frac{p \alpha d}{2U_\infty} \right)$	1/rad ²	64 ^c	$\partial C_n / \partial \psi _T$	1/rad
47	$C_{\ell 0}$		65	∂_T	deg
48	$\partial C_{\ell} / \partial \alpha$	1/rad	66	ψ_T	deg
49	$\partial C_{\ell} / \partial \beta$	1/rad	67	$\phi(0)$	deg
50	$\partial C_{\ell} / \partial \alpha \beta$	1/rad ²	68	$\theta(0)$	deg
51	$\partial C_{\ell} / \partial \beta \alpha $	1/rad ²	69	$\psi(0)$	deg
52	$\partial C_{\ell} / \partial \beta \beta $	1/rad ²	70	$p(0)$	deg/sec
53	$\partial C_{\ell} / \partial \left(\frac{p d}{2U_\infty} \right)$	1/rad	71	$q(0)$	deg/sec
54	$\partial C_{\ell} / \partial \left(\frac{p \alpha d}{2U_\infty} \right)$	1/rad ²	72	$r(0)$	deg/sec

Table 5. Effect of Number of Cycles and Number of Points per Cycle on C_{mq} RMS Deviation in Percent of C_{mq}

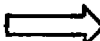

		Number of Cycles 			
		$3\frac{1}{2}$	7	10	15
Number of Points per Cycle 	7	67.0	21.2	10.9	1.0
	15	46.0	14.6	8.2	5.4
	30	31.3	10.9	5.9	3.8
	60	22.0	7.8	4.9	0.5

Table 6. Effect of Measurement Noise on Linear and Nonlinear Coefficients and Their RMS Deviations

α , deg	$C_{m\alpha}$, 1/rad	$E(C_{m\alpha})$, 1/rad	C_{mq} , 1/rad	$E(C_{mq})$, 1/rad	$C_{mq\delta}^2$, 1/rad ³	$E(C_{mq\delta}^2)$, 1/rad ³	$C_{mq\delta}^2$, 1/rad ³	$E(C_{mq\delta}^2)$, 1/rad ³
0.01	-0.2360	0.47 (10^{-5})	-4.001	0.0017	5.8106	0.0008	98.67	0.43
0.02	-0.2360	0.95 (10^{-5})	-3.998	0.0033	5.8108	0.0016	97.44	0.86
0.03	-0.2360	0.14 (10^{-4})	-4.004	0.0050	5.809	0.0024	99.59	1.29
0.04	-0.2360	0.18 (10^{-4})	-3.994	0.0063	5.814	0.0031	97.32	1.63
0.05	-0.2360	0.24 (10^{-4})	-4.007	0.0083	5.809	0.0041	99.53	2.15

Note: $E(\)$ denotes RMS deviation.

Table 7. Tabular Results of Sharp Cone Analysis Using the Asymmetric Program for Fixed Model Aerodynamics

Tunnel-Fixed Process Noise [Eq. (38)]										
	C_{fo}	I_{zx} , slugs-ft ²	Damping		Stiffness		θ_T , deg	ψ_T , deg	Sum of Residuals [Eq. (32)], deg	Data Sampled (see Fig. 17), sec
			t_1 , 1/rad	t_2 , 1/rad	t_1 , 1/rad	t_3 , 1/rad				
Value	-0.57 (10^{-5})	0.0016	2.24	-1.65	0.0163	-0.0056	-0.134	0.152	0.0557	4.40
Deviation	0.4 (10^{-6})	0.0003	0.11	0.12	0.00016	0.00015	0.011	0.013		
Value	-0.10 (10^{-4})	0.0018	1.35	-0.45	0.0154	-0.0054	-0.118	0.159	0.1158	8.44
Deviation	0.1 (10^{-6})	0.0003	0.10	0.08	0.00011	0.00014	0.013	0.014		

Table 8. Tabular Results of Sphere Cone Analysis Using the Asymmetric Program for Fixed Values of $C_{\ell p} = -0.0027$ 1/rad, $t_1 = 0.017$ 1/rad, $t_4 = 0$, $\theta_T = 0$, $\psi_T = 0$

	$C_{m\alpha}$, 1/rad	$C_{m\alpha \alpha }$, 1/rad ²	$C_{m\alpha \beta }$, 1/rad ²	$C_{n\beta}$, 1/rad	$C_{n\beta \alpha }$, 1/rad ²	$C_{n\beta \beta }$, 1/rad ²	C_{mq} , 1/rad
Value Deviation	-0.240 0.005	-1.87 0.11	-1.22 0.16	0.265 0.005	0.927 0.17	1.57 0.09	-1.55 0.64
Value Deviation	-0.189 0.005	-2.70 0.13	-2.02 0.18	0.269 0.004	0.801 0.18	1.53 0.10	1.25 0.58
Value Deviation	-0.172 0.004	-3.06 0.12	-2.20 0.19	0.264 0.002	0.728 0.19	1.62 0.10	1.25 0.50

	C_{nr} , 1/rad	$C_{\ell o}$ $\times 10^6$	I_{zx} , slugs-ft ²	t_4 , 1/rad	t_3 , 1/rad	Sum of Residuals [Eq. (32)], deg	Data Sampled (see Fig. 18), sec
Value Deviation	-4.54 0.63	3.5 0.39	0.0027 0.0006	-3.65 0.20	-0.0016 0.0004	0.0775	5.16
Value Deviation	-12.3 0.60	-1.2 0.2	0.0032 0.0006	0.62 0.20	0.0026 0.0005	0.130	8.32
Value Deviation	-14.47 0.57	-3.5 0.09	0.0028 0.0005	2.72 0.17	0.0032 0.0005	0.174	11.98

APPENDIX A

MATHEMATICAL DEVELOPMENT: ASYMMETRIC VERSION

The parameter identification technique as developed in Section 3.0 considered the 3DOF motion of axially symmetric bodies. In order to provide the greatest versatility in the improved analysis technique as developed in this report, an analogous version considering asymmetric bodies has been formulated. The asymmetric analysis considers the 3DOF motion of bodies with mirror plane symmetry about the x, z plane (see Fig. 1). The governing equations as derived from Eqs. (1) and (2) in the body-fixed coordinate system are

$$\begin{aligned}
 \dot{J} &= \bar{M}_z + \bar{M}_x J_z - pq(I'_z - J_x J_z) - qr(1 + I'_x) J_z \\
 \dot{q} &= \bar{M}_y - (p^2 - r^2) J_y - rp I'_y \\
 \dot{J}p &= \bar{M}_x + \bar{M}_z J_x - qr(J_x J_z + I'_x) + pq(1 - I'_z) J_x
 \end{aligned} \tag{A-1}$$

where the following definitions have been used

$$\begin{aligned}
 J_x &\equiv I_{zx}/I_x & I'_x &\equiv (I_z - I_y)/I_x \\
 J_y &\equiv I_{zy}/I_y & I'_y &\equiv (I_x - I_z)/I_y \\
 J_z &\equiv I_{zx}/I_z & I'_z &\equiv (I_y - I_x)/I_z \\
 J &\equiv 1 - J_x J_z
 \end{aligned} \tag{A-2}$$

with $\bar{M}_x \equiv M_x/I_x$, $\bar{M}_y \equiv M_y/I_y$, and $\bar{M}_z \equiv M_z/I_z$.

The kinematic relations relating the Euler angles to the body-fixed angular rates are given in Eq. (A-3).

$$\begin{aligned}
 \dot{\phi} &= p - \tan \theta (q \sin \phi - r \cos \phi) \\
 \dot{\theta} &= q \cos \phi - r \sin \phi \\
 \dot{\psi} &= (r \cos \phi + q \sin \phi) / \cos \theta
 \end{aligned} \tag{A-3}$$

Integration of Eqs. (A-1) and (A-3) yields the 3DOF angular motion solution for an asymmetric body assuming that the moment expansions as functions of the Euler angles and angular rates are given. For mirror symmetry about the x, z plane in the body-fixed axis system, the moment coefficient expansions in terms of α and β as given in Eqs. (11) and (14) are utilized. The variables α and β are, however, re-evaluated in the body-fixed axis system leading to Eq. (A-4).

$$\beta \equiv \frac{v}{l_\infty} = -\sin \psi \cos \phi + \cos \psi \sin \theta \sin \phi$$

$$\alpha \equiv \frac{w}{l_\infty} = \sin \psi \sin \phi + \cos \psi \sin \theta \cos \phi$$
(A-4)

The parameter extraction method as discussed in Section 3.2 is applied in an analogous manner to the asymmetric analysis. The parametric differential equations required to evaluate the influence coefficients as used in Eq. (21) are derived from Eqs. (A-1) and (A-3) and are shown in Eq. (A-5).

$$\begin{aligned} \dot{P}_{1i} = & Q_{1i} + P_{2i} \sec^2 \theta (q \sin \phi + r \cos \phi) \\ & + \tan \theta (\theta_{2i} \sin \phi + P_{1i} q \cos \phi + Q_{3i} \cos \phi \\ & - P_{1i} r \sin \phi) \\ \dot{P}_{2i} = & Q_{2i} \cos \phi - P_{1i} q \sin \phi - Q_{3i} \sin \phi - P_{1i} r \cos \phi \\ \dot{P}_{3i} = & (Q_{3i} \cos \phi - P_{1i} r \sin \phi + Q_{2i} \sin \phi + P_{1i} q \cos \phi) \sec \theta \\ & + (r \cos \phi + q \sin \phi) P_{2i} \tan \theta \sec \theta \\ J\dot{Q}_{1i} = & M_{1i} - M_{3i} J_x - (J_y J_x + I'_x) (q Q_{3i} - r Q_{2i}) \\ & + (1 - I'_y) J_x (p Q_{2i} + q Q_{1i}) \\ \dot{Q}_{2i} = & M_{2i} - J_y (2p Q_{1i} - 2r Q_{3i}) - I'_y (r Q_{1i} + p Q_{3i}) \\ J\dot{Q}_{3i} = & M_{3i} + M_{1i} J_y - (I'_x - J_x J_y) (p Q_{2i} + q Q_{1i}) \\ & - (1 + I'_y) J_x (q Q_{3i} - r Q_{2i}) \end{aligned}$$
(A-5)

where P_{1i} , P_{2i} , P_{3i} , M_{1i} , and M_{2i} , and M_{3i} are defined as before and $Q_{1i} = \partial p / \partial a_i$, $Q_{2i} = \partial q / \partial a_i$, $Q_{3i} = \partial r / \partial a_i$. The initial conditions for the parametric, kinematic, and dynamic equations as given in Eqs. (A-1), (A-3), and (A-5) are listed below.

$$\begin{aligned} \phi(0) &= a_{N_c-5} & p(0) &= a_{N_c-2} \\ \theta(0) &= a_{N_c-4} & q(0) &= a_{N_c-1} \\ \psi(0) &= a_{N_c-3} & r(0) &= a_{N_c} \end{aligned}$$
(A-6)

$$\begin{aligned}
 P_{1i}(0) &= \delta_{N_c-5,i} & Q_{1i}(0) &= \delta_{N_c-2,i} \\
 P_{2i}(0) &= \delta_{N_c-4,i} & Q_{2i}(0) &= \delta_{N_c-1,i} \\
 P_{3i}(0) &= \delta_{N_c-3,i} & Q_{3i}(0) &= \delta_{N_c,i}
 \end{aligned}
 \tag{A-7}$$

Integration of the parametric and angular motion equations and evaluation of the corrections to the parameters, a_i , are determined in a manner similar to that discussed in Section 3.2 for the axially symmetric analysis.

In addition to the moment coefficients as given in Eq. (14) and the boundary conditions, the product of inertia, I_{zx} , has also been included in the list of parameters, a_i , to be determined. This option was provided in order to circumvent the lack of simple techniques for determining the product of inertia for asymmetric configurations. In Ref. 21, values of I_{zx} as large as 6 percent of I_y have been extracted successfully from generated motion with measurement noise.

NOMENCLATURE

a_i	Aerodynamic coefficients to be extracted, see Section 3.2
a_{i0}, a_{i1}, \dots	Taylor series expansion coefficients as used in Eqs. (12), (14), and (16) ($i = 1, m, n$)
B_i	Diagonal components of the inverse matrix of C_{ij} .
b_{i0}, b_{i1}, \dots	Taylor series expansion coefficients as used in Eqs. (12), (14), and (16) ($i = 1, m, n$)
C_{ij}	$N_c \times N_c$ matrix of influence coefficients, Eq. (24)
C_l	Rolling-moment coefficient, Eq. (7)
C_{l0}	Trim roll torque coefficient, see Eq. (16)
C_{lp}	$\partial C_l / \partial (dp/2U_\infty)$, 1/rad
C_{lq}	$\partial C_l / \partial (dq/2U_\infty)$, 1/rad
C_{lr}	$\partial C_l / \partial (dr/2U_\infty)$, 1/rad
$C_{l\dot{\alpha}}$	$\partial C_l / \partial (d\dot{\alpha}/2U_\infty)$, 1/rad
$C_{l\dot{\beta}}$	$\partial C_l / \partial (d\dot{\beta}/2U_\infty)$, 1/rad
C_m	Pitching-moment coefficient, Eq. (7)
C_{mp}	$\partial C_m / \partial (dp/2U_\infty)$, 1/rad
C_{mq}	$\partial C_m / \partial (dq/2U_\infty)$, 1/rad
$C_{mq\delta^2}$	$\partial C_m / \partial (dq\delta^2/2U_\infty)$, 1/rad ³
C_{mr}	$\partial C_m / \partial (dr/2U_\infty)$, 1/rad
$C_{m\alpha}$	$\partial C_m / \partial \alpha$, 1/rad
$C_{m\dot{\alpha}}$	$\partial C_m / \partial (d\dot{\alpha}/2U_\infty)$, 1/rad
$C_{m\alpha \alpha }$	$\partial C_m / \partial \alpha \alpha $, 1/rad ²

$C_{m \alpha \beta }$	$\partial C_m / \partial \alpha \beta , 1/\text{rad}^2$
$C_{m \alpha \delta^2}$	$\partial C_m / \partial \alpha \delta^2, 1/\text{rad}^3$
$C_{m \dot{\beta}}$	$\partial C_m / \partial (d\dot{\beta}/2U_\infty), 1/\text{rad}$
C_n	Yawing-moment coefficient, Eq. (7)
$C_{n p}$	$\partial C_n / \partial (dp/2U_\infty), 1/\text{rad}$
$C_{n q}$	$\partial C_n / \partial (dq/2U_\infty), 1/\text{rad}$
$C_{n r}$	$\partial C_n / \partial (dr/2U_\infty), 1/\text{rad}$
$C_{n \dot{\alpha}}$	$\partial C_n / \partial (d\dot{\alpha}/2U_\infty), 1/\text{rad}$
$C_{n \beta}$	$\partial C_n / \partial \beta, 1/\text{rad}$
$C_{n \dot{\beta}}$	$\partial C_n / \partial (d\dot{\beta}/2U_\infty), 1/\text{rad}$
$C_{n \beta \alpha }$	$\partial C_n / \partial \beta \alpha , 1/\text{rad}^2$
$C_{n \beta \beta }$	$\partial C_n / \partial \beta \beta , 1/\text{rad}^2$
c_{i0}, c_{i1}, \dots	Taylor series expansion coefficients as used in Eqs. (12), (14), and (16) ($i = 1, m, n$)
D_j	Residual influence matrix, Eq. (25)
d	Reference length (base diameter), ft
d'_3, d'_4, d'_5	Coefficients as used in Eq. (16)
d_N	Nose diameter, ft
E	RMS deviation between experimental data and converged solution, rad
e_0	Trim roll coefficient, see Eq. (16)
e_1, e_2	Proportionality constants relating $\dot{\alpha}$, q and $\dot{\beta}$, r
f_{i0}, f_{i1}, \dots	Taylor series expansion coefficients as used in Eqs. (12), (14), and (16) ($i = 1, m, n$)

g_3, g'_4, g'_5	Coefficients as used in Eq. (16)
\vec{h}	Moment of momentum vector defined in Eq. (2)
h_x, h_y, h_z	Components of moment of momentum vector
I	Transverse moment of inertia for axially symmetric body, slugs-ft ²
I'_x	Dimensionless moment of inertia, Eq. (A-2)
I_{xx} or I_x	Moment of inertia about x axis, Fig. 1, slugs-ft ²
I_{xy}	Product of inertia in x, y plane, Fig. 1, slugs-ft ²
I'_y	Dimensionless moment of inertia, Eq. (A-2)
I_{yy} or I_y	Moment of inertia about y axis, Fig. 1, slugs-ft ²
I_{yz}	Product of inertia in y, z plane, Fig. 1, slugs-ft ²
I'_z	Dimensionless moment of inertia, Eq. (A-2)
I_{zx}	Product of inertia in x, z plane, Fig. 1, slugs-ft ²
I_{zz} or I_z	Moment of inertia about z axis, Fig. 1, slugs-ft ²
$\vec{i}, \vec{j}, \vec{k}$	Unit vectors along coordinate axis, Fig. 1
J	$1 - J_x J_z$
J_x	Dimensionless product of inertia, Eq. (A-2)
J_y	Dimensionless product of inertia, Eq. (A-2)
J_z	Dimensionless product of inertia, Eq. (A-2)
ℓ	Distance between bearing pivot point and mass center, see Fig. 13, ft
\vec{M}	Moment vector acting at mass cg [see Eq. (1) and discussion]
M_{1i}, M_{2i}, M_{3i}	Equal to $\partial \bar{M}_x / \partial a_i$, $\partial \bar{M}_y / \partial a_i$, and $\partial \bar{M}_z / \partial a_i$, respectively
M_x, M_y, M_z	Components of moment vector

$\overline{M}_x, \overline{M}_y, \overline{M}_z$	Equal to \hat{M}_x/I_x , \hat{M}_y/I , and \hat{M}_z/I , respectively, for the symmetric program and M_x/I_x , M_y/I_y , and M_z/I_z , respectively, for the asymmetric program, lbf/slug-ft
M_{yT}	Tunnel-fixed moment, Eq. (38), ft-lbf
M_{zT}	Tunnel-fixed moment, Eq. (38), ft-lbf
N	Total number of time points in fit
N_c	Total number of coefficients to be extracted
n	Number of iterations per case
P_{1i}, P_{2i}, P_{3i}	Equal to $\partial\phi/\partial a_i$, $\partial\theta/\partial a_i$, and $\partial\psi/\partial a_i$, respectively
$P_{1i\ell}, P_{2i\ell}, P_{3i\ell}$	Value of P_{1i} , P_{2i} , and P_{3i} , respectively, at time point ℓ
p	Roll velocity, deg/sec
Q_{1i}, Q_{2i}, Q_{3i}	Equal to $\partial p/\partial a_i$, $\partial q/\partial a_i$, $\partial r/\partial a_i$, respectively
q	Pitch velocity, deg/sec
q_∞	Dynamic pressure of free-stream, psfa
R	Dimensionless inertia ratio, I_x/I
$R_{1\ell}, R_{2\ell}, R_{3\ell}$	Residuals in ϕ , θ , and ψ , respectively, at each time point ℓ , deg
r	Yaw rate, deg/sec
S	Reference area (base area), ft ²
t	Time, sec
t_1, t_2, t_3, t_4	Tunnel-fixed moment coefficients as defined in Eq. (38), 1/rad
t_{max}	Data sample time, sec
U_∞	Free-stream velocity, ft/sec
u	Velocity along x axis, see Fig. 1, ft/sec
$u\ell$	Residual in roll, deg

v	Velocity along y axis, see Fig. 1, ft/sec
v_Q	Residual in yaw, deg
W	Pendulum weight, lbf
w	Velocity along z axis, see Fig. 1, ft/sec
w_Q	Residual in pitch, deg
X	Tunnel-fixed axis, see Fig. 2
x	Body-fixed axis, see Fig. 1
x', y', z'	Rotated axis system as defined in Fig. 3
Y	Tunnel-fixed axis, see Fig. 2
y	Body-fixed axis, see Fig. 1
Z	Tunnel-fixed axis, see Fig. 2
z	Body-fixed axis, see Fig. 1
a	Velocity ratio as given in Eq. (9) or Eq. (A-4)
a_a	Angle of attack as defined in Eq. (33), rad
a_v	Velocity ratio as used by Tobak, Eq. (32)
β	Velocity ratio as given in Eq. (9) or Eq. (A-4)
β_a	Angle of attack as defined in Eq. (33), rad
β_v	Velocity ratio as used by Tobak, Eq. (32)
Δa_i	Corrections to the coefficients a_i
Δt	Integration time interval, sec
δ	Equal to $\sqrt{a^2 + \beta^2}$, rad
δ_{ij}	Kroneker Delta function

δa_i	RMS deviation in extracted coefficient a_i
θ	Pitch angle, see Fig. 2
θ_c	Cone semiangle
θ_T	Artificial tunnel-fixed flow angularity correction, pitch, deg
θ_ℓ	Calculated pitch angle at time point ℓ , deg
θ_{ℓ_0}	Value of θ_ℓ for the given constants, a_i , deg
$\theta_{m\ell}$	Measured pitch angle at time point ℓ , deg
σ	One standard deviation, Gaussian noise, deg
$\sigma_\phi, \sigma_\theta, \sigma_\psi$	Standard deviation of relative uncertainty in ϕ , θ , and ψ measurement, respectively, deg
τ	Computer run time of codes, Eq. (31), sec
ϕ	Roll angle, deg
ϕ_ℓ	Calculated roll angle at time point ℓ , deg
ϕ_{ℓ_0}	Value of ϕ_ℓ for the given constants, a_i , deg
$\phi_{m\ell}$	Measured roll angle at time point ℓ , deg
ψ	Yaw angle, see Fig. 2, deg
ψ_T	Artificial tunnel-fixed flow angularity correction, yaw, deg
ψ_ℓ	Calculated yaw angle at time point ℓ , deg
ψ_{ℓ_0}	Value of ψ_ℓ for the given constants, a_i , deg
$\psi_{m\ell}$	Measured yaw angle at time point ℓ , deg
Ω	Sting roll position as used in Eq. (36), deg

Superscripts

^ Coefficients in plane-fixed or aeroballistic axis system

.

 d/dt

Subscript

o Initial value of coefficient